AD NUMBER

ADB085262

LIMITATION CHANGES

TO:

Approved for public release; distribution is unlimited.

FROM:

Distribution authorized to U.S. Gov't. agencies only; Test and Evaluation; JUL 1984. Other requests shall be referred to Army Research and Technology Lab., Fort Eustis, VA.

AUTHORITY

USAAVSCOM ltr 27 Mar 1995

USAAVSCOM TR-84-D-6

SMALL PORTABLE ANALYZER DIAGNOSTIC EQUIPMENT (SPADE) PROGRAM — DIAGNOSTIC SOFTWARE VALIDATION

P. Berrett and J. M. Laskey

RCA AUTOMATED SYSTEMS
Burlington, Mass. 01803

July 1984

Final Report

Prepared for

APPLIED TECHNOLOGY LABORATORY
U.S. ARMY RESEARCH AND TECHNOLOGY LABORATORIES (AVSCOM)
Fort Eustis, Va. 23604

APPLIED TECHNOLOGY LABORATORY POSITION STATEMENT

This report provides the validation of diagnostic software that can be used in the early detection and identification of rolling element bearing failures in helicopter drive train components. This technique does not rely upon the prior history of the component as did previous techniques. It is suggested that the reader use these results to evaluate current or planned programs while being aware that this technique has not been fully demonstrated on operational aircraft. Results of this contract are being integrated with other R&D programs with the Applied Technology Laboratory which involve the development of multipurpose diagnostic equipment.

Mr. Roger J. Hunthausen, R&M and Subsystems, Aeronautical Systems Division, served as project engineer for this effort.

Citation Format: Full Citation (1F)

Accession Number:
ADB085262
Citation Status:
Active
Citation Classification:
Unclassified
Fields and Groups:
010301 - Helicopters
130900 - Machinery and Tools
Corporate Author:
RCA AUTOMATED SYSTEMS DIV BURLINGTON MA
Unclassified Title:
(U) **Small Portable Analyzer Diagnostic Equipment (SPADE) Program** -- Diagnostic Software Validation.
Title Classification:
Unclassified
Descriptive Note:
Final rept.,
Personal Author(s):
Berrett, P
Laskey, J M
Report Date:
Jul 1984
Media Count:
239 Page(s)
Cost:
$14.60
Contract Number:
DAAK51-82-C-0052
Report Number(s):
USAAVSCOM-TR-84-D-6
Project Number:
1H464204DC32
Task Number:
14
Monitor Acronym:
USAAVSCOM
Monitor Series:
TR-84-D-6
Report Classification:
Unclassified
Distribution Statement:
Approved for public release;Distribution unlimited.
Descriptors:
(U) *DIAGNOSTIC EQUIPMENT, *BEARINGS, DEFECTS(MATERIALS), FRICTION, WEAR, DETECTION, TRANSMISSIONS(MECHANICAL), BREADBOARD MODELS, SIGNATURES, TEST AND EVALUATION

Distribution Change Order refer to Change Authority Field

Identifiers:

(U) *SPADE(Small Portable Analyzer Diagnostic Equipment), AH-1G helicopter, UH-1H helicopter, OH-58 A/C, PE64204A, ASC32, WU033.

Identifier Classification:

Unclassified

Abstract:

(U) The SPADE system is being developed to detect and isolate degraded Army helicopter power train bearings. It is designed to determine the condition of hanger bearings, 42-degree gearbox bearings, and 90-degree gearbox bearings of the UH-1H, AH-1S, and OH-58A, B, and C aircraft. SPADE is expandable to address added helicopter types and bearing or gearbox types. Current SPADE technology has demonstrated a bearing fault detection rate of better than 90 percent with a false alarm rate less than 10 percent. (Author)

Abstract Classification:

Unclassified

Distribution Limitation(s):

01 - APPROVED FOR PUBLIC RELEASE

Source Serial:

F

Source Code:

409516

Document Location:

DTIC AND NTIS

IAC Assigned Accession Number:

MCIC-124036

Change Authority:

950406 - (< MAR 27 DTD LTR VA-AMS-R-TMS EUSTIS>

REPORT DOCUMENTATION PAGE

READ INSTRUCTIONS BEFORE COMPLETING FORM

1. REPORT NUMBER: USAAVSCOM TR 84-D-6	2. GOVT ACCESSION NO.
3. RECIPIENT'S CATALOG NUMBER	
4. TITLE (and Subtitle): SMALL PORTABLE ANALYZER DIAGNOSTIC EQUIPMENT (SPADE) PROGRAM - DIAGNOSTIC SOFTWARE VALIDATION	5. TYPE OF REPORT & PERIOD COVERED: Final
	6. PERFORMING ORG. REPORT NUMBER
7. AUTHOR(s): P. Berrett, J. M. Laskey	8. CONTRACT OR GRANT NUMBER(s): DAAK51-82-C-0052
9. PERFORMING ORGANIZATION NAME AND ADDRESS: RCA Automated Systems, Burlington, MA 01803	10. PROGRAM ELEMENT, PROJECT, TASK AREA & WORK UNIT NUMBERS: 64204A 1H464204DC32 14 033
11. CONTROLLING OFFICE NAME AND ADDRESS: Applied Technology Laboratory US Army Research and Technology Laboratories (AVSCOM), Fort Eustis, VA 23604	12. REPORT DATE: July 1984
	13. NUMBER OF PAGES: 224
14. MONITORING AGENCY NAME & ADDRESS(if different from Controlling Office)	15. SECURITY CLASS. (of this report): Unclassified
	15a. DECLASSIFICATION/DOWNGRADING SCHEDULE

16. DISTRIBUTION STATEMENT (of this Report)

Distribution limited to US Government agencies only; test and evaluation; July 1984. Other requests for this document must be referred to the Applied Technology Laboratory, US Army Research and Technology Laboratories (AVSCOM), Fort Eustis, Virginia 23604.

17. DISTRIBUTION STATEMENT (of the abstract entered in Block 20, if different from Report)

18. SUPPLEMENTARY NOTES

19. KEY WORDS (Continue on reverse side if necessary and identify by block number)

Gearbox bearings
Power train
Diagnostic equipment
Fault detection

20. ABSTRACT (Continue on reverse side if necessary and identify by block number)

The SPADE system is being developed to detect and isolate degraded Army helicopter power train bearings. It is designed to determine the condition of hanger bearings, 42-degree gearbox bearings, and 90-degree gearbox bearings of the UH-1H, AH-1S, and OH-58A, B, and C aircraft. SPADE is expandable to address added helicopter types and bearing or gearbox types. Current SPADE technology has demonstrated a bearing fault detection rate of better than 90 percent with a false alarm rate less than 10 percent.

PREFACE

This report was prepared by RCA Automated Systems under U.S. Army Contract DAAK51-82-C-0052, "Small Portable Analyzer Diagnostic Equipment (SPADE) Program". The contract was administered under the technical direction of Mr. Roger J. Hunthausen of the Applied Technology Laboratory, U.S. Army Research and Technology Laboratories (AVSCOM), Fort Eustis, Virginia. Principal RCA Automated Systems personnel contributing to this development were:

System Analysis	-	R. B. Mark
System Development	-	G. R. Egar, V. Graziani, E. F. Heyl
Data Base Development	-	D. A. Gore
Accelerometer Development	-	R. C. Blanchard
Engineering Management	-	P. Berrett
Program Management	-	J. M. Laskey

Appreciation is expressed for the assistance and support given by Mr. Roger J. Hunthausen in the accomplishment of this program.

Acknowledgement is also given for the assistance provided by personnel of the following organizations:

Bell Helicopter Textron, Inc.	-	Mr. Charles Braddock Mr. Purdue Patel Mr. Lewis Wood
U.S. Army Aviation Development Test Activity (USAAVNDTA) Fort Rucker, Alabama	-	Col. William B. Woodson, Commander Mr. Russell Sharp, USAAVNDTA Mr. Ron Parrish, Northrop Worldwide Aircraft Service, Inc.

TABLE OF CONTENTS

TABLE OF CONTENTS (cont.)

TABLE OF CONTENTS (cont.)

LIST OF ILLUSTRATIONS

LIST OF ILLUSTRATIONS (cont.)

LIST OF ILLUSTRATIONS (cont.)

LIST OF ILLUSTRATIONS (cont.)

LIST OF ILLUSTRATIONS (cont.)

LIST OF ILLUSTRATIONS (cont.)

LIST OF ILLUSTRATIONS (cont.)

LIST OF TABLES

SECTION 1
INTRODUCTION

The SPADE engineering development program was awarded to RCA Automated Systems, Burlington, Massachusetts, on 30 September 1982. The SPADE system is being developed to detect and isolate degraded Army helicopter power train bearings. Under the current program the SPADE system is designed to determine the condition of hanger bearings, 42-degree gearbox bearings, and 90-degree gearbox bearings of UH-1H, AH-1S, and OH-58 A/C aircraft. SPADE is expandable to address added helicopter types and added bearing or gearbox types in the future. Specific requirements for the system are stated in Contract DAAK51-82-C-0052, and will become finalized in the Prime Item Development Specification (PIDS) which is under development as part of the SPADE contract.

The SPADE preliminary design status was presented at a Preliminary Design Review on 18/19 January 1983. The preliminary design was approved and initiation of detail design authorized on 28 January 1983. Real-time signal processing with breadboard SPADE hardware and software during February 1983 revealed that system design modifications were required to satisfy the bearing fault detection requirements of the PIDS. An engineering analysis of the physical phenomena of bearing failures was conducted. Design modifications were defined in May 1983 based on new discoveries about bearing fault characteristics. The program Statement of Work was modified to:

(1) Concentrate on proving the design changes by breadboard implementation, diagnostic software validation, and on-aircraft fault insertion tests at Fort Rucker, Alabama.

(2) Defer detail design and related Integrated Logistic Support (ILS) tasks.

A Special Progress Review (SPR) conducted on 12/13 October 1983 reviewed the SPADE hardware/software design details and the results of the diagnostic software validation effort. The SPR demonstrated:

(1) A significant improvement in definition of bearing fault characteristics

(2) A SPADE system design and breadboard hardware/software performance that satisfied the PIDS requirements

(3) A viable signal processing within SPADE to suppress the helicopter noise and clutter

(4) A technology development resulting in a new tool, SPADE, that provides insight into the world of rotating machinery with potential application to gears, machinery imbalance, and grease lubricated assemblies, as well as bearings.

This report presents a summary of the engineering effort conducted since the January 1983 Preliminary Design Review. The details of the engineering analysis, hardware and software modifications to the PDR design, and test results are described herein. The objectives of the diagnostic software validation have been successfully accomplished. The current SPADE technology has demonstrated a bearing fault detection rate of better than 90 percent with a false alarm rate less than 10 percent.

SECTION 2
SYSTEM REQUIREMENTS

2.1 THE PHYSICAL PHENOMENA OF HELICOPTER BEARING FAILURES

To achieve a useful payload and range, helicopters are designed to be as light as possible, yet strong enough to satisfy flight safety requirements for their operational life. This design trade-off is particularly evident in the drive line. Every element of the drive line is designed to be absolutely as light as possible for the loads which it must carry. To this extent the bearings chosen for helicopter applications are typically dynamically loaded to levels which cause them to have mean lifetimes which are shorter than is commercially common. For a given dynamic loading application, a commercial user might select a medium series ball bearing, whereas a light series bearing would probably be chosen for a similar military helicopter application. By using the light series bearing instead of the medium series for the same load conditions, the L_{10} life of the bearing will be reduced to approximately 1/3. Some of this life reduction can be regained by choosing different bearing materials such as M-50 tool steel rather than the more common 52100 bearing steels, and by specifying better steel refining techniques such as consumable electrode double vacuum melt processing. However, even with the use of better steels and advanced refining techniques, the premium placed on overall light weight results in relatively short bearing lifetimes.

The life of a bearing which is properly lubricated, correctly handled and installed, and of adequate design will be a function of the fatigue of the bearing material. The rotation of a bearing generates cyclic stresses on the raceways and rolling elements which causes flexing of the bearing surfaces. This flexing ultimately results in metal fatigue. During the early stages of fatigue, microcracks form on and below the bearing's surface. Continued cyclic stressing lengthens and expands the microcracks until the bearing fails by spalling. This fatigue damage is inevitable during normal bearing operation.

Unless rolling element bearings wear out prematurely, they will all ultimately succumb to steel fatigue. The bearings used in helicopter gearbox applications generally fail due to subsurface fatigue whereas the major mode of hanger bearings is associated with lubrication and the penetration of dirt and water.

2.1.1 Hanger Bearings

The hanger bearings used on the UH-1 Huey, OH-58 Kiowa, and the AH-1 Cobra helicopters are all extra light series, deep groove ball bearings with pressed steel ribbon cages which are permanently sealed and grease lubricated. In all cases these bearings are directly exposed to the outside environment. Dirt and moisture tend to wear the rubbing seals to the point

at which they are able to penetrate the bearing. Once inside the bearing, the dirt causes rapid wear and the moisture results in corrosion of the raceways. These failures begin as surface microcracks which will expand until the bearing fails due to spalling. The presence of water in the lubricant, whether dissolved or free, has been found to encourage the propagation of cracks. This is believed to be due to migration of the water molecules to the cracks where they tend to break down, releasing hydrogen ions. The hydrogen ions enter the microcracks and react with the steel, making it brittle. Recent efforts to protect the hanger bearings from exposure to dust and water by using tail-boom shrouds have been successful in reducing the number of failures but have not eliminated them.

2.1.2 Gearbox Bearings

The ball and roller bearings utilized in the tail rotor drive gearboxes for the Huey, Kiowa, and the Cobra helicopters are not exposed to the outside environment as are the hanger bearings. These gearbox bearings are internal to the assemblies, oil lubricated, and protected from dirt and moisture by multi-lip positive wiping seals. The input and output shafts of all of the subject gearboxes (42 degree and 90 degree) have a similar contingent of bearings. For each case, the quill is supported by a preloaded duplex pair of ball bearings and a cylindrical roller bearing. The duplex pair absorbs all of the axial thrust loads while the radial loads are distributed between the duplex pair and the cylindrical roller bearing. The most common failure mode of both of these types of bearings, when they are correctly handled and lubricated, is spalling due to subsurface fatigue.

The duplex pairs of ball bearings used in these applications are always preloaded together to increase the assembly stiffness. Subjecting a rolling bearing to a controlled preload causes a certain amount of deflection to take place within the assembly. The addition of further loads increases the total deflection; however, the incremental deflection associated with the additional load will be less than if there was no preload on the bearing's. In addition to increasing the stiffness of a bearing, preloading minimizes the tendency of rolling elements to skid around the races. Skidding of rolling elements within bearings occurs when the balls or rollers pass through a zone where they become unloaded but are still propelled along by the bearing's rotating cage. The action of sliding friction rather than the desired rolling friction causes accelerated bearing wear. The ball bearings in these gearboxes are preloaded to a level sufficient to insure that the balls are never completely unloaded as they travel around the races with normal loads. In these applications the load on individual balls cyclically increases to between 200-250 kpsi in the bearing load zone and then decreases to a few thousand psi as they travel around the stationary outer races. Unless these ball bearings are mishandled or insufficiently lubricated, they will always ultimately succumb to fatigue failure culminating in spalling. Figure 1 depicts the failure sequence.

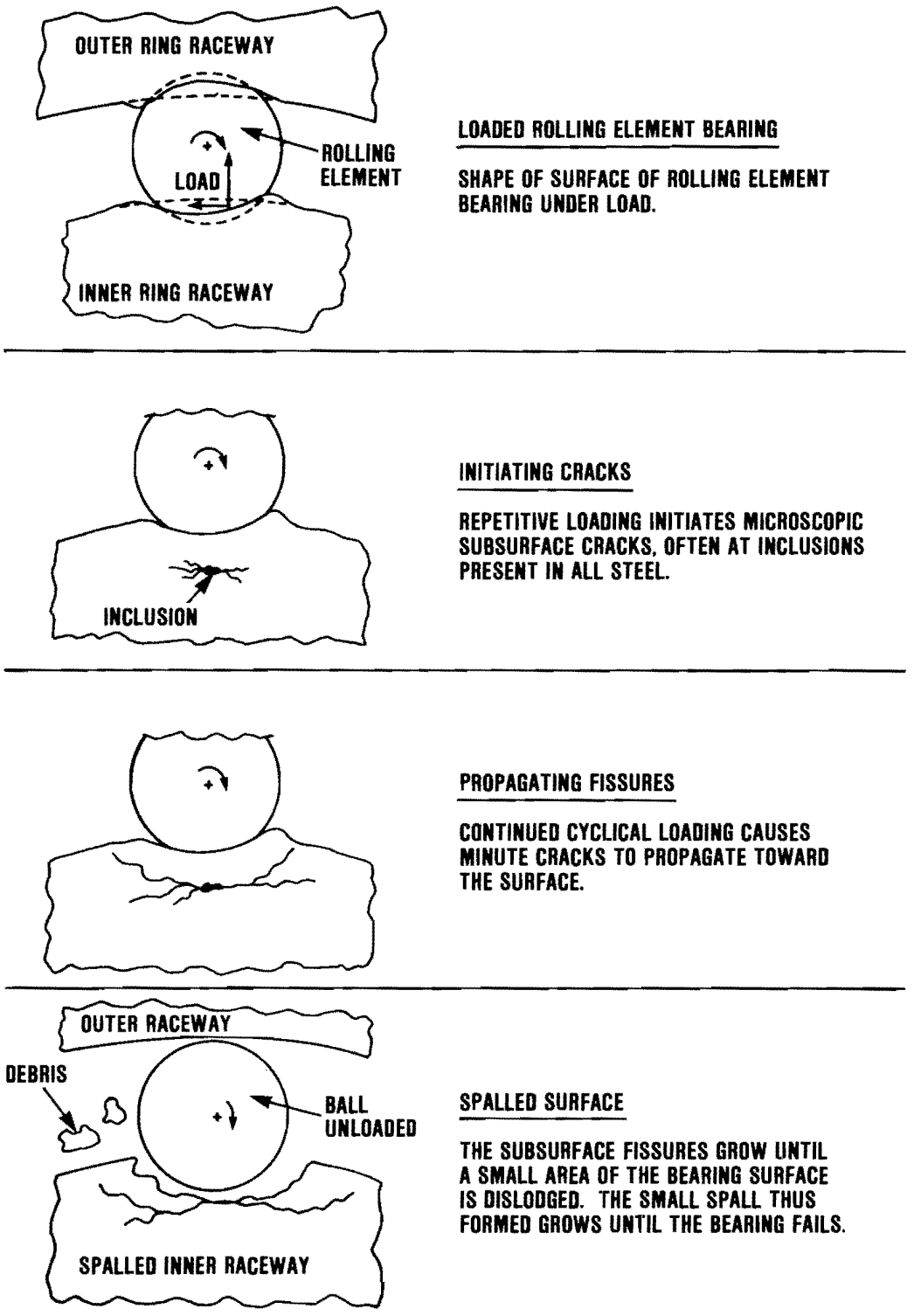

Figure 1. Steel Fatigue Failure Sequence in Rolling Element Bearings

The loads imposed on the cylindrical roller bearings used in these gearboxes differ from the duplex ball bearing loads in two major respects.

(1) These roller bearings are designed to resist a pure radial load and are not preloaded. As a given roller travels around its stationary outer race, it leaves the load zone and enters a no-load zone where there is zero compressive stress on the roller. When the roller is in the no-load zone it tends to no longer rotate about its own axis but rather be dragged along by the retainer. This sliding contact between the roller and the races tends to produce greater wear than would take place with rolling contact. In the extreme, severe skidding results in fatigue spalling of the races and rollers; however, this type of failure is very uncommon in these gearboxes. The most common failure is spalling due to fatigue in the load zone.

(2) There is a stress concentration at the ends of the contact path of the loaded cylinders which tends to shorten the fatigue life. To minimize this problem, the rollers used in these bearings are slightly crowned to more uniformly distribute the stress across the roller's length. This crowning of the rollers has the effect of greatly extending the bearing's life and of causing the ultimate fatigue failure to be located in the middle of the rollers and raceways.

2.1.3 Bearing Failure Summary

In summation, there are many types of bearing failures possible, the majority of which relate to bearing abuse, poor design, and lubrication failure. The military aviation community goes to great lengths to avoid premature bearing failures due to these factors, but when it does occur it leads to a spalling. Even if all premature failures are eliminated, rolling element bearings will always ultimately succumb to steel fatigue. Ring raceways and rolling elements are subjected to cyclic contact stresses that initiate microscopic cracks which propagate. These cracks act as stress risers which over time propagate through the load surface until a small isolated portion of the bearing's surface is dislodged. This fatigue failure, spalling, must be detected before additional damage occurs.

2.2 IDENTIFICATION AND CHARACTERIZATION OF FAULT SIGNALS

SPADE is designed to detect bearing failure and/or incipient failure. SPADE consists of an analyzer unit and its associated cables and sensors (accelerometers). When the sensors are attached to gearboxes and hanger bearings of a helicopter, the vibrational energies released in the vicinity of the bearings under test develop electrical signals that are processed by the SPADE analyzer. The processed signals are compared to threshold levels programmed in the SPADE to sense and indicate a faulty bearing condition. The first prerequisite to this design is the identification and

characterization of bearing fault signals. From this understanding evolves the signal processing required to enhance, discriminate, and measure the fault signal contained in the accelerometer output.

Raw accelerometer signals are characterized by a multitude of components, mostly periodic and mutually coherent. Examples of these are:

(1) FM or AM modulation imposed on higher frequency components caused by load variations generates families of sidebands.

(2) Random and frequent excitations of natural frequencies of shafts, housings, gears and bearing races caused by random asperities and other irregularities in gear teeth and bearing elements.

(3) A mixture of random and coherent noise, at relatively high frequencies, caused by disturbances from gas engine turbine blade interference and exhaust turbulence.

Overall, the accelerometer output has been observed to comprise the bearing failure signal, clutter (noise signals produced by shaft imbalances and gears that are similar to bearing failure signals in repetition rate), and machinery noise (low and high frequency noise signals unlike bearing failure signals). The noise floor of the accelerometer and built-in preamplifier is well below the level of other signals and thus does not contribute significantly to the accelerometer output signals.

RCA studies have shown that for the bearing sizes tested no usable signals are found in the 0 to 10 kHz band and that the system signal-to-noise ratio, dynamic range and gain can be greatly improved by removing the machinery noise which is found in this band. Figure 2 shows a typical accelerometer output signal filtered by a 5 kHz high pass filter. This shows that in spite of the 5 kHz filtering, the waveform comprises mostly 5 kHz fairly narrow-band noise, the narrowness being indicated by the number of cycles in the groups of bursts apparent in the figure. The noise obscures the bearing fault signal in the waveform (obtained from a test cell run of a duplex ball bearing outer race fault implant on an AH-1S, 90-degree gearbox input quill).

Figure 3 clearly reveals a group of isolated bursts occurring at a repetition rate of 345 per second (measured). Section 2.3.1 will show that these bursts correlate with the calculated repetition rate (351 per second) for a fault signal emanated in the outer race of this bearing (correlation is within 2 percent).

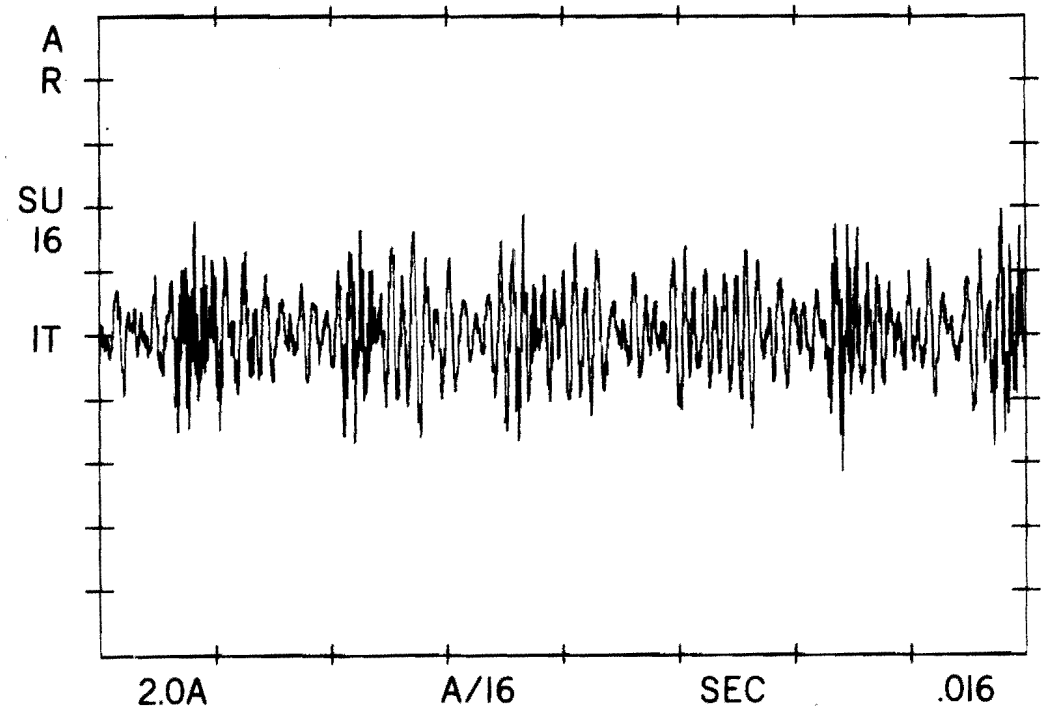

Figure 2. Typical Raw Accelerometer Output Signal

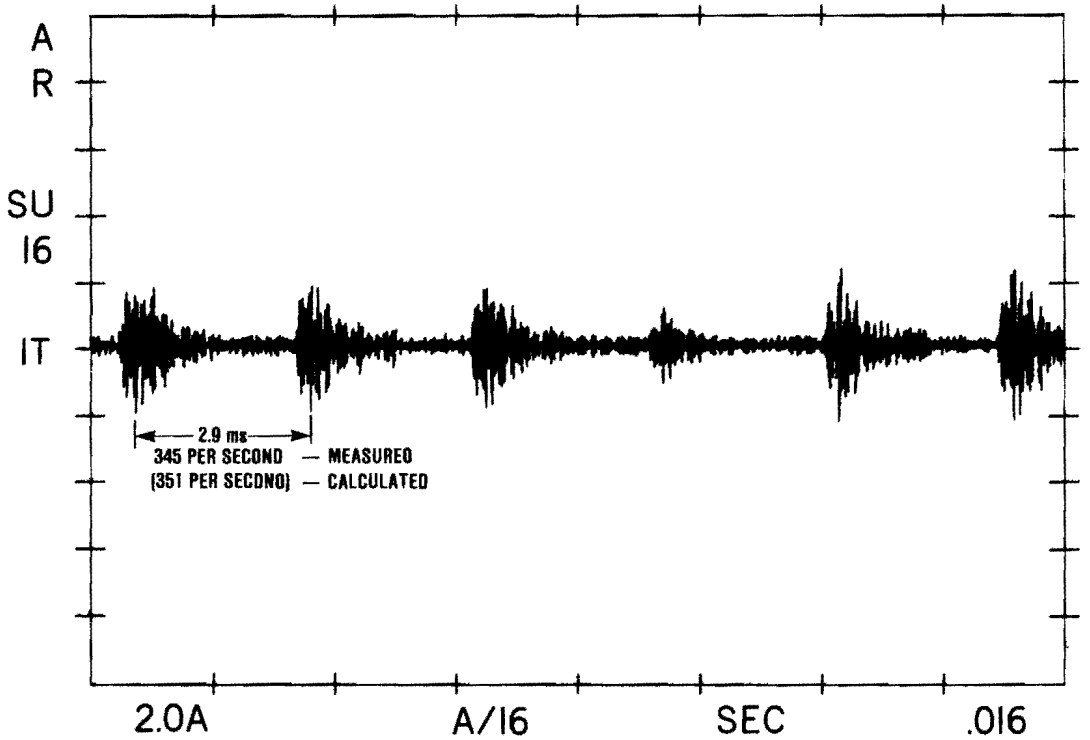

Figure 3. Band-Pass Filtering Reveals Bearing Fault Signal

The filter which revealed the fault signal was a four-pole high pass at 15 kHz which greatly reduced the machinery noise without attenuating the fault signal. Also present was a four-pole low pass at 35 kHz which was found necessary to attenuate the high frequency noise present in aircraft tests.

2.3 CORRELATION OF SIGNALS WITH PHYSICAL PHENOMENA

The forces and moments acting on a loaded roller or ball bearing are shown in Figure 4 and those acting on an unloaded roller or ball bearing are shown in Figure 5. Static forces are the shaft load, deformation of the bearing elements due to designed preloads (includes "press-fit" or "interference fit" of parts), dynamic deformation and thermal deformation.

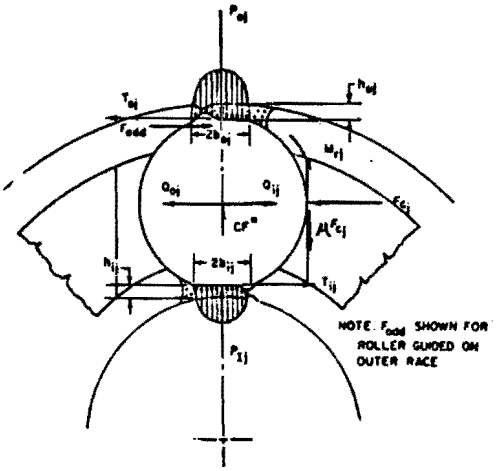

Figure 4. Forces and Moments Acting on a Loaded Roller or Ball Bearing

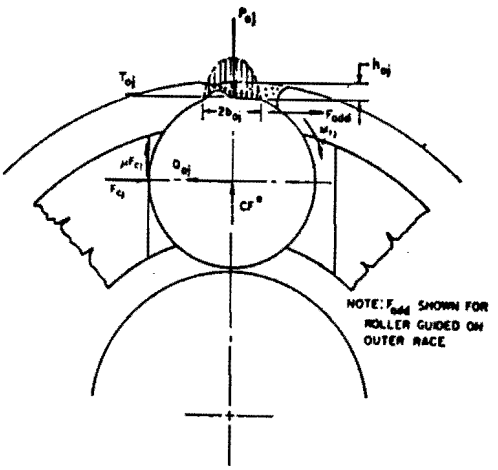

Figure 5. Forces and Moments Acting on an Unloaded Roller or Ball Bearing

Dynamic forces acting on a loaded roller or ball include centrifugal, fluid pressure, traction (fluid frictional drag), and friction. As an example of dynamic deformation, a 0.5-inch-diameter hollow roller with a 0.25-inch-diameter hole will experience a ± 4 percent bulging of its outer surface at 150,000 rpm roller speed. Significant rolling element load changes occur due to such deformations in each of the bearing elements. The summation of all of these forces results in an elastic deformation of the elements. Temperature changes affect the static loading due to the thermal deformation of the elements and the dynamic loading by changing the fluid pressure and traction forces.

For a given bearing operating at a steady-state shaft load and speed, these various forces will be in equilibrium and a summation of all forces will be zero. When a rolling element passes over a fault, such as a crack or spall, a rapid change in the loading occurs and thus a rapid change of force is transferred to the outer race. The force imbalance therefore results in a physical disturbance at the bearing housing. This can occur when a loaded

ball encounters a spall resulting in a sudden release of the loading, or when an unloaded ball encounters a high spot (such as debris), having the effect of a sudden loading. The physical disturbance which results from these loading discontinuities is typically measured as vibration on the outer race.

There are two types of vibration which will occur: forced and free. When a bearing ball or roller passes over a fault, both modes of vibration occur. Forced vibration is motion which is directly caused by, and persists because of, the existence of a disturbing force. As soon as the disturbance is removed, forced vibration ceases. For this reason, the vibration frequency will be directly related to the disturbance frequency. Free vibration exists if the periodic motion continues after the cause of the original disturbance is removed. Any free vibration of a mechanical system will eventually cease because of a loss of energy. The frequency of free vibration is the natural frequency of the system. If the forcing frequency should become equal to the natural frequency of a system, then resonance occurs.

Forced vibration will occur primarily from rotating element imbalances and thus at frequencies considerably below the natural frequency. These will also be primarily sinusoidal in nature and thus not have any components at or even near the natural frequency (discounting some of the more complex waveforms that will be present). A roller traveling over a discontinuity, such as a crack or spall, creates a step change in the bearing loads and thus imparts an energy impulse containing a broad range of frequencies, at least some of which will be at the natural frequency of the bearing and/or sensor. Thus some resonance will occur.

Early attempts at detecting bearing faults by spectral analysis concentrated upon vibration frequencies which were multiples of the shaft rotational frequency. An important assumption made in these investigations was that the bearing components were rigid bodies. This greatly simplified the analysis but obscured the potential advantages of considering the elastic properties of the system. To be more specific, these early approaches only considered forced vibration and did not consider free vibration.

Thus, by measuring vibrations exclusively at the natural frequency of the system elements, the background vibrations caused by shaft imbalance and other sources are ignored and only the impulse related events are measured. For the systems being considered, the only source of an impulse disturbance is due to faults in the bearing.

2.3.1 Defect Repetition Rates

Table 1 provides the repetition rates calculated for inner race (IR), outer race (OR), and rolling element (RE) faults of typical bearings. For a defect (simulated spall) in the OR, the fault frequency is the number of times per second that a ball passes over the spall at the normal operating speed of the shaft supported by the bearing. Since the OR is irrotational, a spall almost always forms in the (fixed) load zone and each ball passes over it in maximum load condition. Figure 3 shows that the amplitude of the fault responses are

TABLE 1. TYPICAL BEARING PARAMETERS

A/C	Bell Helicopter Part Number	Fault Repetition Rates IR	OR	RE	Description/Application
AH-1S	212-040-143	504	357	313	Duplex ball, 42-degree gearbox input and output quill
	212-040-466	192	134	132	Roller, 90-degree gearbox output quill
	212-040-456				Duplex ball, 90-degree
		509	351	327	gearbox input quill
		197	136	126	output quill
UH-1H	204-040-143				Duplex ball,
		503	357	313	90-degree gearbox input quill
		503	357	313	42-degree gearbox input quill
	204-040-310	594	410	378	Roller, 42-degree gearbox input quill

roughly equal, except for one which is considerably smaller than the rest. Figure 6 shows a magnified sample from the same tape recording as Figure 3 but at a different time. The small signal is again present, indicating that the ball which generated it was less loaded than the others. Chance reduction of load by other vibrations could account for the reduced response.

Figure 7 shows the fault signal for an IR implanted spall (AH-1S, input quill, duplex ball). Since the IR rotates, the spall passes through the load zone (once per revolution) and the ball which runs over the spall at this point produces the largest signal. Note that the measured ball-pass frequency of 519 Hz agrees with the calculated value of 509 (Table 1) to an accuracy of 3 percent.

Figure 8 shows the distinctive pattern of a ball spall. The axis of rotation of the ball precesses continuously so that the spall periodically loses its once-per-revolution contact with the races, as indicated by the low amplitude periods of the trace. Since none of the signals above is present when no fault is present, it is concluded that the signals shown result from the inserted spalls.

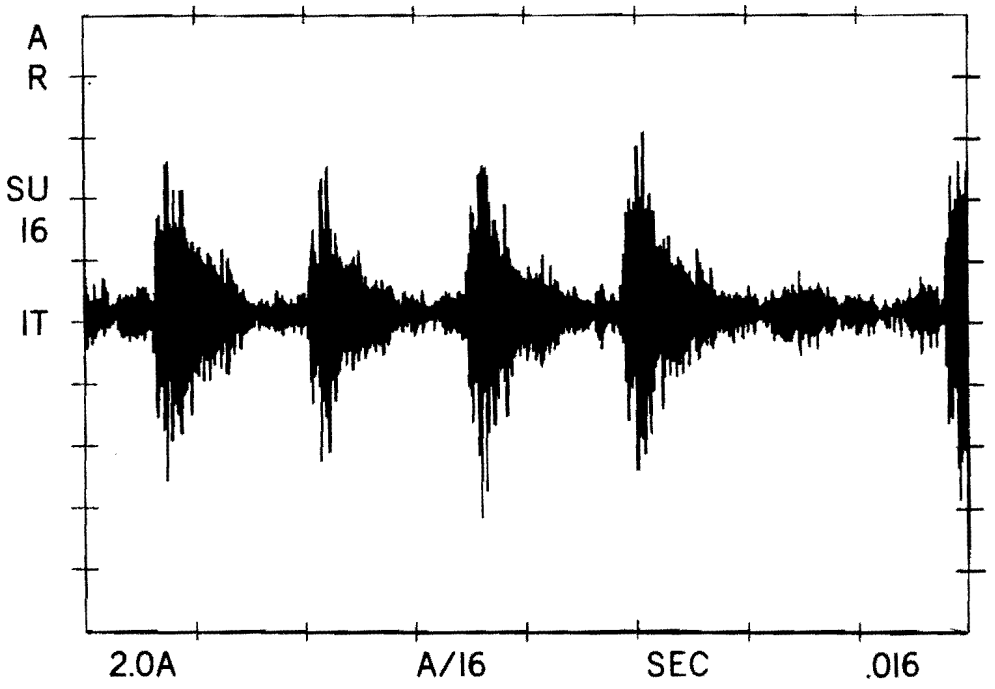

Figure 6. Magnified Band-Pass Filtered Signal

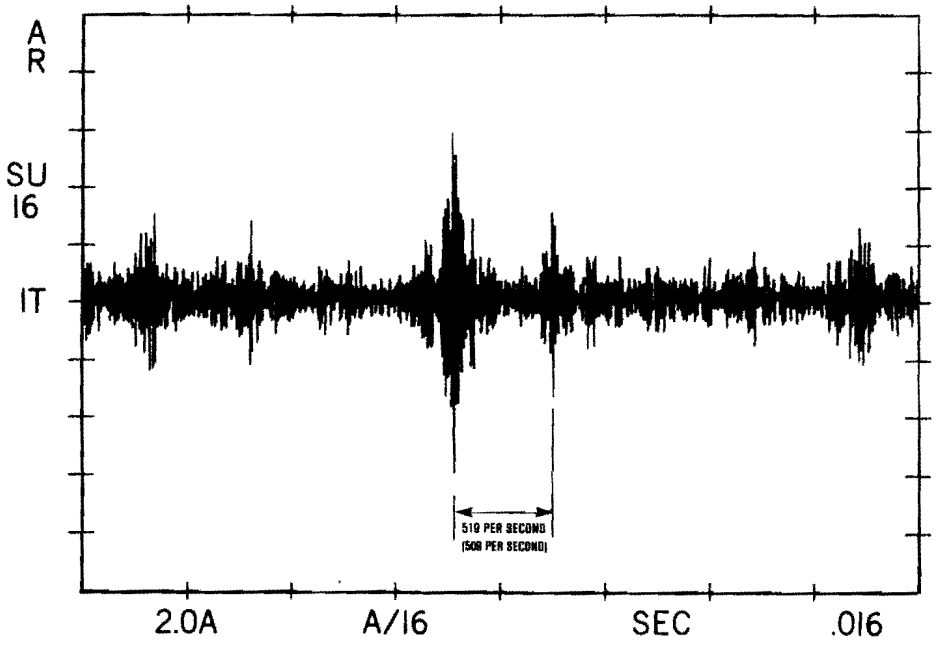

Figure 7. Band-Pass Filtered Signal of an Inner Race Duplex Ball Fault Implant

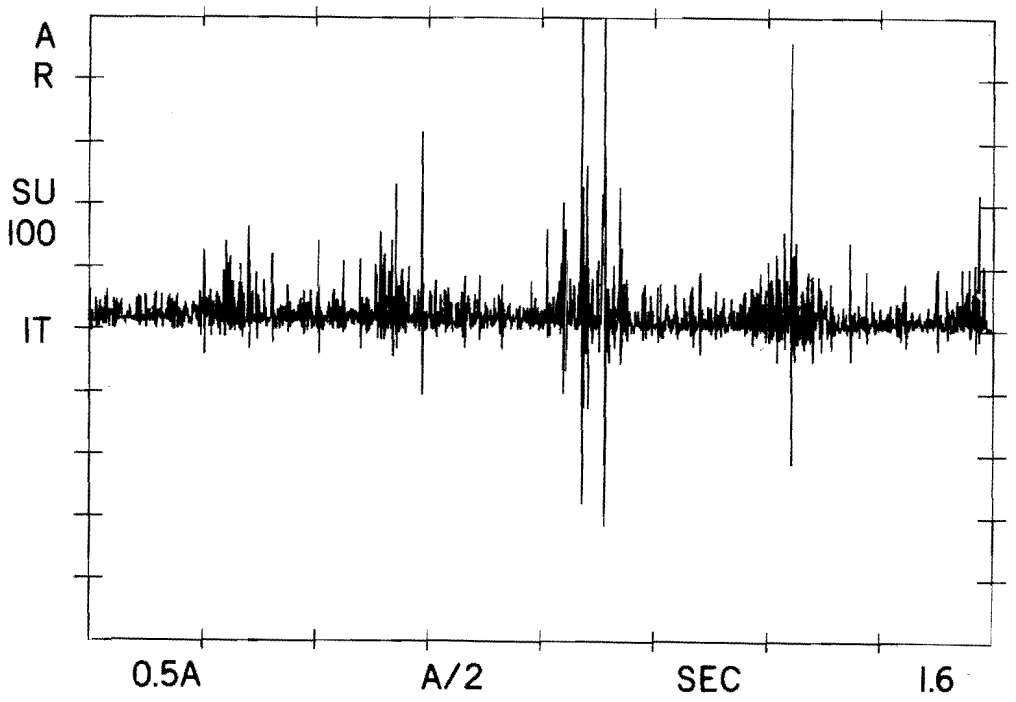

Figure 8. Band-Pass Filtered Signal of an Implanted Ball Fault

2.3.2 Details of Defect Response

Figures 9 and 10 show the details of bearing fault signal bursts for an implant outer and inner race fault, respectively. From Figure 9, several properties of the response are evident:

(1) The background noise is similar in nature to the signal itself, hence is defined as clutter rather than uncorrelated or random noise. This property has a strong effect on the type of signal processing required.

(2) In each figure there is a distinct change in phase of the "carrier" after an initial interval of 0.3 and 0.4 milliseconds respectively. The amount of phase delay is about 180 degrees in the first figure and 90 degrees in the second.

(3) There are rapid (cycle to cycle) variations in amplitude of the fault signal.

(4) The start of the signal is abrupt (allowing for the low-pass filter cutoff at 35 kHz).

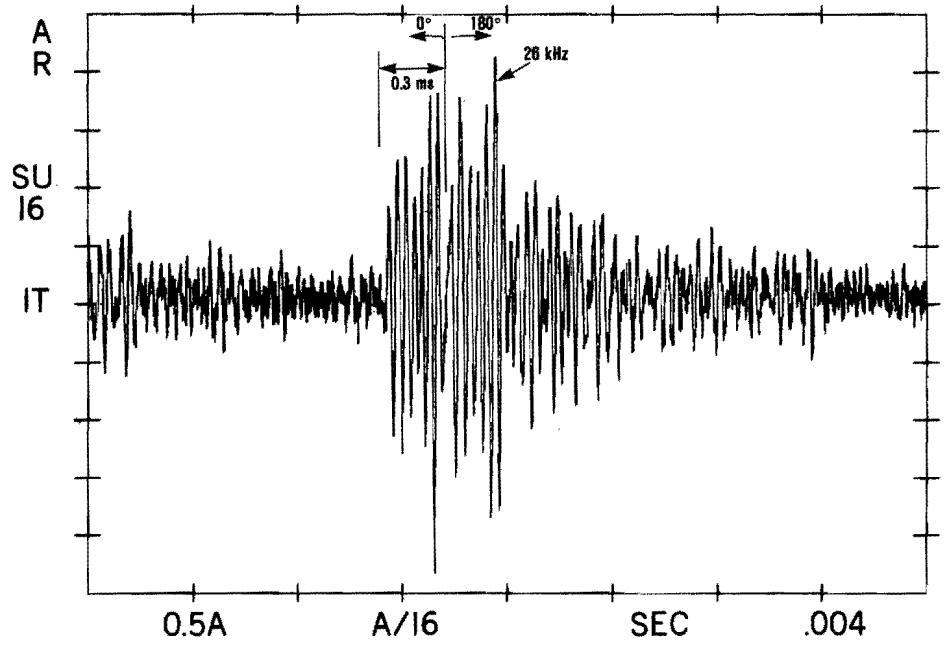

Figure 9. Details of Outer Race Fault Signal

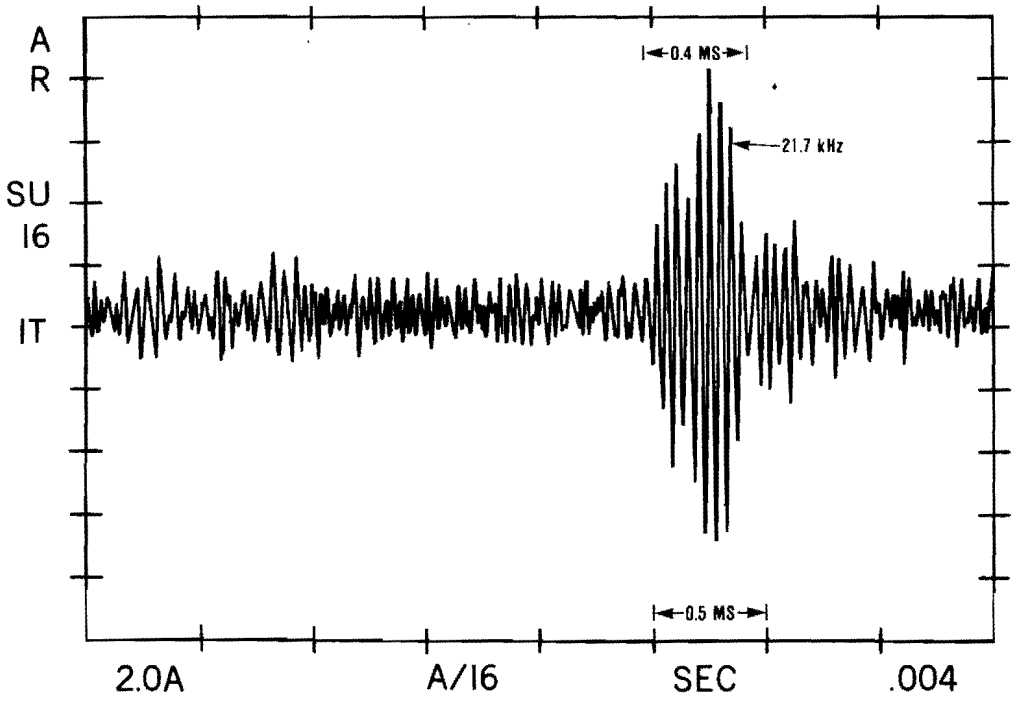

Figure 10. Details of Inner Race Fault Signal

(5) There is no external manifestation of a pulse, spike or sharp change in level at the start of the signal, unless at a level far below the signal and clutter. Therefore, the signal which must be exploited for the detection of bearing faults is the ringing signal shown in Figures 9 and 10.

The phase change of (2) above can be correlated with the size of the fault along the direction of travel of the rolling element. Defining f_o as the rolling element defect frequency, i.e., the frequency at which a point on the ball would contact both of the races alternately, then the frequency of contact with one race is $f_o/2$. The sizes of the implanted faults (simulated spalls) were all proportioned to the diameter of the rolling element. If this ratio is k, the length of the fault on the race or rolling element is kd_b, and d_b is the ball diameter. In one period between contacts of the ball reference point and the race, a distance of d_b is traversed on the race as well as on the ball. The time of passage over the fault is then

$$T_f = \frac{2}{f_b} \times \frac{kd_b}{d_b}$$

Therefore,

$$T_f = \frac{2k}{f_b}$$

Values of k from 0.25 to 0.375 were used in generating the faults, and the resulting passage times of 0.32 ms and 0.47 ms agree well with the measured values of 0.3 to 0.4 ms. (The value of f_b for these cases is 503 Hz.)

Superficially, the pattern resembles the beating of two frequencies. However, this would require equal amplitude components having a frequency ratio of 13/14 (to produce 180-degree interference after seven cycles as in Figure 9). Figure 10 does not show a 180-degree phase change, and neither figure shows the sinusoidal envelope typical of beats. It is therefore concluded that the signal is initiated by the sudden passage of the rolling element into the spall area, which relieves the loads and deformations on the inner race, outer race and rolling element simultaneously, and that the second part of the response (after the phase change) results from the abrupt restressing of the bearing elements as the rolling element comes out of the spall area. Inspection of many traces has shown that the structure discussed above is uniformly present in fault responses.

The cycle to cycle amplitude variations of (3) above are consistent with the presence of more than one mode in the response and with a nonharmonic relationship between the mode frequencies. (Harmonics merely distort the basic waveform without producing cycle to cycle variations.) The shock response of bearing races possesses these properties. Table 2 shows the relationship of the modes and the specific resonance frequencies for the outer races of several bearings used in the tests. Inner race frequencies are not shown, as the inner race is often a tight fit on the shaft, which is

also steel, resulting in large changes from the free race resonance frequencies. The outer races, however, are pressed into a steel ring which is installed in a magnesium housing. The bulk mechanical impedance of magnesium is about one fifth that of steel, so the outer race is relatively free to oscillate in its own modes. The steel ring is included in the calculation of the mode frequencies.

TABLE 2. MODE RELATIONSHIPS AND OUTER RACE RESONANCE FREQUENCIES (kHz)

Mode Relationships:

n	2	3	4	5	6	7	8
k_n	2.683	7.589	14.552	23.534	34.520	47.518	62.514
k_n/k_{n-1}	-	2.8286	1.9175	1.6172	1.470	1.379	1.316
k_n/k_2	1.00	2.83	5.42	8.77	12.87	17.71	23.30

Resonance Frequencies (kHz):

n	2	3	4	5	6	7	8
Part Number							
AH-1S a/c							
212-040-143	3.1	8.8	16.8	27.2	39.8	54.8	72.1
212-040-466	3.3	9.3	17.8	28.8	42.3	58.2	76.6
212-040-456	3.1	8.8	17.0	27.5	40.4	55.6	73.1
UH-1H a/c							
204-040-143	3.1	8.8	16.8	27.2	39.8	54.8	72.1
204-040-310	2.7	7.8	14.9	24.1	35.3	48.6	64.0

For the rectangular cross section of a race, the resonance frequencies, f_n, are given by

$$f_n = k_n \times \frac{h}{a^2\ 12} C_L \qquad n = 2, 3, 4, \ldots .$$

n = mode number

h = thickness of race

a = average radius of race

C_L = velocity of sound in steel: 16,380 feet/second or 4.993×10^6 mm/second

$$k_n = \frac{n\ (n^2 - 1)}{\sqrt{n^2 + 1}}$$

Although the calculated frequencies may be no more accurate than roughly ±20 percent, the ratios are expected to be much more accurate. Modes 4 and 5, which lie in the operating region, have a frequency ratio of 1.6 to 1 which produces beats or partial cancellation every 1.3 cycles on the average.

The abrupt start of the response of (4) above is consistent with excitation by relief of rolling element induced (localized) stresses. Mode numbers up to one-half the number of balls (sixth to tenth modes) can be efficiently excited by the relief of the stress and deformations caused by a single ball.

Rough calculations indicate that the stress relaxation time is of the order of 10 microseconds, allowing efficient excitation of frequencies up to 25 kHz, and higher at reduced amplitudes.

2.4 NOISE AND CLUTTER ENVIRONMENT

This section describes the noise and clutter background signals which are present in the "live" helicopter test environment. Other sections of this report demonstrate that investigation led to an understanding of the bearing fault mechanism that resulted in improvements in the fault signal detection and discrimination process. Similarly, investigation and analysis were conducted to identify and understand the differences between the test cell and "live" helicopter test environments. Selected test specimen gearboxes and hanger assemblies with the same fault implant bearing were operated in both environments to obtain and characterize test signal differences. This section presents the characteristics of background signals that are not due to bearing faults. The following signal sources have been identified as contributors of background noise and clutter:

(1) Low frequency machinery noise
(2) High frequency machinery noise
(3) Shaft imbalances
(4) Gear noise

The first two noise sources are at different frequencies from the carrier of the bearing fault signature, and can therefore be eliminated by band-pass filtering. The second two sources of noise reside at the same frequency as the carrier of the bearing fault signature.

2.4.1 Low Frequency Noise

The major signal source to the accelerometer is machinery noise which has a frequency range from DC to less than 7 kHz. Table 2 shows that the fundamental mode carrier of the bearing fault signature falls in this region. However, the magnitude of machinery noise interference is too great to allow fault detection at the fundamental frequency. Previous work, described in Section 3, indicated that the 0-7 kHz band is ineffective for locating Class C/D bearing faults, and should be strongly reduced.

The frequency response of a resonant accelerometer, excited by helicopter machinery noise and with a resonance frequency of 40 kHz, is shown in Figure 11. Figure 12 shows the frequency response of a nonresonant accelerometer with an integral single-pole 5 kHz high-pass filter. As can be seen by comparing these two figures, the resonant accelerometer is not very effective in eliminating machinery noise, or for that matter enhancing the region around the resonance. To eliminate machinery noise, electronic filtering must be performed. Comparing these figures also shows that the signal rejection in the 5-15 kHz band should be on the order of 40 dB. This amount of rejection requires using a complex filter design and cannot be achieved by using the accelerometer as a mechnical filter.

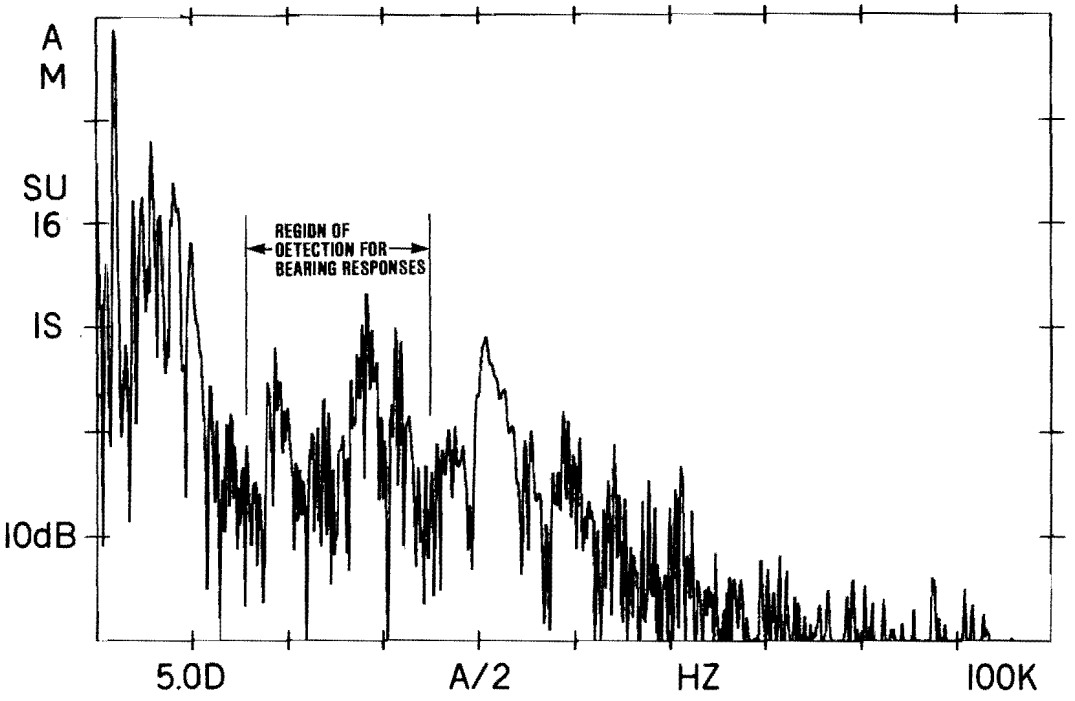

Figure 11. Frequency Response of a Resonance Accelerometer

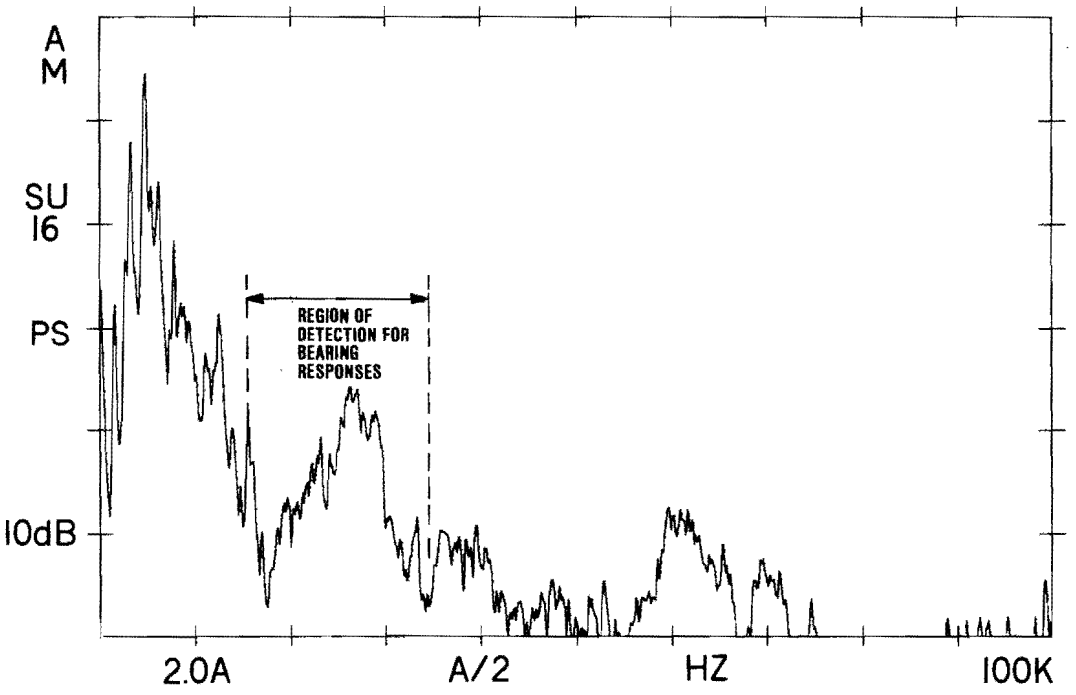

Figure 12. Wide-Band Accelerometer Response

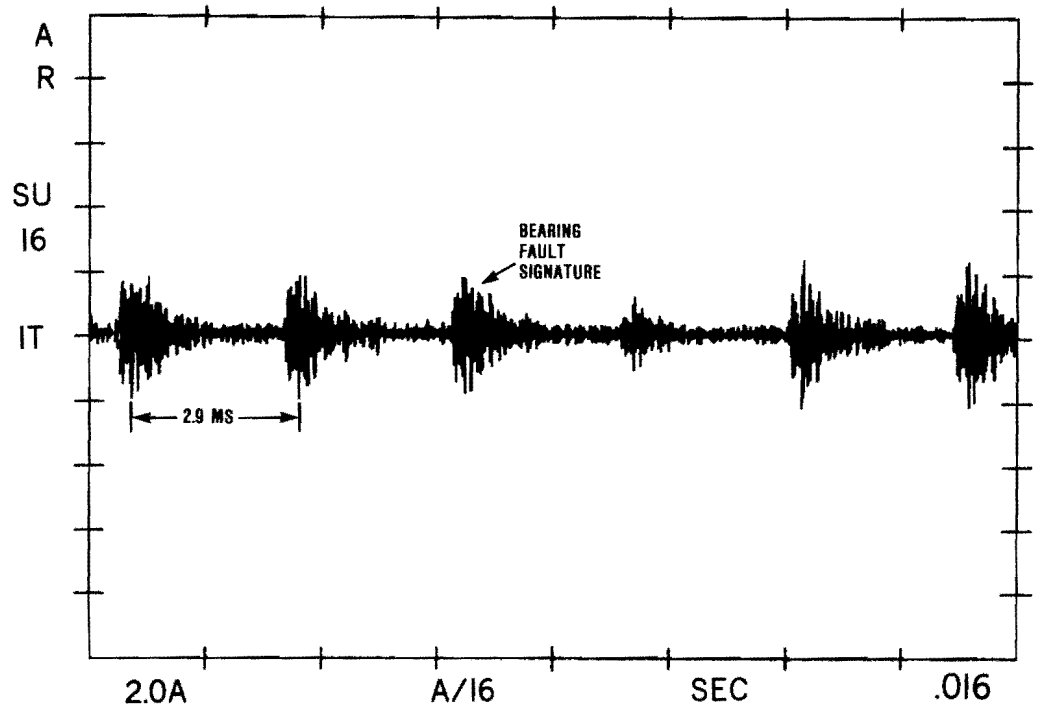

Figure 13. Band-Pass Filtered Signal

Figures 2 and 13 demonstrate the effect of filtering to remove low frequency noise from the signal. Figure 2 shows the raw accelerometer signal and Figure 13 shows the same waveform (at the same signal level) after band-pass filtering between 15-35 kHz.

2.4.2 High Frequency Noise

Figure 14 is a power spectrum of an accelerometer signal obtained from a 42-degree gearbox of a Huey helicopter that shows considerable power in the region of 35-80 kHz. The source of this high frequency noise was not conclusively determined, but was isolated sufficiently to determine that the noise was not the result of bearing faults. Since the final diagnostic process is digital based, this source of noise should be strongly attenuated by electronic filtering to prevent aliasing or excessive bandwidth requirements in the digital process.

2.4.3 Tail Rotor Forces (Shaft Imbalances)

Machinery imbalances can appear to manifest the same effects as bearing fault signatures. Figure 15 shows a 5-kHz high-pass filtered waveform obtained from the 90-degree gearbox of a Cobra which had prior history of tail alignment problems. The waveform consisted of a group of ten pulses per output shaft rotation where two of the pulses are much longer than most. The

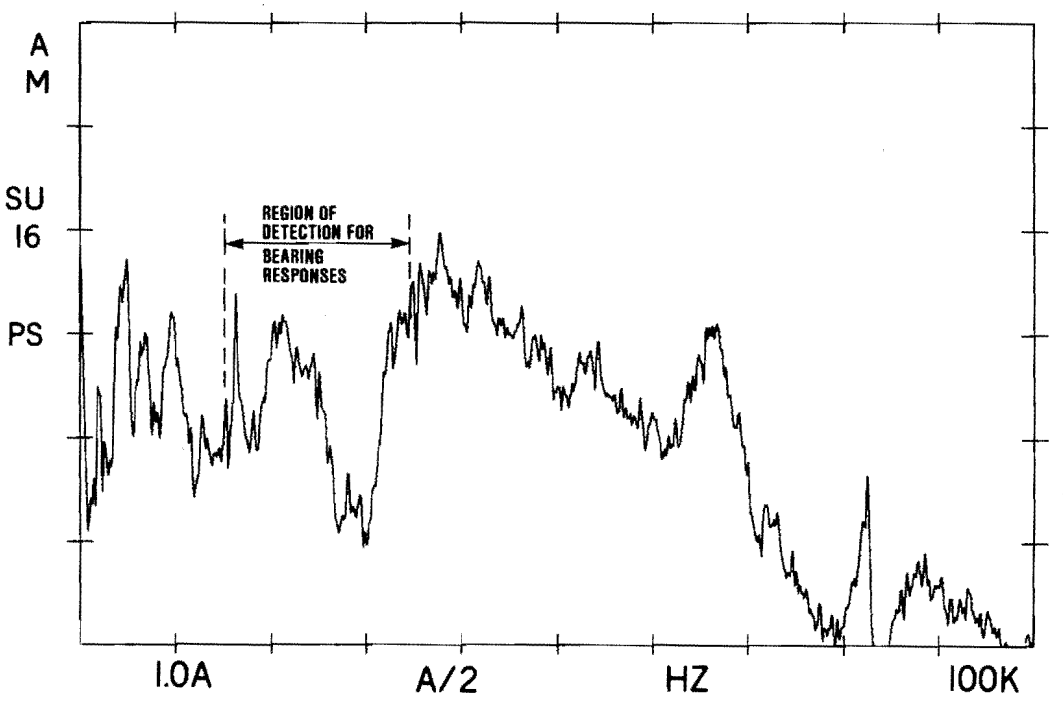

Figure 14. Spectra Showing High Frequency Effects

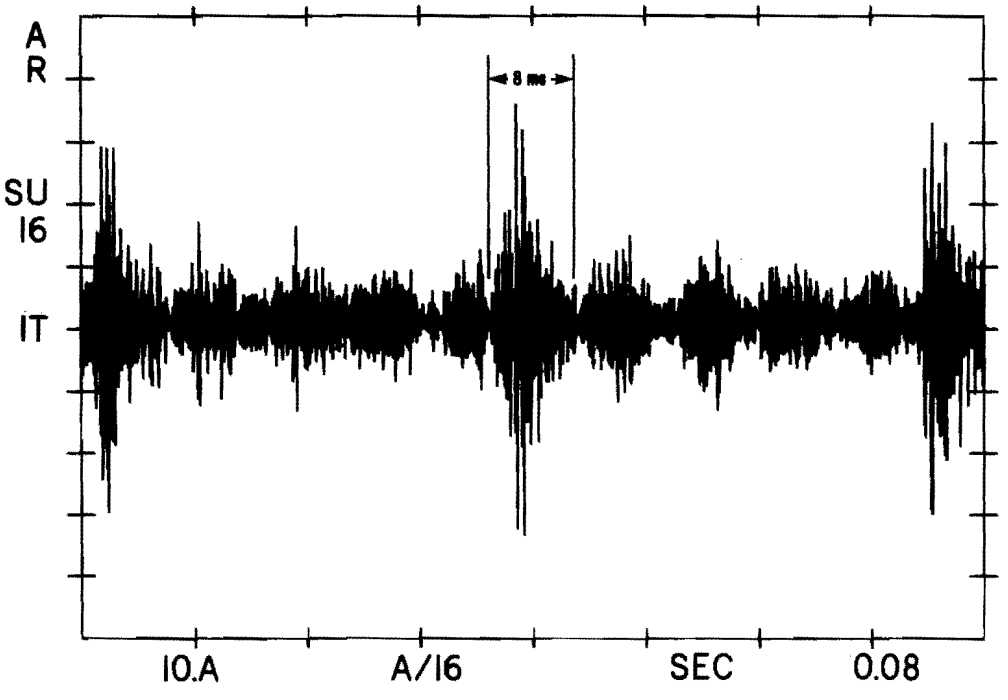

Figure 15. Machinery Imbalance Clutter Waveform (5 kHz High-Pass Filtered)

suspected cause of the two large pulses was tail rotor imbalance. Although the primary mode of the vibration was around 5 kHz, the demodulated waveform shown in Figure 16 reveals that significant energy exists in modes between 15-35 kHz. However, the demodulated pulses shown in Figure 16 had widths greater than 5 msec, which is an order of magnitude greater than bearing fault signatures. The greater pulse length enabled the digital processing described in Sections 5.3 and 7.3 to effectively attenuate these waveforms.

2.4.4 Gear-Mesh Noise

While bearing elements produce a signal when subjected to the unloading and loading effect of a defect, the meshing between the gears produces a similar type of signal as a normal mode of operation. The ringing pulse produced is due to loading when two gears contact followed by an unloading when the two gears separate. Shown in Figure 17 is a 27 kHz narrow band filtered signal which is believed to be caused by gear meshing. Figure 18 shows the spectrum of the demodulated signal.

The significant characteristic of the gear-mesh signatures is the short pulse duration, which is on the order of 150-250 μsec. Due to the difference in the pulse lengths between gear-mesh signatures and bearing signatures, the

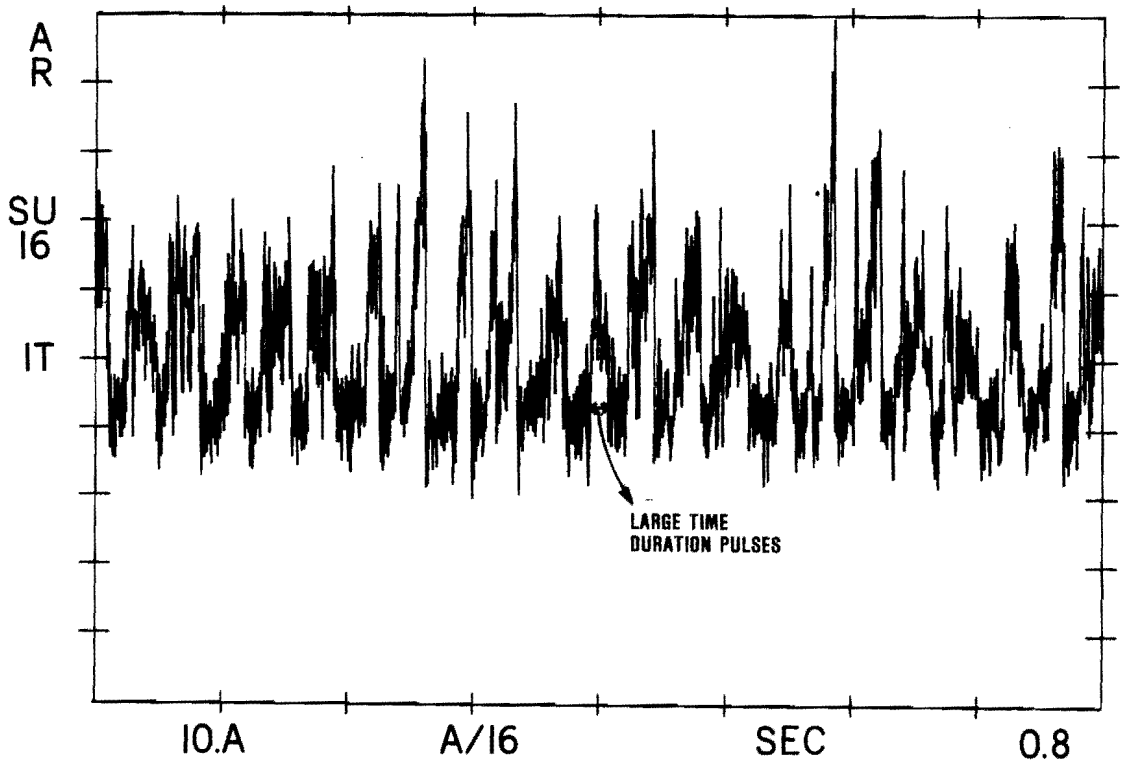

Figure 16. Machinery Imbalance Clutter After Band-Pass Filtering and Demodulation (15-35 kHz Band-Pass)

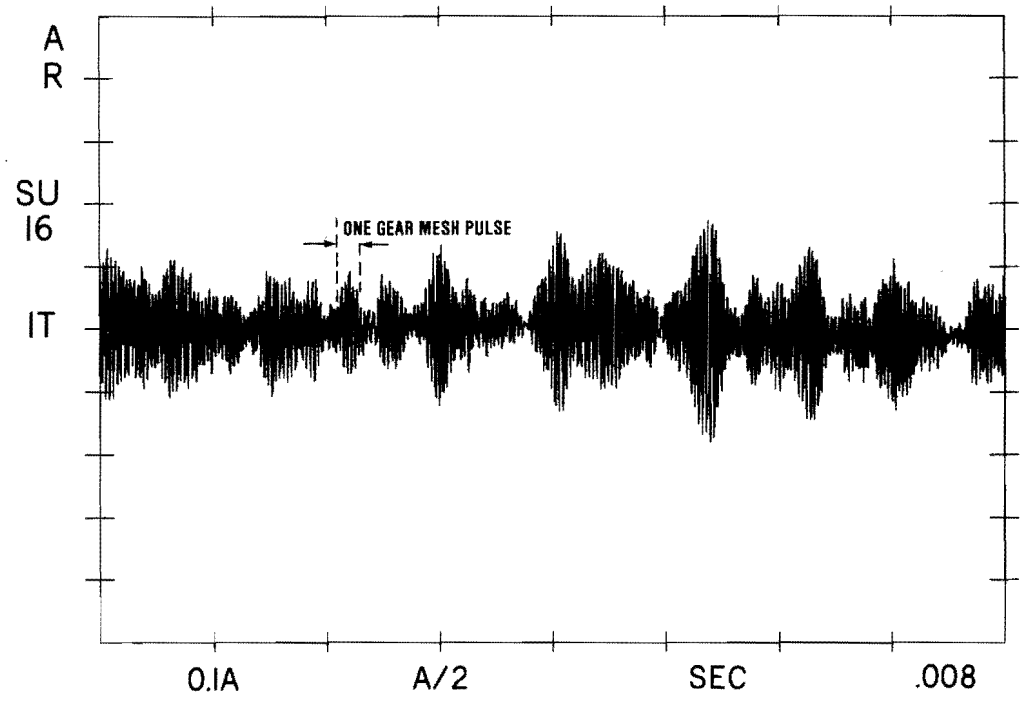

Figure 17. Gear-Mesh Waveform

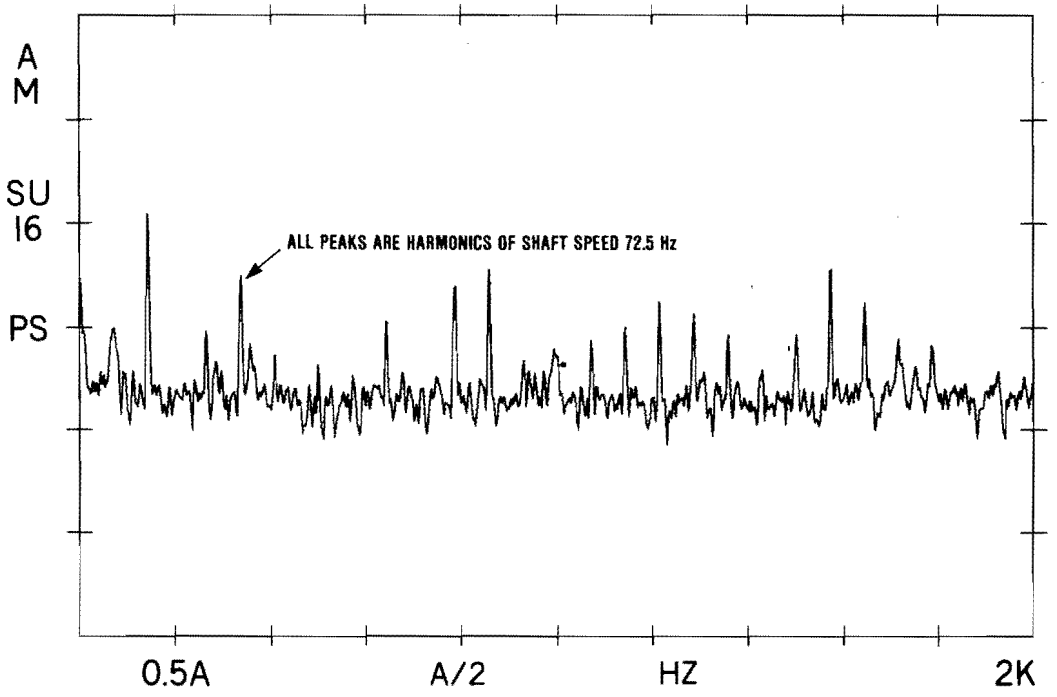

Figure 18. Resulting Spectra from Gear-Mesh Waveform

two pulses can be discriminated on the basis of pulse length. This was accomplished by the digital signal processing described in Sections 4 and 5. The carrier frequency of the gear-mesh pulses appeared to be the same as for corresponding bearing fault signature carriers, suggesting that the manifestation of the gear-mesh waveform was also from the ringing of the outer race. The differences in the waveforms between bearing fault signatures and gear tooth meshing suggest that different signal processing would be effective for gear fault detection.

2.5 PERFORMANCE REQUIREMENTS

The top level performance requirement for the SPADE system set forth in the PIDS is twofold:

(1) A minimum of 90 percent of all helicopter component/part removals resulting from the SPADE system indications shall be valid failures or incipient failures.

(2) The SPADE system, when used in conjunction with the current maintenance and inspection procedures, shall not fail to detect unsafe for flight (Class D; see Table 3) bearing-related component defects more than once every 1000 flight hours (2000 desired). The SPADE system shall be used every 25 aircraft flight hours.

Requirement (1) above is equivalent to a false alarm rate of 10 percent or less. In addition, a goal of 90 percent failure detections has been adopted as a conservative criteria of meeting requirement (2) above, to ensure that SPADE will perform valid fault detection in the field, and that it will be so perceived by the user.

Verifying statistical performance requirements such as those above can demand a massive data collection program, particularly if changes in the data measuring devices (accelerometer, preamplifier, mount, connector, and cable) become necessary. A much more economical approach lies in using statistical analysis to trade off fault signal-to-noise ratio for sample size, i.e., number of aircraft tested. Table 4 shows the signal-to-noise ratios for 90 percent confidence of meeting the 90 percent probability of detection and 10 percent false alarm rate for tests on 2 to 20 aircraft. Detailed explanation of the sampling process is given below, and Section 6.2 discusses the process of setting limits to obtain the required performance.

It is an unfortunate property of samples that the calculated mean and variance of the sample yields only a very low confidence (defined essentially as the probability of being correct). For a given sample size, confidence can only be obtained by increasing the variance as shown in Figure 19. Part C of Figure 19 shows a typical set of baseline and fault measurements at the SPADE signal processor output, i.e., through all filtering, Fast Fourier Transform (FFT), spectral windowing and any other signal processing, for a particular bearing. If this same measurement is made on at least one other aircraft, the data can be combined and the sample distribution can be

TABLE 3. DEFINITION OF BEARING FAULTS
(DEGRADED PART CLASSIFICATION)

BALL BEARING DEFECT CATEGORY	
CATEGORY A	NO DEFECT.
CATEGORY B	INITIAL SPALLING: ONE OR MORE VOIDS OR IRREGULARITIES IN THE BALL PATH OR ON THE BALL ITSELF NOT EXCEEDING AN AREA DESCRIBED BY 0.05 X BALL DIAMETER WIDE OR 0.20 X BALL DIAMETER LONG.
CATEGORY C	MODERATE SPALLING: ONE OR MORE VOIDS OR IRREGULARITIES IN THE BALL PATH OR ON THE BALL ITSELF BETWEEN THE UPPER LIMIT OF CATEGORY B AND NOT EXCEEDING AN AREA DESCRIBED BY 0.30 X BALL DIAMETER WIDE BY 0.40 X BALL DIAMETER LONG.
CATEGORY D	ADVANCED SPALLING. BEARING STILL OPERATIONAL, BUT WITH ONE OR MORE VOIDS OR IRREGULARITIES IN THE BALL PATH OR ON THE BALL ITSELF GREATER THAN THE UPPER LIMIT OF CATEGORY C.
CATEGORY E	FUNCTIONAL FAILURE: BEARING JAMMED OR CONTAINS A BROKEN COMPONENT.
ROLLER BEARING DEFECT CATEGORY	
CATEGORY A	NO DEFECT.
CATEGORY B	INITIAL SPALLING ONE OR MORE VOIDS OR IRREGULARITIES IN THE ROLLER PATH OR ON THE ROLLER ITSELF NOT EXCEEDING AN AREA DESCRIBED BY 0.15 ROLLER DIAMETER CIRCUMFERENTIALLY OR 0.30 X ROLLER LENGTH AXIALLY.
CATEGORY C	MODERATE SPALLING: ONE OR MORE VOIDS OR IRREGULARITIES IN THE ROLLER PATH OR ON THE ROLLER ITSELF BETWEEN THE UPPER LIMIT OF CATEGORY B AND NOT EXCEEDING AN AREA DESCRIBED BY 0.30 X ROLLER DIAMETER CIRCUMFERENTIALLY ACROSS THE TOTAL WIDTH OF THE ROLLER OR ROLLER PATH.
CATEGORY D	ADVANCED SPALLING: ONE OR MORE VOIDS OR IRREGULARITIES IN THE ROLLER PATH OR ON THE ROLLER ITSELF GREATER THAN THE UPPER LIMIT OF CATEGORY C.
CATEGORY E	FUNCTIONAL FAILURE BEARING JAMMED OR CONTAINS A BROKEN COMPONENT.

calculated and plotted as in part A of Figure 19. Here again the signal is the difference of the mean values of the two distributions and the signal-to-noise ratio is obtained by dividing by the one sigma value of the noise alone (the usual peak-to-peak signal divided by rms noise). This distribution is an estimate of the distribution of the parent population, i.e., all similar bearings in all of the same aircraft model designation. However, the probability that the distribution of the parent population is really this good is quite small. If, as shown in part B of Figure 19, we increase the standard deviation of the sample sufficiently to obtain 90 percent confidence that the parent population distribution is correctly represented (i.e., is included within the expanded distribution), we can set a threshold at the 10 percent false alarm rate point and then, for that threshold, determine the probability of detection (P_{DET}) from the signal plus noise curve of part B. Details of the probability distributions and the calculation of probability of detection (P_{DET}) and probability of false alarm (P_{FA}) are shown in Appendix H, which also shows that a signal-to-noise ratio of 2.5 to 1 is required to obtain the required 10 percent P_{FA} and 90 percent P_{DET}. As discussed above, additional signal noise is required to generate reasonable confidence in field results.

TABLE 4. SIGNAL-TO-NOISE REQUIREMENTS FOR VARIOUS CONFIDENCE LEVELS AND SAMPLE SIZES

S_{s+n} Multipliers for Signal Plus Noise:

Sample Size	Confidence 80%	90%	95%
3	5.39	7.76	11.09
4	3.84	5.08	6.75
5	3.35	4.20	5.37
10	2.49	3.07	3.64
20	2.34	2.78	3.20

S_n Multipliers for Noise:

Sample Size	Confidence 80%	90%	95%
3	4.85	6.85	9.70
4	3.25	4.15	5.45
5	2.75	3.25	4.10
10	1.80	2.05	2.30
20	1.65	1.75	1.85

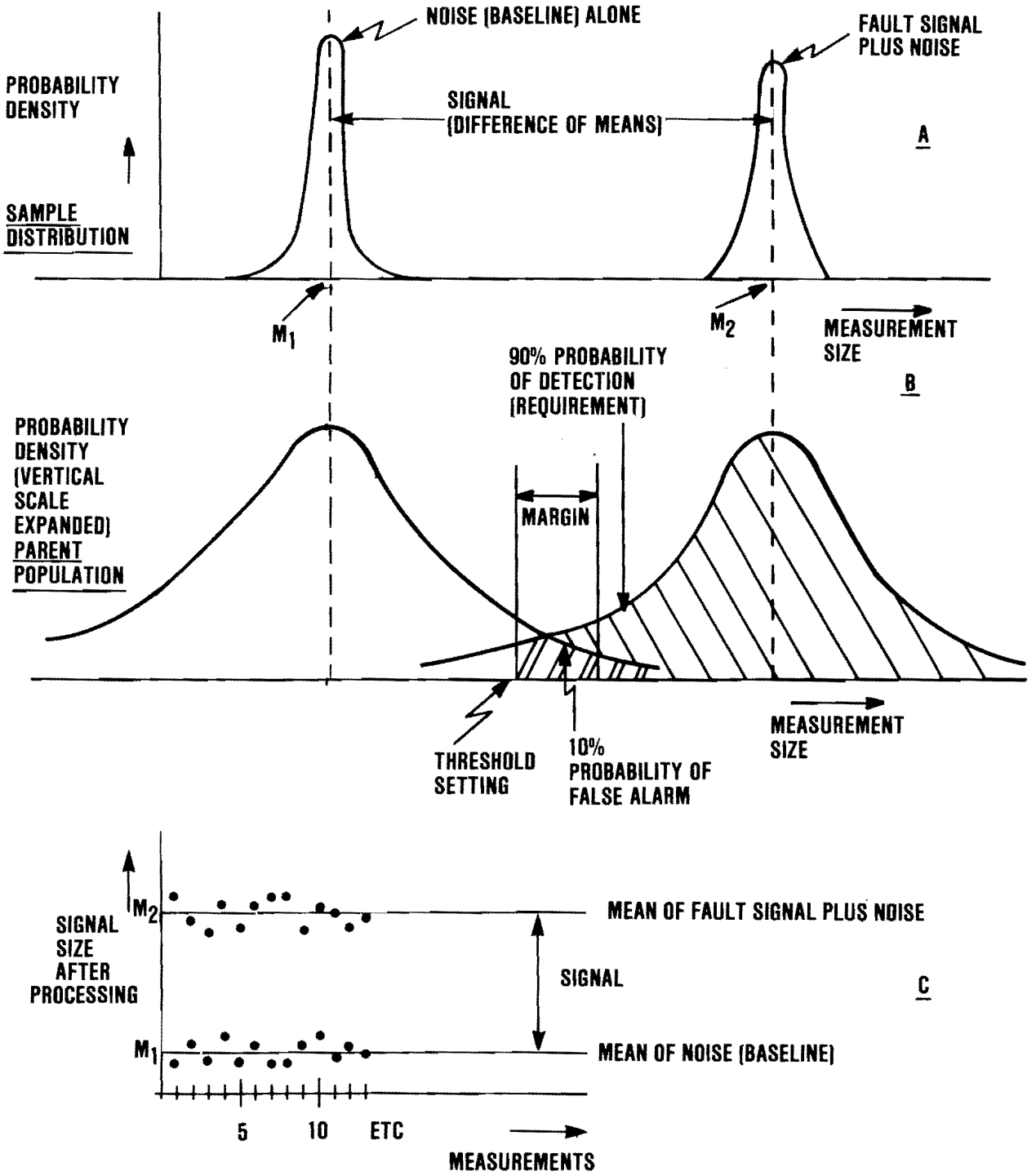

Figure 19. Growth of Variance for Confidence in Parent Population Distribution

SECTION 3
PRIOR RESEARCH AND TRANSITION FROM PRELIMINARY DESIGN REVIEW

Significant design enhancements were incorporated in SPADE after the Preliminary Design Review (PDR). These enhancements resulted from an improved understanding of bearing fault phenemona and led to the current design described in other sections of this report. This section summarizes the basis and rationale for these engineering design enhancements.

During the initial 3 months of contract effort the preliminary design of hardware and software was completed, two breadboard SPADE analyzers were completed and ready for software integration, test stand data acquisition on UH-1H gearbox assemblies was completed, and initial aircraft data acquisition at Fort Rucker, Alabama, was completed. Although computer simulation and analysis of data base fault implant recordings detected critical weakness in the Advance Development Shock Profile Area (SPA) algorithm, RCA had developed concepts to enhance the algorithm's performance. A PDR of the SPADE Engineering Development was conducted on 18/19 January 1983. The preliminary design presented at that time was approved and released for detail design implementation.

Subsequent to the PDR, RCA initiated real-time processing of data base recordings using breadboard hardware and software. Analysis of test data resulted in critical observations and discoveries concerning the technology of bearing vibrational analysis relevant to the SPADE program. The four topical areas which follow discuss these discoveries, their impact on the SPADE preliminary design, and the basis for the enhanced design effort that was accomplished.

3.1 SPADE CONCEPT LEGACY

The SPADE Engineering Development program derived its bearing fault detection concept from the encouraging prototype test results of the SPADE Advance Development contract (SKF Industries, Inc.). The final report of the Advance Development contract[1] summarized the concept as follows:

- "Discrepant parts such as pitted, spalled, brinneled or skidding bearing elements release abnormal amounts of frictional and/or kinetic energy."

- "High frequency vibrational analysis utilizes the transponder resonant output at frequencies several orders of magnitude above the dynamic event frequencies of the machinery."

---

[1]David B. Board, SMALL PORTABLE ANALYZER DIAGNOSTIC EQUIPMENT (SPADE), Advance Development Prototype Report, SKF Industries, Incorporated, AVRADCOM TR-80-F-3, September 1979.

Figure 20 shows the concept of a shock pulse, with a fast rise time pulse of very narrow width incident upon a resonant sensor. Figure 21 shows the frequency response of that resonant sensor (this diagram taken from Reference 1). It shows that the sensor is resonant at 40 kHz (with a

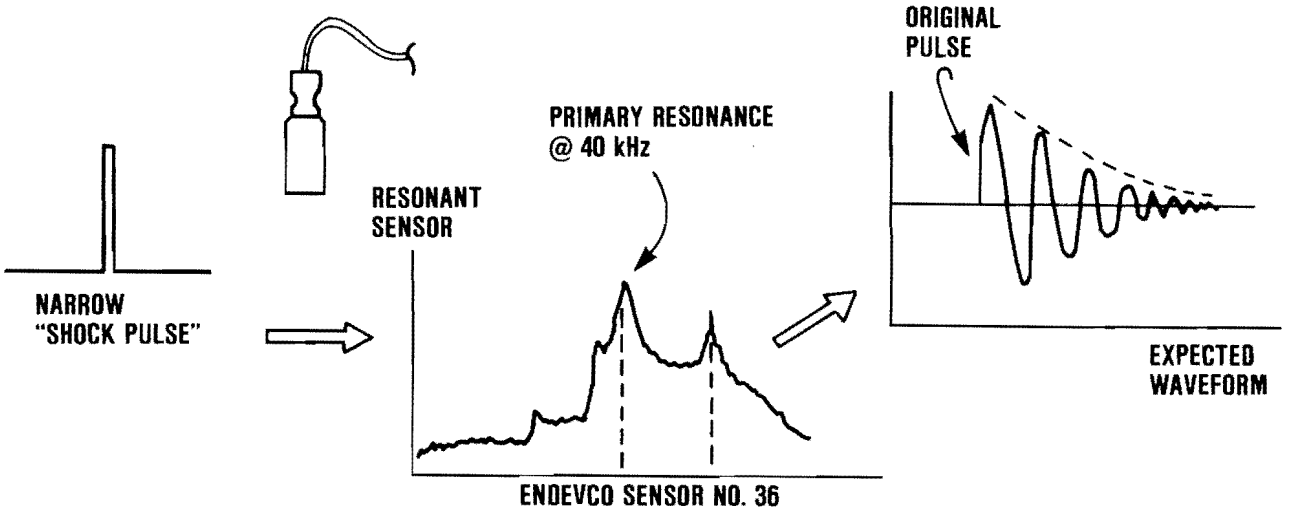

Figure 20. Shock Pulse Waveform

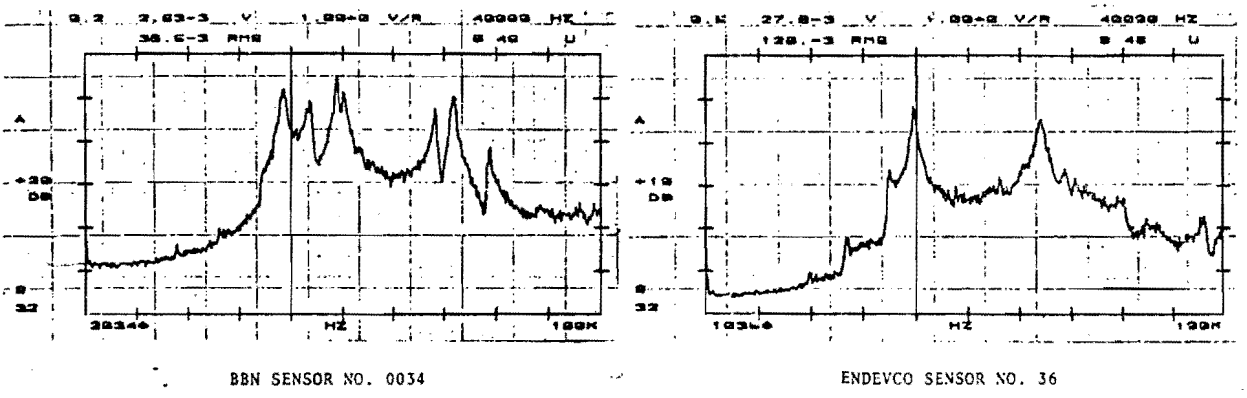

Figure 21. Resonant Sensor Frequency Response

secondary resonance somewhere around 60 kHz). The expected waveform resulting from the shock pulse exciting the sensor is shown in Figure 20. This waveform is a ringing response at the frequency of the resonant sensor, dying out after the shock pulse excites it to its initial (and maximum) peak value. A block diagram (Figure 22) of the Advance Development SPADE hardware is shown as it was used with the resonant sensor approach. The hardware processing consisted of amplification, a resonant tank circuit tuned to the resonance of the sensor, and a detector. A pictorial diagram in Figure 22 shows the sequence of spikes which would be the expected waveform resulting from detecting a sequence of the ringing waveforms generated from the narrow shock pulse incident upon the resonant sensor and the tuned resonance in the SPADE hardware. The SPA, also shown in the diagram, was developed from hardware pulse processing. The SPA diagram was accompanied by a quotation taken from Reference 1: "a curve of shock pulse rate as a function of shock pulse amplitude". This is the key concept inherited from the SPADE Advance Development Effort, which indicates that a high frequency shock pulse rings a resonant sensor. The SPADE Advance Development Prototype system was also shown in diagram form as having a red, a yellow and a green indicator light indicative of the condition of the bearings being either bad, marginal or in a pass condition.

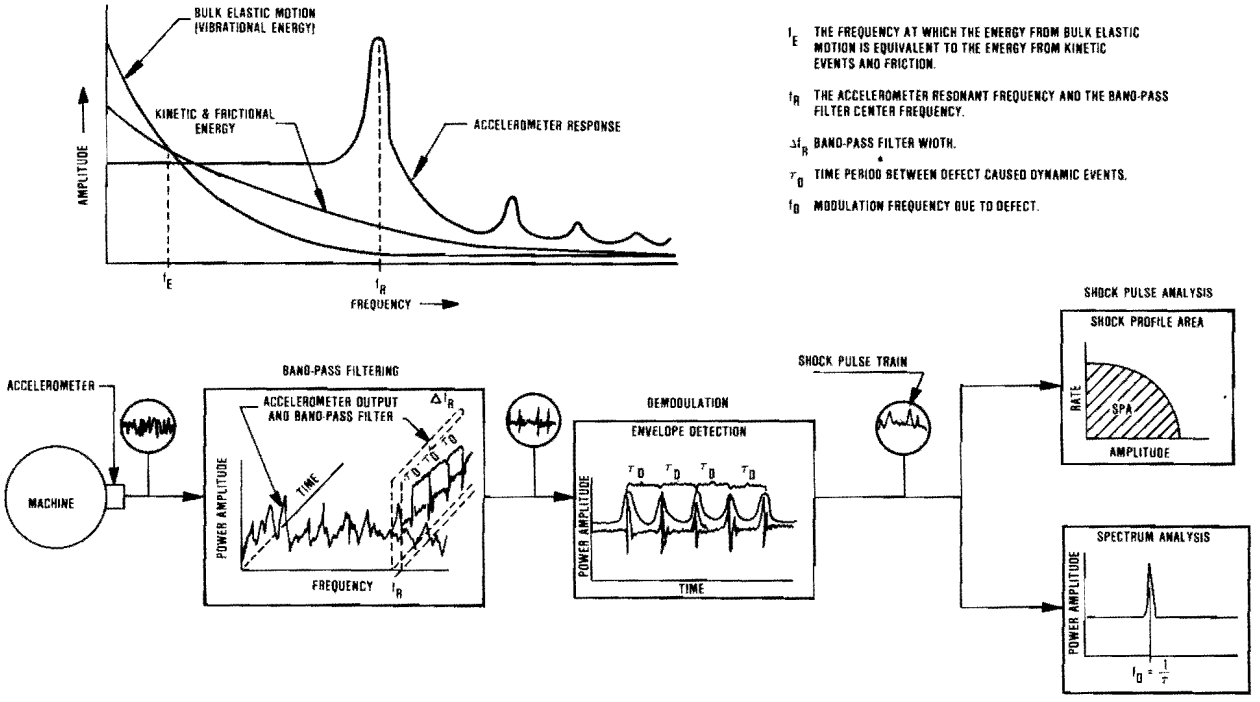

Figure 22. Advance Development Model SPADE System Block Diagram

3.2 RCA SPADE CONCEPT

The RCA SPADE concept (proposal to PDR timeframe) was based on a narrow shock pulse waveform (similar to Figure 20) incident upon a wide-band sensor. A supporting diagram detailed the frequency response of this wide-band sensor. The RCA system has a sensor (accelerometer) which is essentially flat up to and beyond 60 kHz, with the exception of a built-in roll-off frequency below 5 kHz (intended to prevent sensor saturation due to low frequency machinery noises). The RCA design featured an electronic filter, tunable over the frequency range of 20-35 kHz. The incident shock pulse was to be detected and amplified by the wide-band sensor, and transmitted to the electronic tunable filter, to generate the same damped ringing waveform as in the case of the Advance Development version of the SPADE system. The RCA wide-band sensor and electronic tunable filter were functionally the electronic analog of a mechanically resonant sensor. Figure 23 details the SPADE system as presented by RCA at the time of the proposal and the PDR.

3.2.1 Fault Signature Waveform Investigation

Availability of breadboard hardware and software following the PDR enabled RCA to conduct real-time data processing and investigation of the fault signature waveforms. RCA found evidence that the signals in the fault signature are not the result of shock pulses which excite the resonant

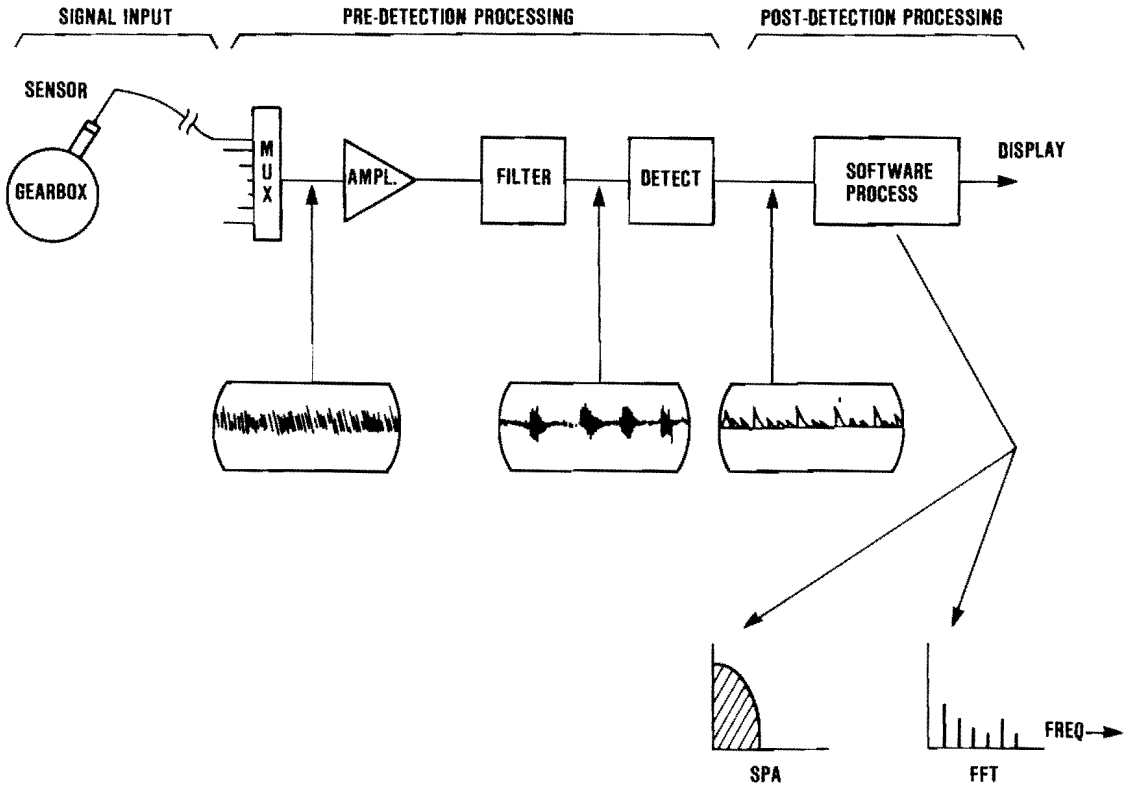

Figure 23. RCA Proposed SPADE Block Diagram

circuit. A digital storage oscilloscope recording (Figure 24) details an actual waveform of a faulty bearing vibrational signature. The data was recorded during fault implant tests conducted for RCA by BHTI (Bell Helicopter Textron, Incorporated) at their test facility in Fort Worth, Texas. There are three factors which support the conclusion that this is not the waveform created and caused by a shock pulse:

(1) The rise time of this pulse is not instantaneous on the first ringing waveform; it takes three or four more cycles of ringing before the signal reaches its maximum amplitude.

(2) The frequency of ringing is not the frequency of a resonant accelerometer or resonant filter. The interpretation is that the waveform is caused by the ringing of bearing structures, specifically the outer race of the bearing which had the fault implanted.

(3) A phase cancellation is found in the middle of the ringing waveform. Such cancellation is seen on many of the waveforms that were recorded and analyzed by RCA in the fault implant program. The rationale for this phase cancellation is as follows: the waveform is a composite of two damped ringing signals, the first one caused when the ball or roller enters the fault zone in the bearing, and the second one (superimposed upon the first) caused when the ball or roller exits from that fault area. On entering the fault area there

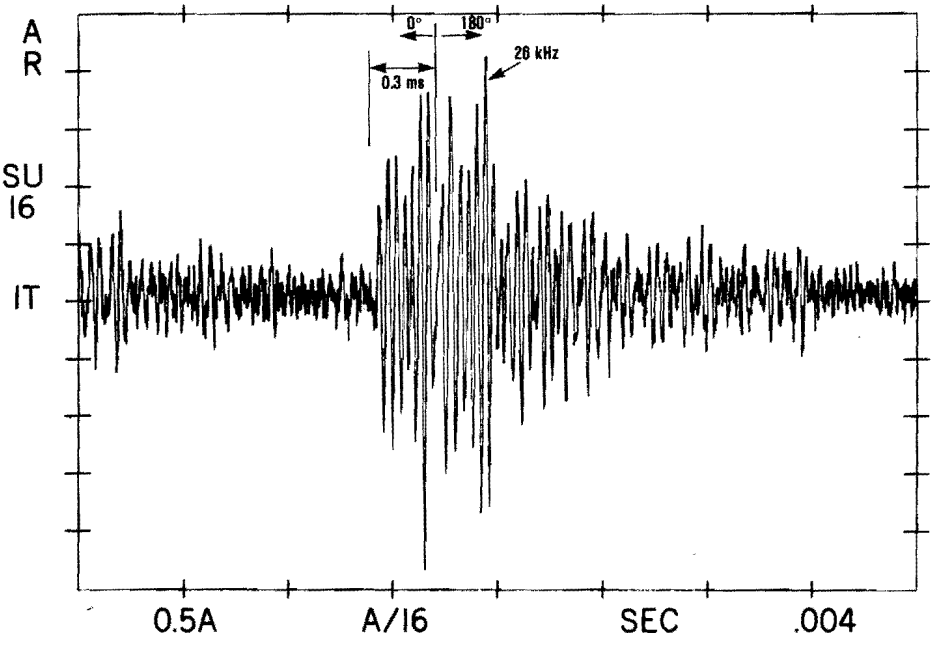

Figure 24. Fault Signature Waveform

is a sudden release of stresses which produces vibrational energy. Upon exiting the fault there is again a change in the stress in the bearing housing (caused by sudden compression of the rolling element) that results in a second ringing. When the second ringing is out of phase with the first, it will cause a phase cancellation in the midst of the waveform. This discovery of the nature of the ringing waveform (plus other yet to be discussed concerns and discoveries) led RCA to the conclusion that both hardware and software for the SPADE would require modifications to satisfy the requirement of the PIDS.

3.2.2 Shock Pulse Detection

The RCA design concept review at this time addressed the question: "Is the RCA concept to use a wideband sensor instead of a resonant sensor the cause of the missing shock pulse, or was it always missing?" Waveforms are presented which were taken from an ATL tape recording, dated August 1976, of the vibrational signal from a fault implanted gearbox. There is also a photograph of the fault implant, an inner race fault extending across the area of roller contact, identified as fault implant BHC-024 (Figure 25). There are three waveforms shown (Figures 26 through 28). First, the wide-band time domain waveform (Figure 26), shows that the signal consists predominantly of low frequency machinery noise. An unfiltered frequency domain spectrum of the waveform is shown in Figure 27. The third and most important waveform (Figure 28) is the output of a digital oscilloscope of the same signal having been passed through a high-pass filter (at 15 kHz with 24 dB per octave response). This waveform exhibits the same characteristics as previously discussed, which evidences that it is not the result of a shock pulse exciting a resonant mechanical filter. The waveform in Figure 28 has three characteristics which support this conclusion. First, the wave front takes several cycles to reach its full height. Secondly, the frequency of the ringing waveform is approximately 25.5 kHz while the sensor is resonant at a much higher frequency of 100 kHz (an M-8 type resonant sensor). And the third factor is a phase cancellation which is clearly seen in the waveform.

For the purpose of supporting later arguments, this same waveform was passed through a narrow-band filter. The resulting time domain waveform (Figure 29) shows that the fault signature is still present after passing through the narrow-band filter, but it is degraded and has lost much of the prominent signature of the fault conditions. The conclusion to be drawn from this is that using a resonant narrow-band filter in the system degrades the ability of the SPADE system to see and detect fault conditions. Two conclusions are therefore reached: (1) Frequency response (resonance) of sensor and/or tuned filters is not critical. (2) Wideband signal processing to preserve the complex waveform (up to pulse detection) is important to maximize the detected fault signal.

This discussion presented the underlying concept upon which the prior AVRADCOM Advance Development SPADE technology had been based (and which RCA had adopted in its proposal stage and in its development of hardware and

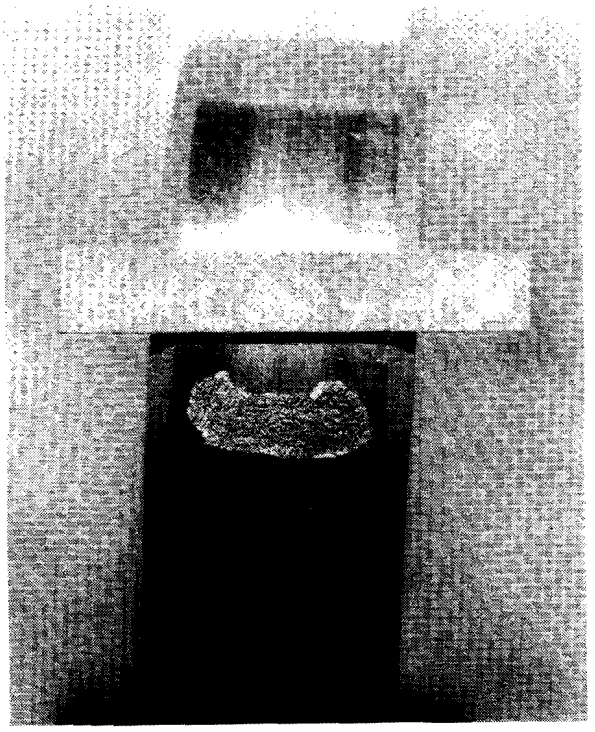

Figure 25. Fault Implant, Inner Race of Roller Bearing ATL Implant BHC-024

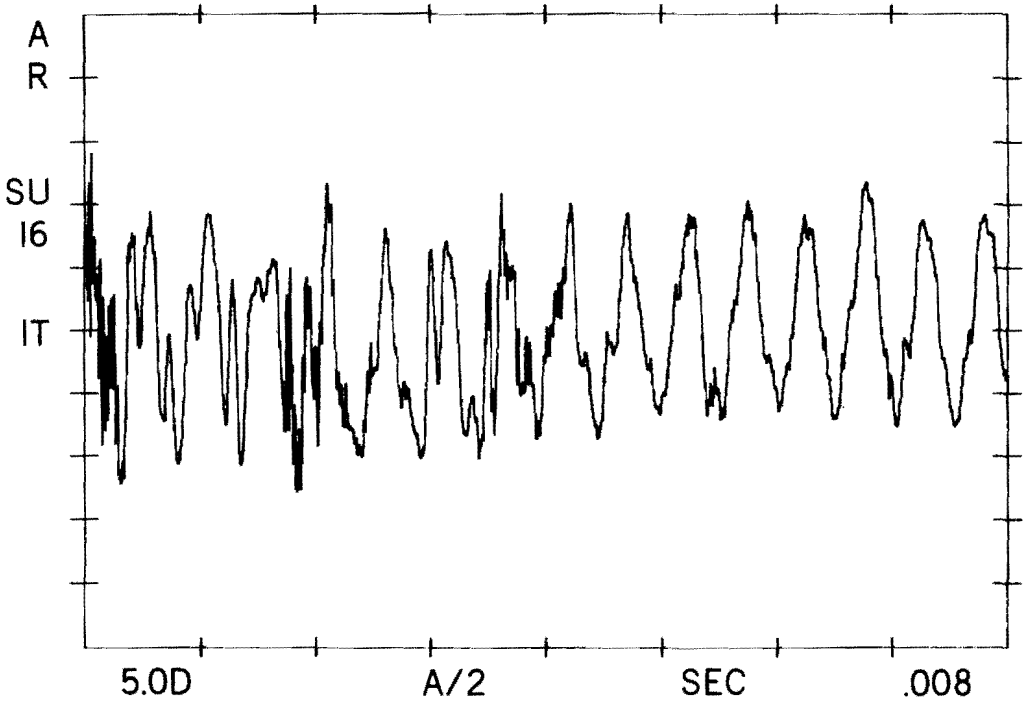

Figure 26. Waveform of Fault Implant BHC-024 Unfiltered Time Domain Signal

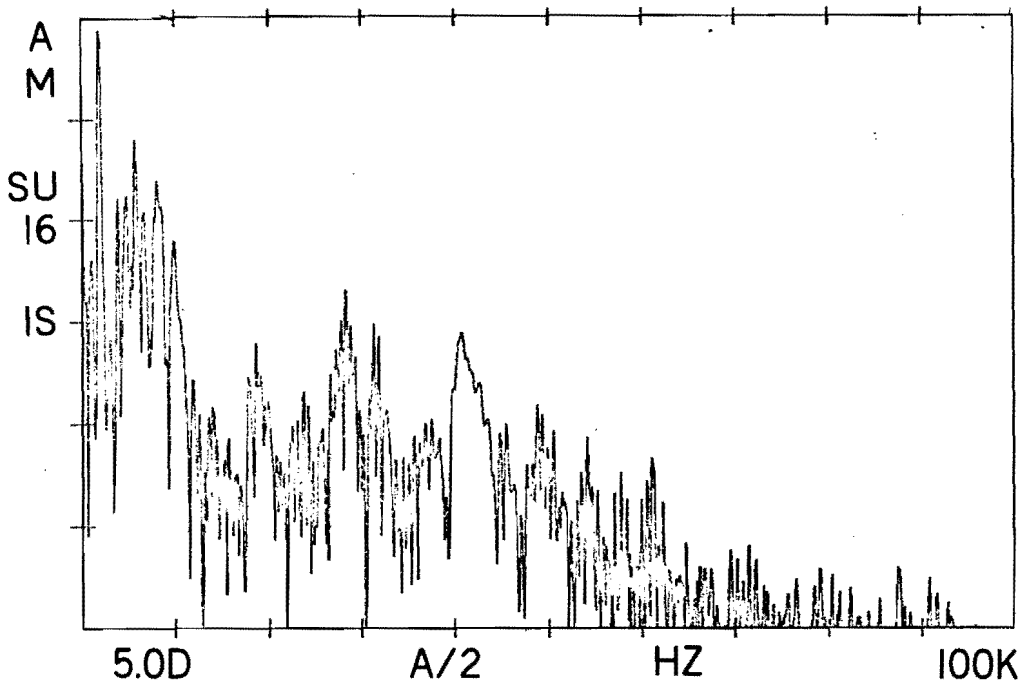

Figure 27. Waveform of Fault Implant BHC-024 Unfiltered Frequency Domain Spectrum

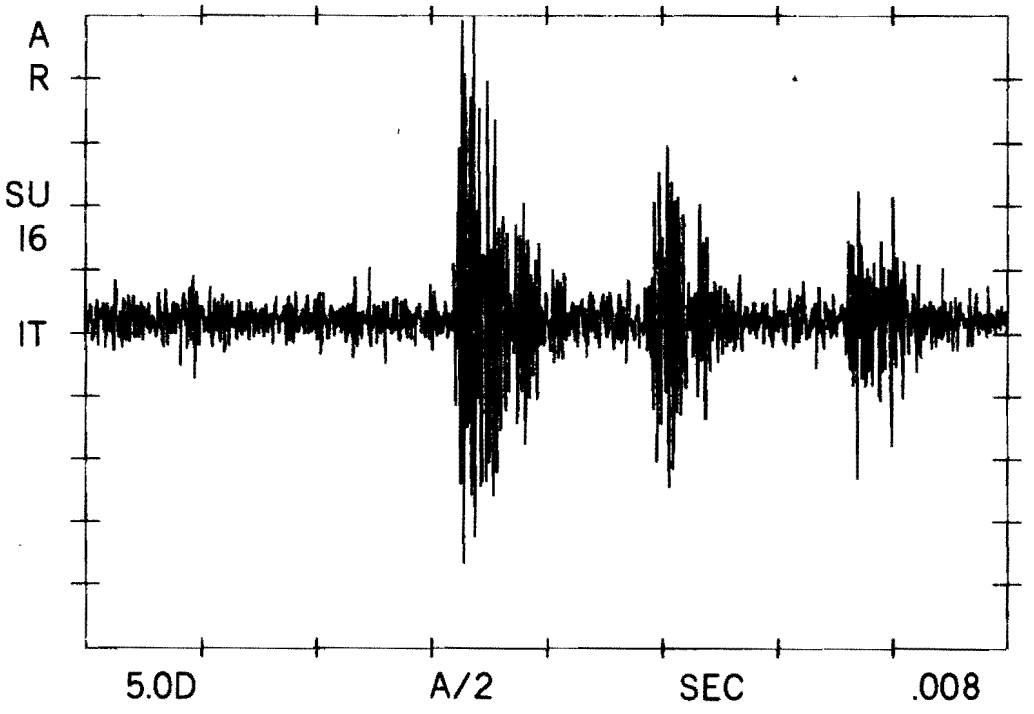

Figure 28. Waveform of Fault Implant BHC-024 Filtered Time Domain

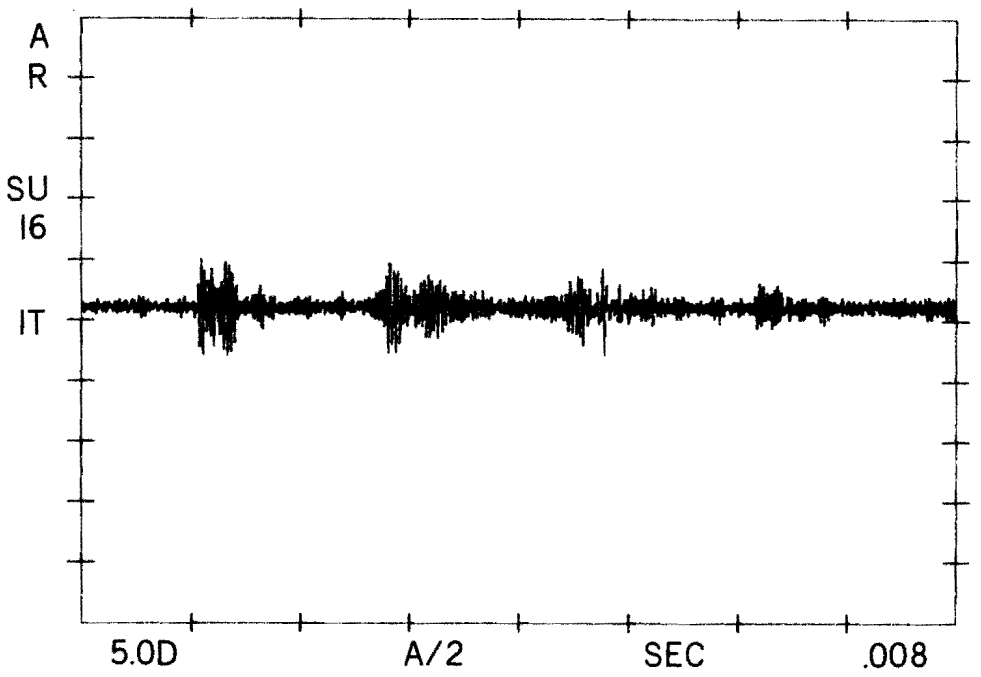

Figure 29. Waveform of Fault Signature Narrow Filtered Showing Signal Degradation

software concepts up to the time of the PDR), and also the technical discoveries made by RCA subsequent to the PDR which led to hardware and software redesign activity for SPADE.

3.3 ASSESSMENT OF SPADE PDR DESIGN PERFORMANCE

The following discussion assesses the performance capabilities of the SPADE design at the time of the PDR. The two plots shown in Figures 30 and 31 reflect the SPA performance analysis presented at the PDR.

As a matter of background, this SPA analysis was performed with data taken from the Bell Helicopter test cells on magnetic tape recordings, and RCA-conducted tests of a number of aircraft monitored and recorded on magnetic tape at Fort Rucker. Specific data presented in these two diagrams is relative to the output shaft monitoring of the 90-degree gearbox on the UH-1 helicopter. It was obtained by processing digitized waveforms through a software simulation implemented on RCA's VAX computer.

The SPA baseline diagram (Figure 30) shows that (with no faults inserted) the enhanced and normalized SPA gave uniform performance. This could only be assumed, however, if one of the aircraft monitored at Fort Rucker actually had a faulty bearing, and this was accepted at the time. Using the baseline established on this assumption, the fault detection diagram of Figure 31 shows reasonable fault detection prognosis.

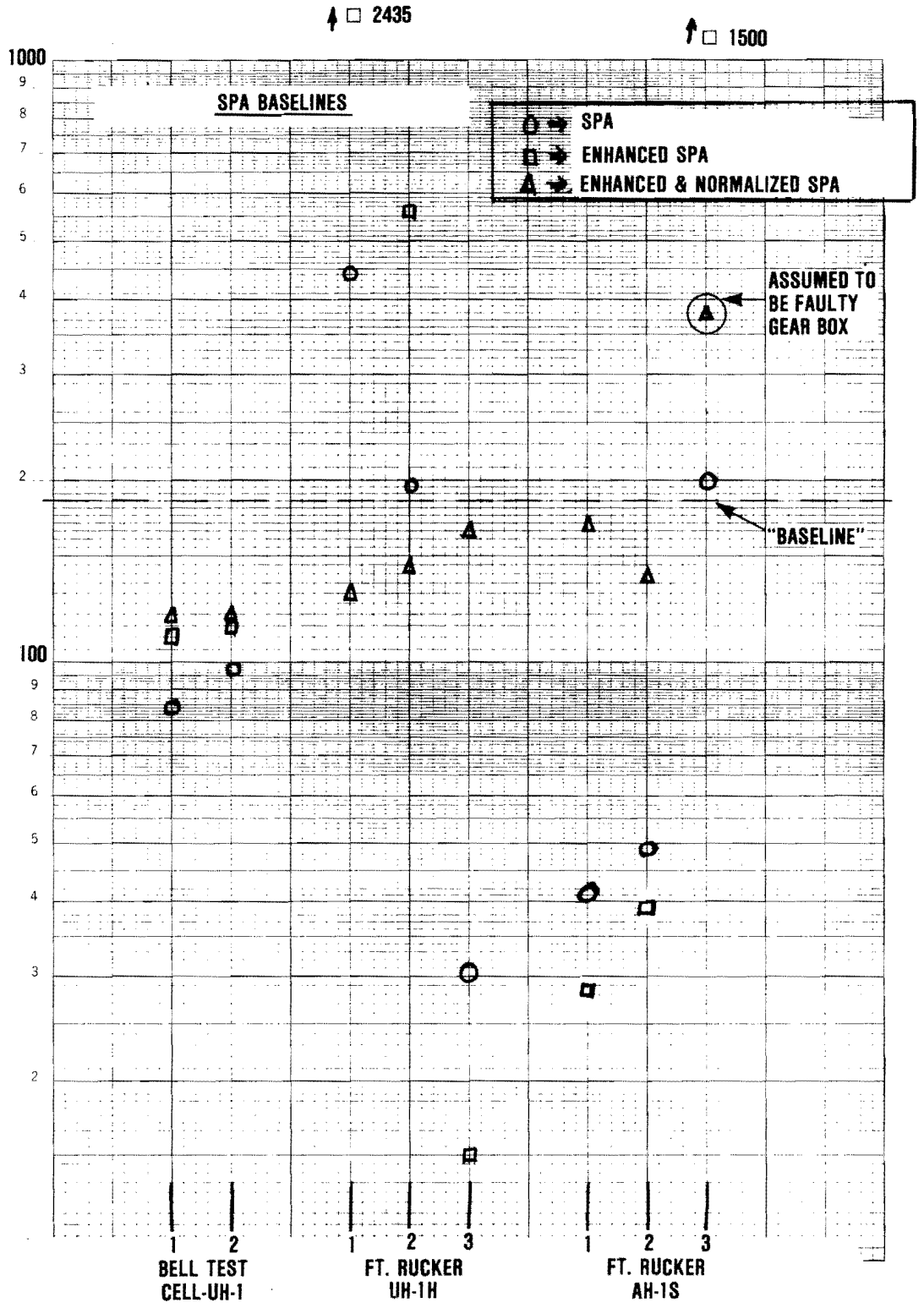

Figure 30. UH-1 Analysis Results, SPA Baselines

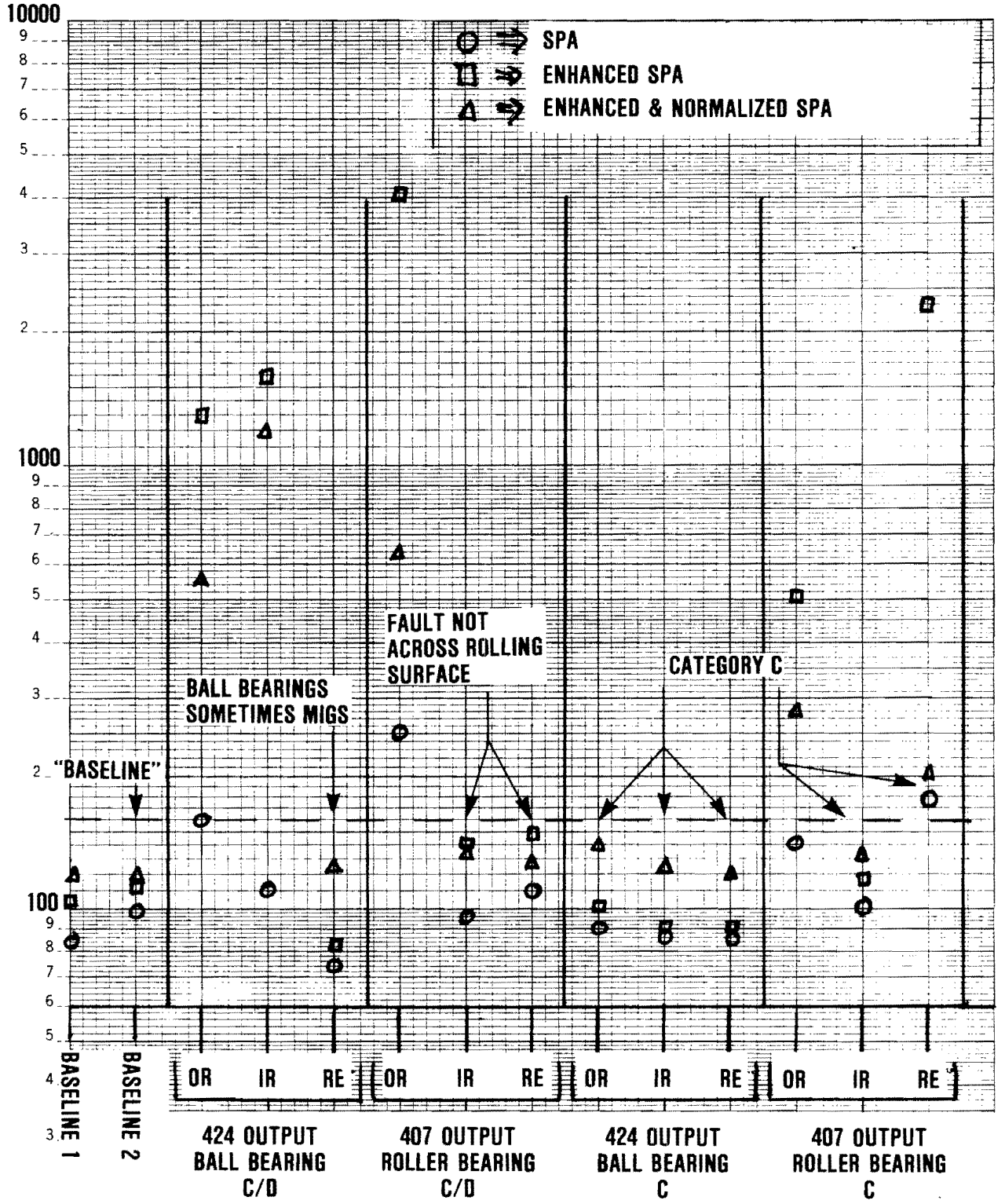

Figure 31. UH-1 Analysis Results, SPA Fault Detection

It is also noted that the original fault implants on roller bearings did not exhibit detectable fault signatures. This was not accepted as a failure of the SPA, but instead was interpreted to mean that fault implants should have been inscribed all the way across the contacting surfaces of roller bearings and/or their raceways. Also noted was the sporadic nature of the vibrational signature as seen in ball bearings in which there could be two tenths to five tenths of a second of very clear fault signature followed by half a second or greater period with an entire lack of fault signature. Such performance is caused by the precession of the ball relative to the fixed axis of rotation so that the fault experiences intermittent periods of race contact.

3.3.1 Impact On PDR Design

Data analysis revealed three "surprises" which impacted the design requirements and led to both hardware and software modifications for the SPADE. The first of these pertained to "Helicopter Vibrations". RCA analyzed the fault signature involved with a specific helicopter at Fort Rucker whose fault signature at the 90-degree gearbox output shaft "appeared" to have a fault condition (see Figures 32 and 33). Careful analysis of the waveform showed that the signature is different from the signature of fault implants observed in the Bell Helicopter test cell. The most significant difference with this Fort Rucker aircraft waveform is the width of the ringing fault pulse. Its duration was 10 to 20 milliseconds in length, exceeding by almost an order of magnitude the pulse width of signals seen on fault implants. Also, the repetition rate of the ringing pulse burst is at the blade passing frequency of the tail rotor blade. The conclusion reached is that the Fort Rucker aircraft had an imbalanced condition on its tail rotors and that it did not have fault conditions on its bearings. To this date the condition of the tail rotor gearbox on that aircraft at Fort Rucker has not been validated by disassembly and inspection. RCA proceeded in the design of the SPADE hardware (and particularly in the software) on the basis that helicopter vibrations of this nature can cause ringing pulses which look somewhat like fault conditions, but can be discriminated with respect to fault conditions by the width of the pulse. This basic premise for the current SPADE design is stated as follows: "Bearing fault signatures observed from test stand data have time durations from 300 microseconds to 1200 microseconds." The detection strategy had changed from caring only about pulse height to also being concerned about pulse time duration.

The second major requirement change pertains to the nature of the signal. The fault signature is not a narrow pulse at a known ringing frequency but is a pulse of complex waveform with a finite rise time. It has a predominant ringing frequency which depends upon the outer race of the bearing involved and its natural mode frequencies. It is therefore important that the hardware signal paths in the SPADE system process this waveform on a wide-band basis to preserve its intricacies. Stated in another sense, the waveform would be seriously degraded by a narrow resonant processing system.

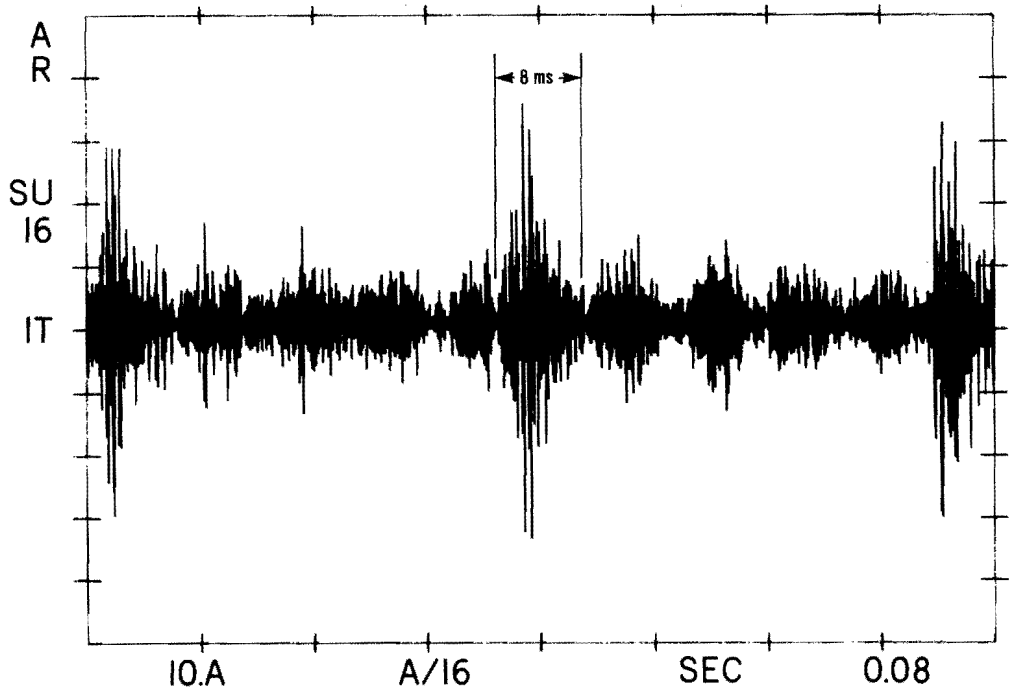

Figure 32. Waveform of Fort Rucker 90-Degree Output Predetection

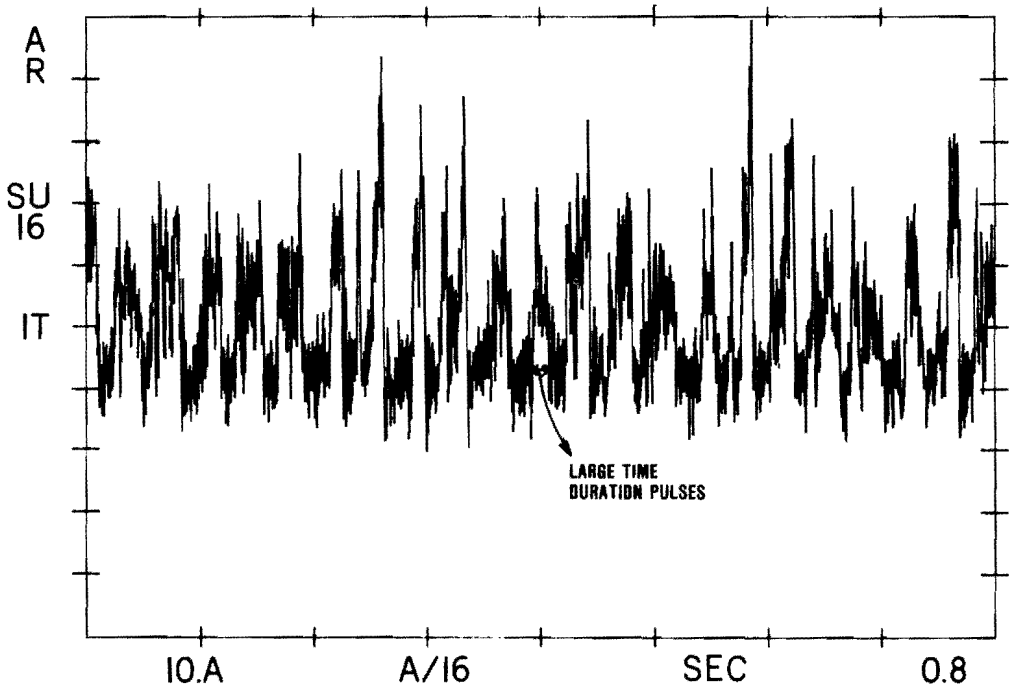

Figure 33. Waveform of Fort Rucker 90-Degree Output Post Detection

The third major requirement change pertains to acoustic noise. Oscillograph observations showed acoustic noise at frequencies of approximately 50 kHz, as observed in the taped instrumentation waveforms taken on live aircraft at Fort Rucker. Not all of the tapes showed this high frequency noise response, but perhaps one or two out of three did. RCA's interpretation is that this is high frequency acoustical noise associated with the gas discharges from helicopter engines. It should be remembered that while SPADE is performing its vibrational analysis, the main rotor on the aircraft is at 100 percent of its normal rated speed, the engines are running, and there is a considerable amount of acoustical noise. The SPADE sensors are vibrational sensors, and thus are susceptible to picking up noise in the acoustical and above acoustical frequency ranges. The impact for SPADE hardware design is that filtering hardware is required to eliminate this large amplitude of acoustical signature which is present on at least some of the aircraft recordings.

3.3.2 Hardware Design Changes

Three specific hardware design changes were determined to be required in response to the technical problems observed and discussed above.

(1) The addition of a common mode rejection amplifier at the front end of the SPADE hardware. The hardware as designed in the PDR assumed a bearing fault signal in the 50-100 millivolt region. However, data taken from the Bell Helicopter recordings has clearly shown that fault signatures and their signals will actually be considerably smaller, perhaps in the 10 millivolt (maximum) region. RCA's concern was that common mode noises picked up on the signal transmitted from the sensor to the analyzer would be of such magnitude as to interfere with the detectability of the fault signals. The front end was redesigned so that the inputs are balanced, giving far superior common mode rejection.

(2) The commutating resonant filter had to be replaced by a multi-pole band-pass filter to allow a wide frequency band and improve the signal-to-noise ratio. The filter improves the signal-to-noise ratio by essentially preserving the complex waveform which is the ringing fault pulse. The band-pass filter is formed from two filter sections: an eight-pole high-pass filter with 15 kHz cutoff and a 48 dB per octave low frequency attenuation, and a six-pole low-pass filter with a cutoff at 35 kHz and 36 dB per octave roll-off. Together these two filters provide a band-pass spreading from 15-35 kHz.

(3) The analog peak detector was replaced with a digital envelope detector. The previous peak detector was found to produce aliasing of the complex input waveform which we now know to be the characteristic fault signal that we are trying to detect. The simple peak detector hardware is replaced by an improved envelope detector design discussed in Section 4.

SECTION 4
SPADE SYSTEM ARCHITECTURE

This section defines a SPADE system architecture which will achieve the performance requirements specified in Section 2.5. The Engineering Development Program was premised on the use of high frequency vibration techniques (greater than 10 kHz) for the basic detection mechanism. The technique involves deconvoluting transient ringing pulses to extract event and magnitude information for bearing defect analysis. The deconvolution technique adopted was an incoherent demodulation approach.

4.1 PROCESSING BASED UPON UNIQUE SIGNATURES

One of the major achievements of the post PDR effort has been the identification of the source of a bearing fault signal as well as the signature of bearing defects. This identification allowed the signal detection process to be optimally designed to detect this signature. The bearing defect for a class C/D defect was shown to be a ringing pulse of a frequency between 15-35 kHz with a time duration of between 300-1200 sec. As a result, the architecture was tailored to detect this pulse. The SPADE processing approach is quite broad and allows considerable flexibility in the system architecture and detection process. The signal flow through the detection process is shown in Table 5. Paragraph references are provided for descriptions of module requirements and implementation techniques.

Table 5 shows that the signal processing chain is quite modular. In fact, the implementation can be done completely in hardware or, with today's technology, almost entirely in software. The system implementation in this design was, for the most part, accomplished in software to allow flexibility for future applications. The requirements for each of the modules are provided in the following paragraphs.

4.2 BAND-PASS FILTERING

The first step in the processing is the removal of the low frequency machinery noise, as shown in Figures 2 and 13. Note that scaling of the plots is the same and the bearing fault signature can be seen embedded in the machinery noise. Since the demodulation process which follows the filtering is not linear, it is important that the low frequency machinery noise be attenuated far below the level of the possible bearing fault signatures. Therefore the performance of the band-pass filtering is one of the most critical performance factors of the system. The reason for this is that the residual components of machinery noise introduce random signals which decrease the signal-to-noise ratio once the waveform is demodulated. Those random signals also raise the noise floor of the FFT and hence degrade the signal-to-noise ratio. Since the final processing steps are digital,

TABLE 5. ARCHITECTURE OF SPADE FAULT DETECTION PROCESS

System Module Flow	Function	Requirement Paragraph	Implementation Paragraph
Accelerometer Input ↓ Noise Filter	Remove extraneous noise originating from sources such as machinery	4.2	5.1.1, 5.1.2
↓ Demodulation	Carrier modulation detection	4.3	5.3
↓ Pulse Processing	Separate pulses of different time duration from other modulating effects such as gear and shaft noise	4.4	5.4
↓ Post-Detection Processing • Time • Frequency	Time domain processing	4.5, 4.5.1	5.4, 5.4.1
	Frequency domain processing	4.5, 4.5.2	5.4, 5.4.2
↓ Decision Analysis	Evaluate performance against decision criteria	4.6	5.5
↓ Pass/Fail			

an upper frequency limit must be established to avoid aliasing. The 35 kHz limit was chosen primarily because most bearing fault signatures are in the range below 35 kHz. A secondary reason for choosing this frequency was to remove the strong high frequency noise which was observed in aircraft data base recordings, as described in Section 2.4.

Based upon the need for eliminating low frequency machinery noise and the aircraft high frequency noise, the preliminary step in the signal processing is to strongly attenuate signals outside the frequency range of interest (15-35 kHz). The frequency range boundaries are somewhat arbitrary. The machinery noise encountered was usually below 15 kHz and the aircraft high frequency noise encountered in the field was usually above 35 kHz.

Two alternative filtering strategies were evaluated for the architecture. The first strategy was to employ a fairly steep band-pass filter which had a pass band in the range of 15-35 kHz. This approach would remove the obstructing noise from the signal and let the bearing pulse signature pass through. In the range of 15-35 kHz several modes of the bearing race ring can exist and the pulse structure will usually be multimode. The second approach was to have a very sharp narrow-band filter which is precisely

aligned on one of the resonance frequencies of the race. The width of the filter is designed so that the spectral width caused by modulation of the ringing pulse could be accommodated. This approach promised a higher signal-to-noise ratio at the cost of a very complex filter, particularly since the filter would have to be tunable, and an adaptive algorithm would be required to tune the filter to precise resonance frequencies. The two approaches were compared (Figures 34 through 37) by analyzing a bearing fault which produced a ringing signal at a frequency of 27 kHz. The fault signal was analyzed using a band-pass filter consisting of a 15 kHz eight-pole high pass and a 35 kHz six-pole low pass. Next, the fault signal was analyzed using an elliptical band-pass filter which had a very sharp roll-off with a center frequency of 27 kHz and a 3 kHz pass band. (This filter is described in Appendix F.)

The test results are shown in Figures 36 and 37; there is no significant difference in performance. Therefore, on the basis of cost effectiveness the fixed band-pass filter of 15 kHz and 35 kHz was selected.

4.3 DEMODULATION

Demodulating the carrier to recover the pulse shape is an important process in the signal detection chain. As described in Section 4.1, one of the important features of the fault signature which can be exploited to enhance the detection process is the time duration of the fault pulse. Therefore, recovery of the pulse fault shape is critical to the detection process. Also, any random noise which can be eliminated will decrease the noise floor in the power spectrum making the spectral lines more detectable.

At the time of this study there appeared to be no apparent advantage to either coherent demodulation or incoherent demodulation, so the simpler form of incoherent demodulation was adopted. However, the incoherent demodulation process is complicated by the character of the pulse and the nature of the noise in the system. Digital implementation offered considerable performance advantages over the conventional analog peak detector often used in AM demodulation, so this method was chosen. Details of the digital demodulation implementation are discussed in Section 5.3.1.

4.4 PULSE PROCESSING

As described in Section 2.4, there are other signals in the helicopter environment which have pulse modulated waveforms in the frequency range of 15-35 kHz. Bearing faults were shown to have a signature which has different characteristics than other signal phenomena normally found in the helicopter environment. One unique property identified is the time duration of the pulse. Analysis of the waveform in the time domain provides the opportunity to discriminate extraneous pulses from pulses characteristic of bearing failure. However, if the data is transformed into the frequency domain, the ability to discriminate based on pulse duration is lost. In the frequency domain, the possibility of discrimination exists provided the other types of phenomena have a different frequency. However, frequency discrimination can

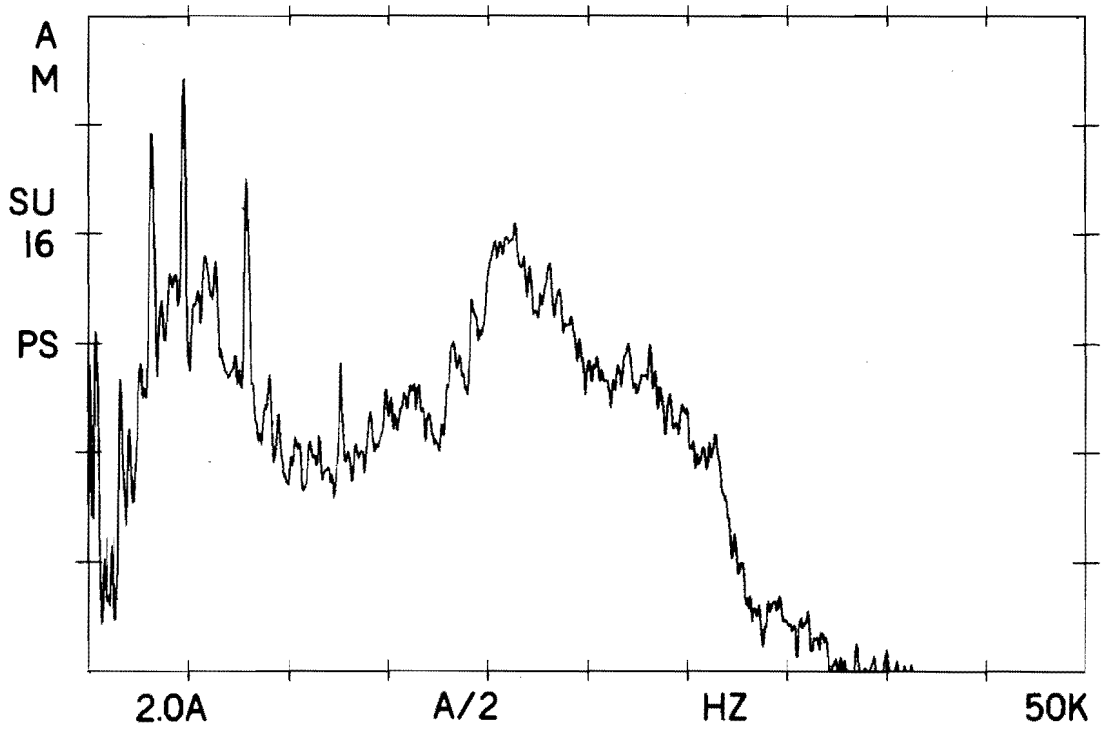

Figure 34. Original Power Spectrum

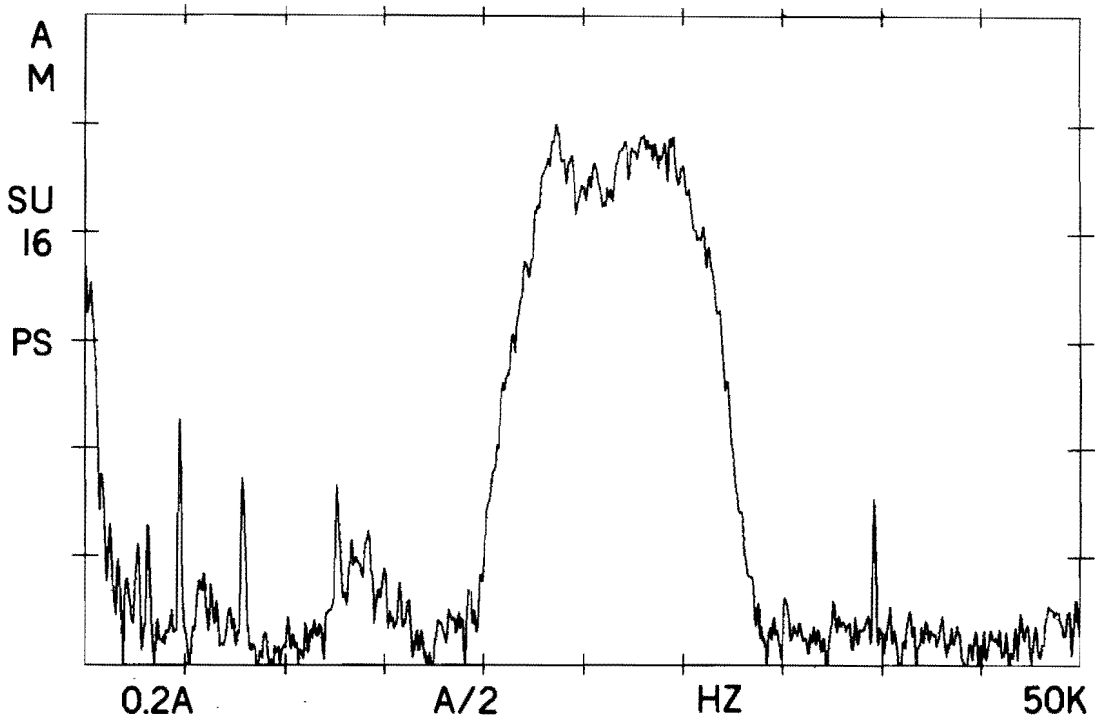

Figure 35. Power Spectrum After Application of Band-Pass Filter

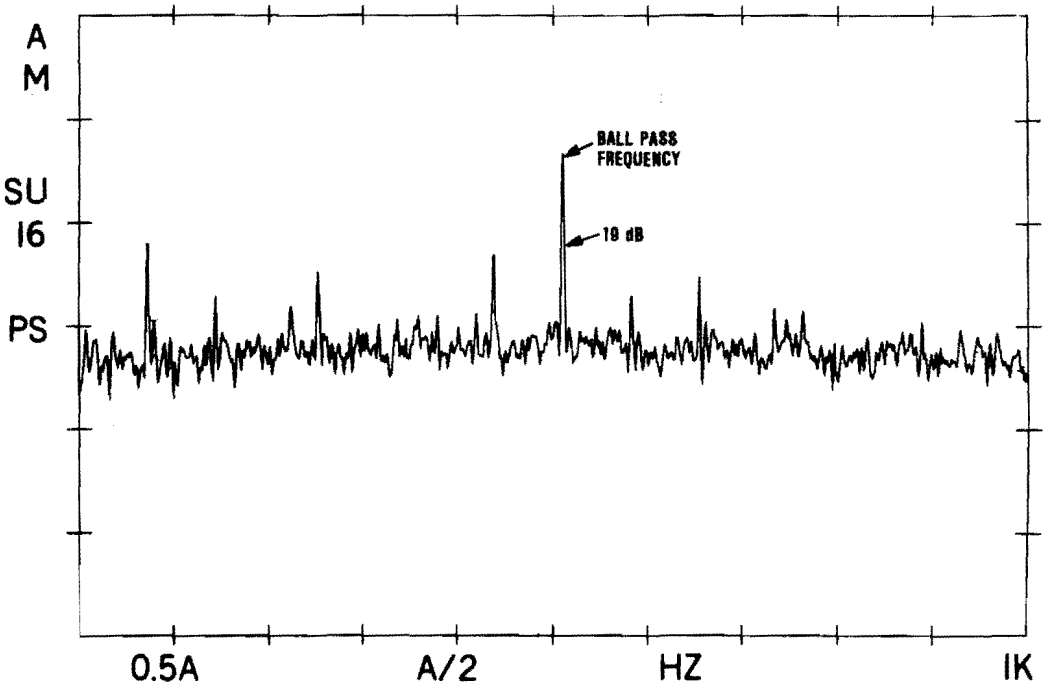

Figure 36. Bearing Fault Signal Obtained With Wide Pass-Band Filter (15-35 kHz)

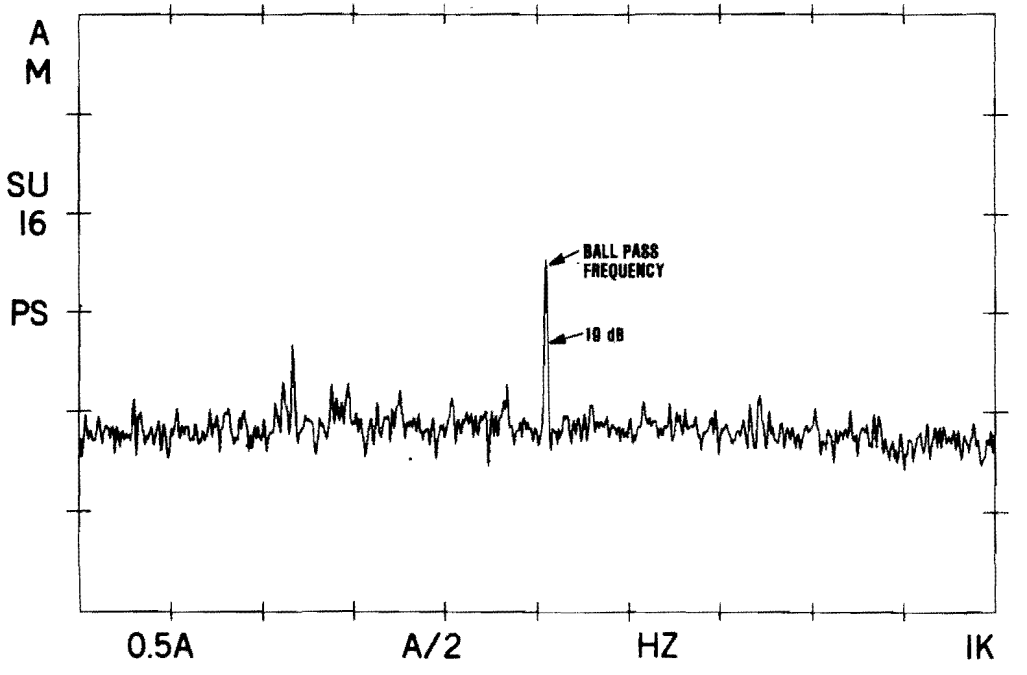

Figure 37. Bearing Fault Signal Obtained With Narrow Pass-Band Filter (27 kHz Center; 3 kHz Pass Band)

be complicated when a frequency of interest (such as a ball-pass frequency) is close to an unwanted frequency (such as a harmonic of a shaft frequency); this is sometimes the case. For the time domain algorithm which is required for detecting ball faults as well as extremely gross faults, there would be no separation. One of the signal processing achievements of the SPADE design is the ability to discriminate the bearing fault signatures from other signatures. The implementation details are presented in Sections 5.1.1, 5.3.2 and 5.3.3. The technique employs a matched filter to enhance the bearing fault and a nonlinear filter to discriminate the bearing fault signal from other phenomena in the waveform.

4.5 POST DETECTION

This section defines the signal processing which is performed after bearing fault type signatures have been identified. The post-detection signal processing is a combination of a time domain processing technique (described in Chapter 3) and a frequency domain processing technique (based upon spectral components of the band-pass frequencies).

4.5.1 Time Domain Processing

The time domain processing algorithm consists of two parts. The first part is based upon integrating the digital processed waveform over a fixed time interval and correcting for the signal gain of the measurement hardware. This technique is identical to the shock pulse analysis technique (the original prime measurement technique of the SPADE design). However, the measurement is then enhanced by the digital processing in order to remove nonbearing signatures. The second technique developed for the time domain processing is based upon the statistical properties of the digitally processed waveform. Although this technique was developed independently, it is similar to the kurtosis measurement technique reported by Dyer and Stewart.[2] Development of the statistical time domain method was required to achieve a technique that would be independent of signal level, power level, and temperature of the gearboxes and bearing assemblies. The statistical properties of the waveform are moments of the waveform as compared to the average level of the signal.

4.5.2 Frequency Domain Processing

The frequency domain processing is based upon the assumption that the shaft speed remains constant in time during the test period. If the shaft speed is constant, the bearing fault signatures of inner and outer race faults will be periodic in time. By transforming the time domain waveform into the frequency domain, the periodic waveforms which characterize a particular bearing ball-pass frequency can be found. The spectra which result from bearing faults appear as narrow lines in the spectrum, as shown in

---

[2]D. Dyer and R.M. Stewart, "Detection of Rolling Element Damage by Statistical Vibration Analysis," Journal of Mechanical Doings, April 1978, pp. 229-235.

Figure 38. Because the fault signal is periodic, the frequency lines are very narrow, which requires very high spectral resolution in order to achieve a high signal-to-noise ratio.

After the spectrum is computed, the problem remains to interpret the spectrum and determine bearing fault lines from spectral lines which are due to residual clutter and other background signal phenomena. The ultimate result of the frequency domain signal process is a numerical value which represents the severity of a particular bearing fault signature.

In conclusion, the following steps are required for the frequency domain signal processing:

1. Measure high frequency resolution of the digitally processed waveform.

2. Identify features in the spectra that represent bearing fault signatures.

3. Extract from the spectra those features which represent bearing fault signatures, and compute a numerical value which represents the severity of the fault.

The requirements and implementation details for each of these steps are presented in Section 5.4.2

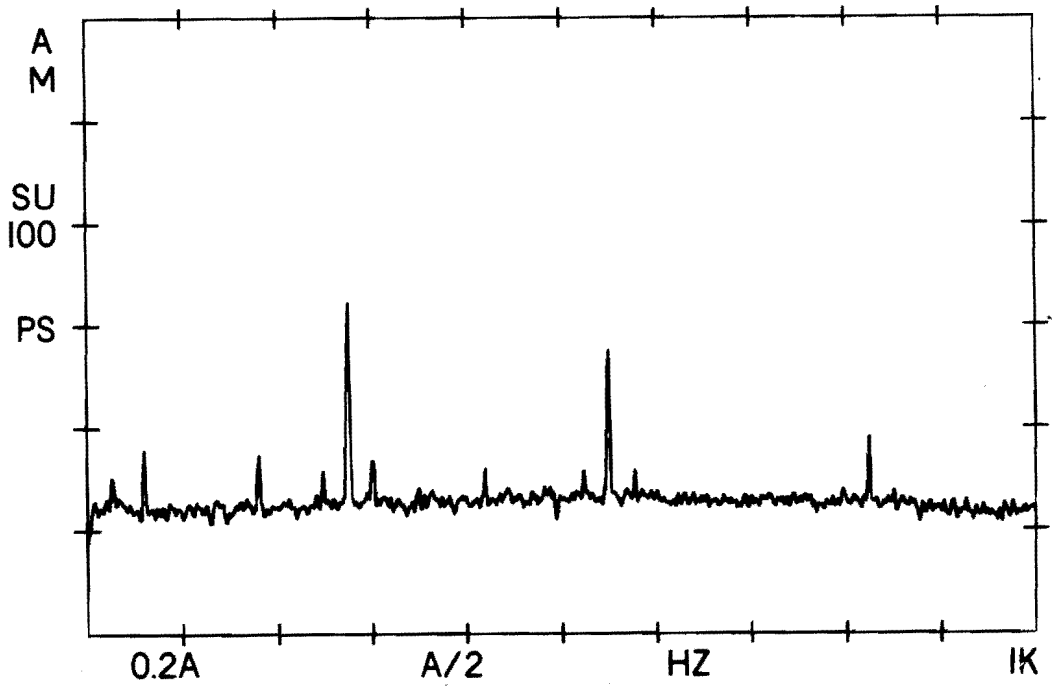

Figure 38. Frequency Domain Spectra of a Bearing Fault

4.6 DECISION ANALYSIS

The decision analysis process determines if a particular bearing assembly or gearbox assembly has a faulty bearing. In the signal processing described thus far, the SPADE analyzer has been functioning as a meter, in essence, simply making a measurement. The task of this module is to implement a decision criterion based on the signal processing measurements from the bearing or gearbox assembly. To do this, a knowledge base must be assembled for use by the decision module. The following observations are relevant for this decision analysis function:

Observation #1 - Bearing rolling element faults are not effectively detected in the frequency domain.

(1) The defect on the rolling element of a ball bearing precesses in and out of the load zone as the ball rotates in the bearing race (see Figure 39). This produces a sporadic pattern of fault signatures which are not detected effectively by the frequency domain technique.

(2) Roller bearing rolling element faults are not readily detectable, primarily because the resulting spectral lines are weak due to broadening, i.e., the signal broadens in frequency and decreases in amplitude. (See Figure 97 for an example.) This broadening is assumed to be due to the rollers skidding out of a fault zone and disrupting the normal coherent repetition rate.

Observation #2 - Gross faults destroy coherent repetition rate from fault signatures.

Figure 40 shows the inner and outer race gross defects which were implanted on an OH-58 hanger bearing. The bearing was reassembled and run on an OH-58 tail boom and test data were recorded. The resultant band-passed demodulated waveform and the digital processed waveform are shown in Figure 41. It is apparent that the characteristic bearing fault signature is not present in either signal. The gross level of the fault (well beyond the C/D fault level) has completely degraded the coherent repetition rate from the fault signature.

Observation #3 - Progression of Bearing Faults

In real life, bearing failures begin as very small spalls which grow into large areas of damage. In order to effectively set bearing fault threshold limits (SPADE analyzer test criteria for pass/fail decisions), an elementary model of the behavior of detected signal level (as a function of the bearing fault level) is required. Fault progression tests were performed on a sample of four OH-58 hanger bearings. A single category B/C level spall was simulated on each bearing as the initial implant. Progressively, the spall areas were enlarged to "extended" Category D level in five separate steps. Data was recorded for each step as the fault level increased. The results are shown in Figures 42 through 44.

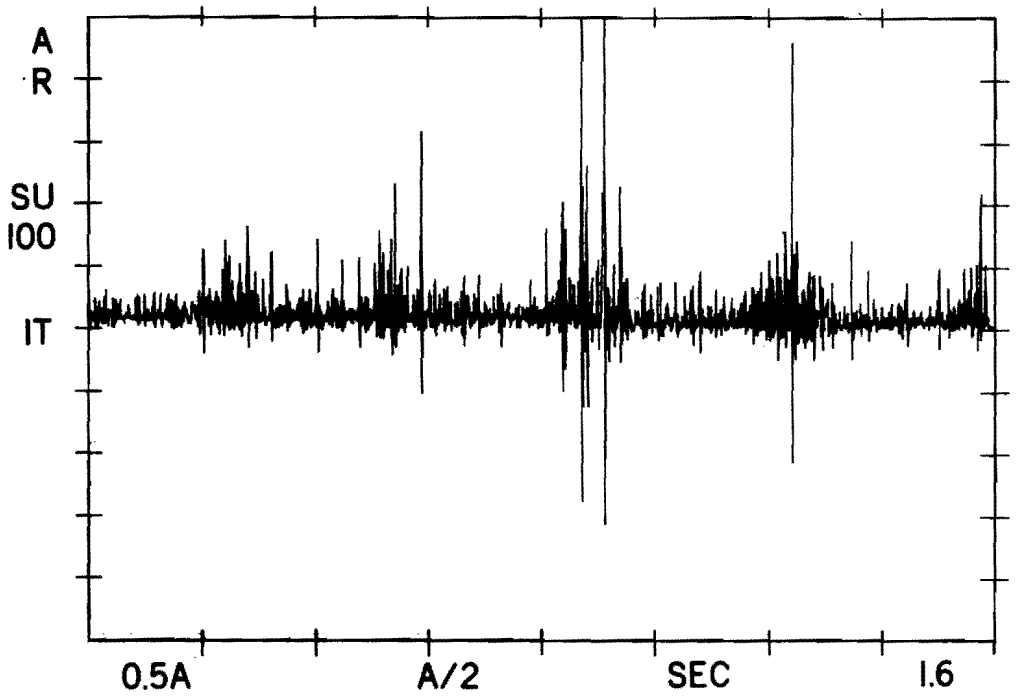

Figure 39. Typical Sporadic Pattern of Ball Bearing Rolling Element Fault

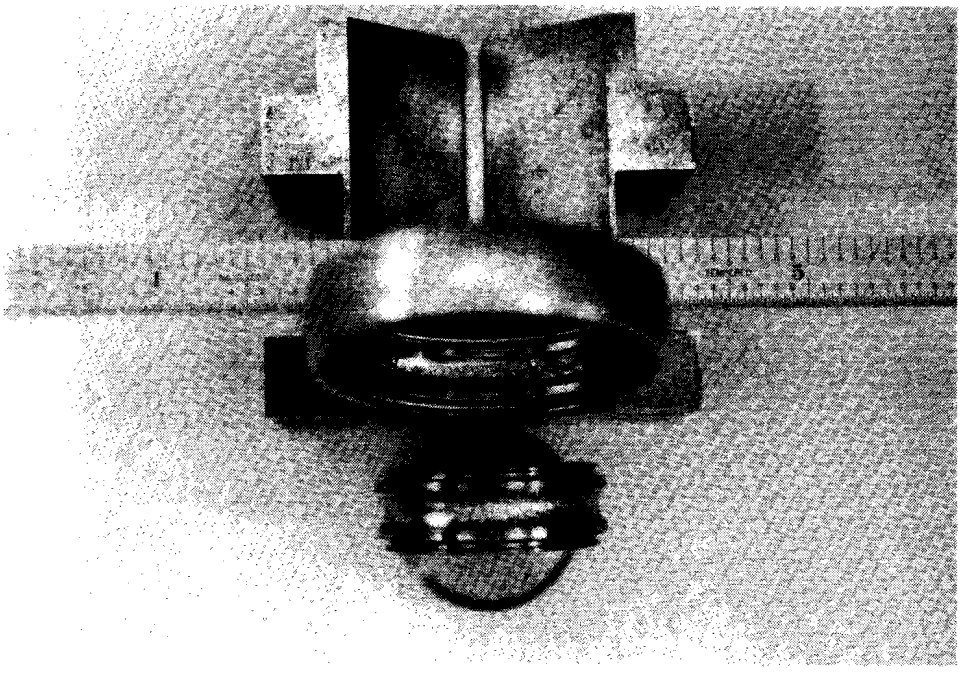

Figure 40. Inner and Outer Race Gross Fault Implants

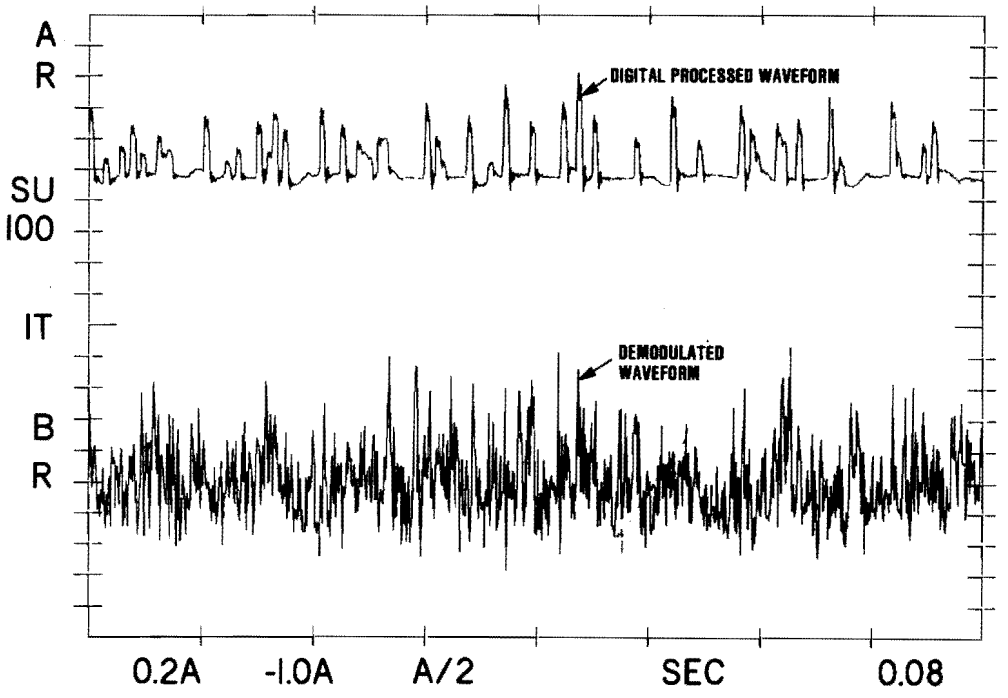

Figure 41. Band-Pass Demodulated Output and Digital Processing Output from Gross Level Bearing Fault Implant

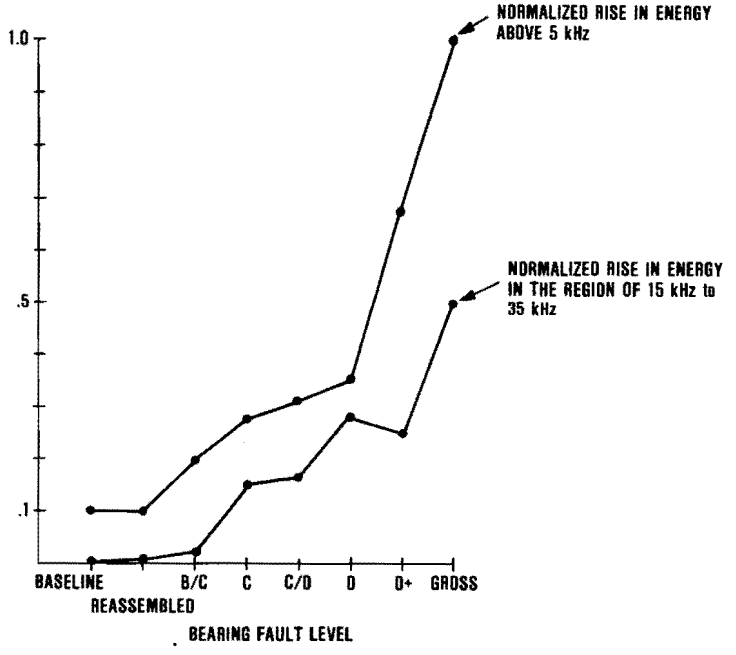

Figure 42. Signal Level as a Function of Bearing Fault Level

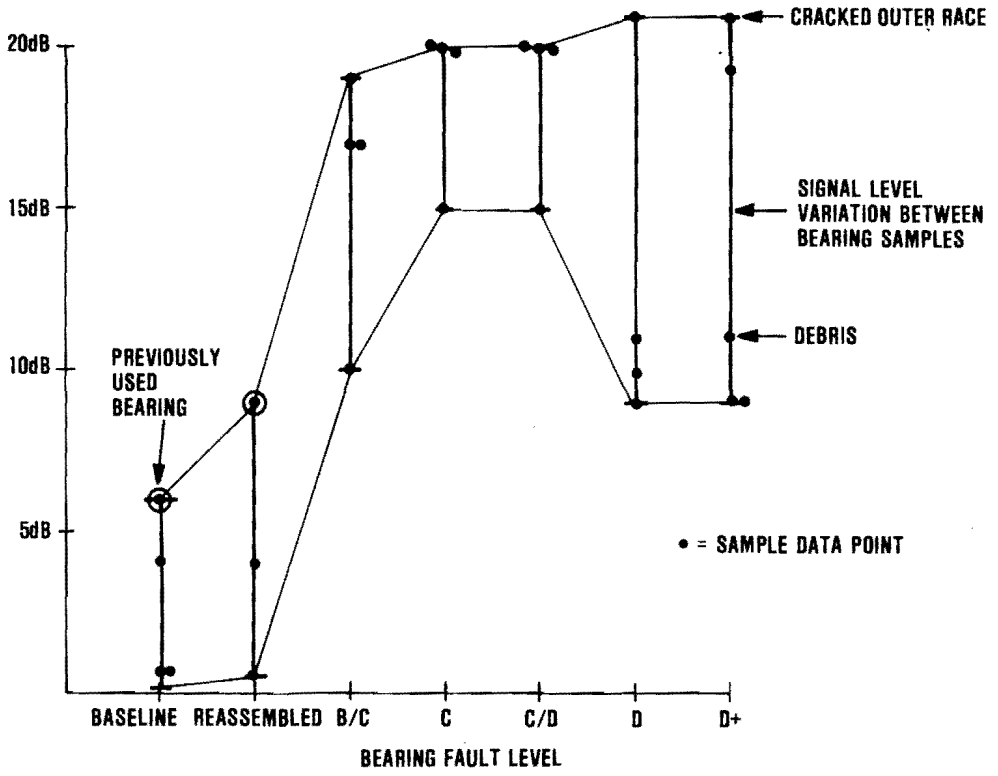

Figure 43. Normalized Plot of Spectral Signal Level as a Function of Bearing Fault Level

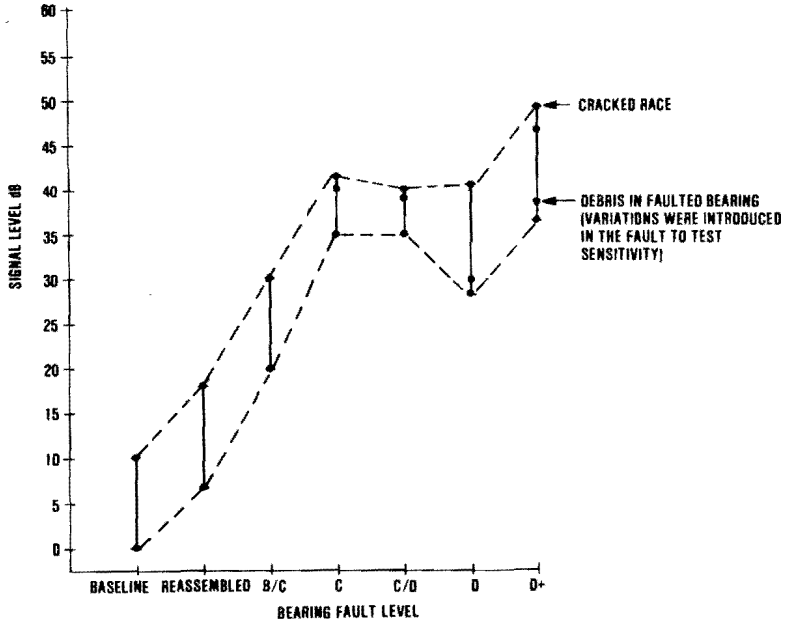

Figure 44. Typical SPADE Processing Signal Level as a Function of Bearing Fault Level

The first variable plotted in Figure 42 is the total signal level (above 5 kHz) as a function of bearing fault level. The signal rise between baseline (no fault) and an extremely gross fault level is approximately 10 to 1.

However, 70 percent of this rise in signal level occurs in the region between D and gross fault levels. The second curve shown in Figure 42 is the rise in signal level (15 kHz to 35 kHz) which occurs as a function of bearing fault level. The rise in signal from baseline (no fault) to an extremely gross fault level is 50 to 1, with a 15 to 1 rise in signal from baseline (no fault) to Class C fault level. This effect is not surprising since most bearing fault detection schemes operate in this region. While the 15 to 1 rise seems large, the ratio will significantly decrease when applied in an environment with other noise sources.

The data plotted in Figure 43 shows a normalized curve of spectral signal peaks (in dB) as a function of bearing fault level. There is signal rise (19 dB) as the fault level increases from baseline (no fault) to B/C level fault. However, after the B/C fault level point, the signal level remains relatively constant. When the data is plotted as signal level after SPADE processing (Figure 44), the curve reveals an average signal level separation of 35 dB between baseline (no fault) and a C/D fault level condition. Also, note that the spectral technique provided definitive signal levels for extended D-level faults. The roll-off of the spectral technique signal level occurs well beyond the extended D-level fault category.

Based upon these observations, the following approaches were adopted for the decision analysis process:

(1) Bearing rolling element faults are to be detected by the time domain analysis (SPA technique).

(2) The signal level will be used to monitor gross fault levels. (It is anticipated that further research will determine a definitive signature for the gross fault condition, which will make its detection more effective.)

(3) The spectral technique will be the prime method of detecting bearing faults on the inner and outer race for fault levels up to and including the extended D-level.

As in any experience-based situation, knowledge will grow as more research and testing occurs. Therefore, the three basic approaches which form the basis of the decision element will grow and possibly others will be included later as more data is gathered. This element is not a static module but will evolve and improve as the knowledge data base is increased. Details of the decision analysis implementation are presented in Section 5.5.

SECTION 5
DEVELOPMENT OF SIGNAL DETECTION METHODS

5.1 PREDETECTION FILTERING AND PROCESSING

5.1.1 Low-Frequency Machinery Noise Filter

To provide the required low frequency filtering, an eighth-order high-pass Butterworth filter was designed, built and tested. The filter, shown in Figure 45, was designed to realize the following transfer function:

$$T(S) = \frac{S^8}{(S^2 + 1.960S + 1)(S^2 + 1.667S + 1)(S^2 + 1.11S + 1)(S^2 + 0.390S + 1)}$$

Both 5 and 15 kHz cutoff frequencies are programmably selectable.

The Butterworth filter design was chosen because it has a flat pass-band response and is also easy to implement actively, thus eliminating the need for inductors in the circuit. Wide bandwidth LF347 operational amplifiers were chosen for the design because a general-purpose operational amplifier is not suitable for the 15 - 35 kHz frequency band of interest.

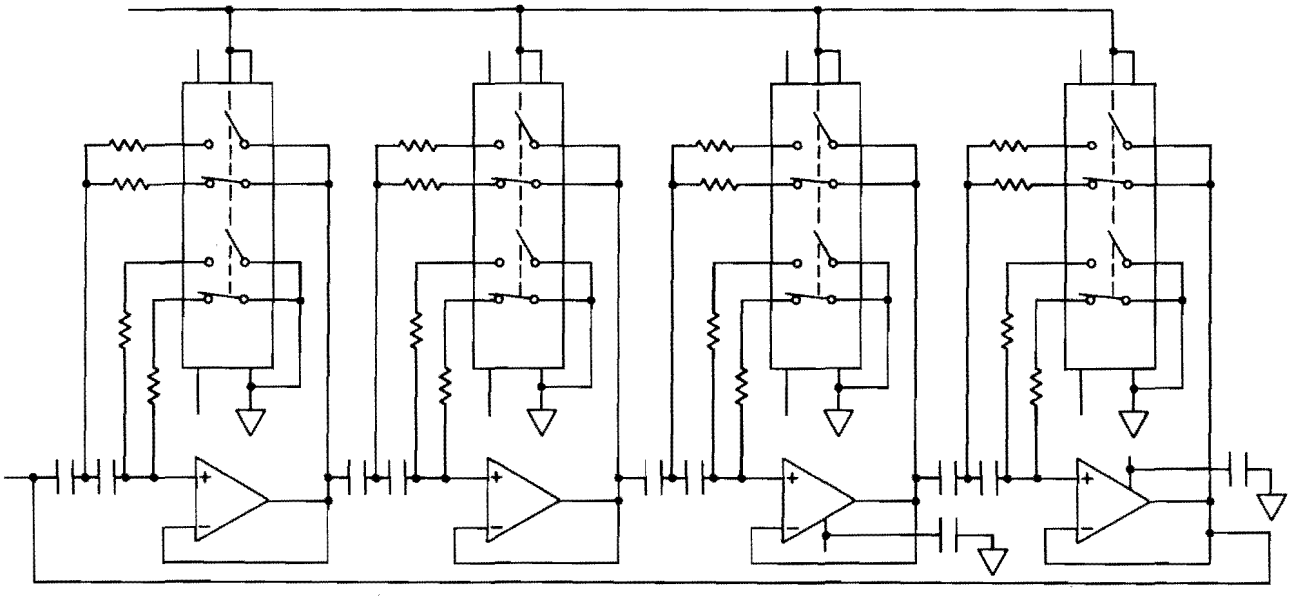

Figure 45. 5/15 kHz Butterworth High-Pass Filter Design

An eighth-order filter was chosen because it was found that the band-pass filter with the sharpest cutoff possible yielded the best fault-detecting capability. Butterworth filters of greater than eighth order do not yield significantly sharper cutoffs.

Figure 46 shows the power spectrum of a typical accelerometer output on a faulted aircraft bearing. Figure 47 shows the spectrum of the same signal after passing through the breadboard band-pass filters. In bench tests the filter was found to roll off at about 60 dB per octave at its steepest point with a stop band attenuation of about 60 dB.

5.1.2 High-Frequency Aircraft Noise Filter

The sixth-order low-pass Butterworth filter shown in Figure 48 was designed and implemented. The filter, which has a 35 kHz cutoff frequency, realizes the transfer function:

$$T(S) = \frac{1}{(S^2 + 1.923S + 1)(S^2 + 1.408S + 1)(S^2 + 0.518S + 1)}$$

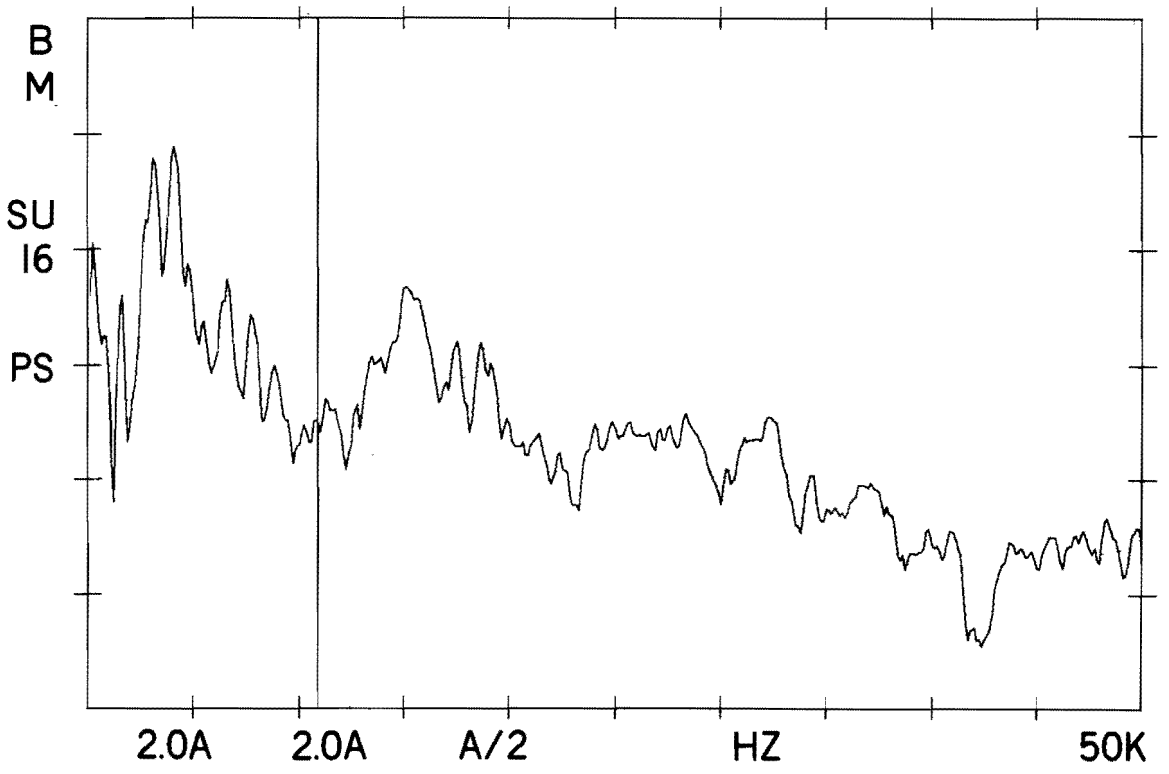

Figure 46. Typical Accelerometer Output from a Faulted Bearing (Frequency Domain)

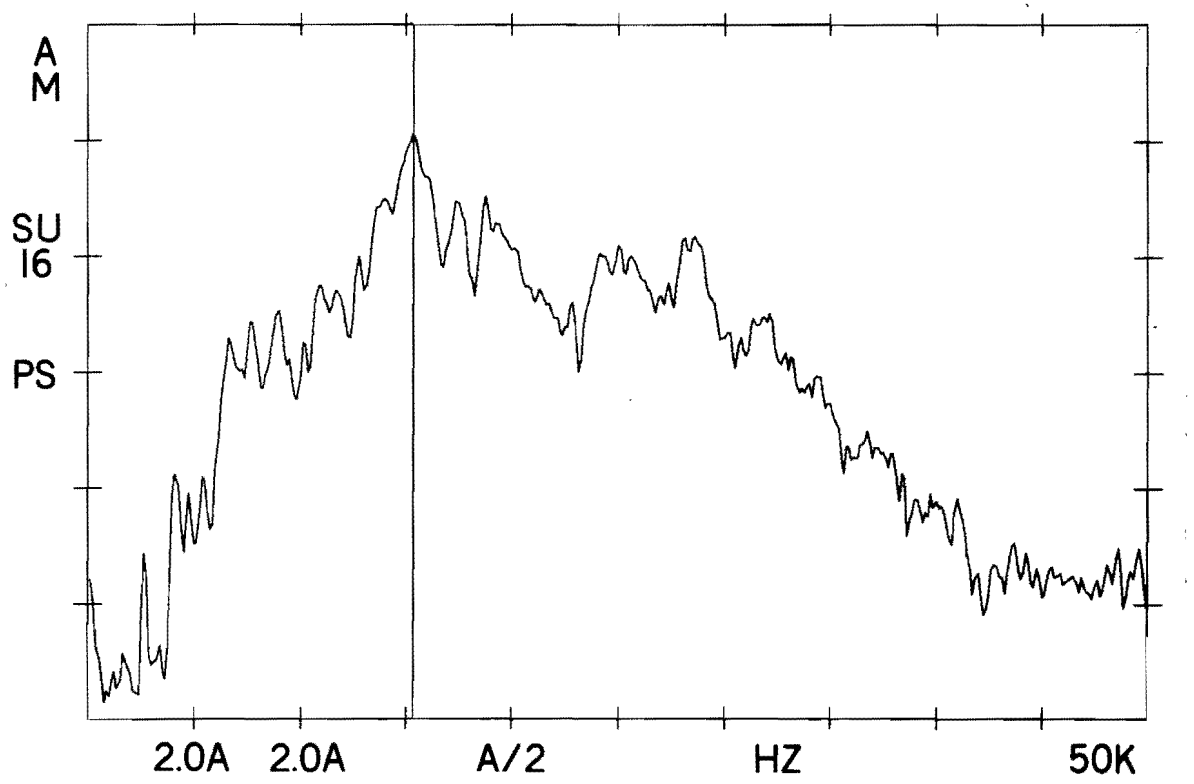

Figure 47. High-Pass Filtered Accelerometer Output (Frequency Domain)

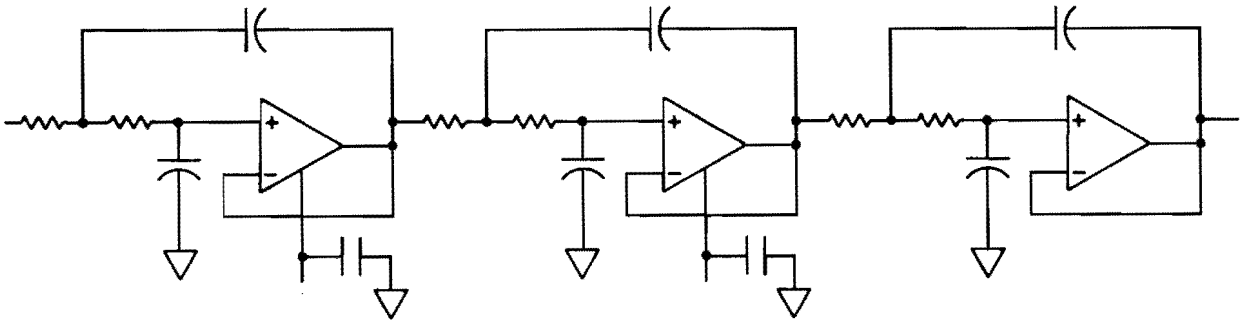

Figure 48. 35 kHz Butterworth Low-Pass Filter Design

The Butterworth filter was chosen for the low-pass filter implementation for the same reasons as the high-pass Butterworth described in the previous section: flat pass-band response and ease of implementation. Because of the high frequencies involved, LF347 wide bandwidth operational amplifiers were used. For this application, a sixth-order filter was sufficient to eliminate the aircraft noise frequencies greater than 35 kHz.

Figures 46 and 47 show the unfiltered and filtered waveforms of an accelerometer output, respectively. The low-pass filter provided a stop band attenuation of 25 to 30 dB.

The 35-kHz low-pass filter combined with the 5/15-kHz high-pass filter described in the previous section yielded an effective wide-band filter. The two filters are implemented separately because the low-frequency noise is so large in amplitude that after it is filtered out, the remaining signal is very small. Therefore, the signal-to-noise ratio is improved by amplifying the signal before the high-frequency aircraft noise is filtered out. This signal flow is shown in Figure 49.

5.1.3 Accelerometer Development

Two vendors supplied six accelerometers each, designed to the requirements of RCA specification RCB-002C (see Appendix A) for test and evaluation. (Note that the specification requires close control of the accelerometer response in the 20 - 35 kHz frequency range.) RCA tested each of the twelve sensors on a B&K high frequency shaker table. The results of these tests and consequent specification changes are described below.

Of the six sensors received from vendor A, two sensors failed initial tests and were returned to the vendor for corrective action. Neither sensor was repaired prior to the end of the test phase, thus they were not further evaluated.

Tests of the remaining four accelerometers were performed on the setup sketched in Figure 50. All tests reported herein were run with the sensors screwed down on the beeswax-coated shaker table to guarantee good high-frequency transmission. The primary reference for performance evaluation was a sensor that is an integral part of the B&K high-frequency exciter. While the absolute precision of the reference sensor is not guaranteed by B&K, tests using two models of vendor A's commercial accelerometers (both 80 kHz or higher units) indicate a reference sensor response that is flat within ± 1 dB at least to 40 kHz. Further, since scatter among sensor responses is more important than absolute precision, the primary value of the reference sensor is in establishing the response variation among a group of sensors.

The band limit filter shown in Figure 50 was essential in making measurements with the RMS meter. The filter ensured that the harmonic content of the

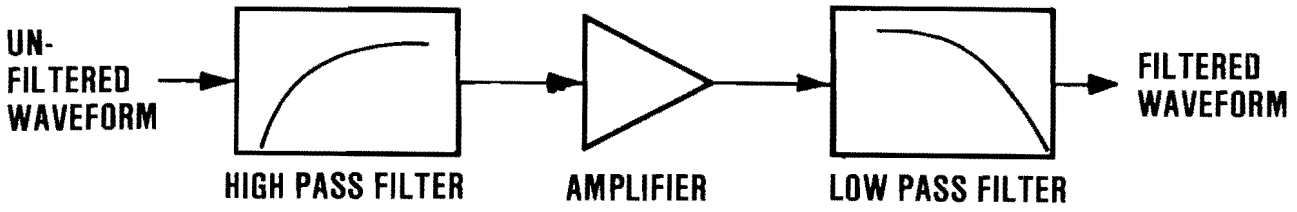

Figure 49. Filter System Block Diagram

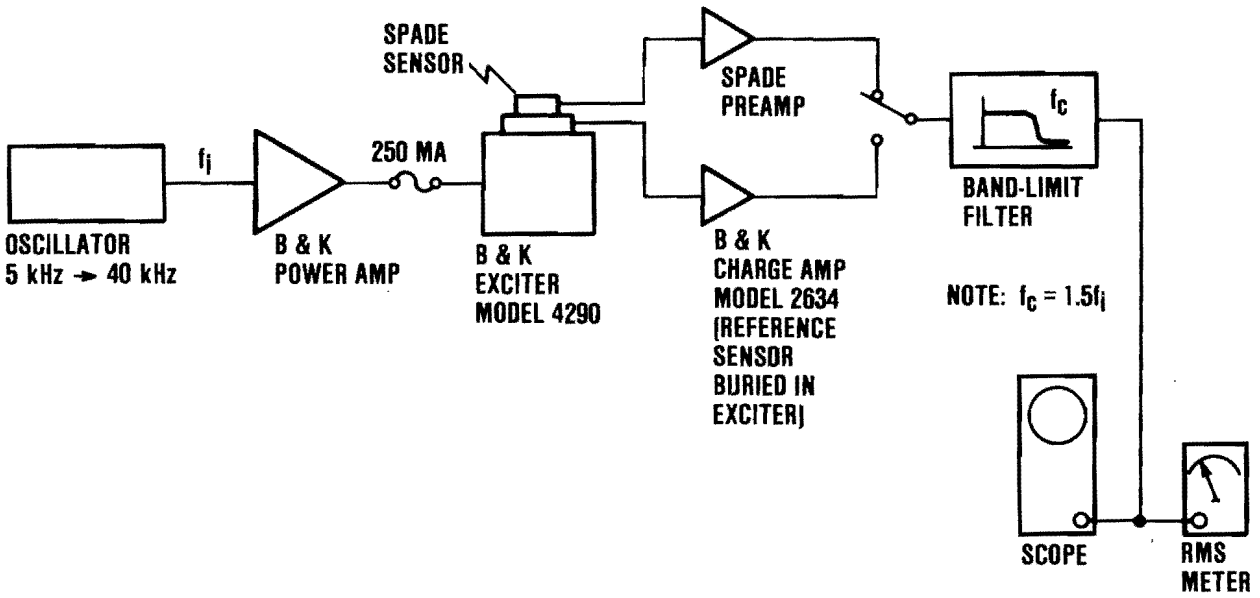

Figure 50. SPADE Accelerometer Test Setup

exciter drive signal due to the 56 kHz natural frequency of the exciter (particularly at 18.7 kHz (56/3) and 28 kHz (56/2)) did not yield measurement errors.

Results of the tests on vendor A sensors are shown in Figure 51. The four curves are plotted on an absolute scale. The frequency response of sensor threaded #1 has a pronounced effect on increasing the spread of the scatter. It is reasonable to assume that this sensor can be readjusted by the vendor to within the range of the other sensors. Even if this were done, the degree of scatter among these units indicates small probability of meeting the RCA specification requirements (±10 percent around a "specified" nominal curve). This accelerometer design failed to satisfy the SPADE sensor requirement.

The configuration of the vendor B sensor is shown in Figure 52.

Vendor B's six sensors exhibited substantially better performance than the vendor A units (see Figure 53). It is clear that the frequency response scatter is much tighter than for the vendor A's sensors. Nevertheless, these results also show that the Vendor B's accelerometers do not comply with the original RCA specification although their submitted test data indicates closer compliance than RCA's test, a result vendor B attributes to their superior reference accelerometer. (This latter claim is not supportable since the B&K sensor, whatever its departure from an ideal, flat response, is not responsible for scatter among six units tested.)

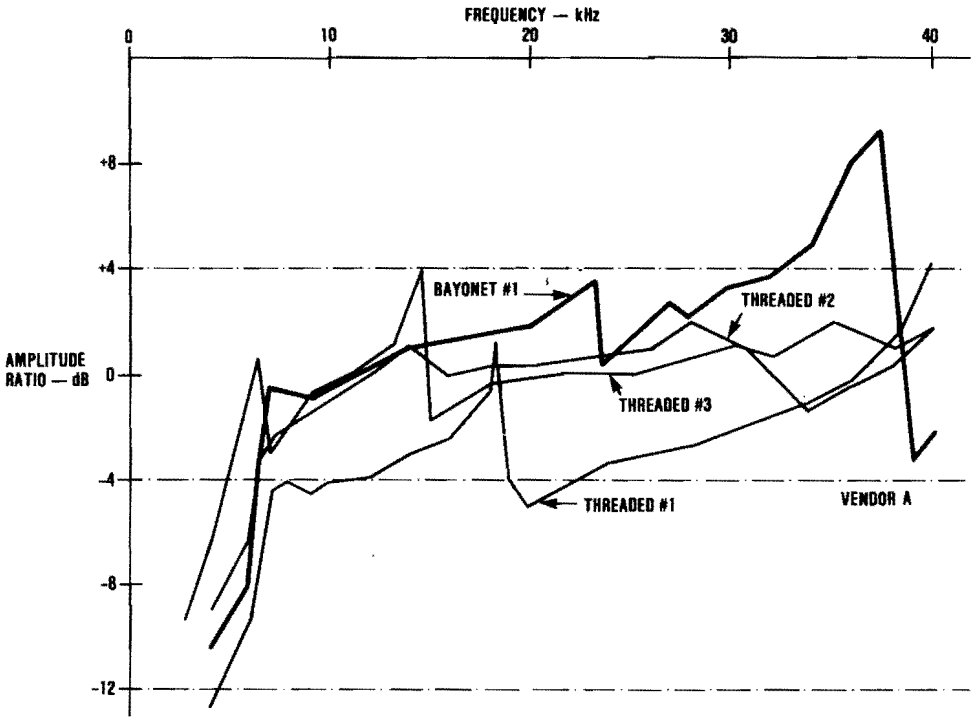

Figure 51. Frequency Response of Four Vendor A Sensors

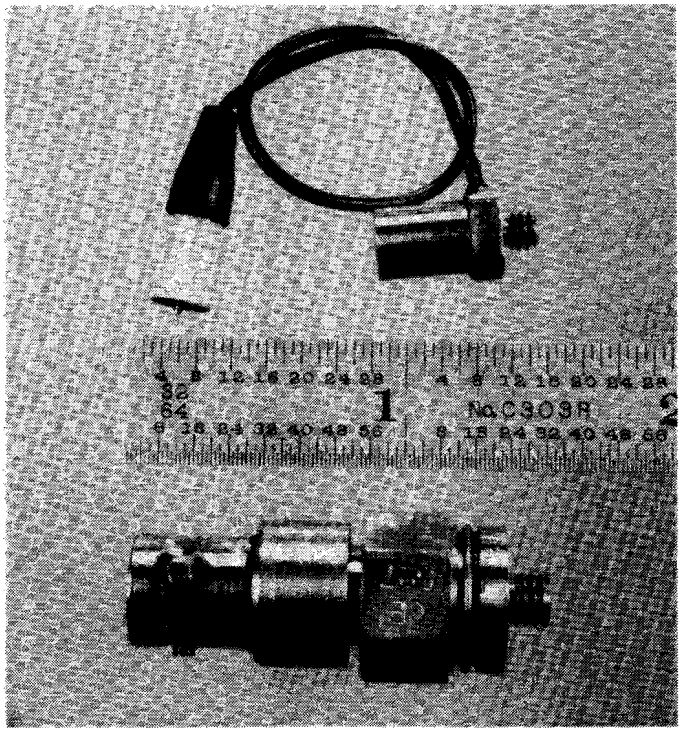

Figure 52. Vendor B's SPADE Sensor and Miniature Accelerometer

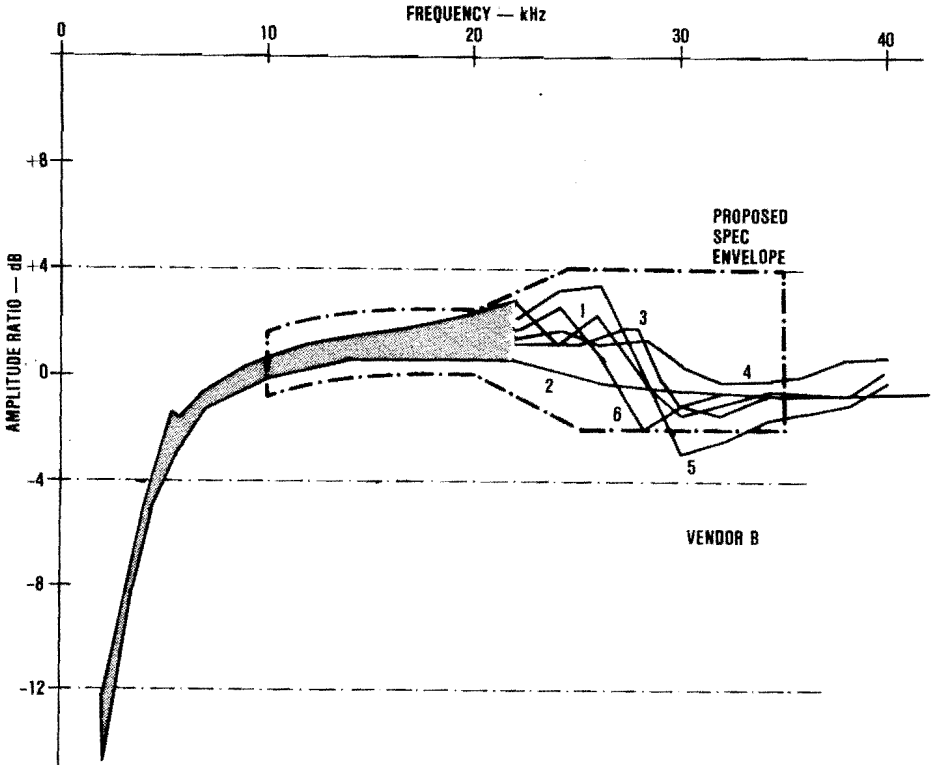

Figure 53. Frequency Response of Six Vendor B Sensors

The original sensor procurement specification was written prior to the PDR. Since then, the SPADE analyzer design using a resonant filter following the sensor was abandoned. This means that the test set can no longer compensate for an arbitrary "nominal" response. Rather, because of the use of a wide band of frequencies during data reduction, a sensor with a relatively flat frequency response is desired.

Accordingly, the specification was revised to reflect this change: to provide for control of the output down to 10 kHz and to accommodate the greater scatter at the higher frequencies. This new Specification RCB-003A is given in Appendix A.

Figure 53 depicts the proposed frequency response envelope incorporated into the new specification. (Five of the six Vendor B sensors satisfied this requirement.) These limits are not as tight as might be desired for a uniform response, but cost is a strong factor in this requirement since there are to be twenty sensors per test set. Accordingly, the specification change was carefully constructed to allow at least one of the two current vendors to comply without further development or production cost increases.

The acquisition of a B&K exciter afforded an opportunity to investigate the deviation of a sensor's response when it is mounted to the exciter table with

an intermediate mounting device rather than directly. (All preceding responses were taken with the sensor stud-attached to the table surface.) The various SPADE sensor mount configurations evaluated are shown in Figure 54.

All mount configurations were observed to cause gross distortion of the response, even for the most straightforward mount designs, as for example, a short pedestal. An example of this effect is seen in Figure 55 where a miniature accelerometer was tested using a direct mount, and a simple 1/2-inch cube mount.

A similar test on a SPADE prototype sensor (by Vendor B) is presented in Figure 56. Note that the greater mass of the SPADE sensor has grossly lowered the frequency of the resonance/antiresonance peaks and the peak amplitude, but the general character of the effect is the same as for the miniature accelerometer.

Thirdly, an example of the use of a special mount for OH-58 hanger brackets is shown in Figure 57. Again, the modification to the relatively flat response of the direct-mounted sensor is dramatic.

An offset aluminum mount with a SPADE accelerometer (by Vendor A) is shown in Figure 58. This combination exhibits the largest deviation of the group from the direct-mounted response.

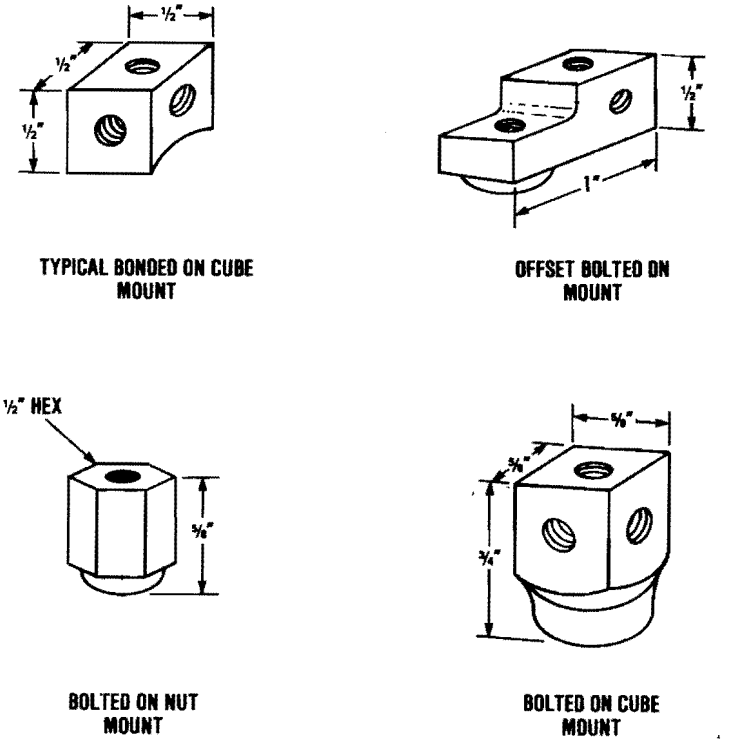

Figure 54. SPADE Sensor Mount Configurations

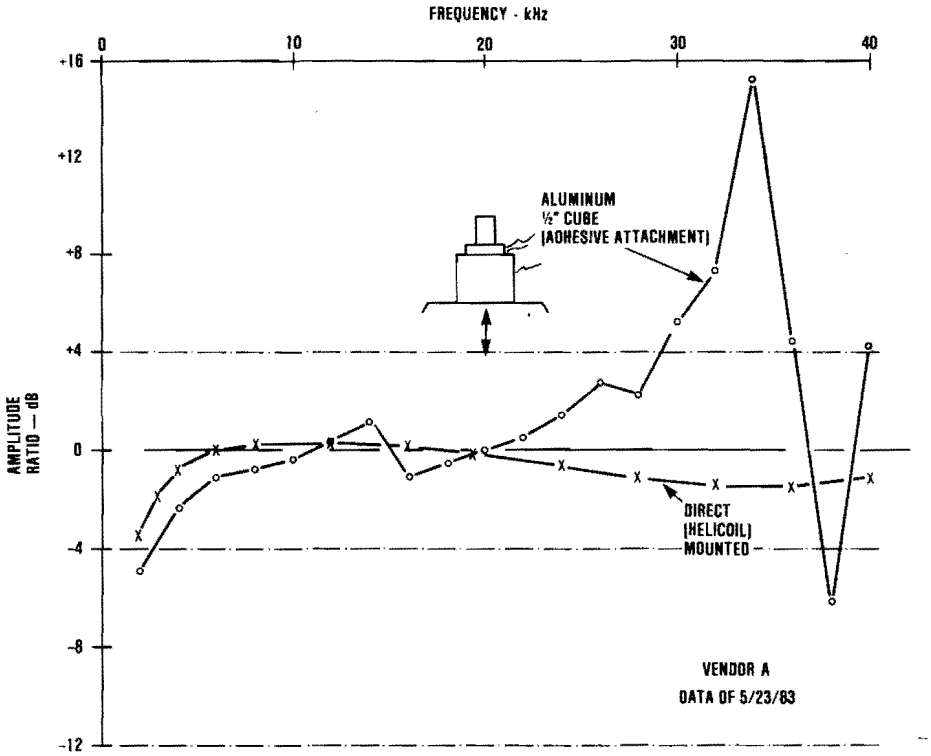

Figure 55. Effect of Simple Cube Mount on Accelerometer Response

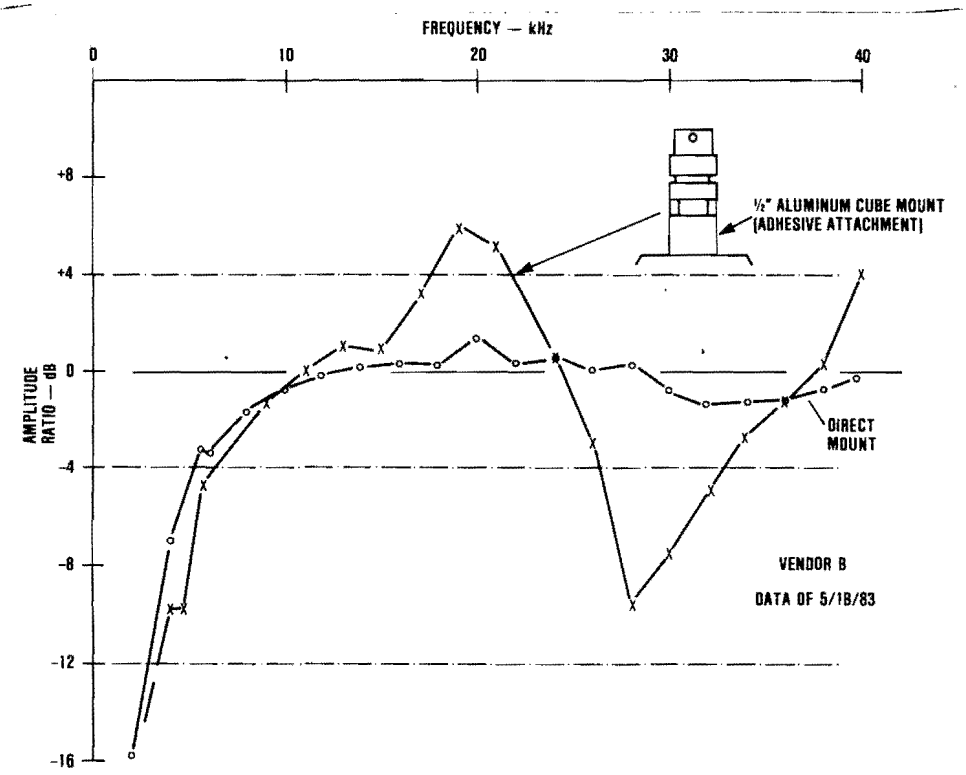

Figure 56. SPADE Sensor Mount Effect

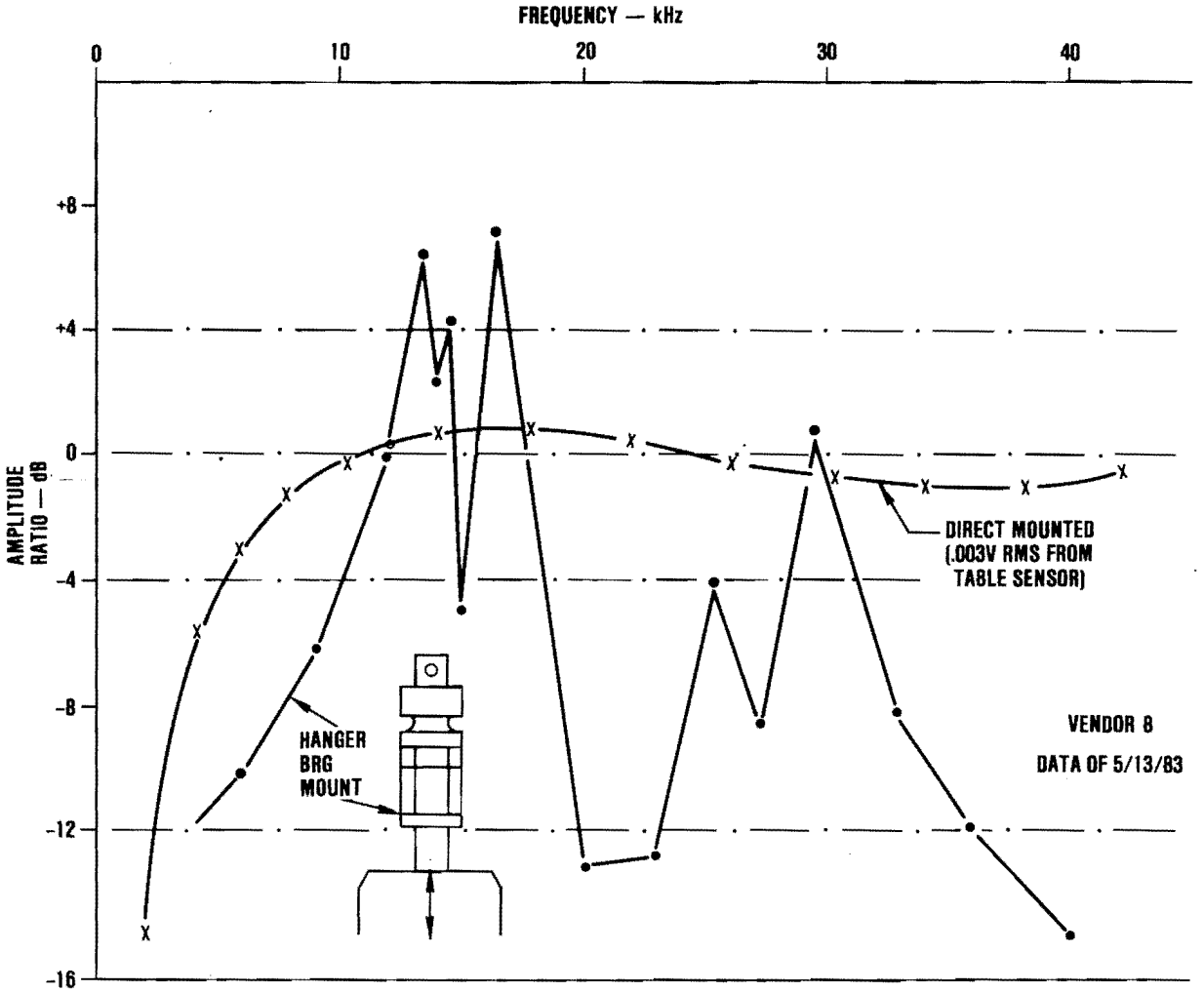

Figure 57. Hanger Bearing Mount

Consider also that these tests were run on a shaker (or exciter) whose actual motion was constrained by independent acceleration feedback to be constant over the test frequency span, i.e., reaction loads of the sensor-under-test were not allowed to alter the motion at the base of the mount. In the typical SPADE application, unless the mount is applied to a relatively massive structure, additional dynamic effects will be present between the vibration source (bearing flaw) and the sensor mount base.

Such results should not be construed to preclude the use of these mounts in bearing analysis applications, for there is almost certainly useful spectral power available notwithstanding the distortion of the frequency-domain response. Such plots serve primarily to alert the designer to the attenuation at certain frequencies that may be of interest in the application of pass/fail criteria.

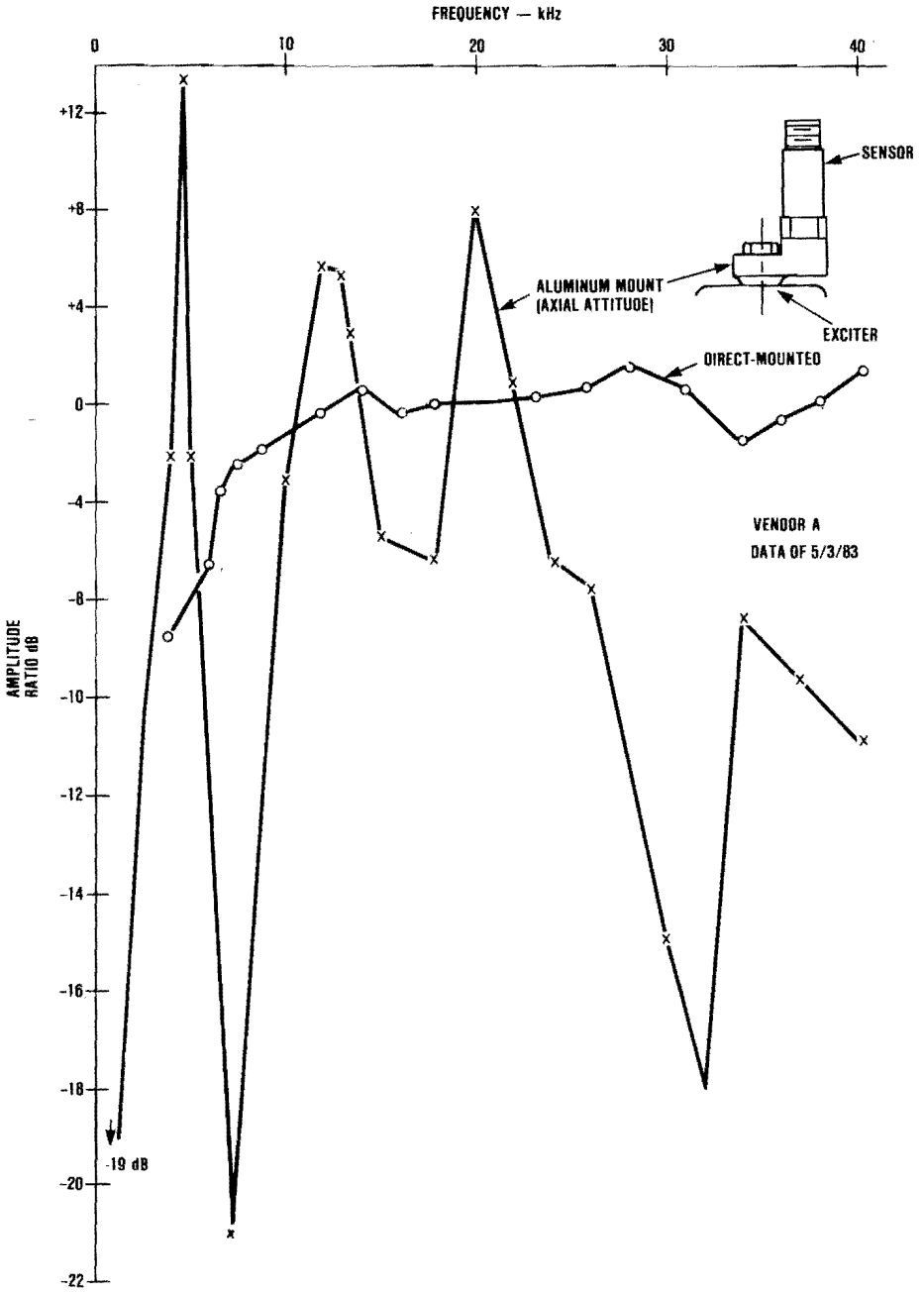

Figure 58. Offset Mount Response

5.1.4 Grounding, Shielding and Self-Induced Noise Minimization

In order to attain the best possible signal-to-noise ratio, careful attention was given to every technique that would achieve this objective. The areas that influence signal-to-noise ratios are cabling, front end design, circuit layout, decoupling and grounding. Each of these areas will be briefly addressed.

5.1.4.1 Cables

Two types of cables exist between the sensors and SPADE: a signal cable which interfaces with the sensors and a fan-out cable which interfaces the signal cable to SPADE. The signal cable consists of twelve shielded cables which are connected to mating ends of the fan-out cable. The fan-out cable contains twelve shielded cables enclosed in a braided shield which is returned through P1/J1 to the SPADE chassis.

5.1.4.2 Front End

The optimum amplifier configuration to minimize common mode noise is an instrumentation amplifier. This is the circuit utilized as the input stage for the multiplexed sensors. An instrumentation amplifier has excellent rejection of power supply noise as well as externally induced common mode noise on the signal cables. In the present configuration the front end instrumentation amplifier does not have both signal inputs wired to the selected transducer (as would be the ideal case) because of the requirement for additional multiplexing and control. Any future implementation of SPADE should include multiplexing of both signal leads to the instrumentation amplifier input.

5.1.4.3 Board Circuit Layout

Two printed circuit wiring boards were designed for the SPADE analyzer: the signal processor and MUX/ADCON. Both printed circuit wiring boards contain analog and digital circuitry. Careful board design and layout was undertaken to minimize any interaction between analog and digital signals. Both boards were designed for minimum interconnection lead lengths and optimum signal flow.

5.1.4.4 Decoupling

Standard analog and digital power supply decoupling techniques were employed on both boards.

5.1.4.5 Grounding

The MUX/ADCON board contains both analog and digital signals and their respective grounds. This board has a TRW flash converter where the analog signal is converted to a seven-bit digital output. As recommended by TRW, both the analog and digital grounds are tied together at the ground pins of the converter chip.

5.2 INITIAL SIGNAL PROCESSING

One of the critical requirements of the SPADE system, as pointed out in Section 4, is a linear response over the frequency range of the accelerometer. The linearity of the response must have a dynamic range of 50-60 dB. Before any processing for detecting bearing failures can begin,

the measurement chain must be checked for linearity. Possible sources of error are a saturated or defective accelerometer. A saturated accelerometer which may be caused by an extremely bad gearbox, or a defective accelerometer, are equally disruptive. A defective accelerometer discovered in a field test had given a signature which, after signal processing, appeared to indicate a bad bearing. As a result, the first step in the processing of accelerometer signals is a confidence test in the linearity of the chain. The test involves checking the signal before the band-pass filter and verifying that the signal is not saturated and that the signal has acceptable peak to average ratios.

5.3 SIGNATURE PROCESSING

This section describes the demodulation and fault signature processing which enhances the fault signature from the background clutter. As discussed in Section 4, this processing is implemented in three steps:

(1) Incoherent digital demodulation and the associated nonlinear filtering to recover the signal outlines from the raw data.

(2) Use of a matched filter to enhance the bearing pulses.

(3) Nonlinear filtering to remove pulses which are not bearing fault signatures.

These three steps are described in detail in the following sections.

5.3.1 Digital Demodulation of Bearing Fault Signatures

The demodulation technique implemented was incoherent demodulation. The signal was contaminated by large random spikes which complicated the demodulation process. A nonlinear filtering technique, a data cleaner (originated by References 3 and 4), was used with success. This filtering technique is described in the following paragraphs.

Figure 59 depicts a marginal signal case of a bearing fault implant where the fault signal was not discernible by eye. Clearly the signal contains a large number of random spikes. Figure 60 shows the bearing fault signal expanded in considerably more detail so that the nature of the spikes and the signal, in general, could be more closely examined. As shown by Figure 60 the 'noise' in the signal consisted primarily of complex sinusoidals rather than Gaussian noise. Also, the spikes appeared not to be directly involved in a

---

[3]Martin and Thomson, "Robust-Resistant Spectrum Estimation," Proceedings of the IEEE, Vol. 70 No. 9, Sept. 1982, pp. 1097-1115

[4]D. J. Thomson, "Spectrum Estimation Techniques for Characterization and Development of the WT4 Waveguide, Part I," Bell Systems Journal, Vol. 56, pp. 1769-1815, 1977

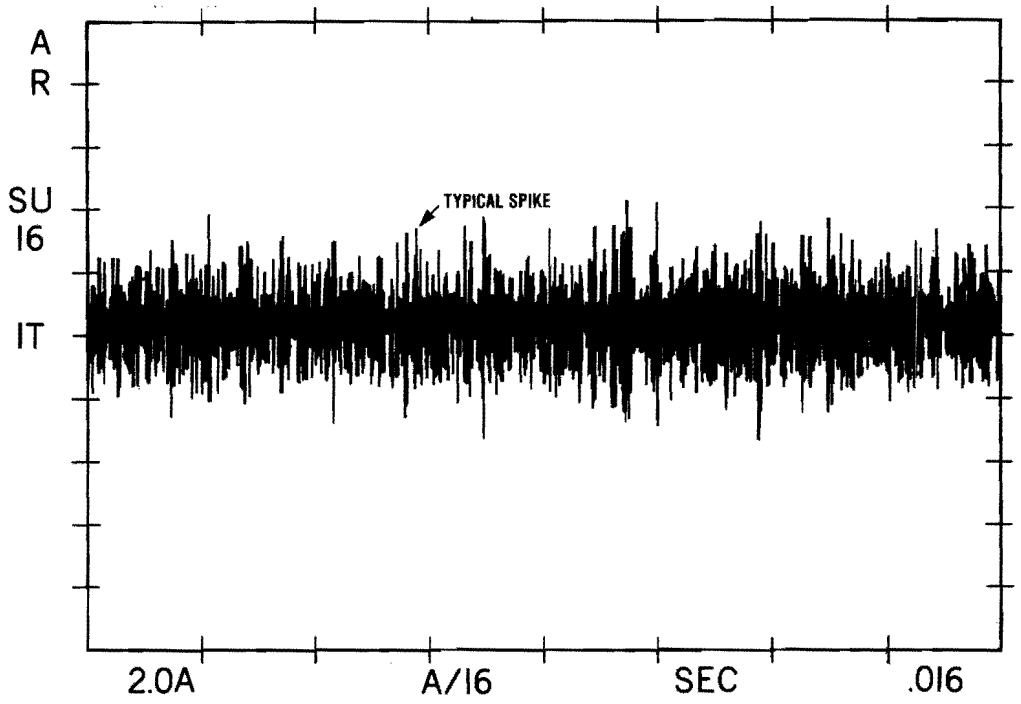

Figure 59. Marginal Signal Case

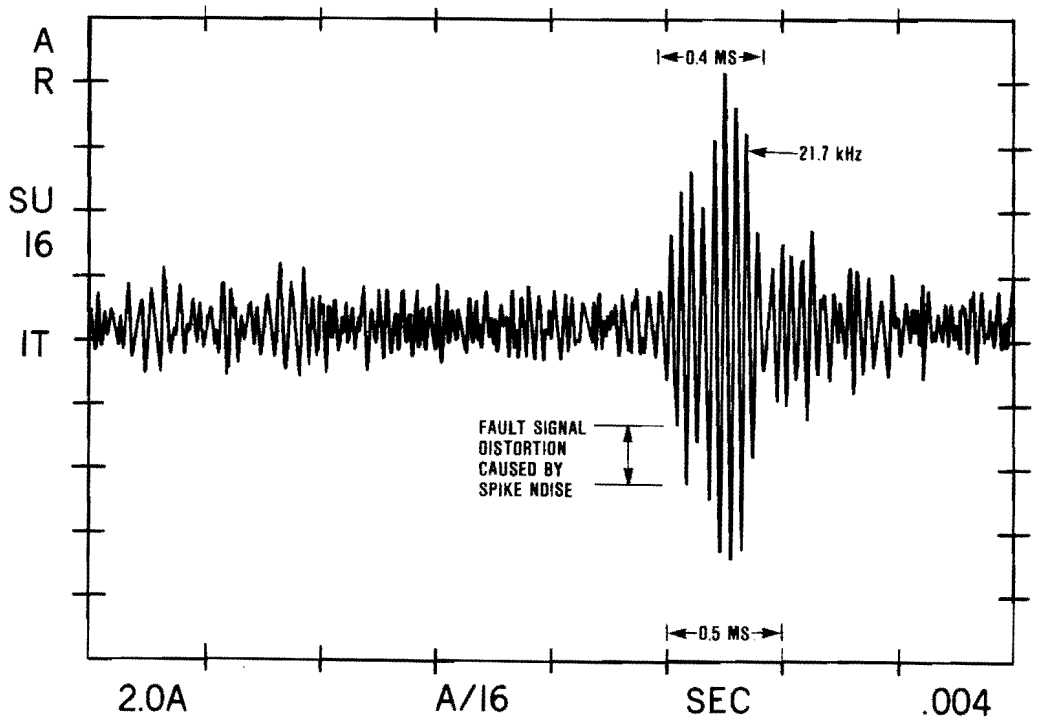

Figure 60. Expanded Signal

fault signature (it was established that a fault signature produced a demodulated pulse that was between 300-1200 microseconds in duration). The random spikes were due to the interaction of the various modes of the bearing fault signature. If the signal is envelope detected in its present state, then the spikes will be random and produce a large clutter component in the spectrum. The conventional approach is to narrow band-pass filter the signal so that only one mode is present. However, due to the complexity of a tunable filter as described in Section 4.2, a digital filtering approach was implemented in order to remove the spikes caused by the interaction of the modes of the bearing fault signature. As shown in Reference 5, a signal contaminated with glint noise has the same features as the spikes which were present in Figure 59. References 3 and 6 showed that considerable improvement in the spectrum could be obtained if the spikes were removed before the application of the spectral estimation procedure.

In order to improve the spectral estimation procedure, the signal was passed through a 'data cleaner' as described in Reference 7. The data cleaner is a nonlinear filter which passes the normal signal while eliminating the unwanted signal. The process is the same as adaptive interference cancellation except that interference in this case is a random signal. The critical requirement for achieving this improvement is to have the algorithm recognize the signal in the presence of noise, and the success of accomplishing this feat determines the effectiveness of the process.

The basis for this algorithm will be explained using Figure 61. In this figure, two signals and their respective spectral components are depicted. Signal A is a random signal, Signal B is a sinusoidal component, and Signal B is much smaller in amplitude than Signal A. As shown in the figure, there will be some variance in the spectral estimation process. Now let us assume that the two signals are added together and the spectrum is as shown in the combined case of the figure. The sinusoidal Signal B, if sufficiently small, may not be visible in the spectrum because its amplitude may not be above the variance in the random Signal A. In cases where the variation reduction is 1/N (as in the averaging of FFT power spectrum), the variation reduction has a diminishing return as N becomes larger. (For example, an averaging limit of 16 times in the power spectrum limits the reduction in the power spectrum to 1/16.) Therefore, the more the random Signal A can be eliminated by a nonlinear filter (data cleaner), the better the resolution of Signal B.

As noted earlier in this report, the effectiveness of the nonlinear filtering operation is directly related to the ability of the filtering algorithm to

---

[5]D. J. Thomson, "Spectrum Estimation Techniques for Characterization and Development of the WT4 Waveguide, Part II," Bell Systems Journal, Vol. 56, p. 1993, Figure 8, 1977.

[6]Martin and Thomson, op.cit., p. 1109, Figures 14-17.

[7]Martin and Thomson, op.cit., p. 1111, Figure 27.

identify signal versus unwanted noise. In the bearing fault detection problem, fault signatures are 300-1200 microseconds in duration, which is much longer than the random spikes. The algorithm used to accomplish this task is shown in Figure 62 and the block diagram is shown in Figure 63.

The block diagram shows the nonlinear filter embedded in the incoherent demodulator. The nonlinear filter is based upon the observation that a large spike is of limited time duration so that eliminating the smallest element in the chain will eliminate the spike. The length of the chain was chosen so that the transition time through the Z^{-1} delay elements was small compared to the length of a fault signature; thus, the fault signature would pass through relatively unchanged. The linear smoothing filter is employed to smooth out the discontinuities resulting from the 70-20 kHz data rate reduction of the nonlinear filter. A matched filter was employed to further enhance fault signatures for analysis downstream. The effectiveness of this process is illustrated by Figures 64 through 69 where the same raw input

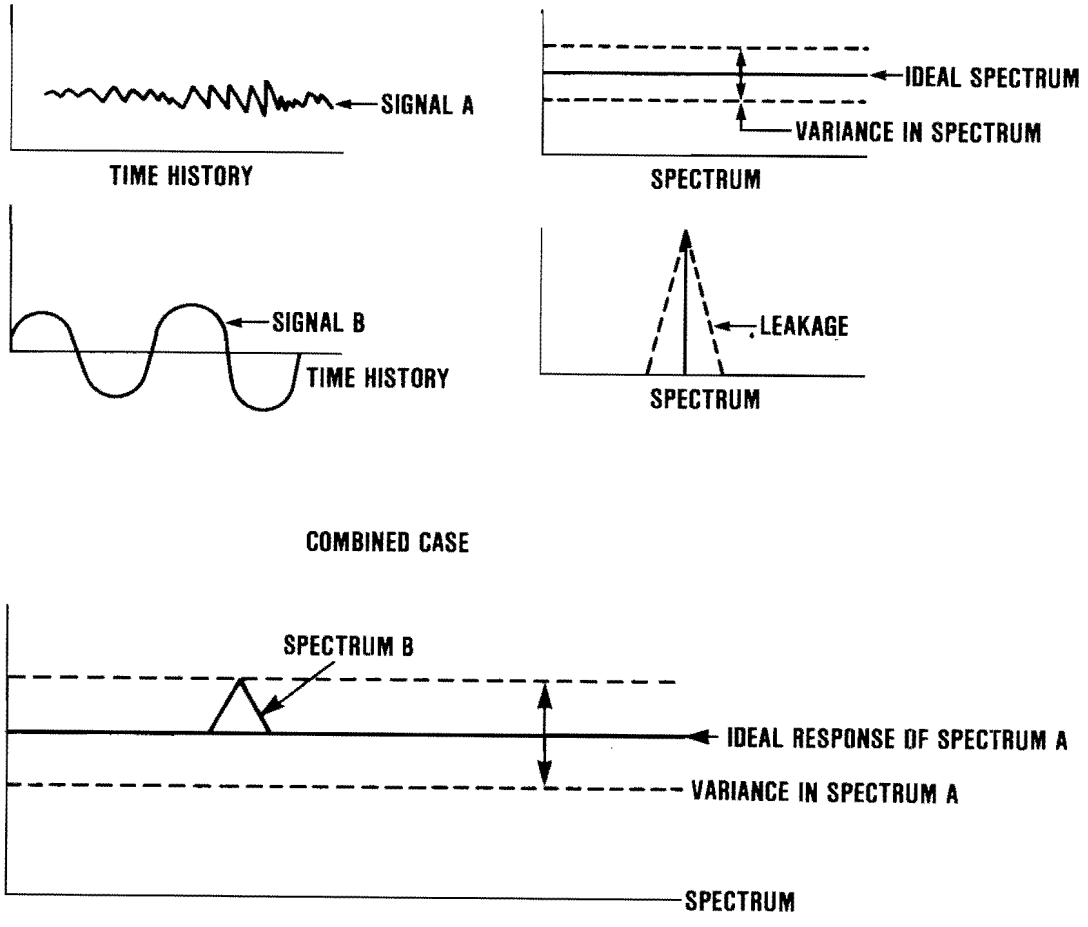

Figure 61. Data Cleaner Example

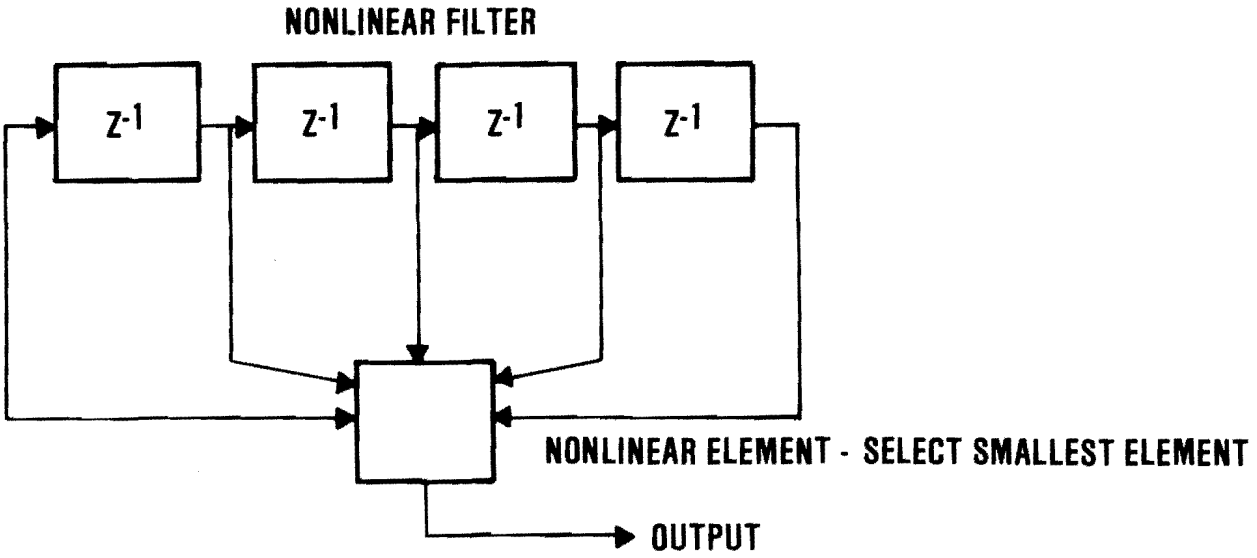

Figure 62. Nonlinear Filter Algorithm

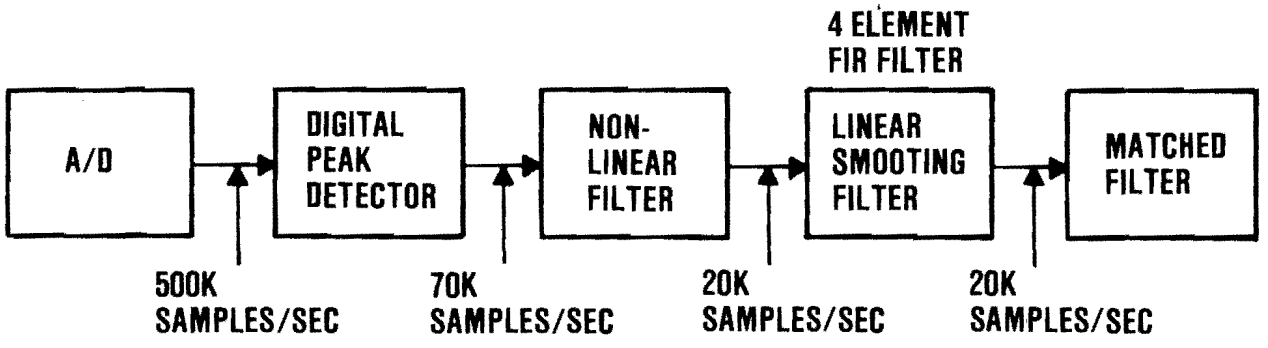

Figure 63. Block Diagram of Nonlinear Filter

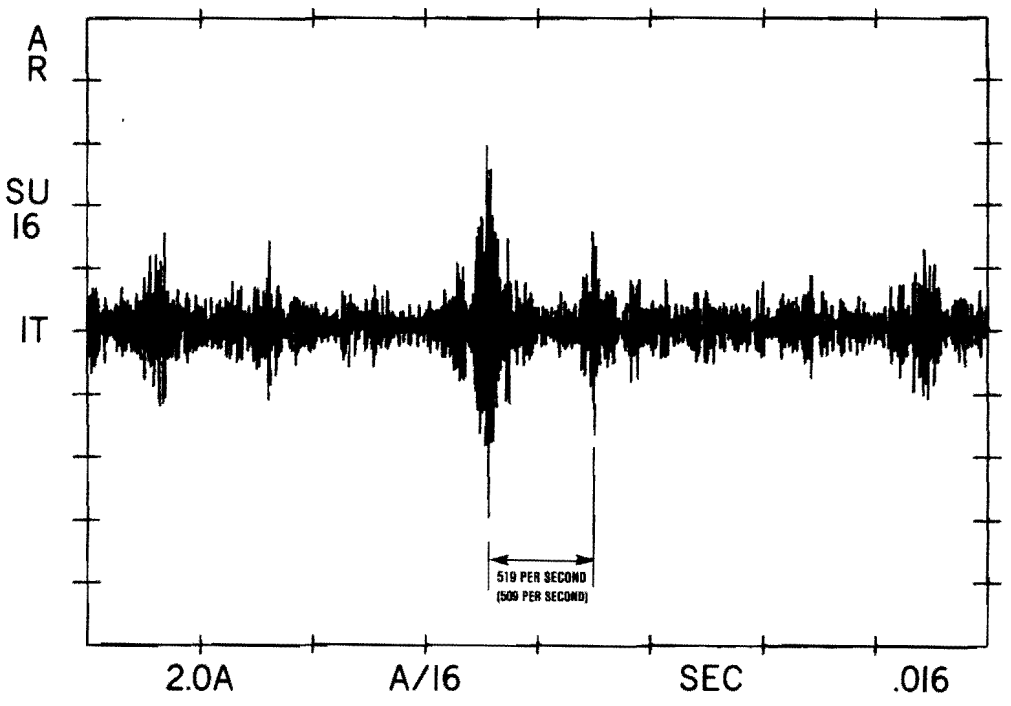

Figure 64. Raw Signal

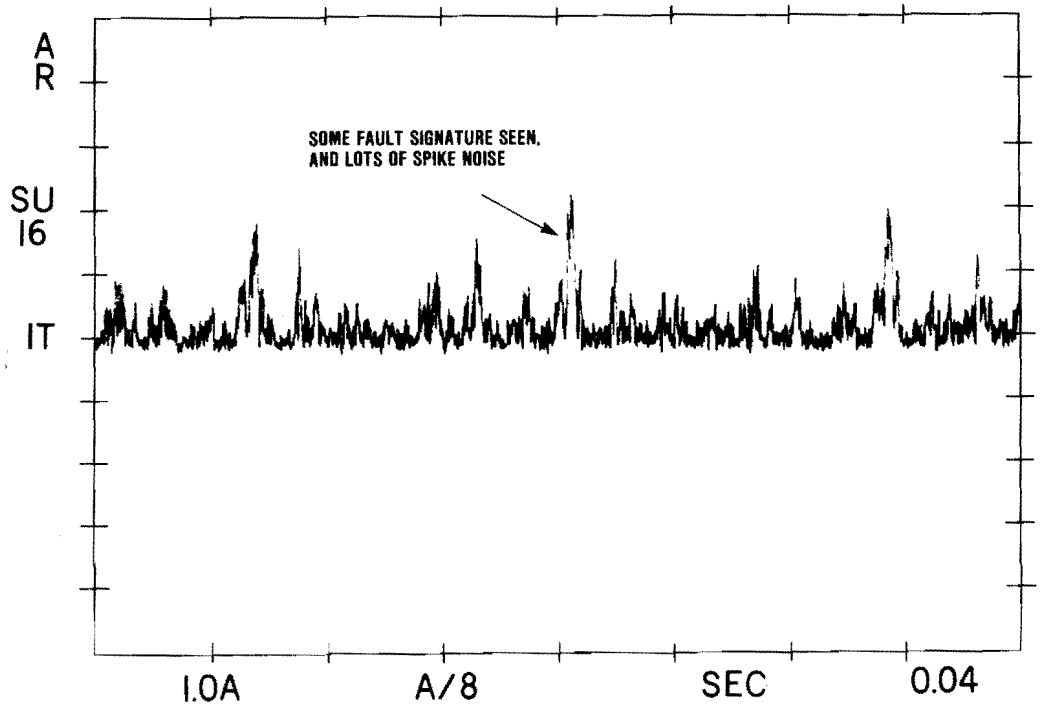

Figure 65. Digitally Demodulated Signal

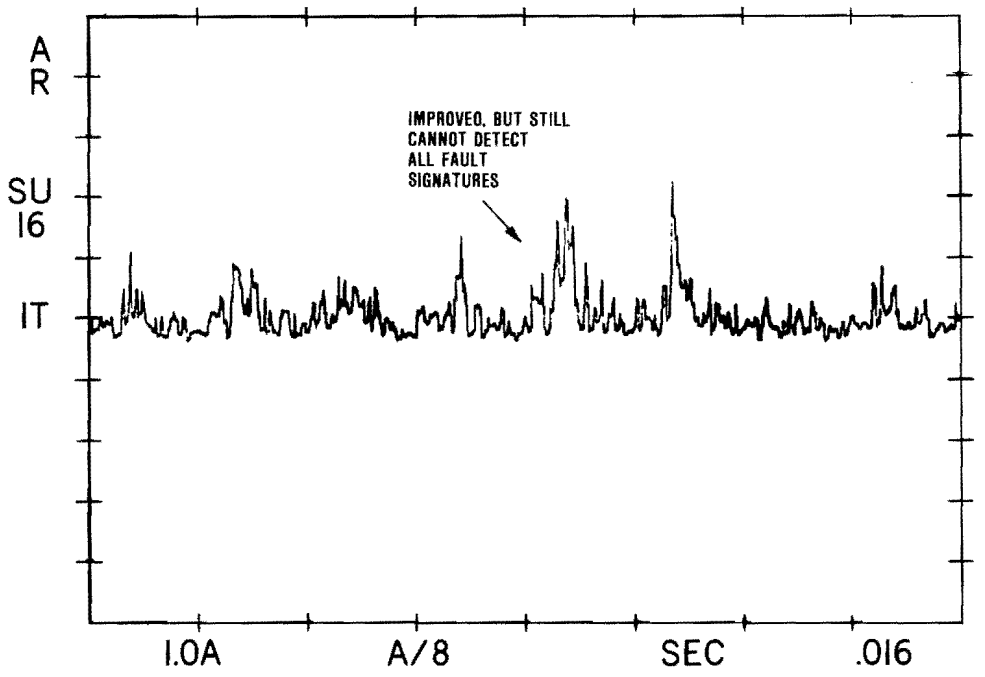

Figure 66. Output of Nonlinear Filter

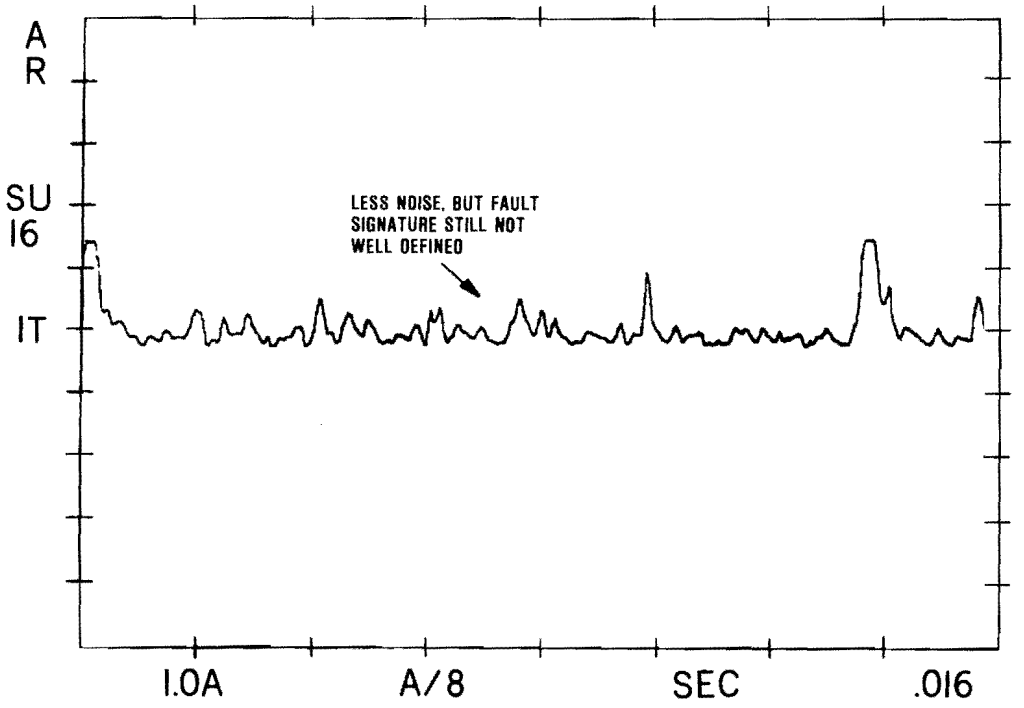

Figure 67. Output of Linear Filter

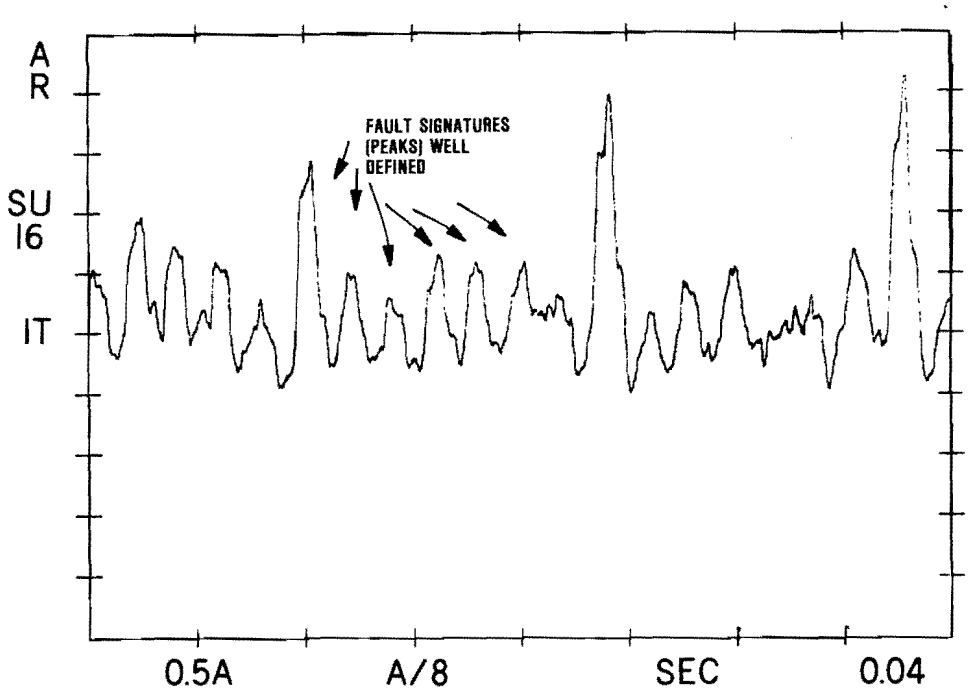

Figure 68. Output of Matched Filter

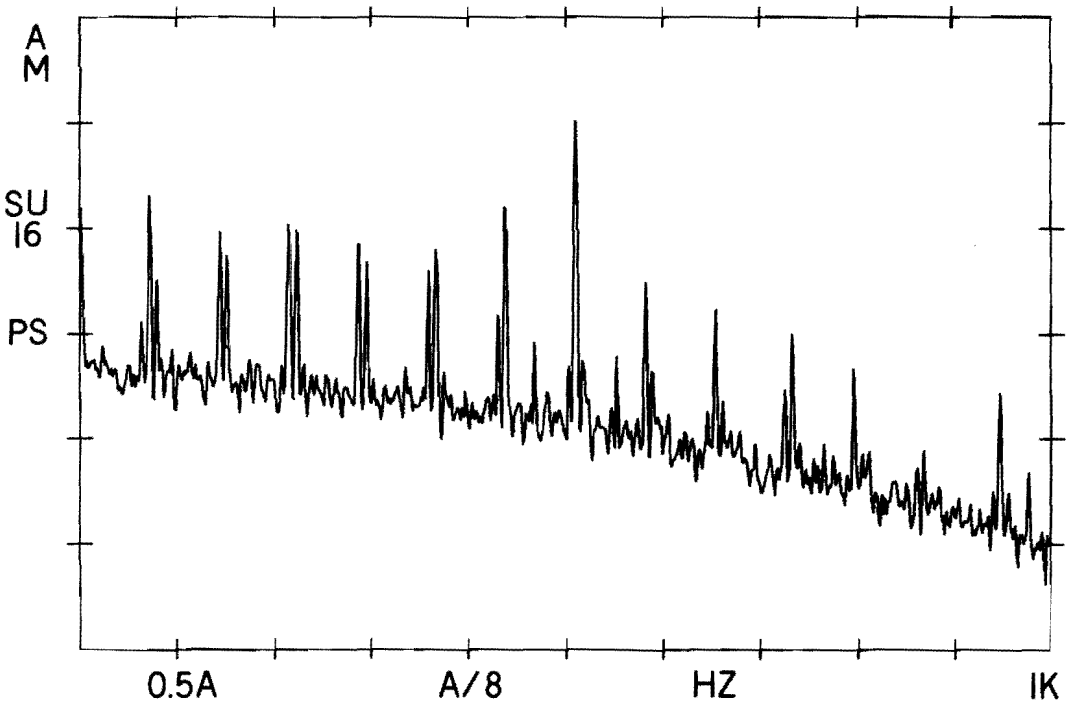

Figure 69. Demodulated Spectrum

signal, shown in Figure 64, is traced through the various process steps. As can be seen by comparing Figures 64 and 68, a significant signal-to-noise ratio improvement has been achieved.

An example of the increase in spectral resolution achievable with this process is shown in Figures 70 and 71. Both represent the spectrum of the same raw signal (Figure 64) except that the spectrum in Figure 71 has been processed with the nonlinear filter. As shown in Figure 71, there are spectral lines which became observable after applying the nonlinear filtering process which were not observable from simple demodulation.

5.3.2 Matched Filtering

This section describes the use of a digital matched filter to detect transient ring pulses caused by bearing defects. In a previous section the nature of the transient pulses as well as their causes were described. The pulse, after being processed by incoherent demodulation, nonlinear filtering, and linear smoothing, results in a waveform as shown in Figure 68.

The role of the matched filter in the detection process, as illustrated in Figure 72, is to enhance the bearing fault pulse from the noise environment. The decision element following the matched filter is nonlinear, and hence the enhancement features provided by the matched filter are essential to the performance of the decision element. The detailed performance of these

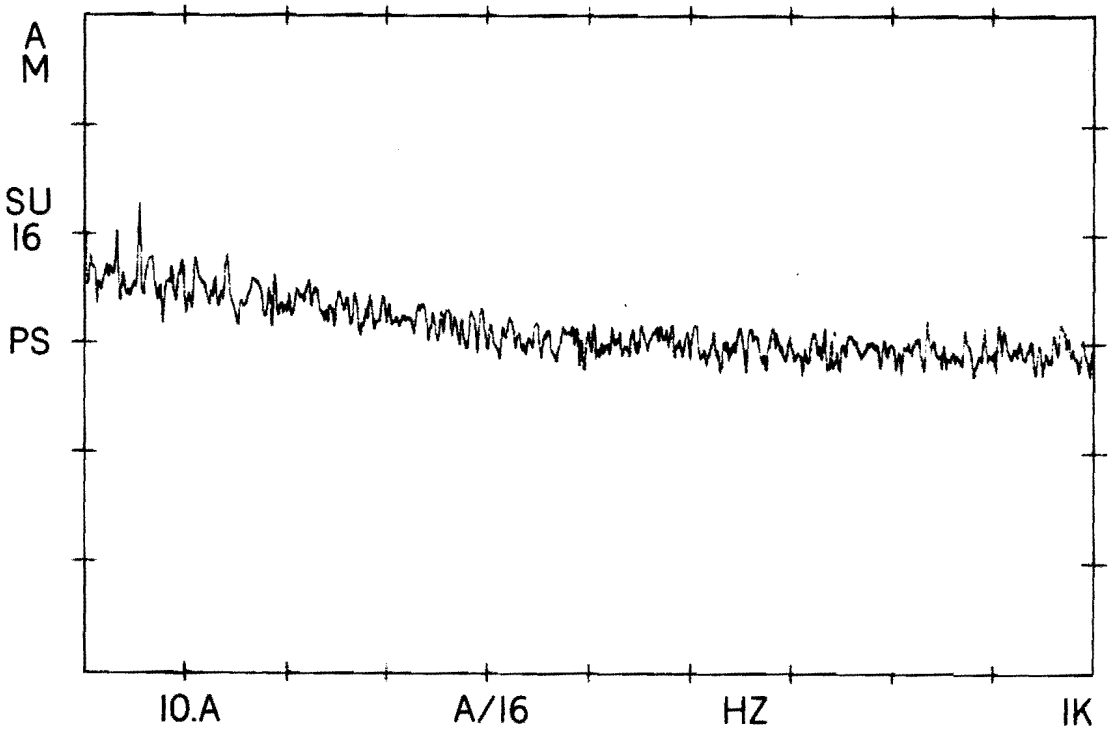

Figure 70. Spectrum due to Simple Demodulation

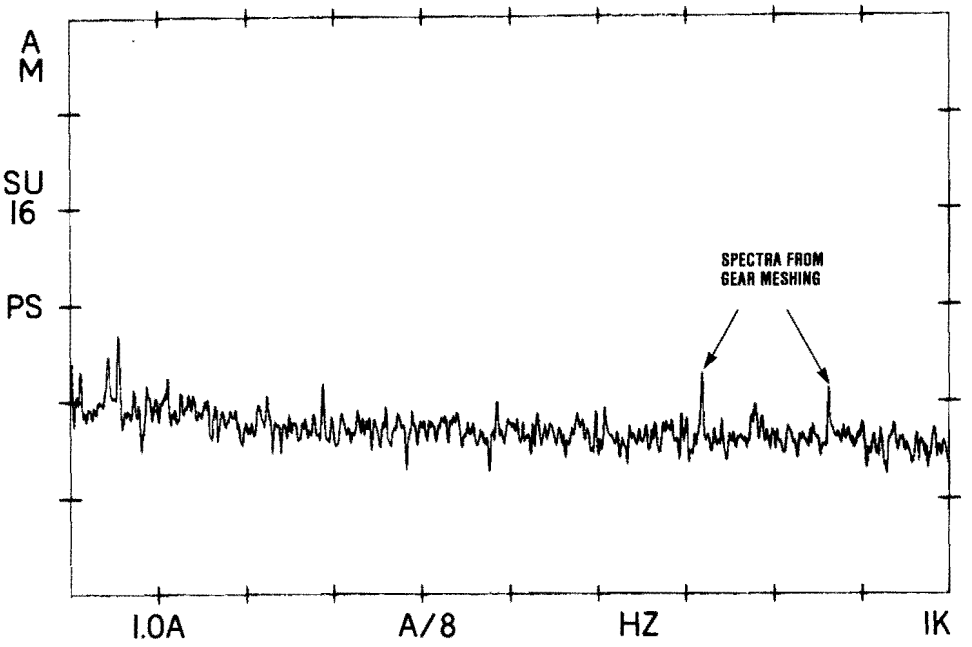

Figure 71. Spectrum due to Nonlinear Filtering

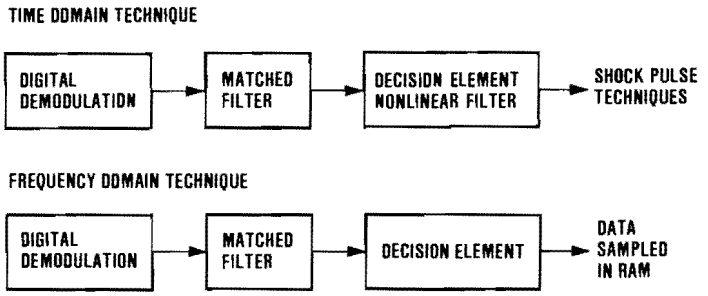

Figure 72. Matched Filtering Application

modules will be discussed in the following paragraphs, and the concept of a matched filter will be defined. A general background on the subject of matched filters can be found in Reference 8.

A matched filter is one which maximizes the signal-to-noise ratio for a given signal and a given noise source. The noise in the system consists of sources other than white Gaussian noise. However, for this study the noise source was considered Gaussian and excellent results were obtained with this assumption. A matched filter which is designed for white Gaussian noise has the property that the time reversed pulse shape is the impulse response of the matched filter. An example of this property can be seen in Figure 73.

---

[8]DiFranco and Rubin, Radar Detection, Prentice Hall, 1968.

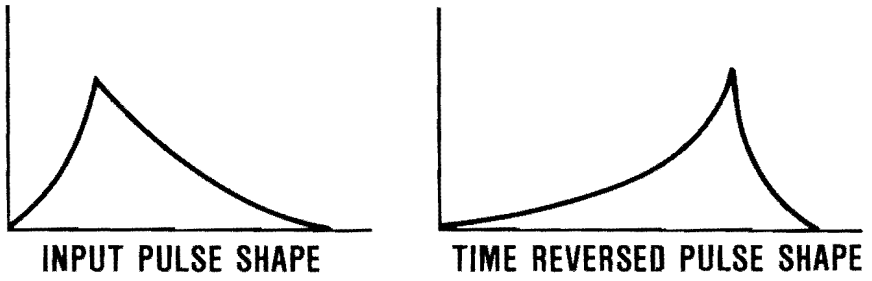

Figure 73. Impulse Response of a Matched Filter

This property makes matched filters which are realized by Finite Impulse Response (FIR) filters easy to implement.

The first step in the design of a matched filter is to define the reference pulse. Unlike a typical communication problem, the bearing fault pulses are not deterministic. Bearing fault signatures have a somewhat random shape and time duration due to factors such as the possible phase reversal described in Section 2.2. Hence, the reference pulse is not uniquely defined but rather requires some subjective evaluation. The most important parameter of a bearing fault pulse is not the actual shape of the pulse but its time duration. Therefore, a square pulse of a time duration of 1200 μsec was adopted as the reference pulse. The square reference pulse shape, while not optimum, was a good compromise in that further attempts at optimization would only lead to a marginal increase in performance.

Due to aliasing considerations, the sampling rate of the matched filter was set at 20 kHz (50 μsec sampling intervals). A 1200 μsec reference pulse required 25 elements in the FIR implementation. Due to the uniform weighting of the waveform resulting from the selection of the square reference pulse, the matched filter could be simplified to the following form.

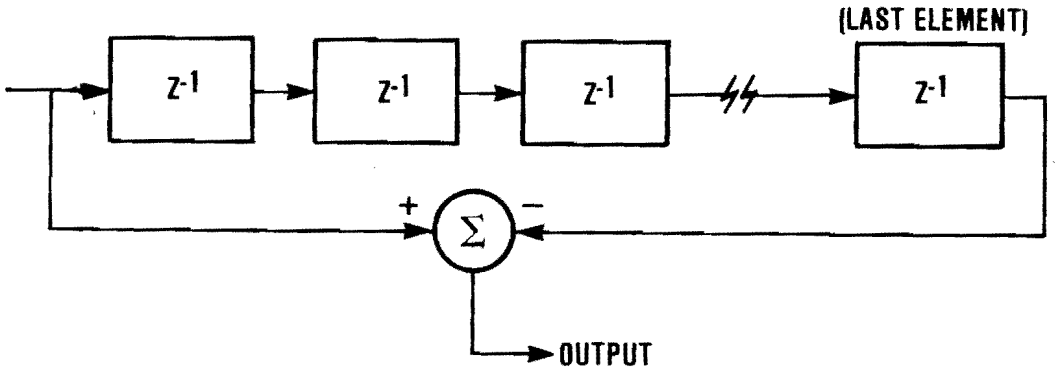

In this implementation of the matched filter, the initial state is important and hence the filter's delay elements must be initialized to zero before execution.

Performance results of the matched filter can be seen in Figures 74 through 78. In Figure 74, the reference input waveform into the matched filter represents the signature for an inner race fault where the ball-pass frequency was 503 Hz. Since the fault is an inner race type, the signature has large pulses every time the shaft rotates into the load zone. These large pulses are evident in Figure 74. Figures 75 and 76 show the time and frequency response for an 800 μsec matched filter and Figures 77 and 78 show the time and frequency response for a 1500 μsec matched filter. As can be observed in Figures 74, 75 and 77, matched filtering enhances the signature of bearing faults and the 800 μsec matched filter was considerably better than the 1500 μsec matched filter. Also, note that the matched filter is a linear filter and does not directly affect the frequency components of the fault signature, as can be seen in Figures 76 and 78. The nonlinear properties of the decision element are responsible for improving the frequency component definition.

5.3.3 Pulse Width Identification

This section presents the details of the decision element module which processes the waveform from the matched filter for both the time domain and frequency domain analysis. The decision element is a nonlinear filter which is designed to pass known good signals and reject known bad signals. The technique is similar to the concept of the data cleaner which was introduced earlier. The data cleaner approach was utilized to filter out large amplitude

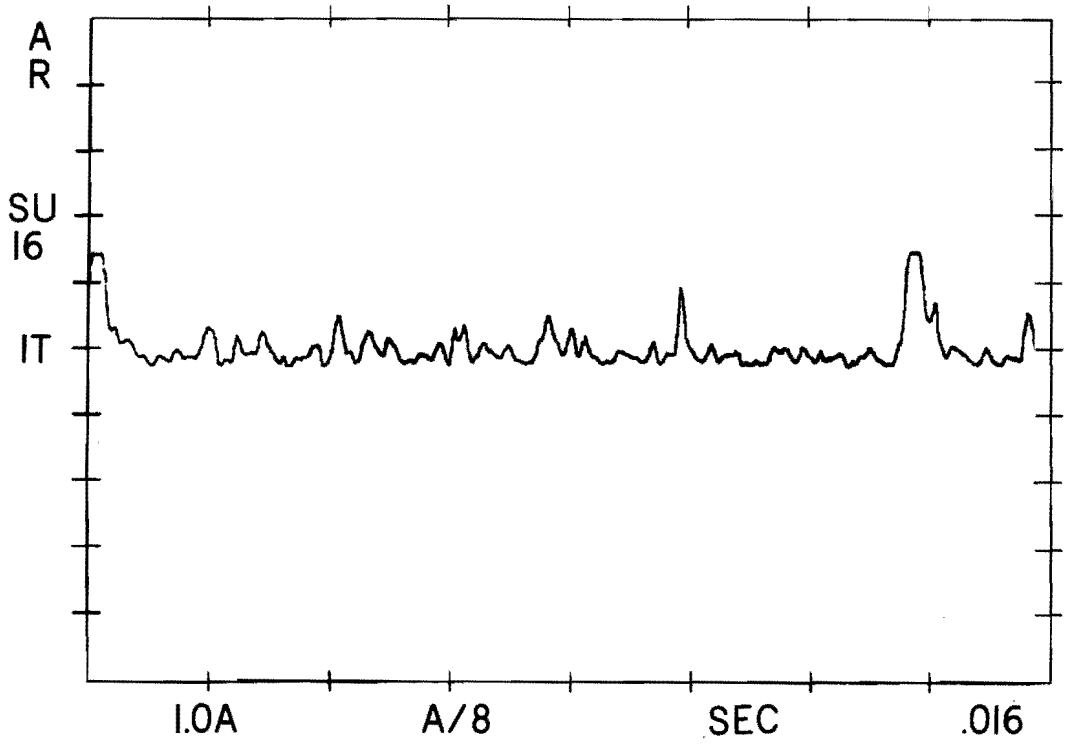

Figure 74. Input into Matched Filter

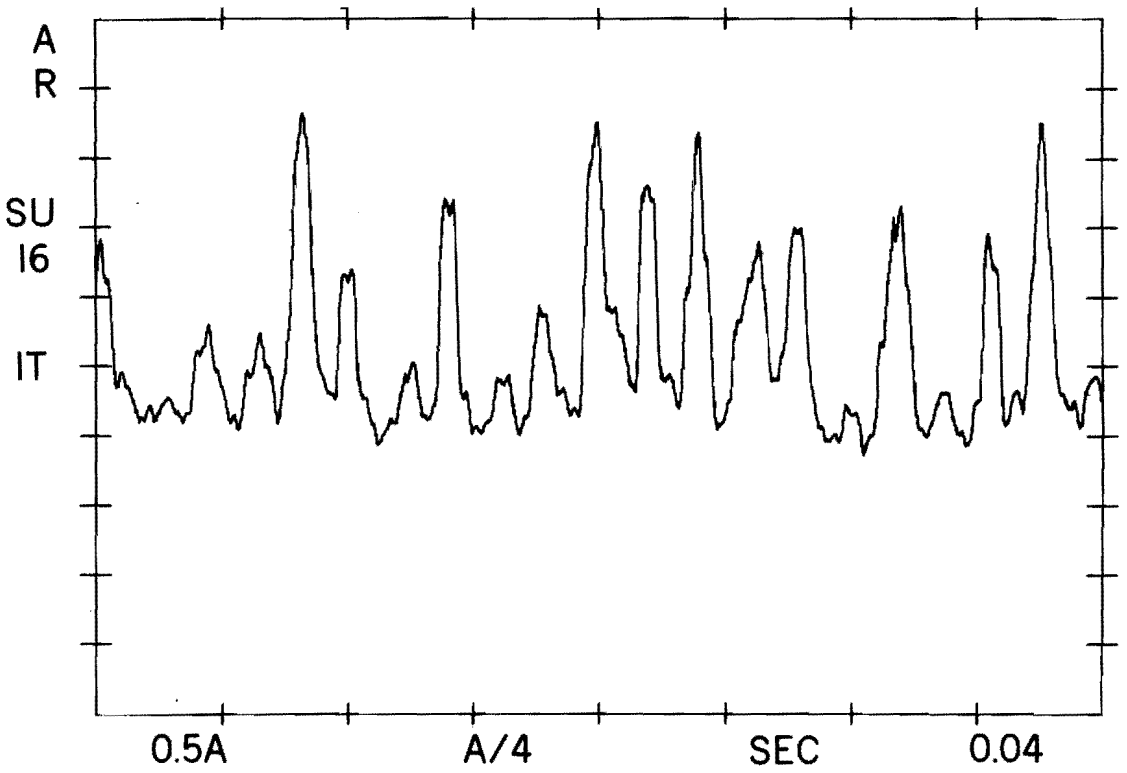

Figure 75. Output of 800 μsec Matched Filter Time History Response

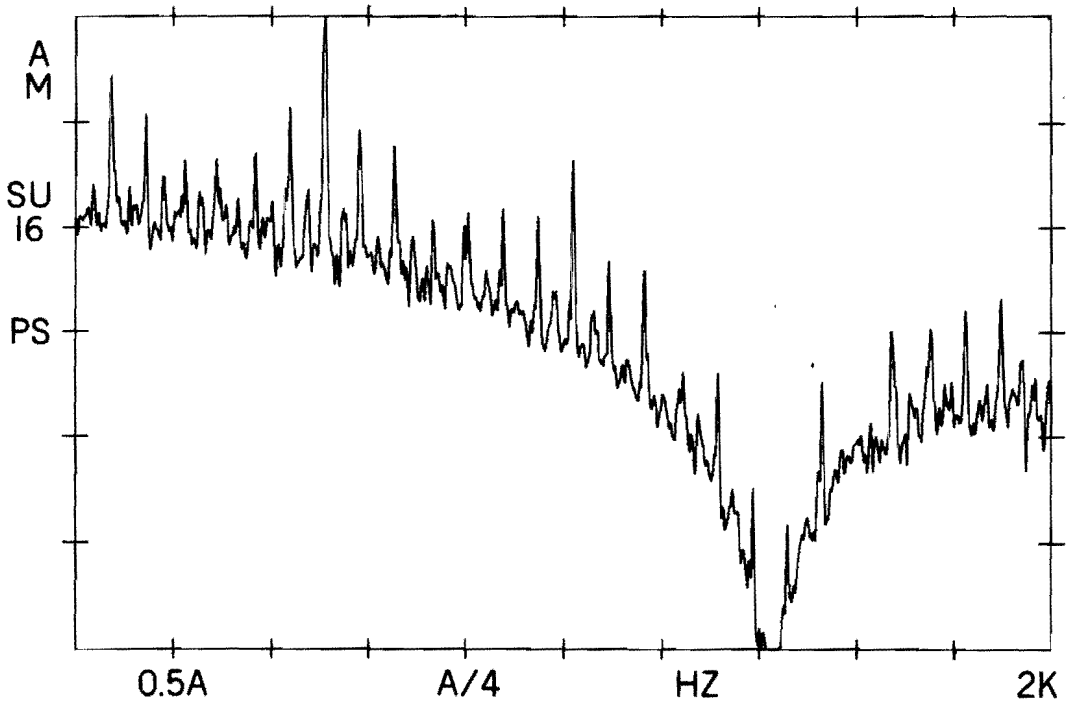

Figure 76. Output of 800 μsec Matched Filter Frequency Response

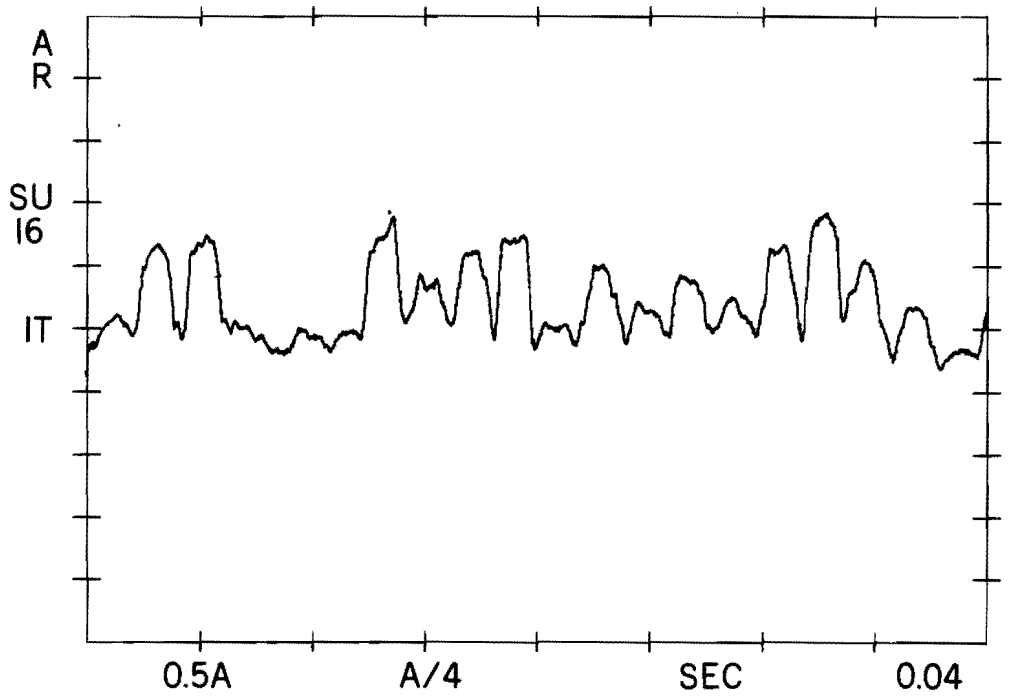

Figure 77. Output of 1500 μsec Matched Filter Time History Response

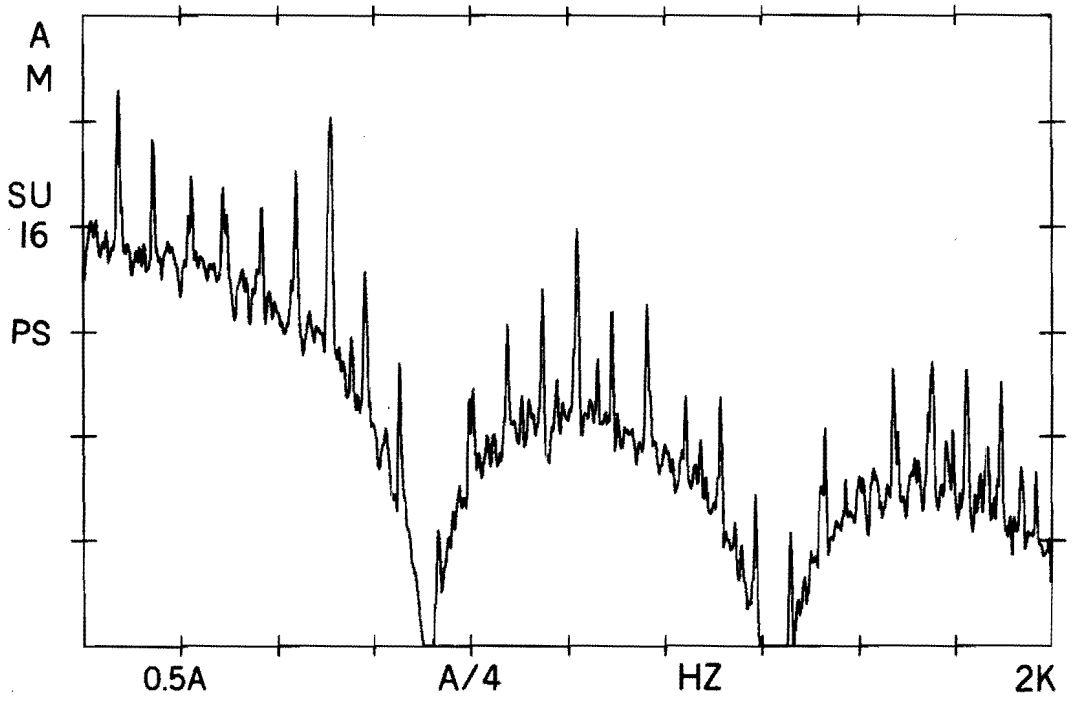

Figure 78. Output of 1500 μsec Matched Filter Frequency Response

random spikes in the time domain. In this application, the data cleaner is designed to filter out pulses which do not have time durations of a specified length.

The parameter which is used for the decision element data cleaner is the pulse duration or more precisely the measurement of the rise time of the pulse. As stated earlier, the criterion for bearing failure signatures has been a pulse of 300-1200 μsec time duration. These pulses appear at the matched filter output with rise times which do not exceed 1200 μsec. If other consistent information was known about the bearing signatures (information regarding a single signature), then this information could also be incorporated into the algorithm. The algorithm used to perform this data cleaning is illustrated in Figure 79.

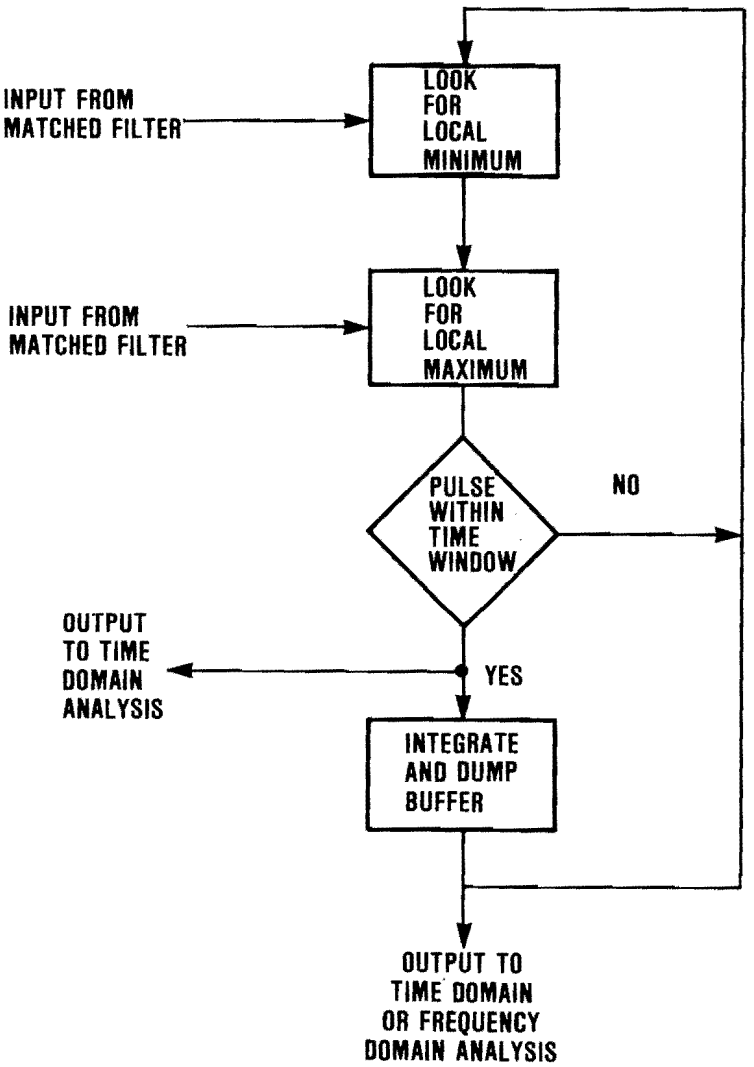

Figure 79. Flowchart of Decision Element Data Cleaner

The procedure illustrated by Figure 79 has been implemented in the following manner. Data is sampled from the matched filter until a local maximum is found. A pulse is then determined to exist of a magnitude equal to the difference between the pulse maximum and the pulse minimum. Next the rise time (defined as the time difference between the minimum and the maximum) is checked against a lower limit of 250 μsec and an upper limit of 1200 μsec. If the pulse rise time is in this window, then the pulse is accepted as a signature which might be a valid bearing signature. Otherwise the pulse is discarded as not being valid. The data describing a valid pulse are input to an integrate and dump circuit which integrates the pulse energy over a given time duration. This step also serves as a down sampling mechanism for the data which is to be converted to the frequency domain by an FFT algorithm. Some practical applications of this data cleaning process can be seen from three examples.

(1) The first case illustrates how gear-mesh noise can be suppressed. Figure 80 shows the demodulated band-passed signal of a gear fault. The fault signature in this figure is quite different from the fault signature associated with bearing faults. Figure 81 shows the spectrum of the demodulated signal without the digital processing. Figure 82 shows the spectrum of the demodulated signal after digital processing to suppress the unwanted signature. A comparison of Figures 81 and 82 clearly depicts the ability of the digital processing to suppress the gear fault noise. Similarly, a case in which the gear-mesh noise and a bearing fault are combined is shown

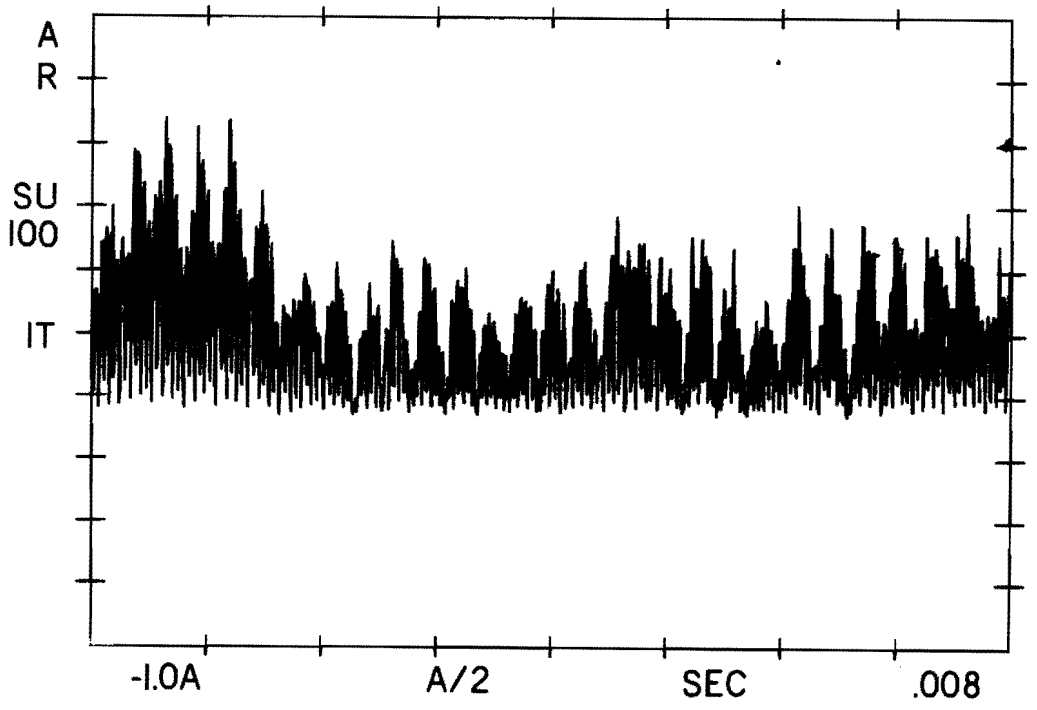

Figure 80. Demodulated Band-Passed Signal of a Ring Gear Fault

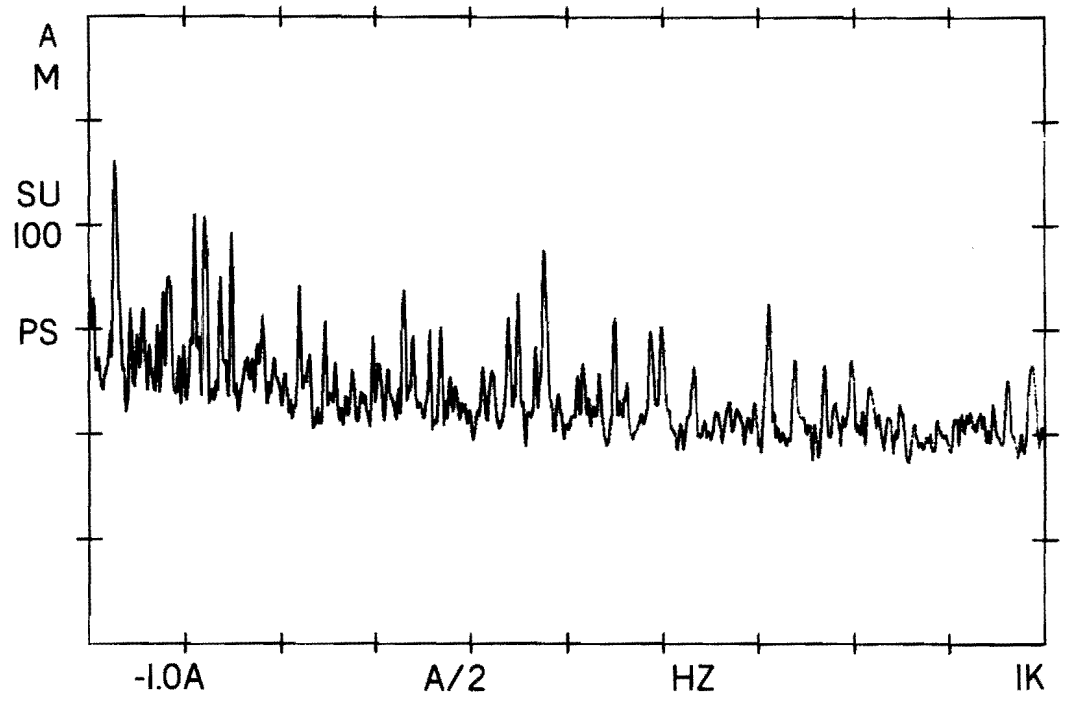

Figure 81. Unfiltered Spectral Response

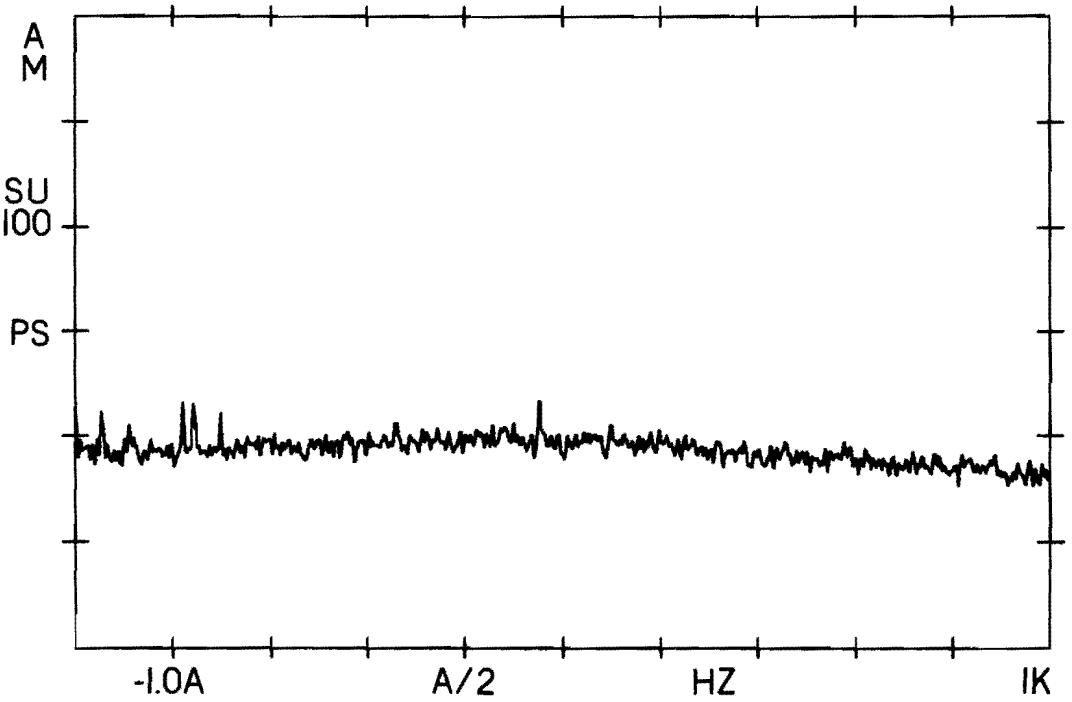

Figure 82. Filtered Spectral Response

in Figures 83 and 84. The digital processing in Figure 83 was optimized (250 μsec matched filter) for detecting the gear-mesh noise. The digital signal processing in Figure 84 was optimized (1200 μsec matched filter) for detecting bearing fault signatures. As can be seen in the comparison, the gear-mesh noise was effectively suppressed.

(2) The second example is shown in Figures 85 and 86. Figure 85 shows the spectral response of an outer race fault which has not been processed with the pulse width data cleaner. Figure 86 shows the enhanced spectral response of bearing fault frequencies after processing by the data cleaner.

(3) The third example shown in Figures 87 and 88 indicates similar improvement for an inner race fault case. As can be seen, considerable improvement is obtained in eliminating spectral lines which were believed to be due to machinery noise which had pulse lengths much greater than those associated with bearing fault signatures.

5.4 POST-DETECTION PROCESSING

The objective of the SPADE post processing module is to process the digitally filtered waveform and reduce the waveform to a few numbers for processing by the decision module (presented in Section 5.5). Two distinct types of post

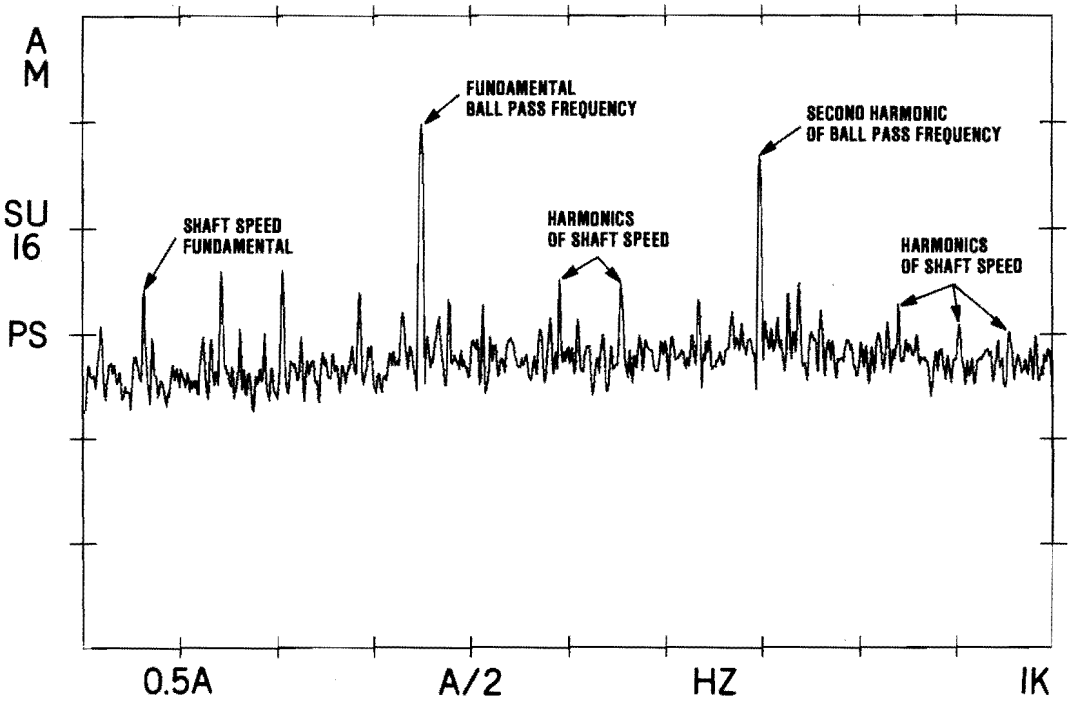

Figure 83. Combined Gear-Mesh Noise and Outer Race Fault Signal - 250 μsec Matched Filter

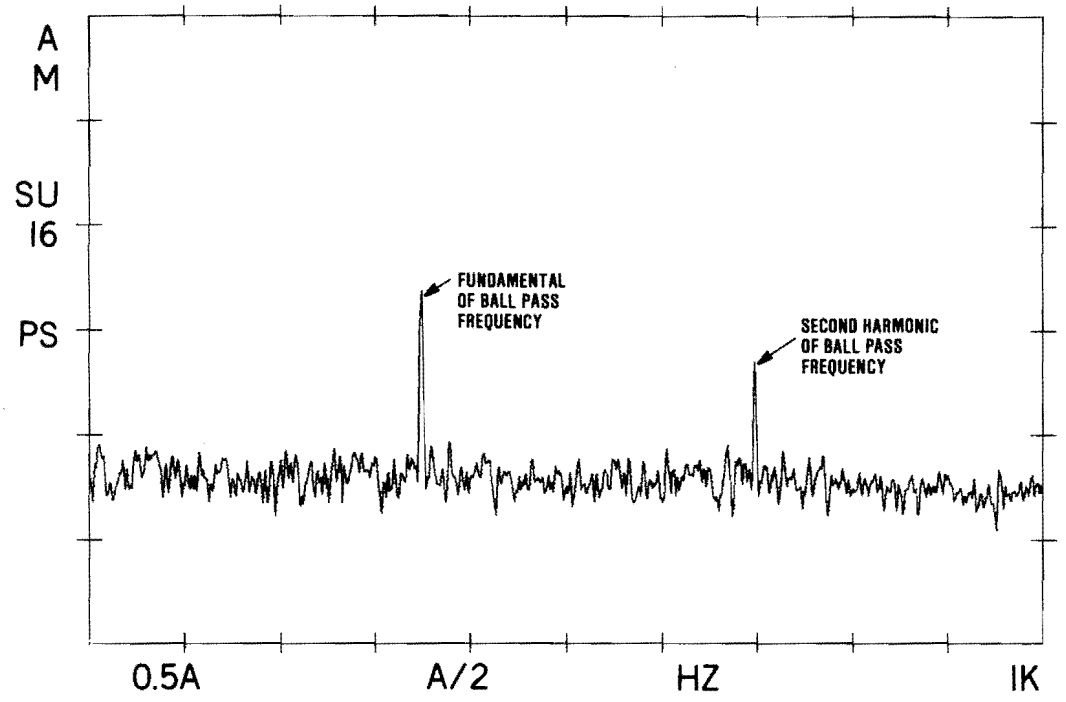

Figure 84. Outer Race Fault Signal After Gear-Mesh Noise Suppressed

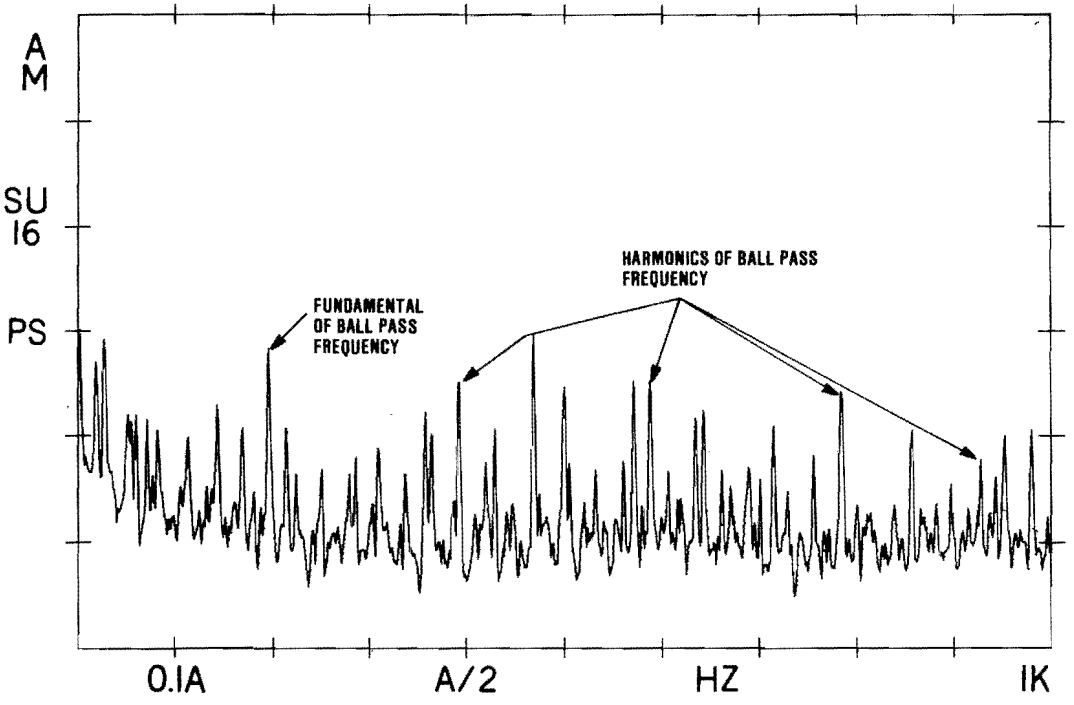

Figure 85. Outer Race Fault/Unprocessed Signal

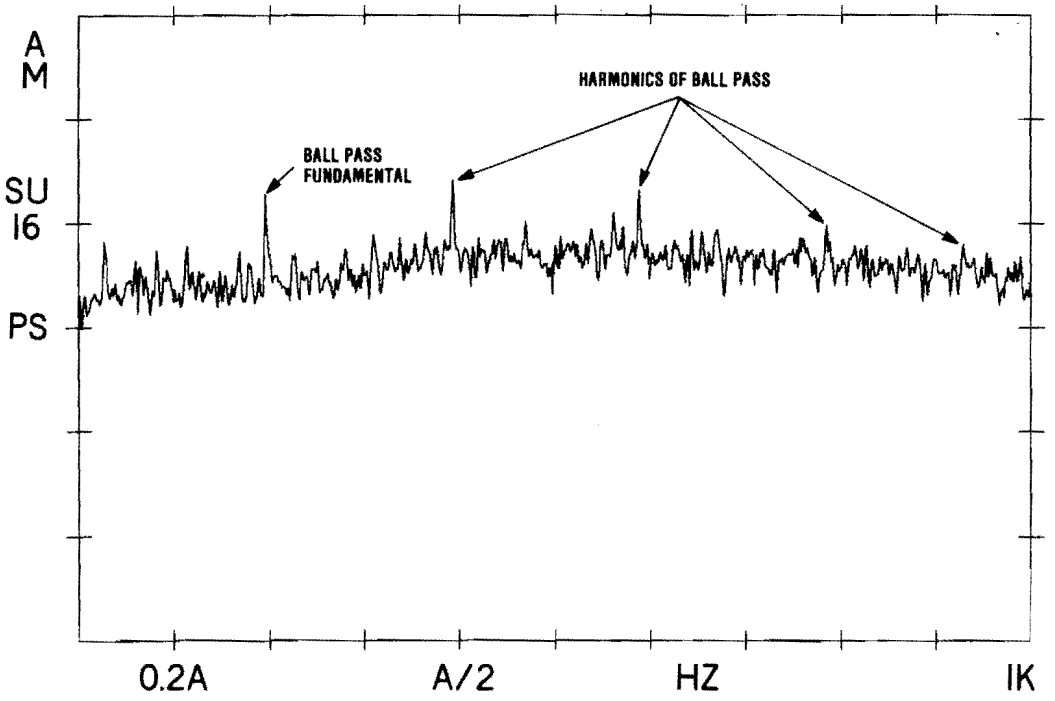

Figure 86. Outer Race Fault/Digitally Processed Signal

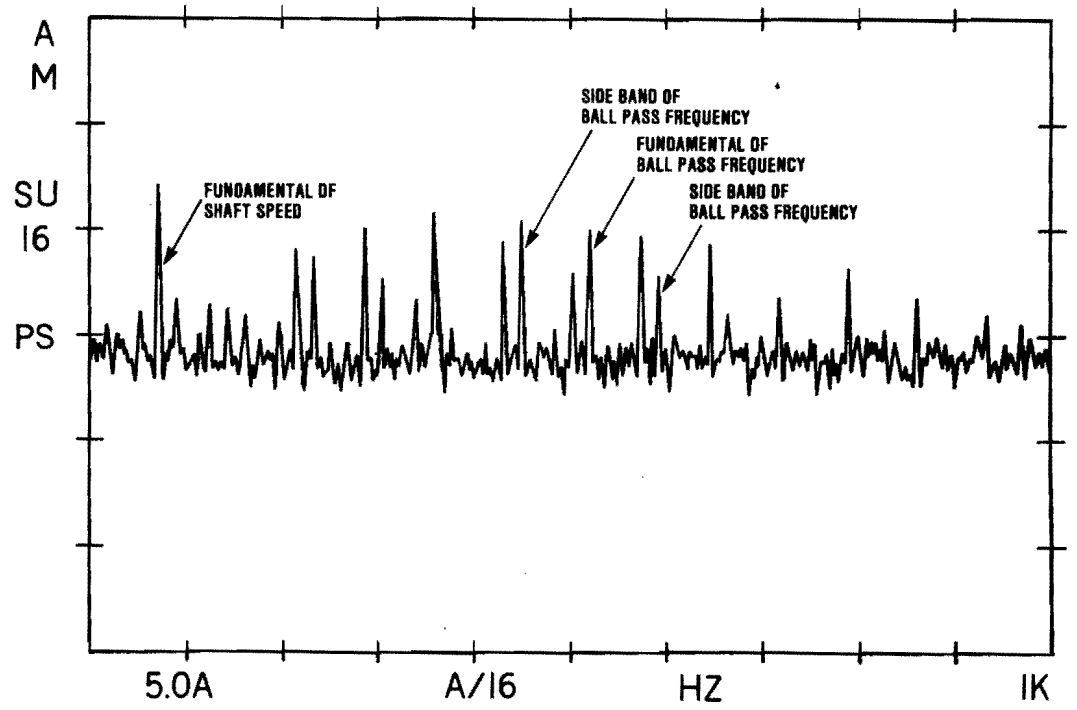

Figure 87. Inner Race Fault/Unprocessed

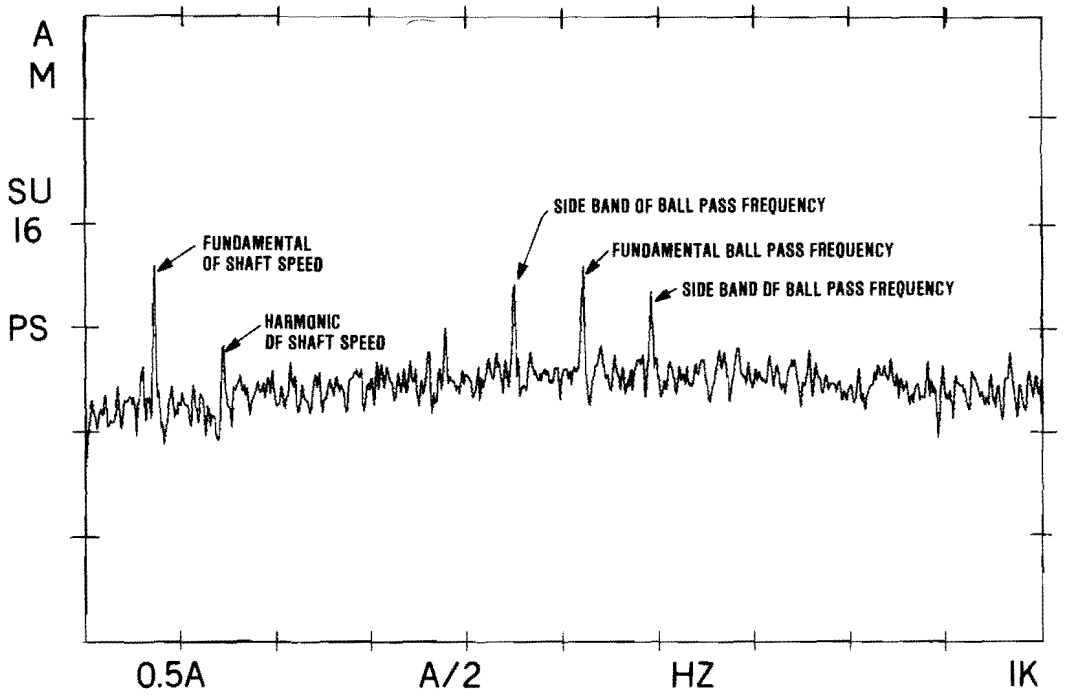

Figure 88. Inner Race Fault/Digitally Processed

processing are employed in the SPADE system: a time domain process which is a modification of the original SPA type technique, and a frequency domain technique which filters the signal into its frequency components.

5.4.1 Time Domain Processing

The time domain technique post processing is illustrated by the following diagram.

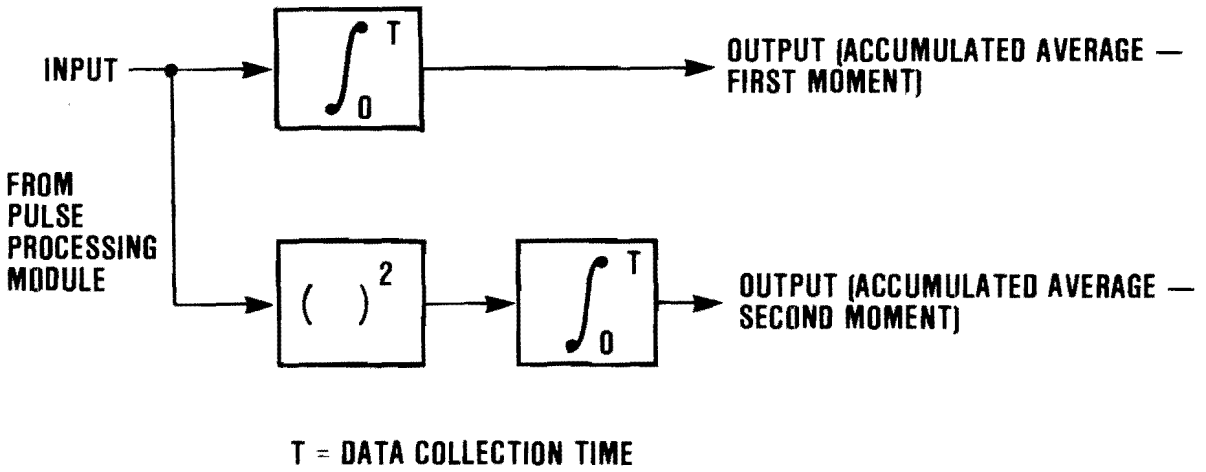

The processing consists of two paths. The first path simply accumulates the sum of the output of the pulse processing module, and the second path squares the output of the pulse processing module and accumulates the sum. It was anticipated that a statistical relation between these summations could be obtained for fault detection. However, as shown in Section 8, the time domain method performed very poorly.

5.4.2 Frequency Domain Post Processing

The steps involved in the frequency domain analysis post processing technique are shown in the following flowchart and described in the following paragraphs.

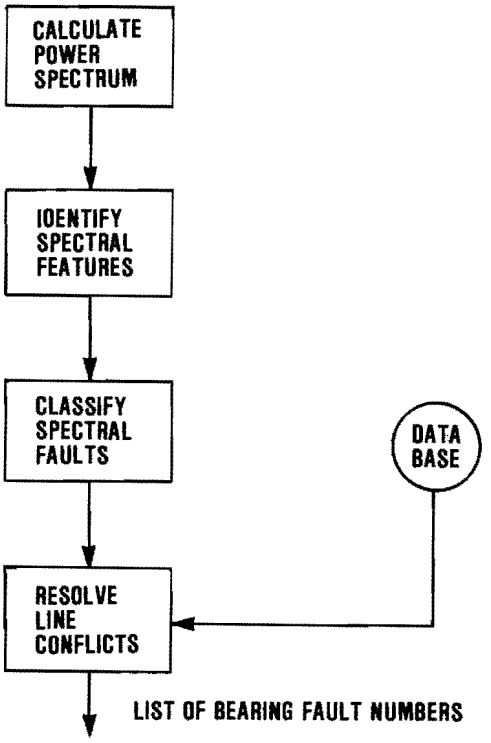

5.4.2.1 Calculation of Power Spectra

In calculating the power spectra, the following points will be addressed:

(1) Method of Power Spectrum Calculation
(2) Digital Noise in the Spectral Calculation
(3) Spectral Resolution
(4) Variance Reduction

5.4.2.1.1 Method of Power Spectrum Calculation

The method chosen for calculating the power spectrum was the FFT. The reasons for this selection are as follows:

(1) The FFT is much more effective at low signal-to-noise ratios than parametric methods.

(2) Due to the nature of the spectrum, which consists mainly of line spectra, parametric methods are not particularly effective.

(3) The FFT could be accommodated within the limited SPADE analyzer RAM space for storing spectral data while providing architectural flexibility.

5.4.2.1.2 Digital Noise

Digital noise is introduced into the spectrum as a result of A/D quantization and round-off error from the integer calculations in the FFT process.

(1) A/D quantization noise - The A/D noise is due to the precision of the A/D converter. For the case of the SPADE design which utilizes a seven bit A/D, the noise is around -42 dB of full scale signal. If finite gain intervals and oscillating waveforms are taken into account, the noise floor of the A/D could be around -24 dB of peak value.

(2) Round-off Error in FFT Calculation - The FFT calculations are done using 2's complement 16 bit arithmetic. The architecture of the TI-TMS320 is not set up to efficiently handle floating point arithmetic, and the available RAM for FFT storage did not lend itself to 32 bit arithmetic. As a result, 16 bit arithmetic was the only alternative. The purpose of this section is to assess the noise impact of 16 bit arithmetic. The worst-case analysis for the FFT is presented as follows:

$$\frac{\text{RMS(error)}}{\text{RMS (signal)}} = \frac{\sqrt{N}\, 2^{-b}\, (0.3)\, \sqrt{8}}{\text{duty factor}}$$

Duty factor = normalized RMS of the input signal
b = number of bits in arithmetic
N = number of points in FFT; i.e., 1024

The following results are obtained for typical FFT sizes and duty factor extremes:

RMS ERROR / RMS SIGNAL (dB)	N	DUTY FACTOR
-67.65	1024	1.0
-47.65	1024	0.1
-61.63	4096	1.0
-41.63	4096	0.1
-49.6	64K	1.0
-29.63	64K	0.1

The values presented here indicate that, for the 1024 point FFT, the noise power is sufficiently low for any practical duty factor.

5.4.2.1.3 Frequency Resolution

This section defines the optimum frequency resolution for the power spectrum measurement. If the spectral lines which characterize a bearing defect are true line spectra, then the spectral height of the peaks should be related by $1/f_r$ where f_r is the width of the spectral resolution. A bearing defect was measured with varying degrees of spectral resolution, and the results are shown in Figures 89 through 92 and summarized in Figure 93. The conclusion is that spectral resolution does not rise nearly as fast as $1/f_r$, which would indicate that bearing defects do not generate true line spectra. A possible explanation is broadening due to nonconstant speed.

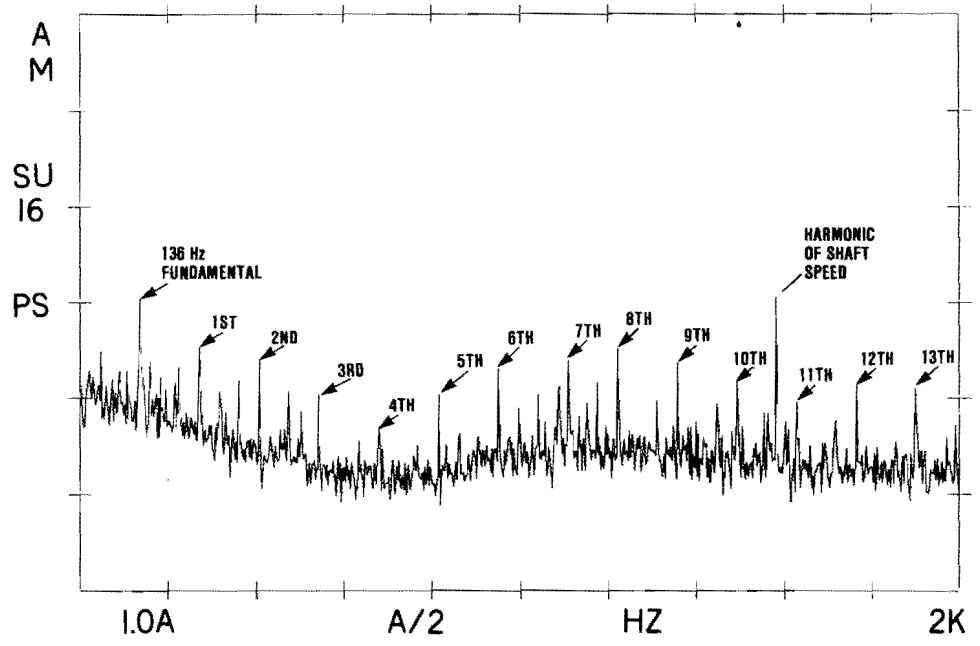

Figure 89. Spectral Resolution at 2 kHz

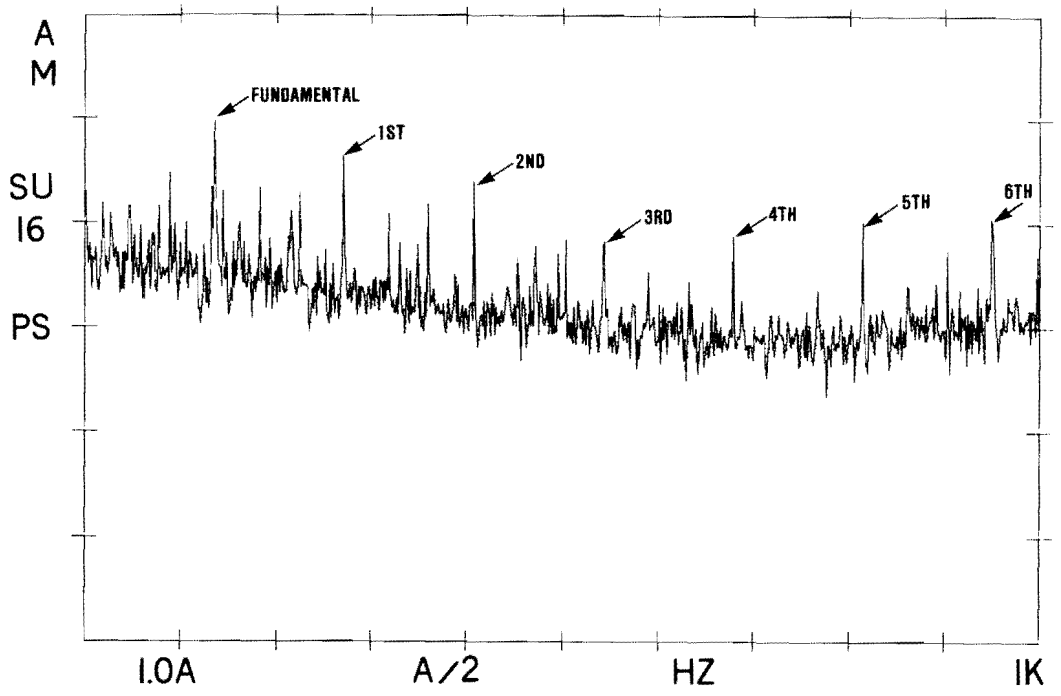

Figure 90. Spectral Resolution at 1 kHz

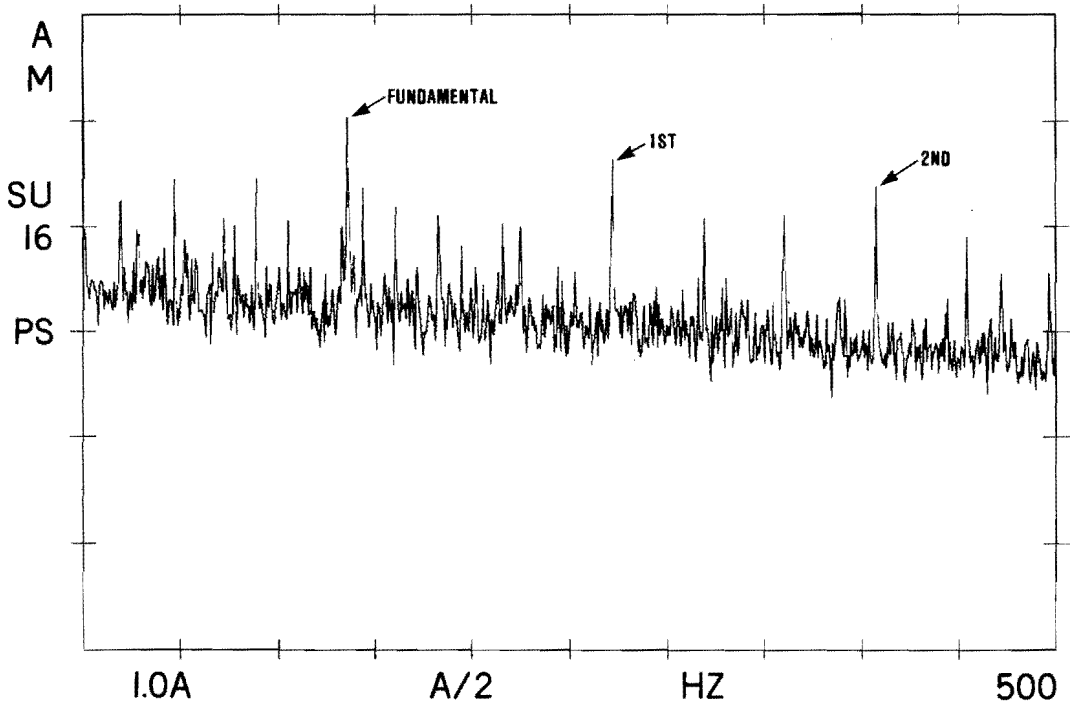

Figure 91. Spectral Resolution at 500 Hz

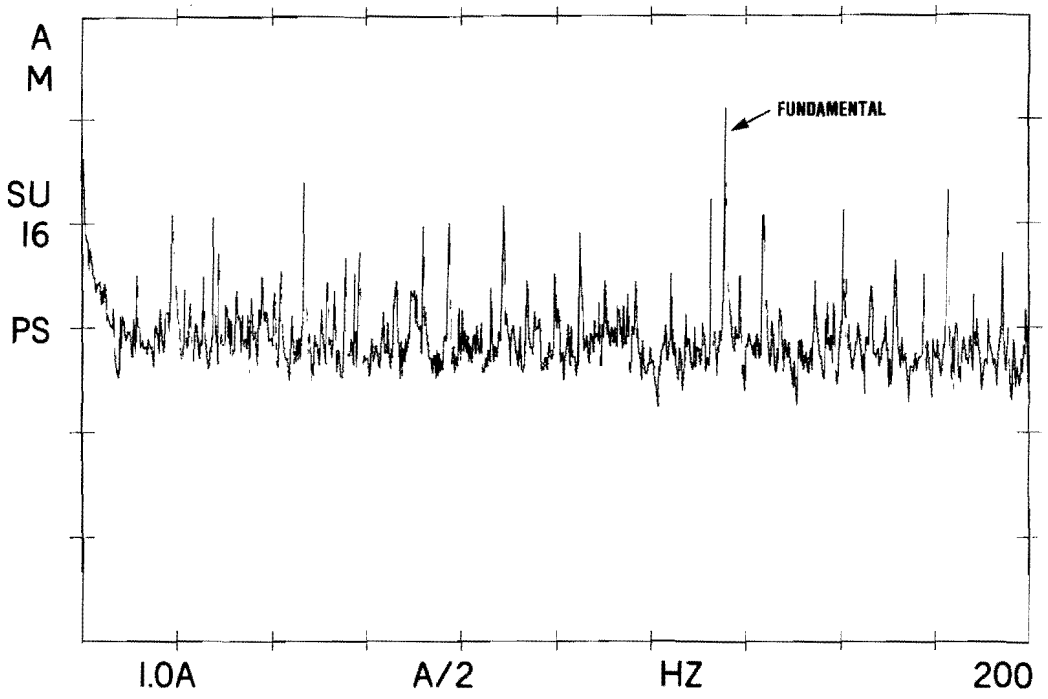

Figure 92. Spectral Resolution at 200 Hz

SPECTRAL HEIGHT	FREQUENCY RESOLUTION
15 dB	2.5 (2K FREQ RANGE)
18 dB	1.25 (1K FREQ RANGE)
20 dB	.625 (500 Hz FREQ RANGE)
24 dB	.25 (200 Hz FREQ RANGE)

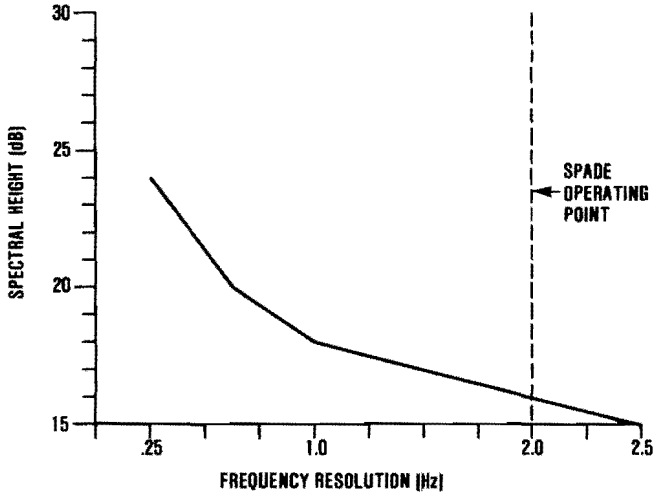

Figure 93. Increase in Spectral Peak Heights with Increased Spectral Resolution

The width or range of the power spectrum measurement is important. The spectral lines which originate from bearing defects contain the fundamental and harmonic of displacements of the shaft speed or any other modulating influence on the bearing fault signature. Table 6 shows the corresponding energy of a bearing fault as a function of frequency range. Note that there is a trade-off between spectral height versus number of peaks in range versus resolution. The operating point for the SPADE unit is 1K frequency range and 2 Hz resolution. From the results shown in this section, this should be a very satisfactory range. If a frequency resolution greater than 2 Hz is needed, a Zoom FFT can be implemented. The details of this implementation are shown in Appendix G.

TABLE 6. MEASURED ENERGY AS A FUNCTION OF FREQUENCY

Frequency	Energy (dB)
2 kHz	32.76
1 kHz	29.83
500 Hz	25.26
200 Hz	24

5.4.2.1.4 Variance Reduction

As shown in Figure 94, a single FFT measurement contains considerable noise in the spectrum. Figure 95 shows that the noise or variance can be considerably reduced by averaging the power spectra. The reduction of variance in a power spectra is 1/N, where N is the number of spectra averaged.

The optimum value for the number of spectral averages was determined to be 128. This value was chosen primarily to provide variance reduction needed for detection of Class D faults.

In FFT-based power spectrum analysis, the question of the type of window to be used in the spectral estimate arises. The purpose of the window is to reduce variance. However, the choice of the window depends upon the type of spectrum that is encountered. Figure 96 shows the result of an averaged power spectrum computation with a constant rectangular window, and Figure 97 shows the power spectrum measurement with a conventional Hanning window. The constant rectangular window gave slightly better results and thus was used instead of the conventional Hanning window.

5.4.2.2 Identification of Spectral Features

Rather than searching for a particular peak in the spectrum, the philosophy taken in the SPADE system was to reduce all spectral features of the power spectrum to a list structure which defined the following properties of each feature:

(1) Frequency
(2) Amplitude of Spectral Peak
(3) Area under Spectral Peak

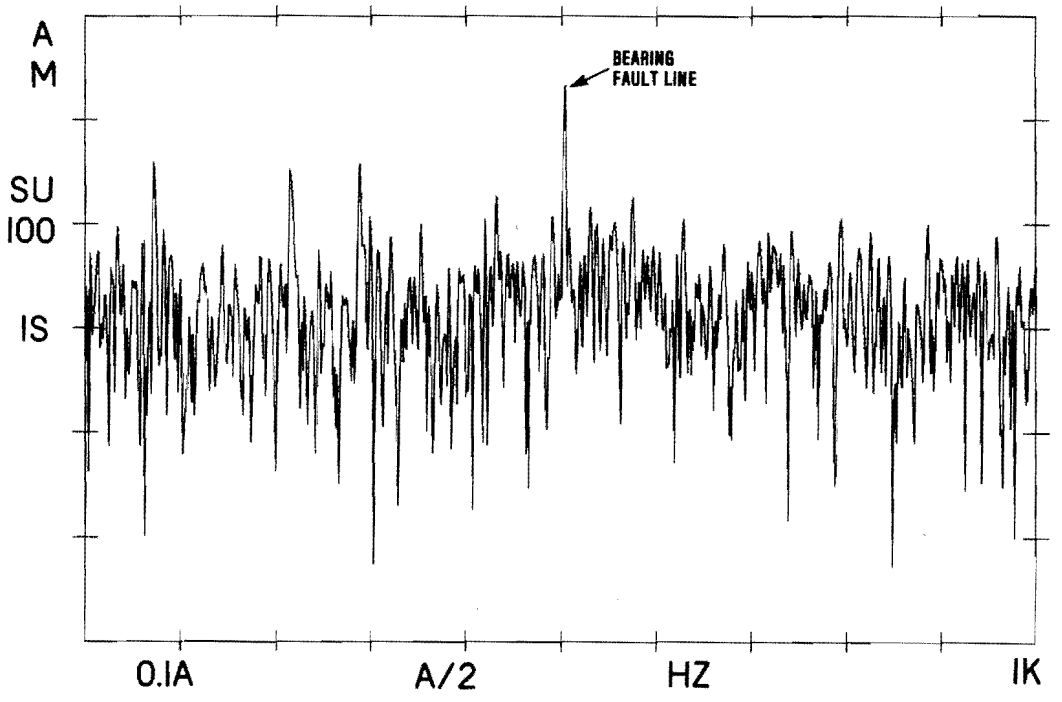

Figure 94. Single FFT Measurement (Considerable Noise)

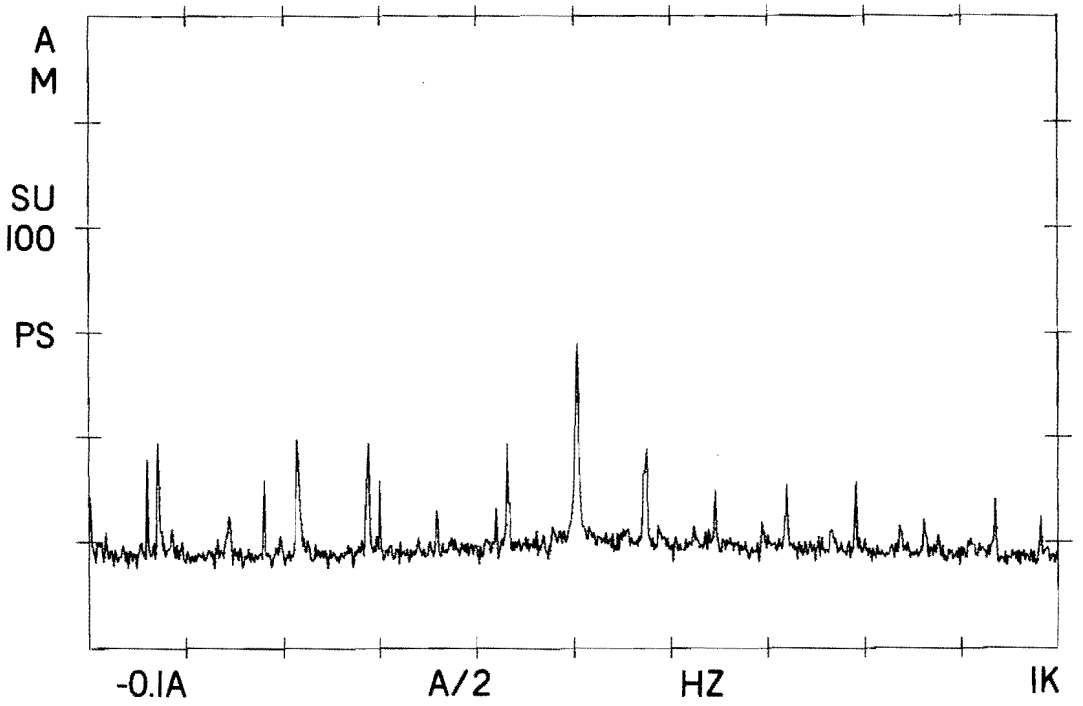

Figure 95. Averaged Spectra with Uniform Window (Reduced Noise)

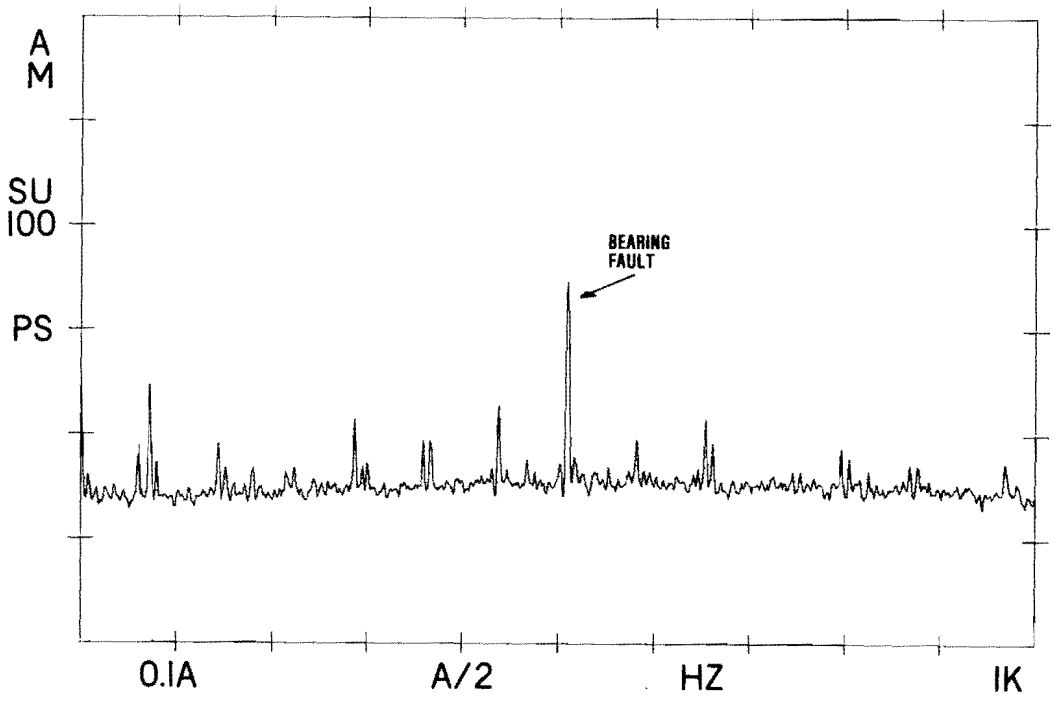

Figure 96. Averaged Spectra with Hanning Window

The frequency of the spectral peak is defined as the frequency bin in the region of the peak which has the highest energy level. The amplitude of the spectral peak is defined as the level difference between the maximum level and the minimum level of the peak. The minimum level of the peak is defined as the point where the power spectrum local increases. In the case of an unsymmetrical peak, the lesser of the local minimums is used. The rationale for this is that an unsymmetrical peak is caused by two spectral lines being close to each other and the lower minimum more closely represents the true level of the peak. The process is illustrated as follows:

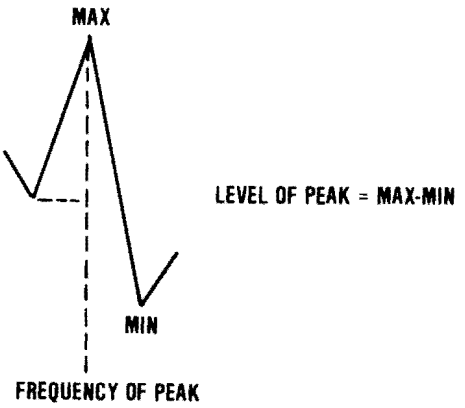

At this stage of the processing, no decision is made on whether a spectral peak is a bearing fault signal or not.

Figure 97 shows the progression of the spectral lines from a class C/D fault to a gross fault. Generally, the mechanism which causes this change in spectral character is that the defect becomes severe enough to upset the repetition rate of the shock pulse. This causes the spectral lines to broaden and decrease in amplitude, as shown in the illustration below.

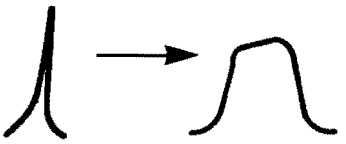

Although the amplitude of the signal decreases, the power in the peak increases due to the increased area of the peak. Therefore, another quantity must be defined in order to account for this effect. This quantity is the area under the peak and is defined by the shaded area shown in the illustration below.

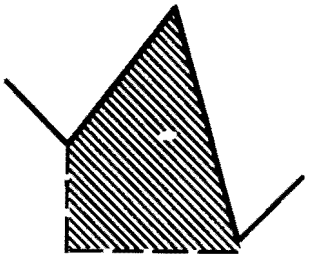

5.4.2.3 Classification of Spectral Lines

This section describes how the list of identified peaks is reduced to a list of numbers representing the level of bearing failure for each of the possible bearing failure types. Each bearing assembly has two failure modes detectable by frequency domain techniques: inner race fault and outer race fault. (Ball or roller faults are not readily detectable by the frequency

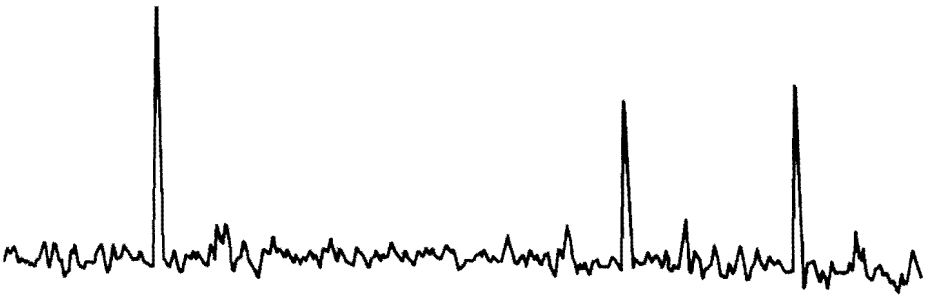

LINE SPECTRUM TYPICAL OF C/D FAULT

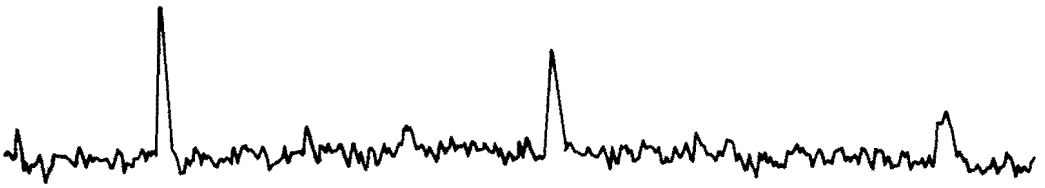

LINE SPECTRUM IN TRANSITION

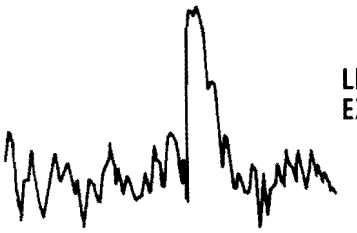

LINE SPECTRUM TYPICAL OF
EXTREMELY GROSS FAULTS

Figure 97. Spectral Broadening Due to Bearing Fault Progression

domain technique.) A bearing failure will generate the following general fault pattern.

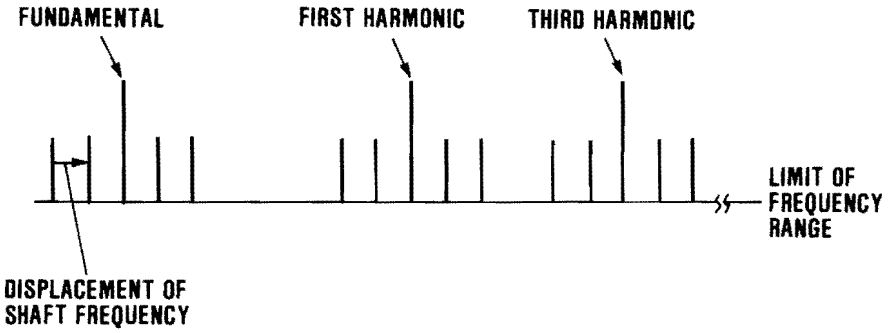

From the list of spectral peaks identified in the previous module, an attempt is made to match the spectral lines with the pattern presented above. The following rules are employed in analyzing spectral peaks:

(1) The fundamental and all shaft-related harmonics are removed from the list of the spectra.

(2) A bearing signature is valid only if a fundamental or second harmonic exists above a certain threshold. (Threshold is determined from the data base.) A side band alone cannot indicate a bearing signature.

(3) For a side band to be valid, the left and right side bands must exist and be within a factor of two of each other in amplitude.

(4) The shaft speed is not known exactly at the running of the test; therefore, as much as ± 1.5 percent uncertainty exists in the shaft speed. This results in ± 7.5 Hz in frequency error at 500 Hz. As a result, several bearings will be indistinguishable from one another.

(5) Once the fundamental or second harmonic of the bearing frequency has been found, this frequency can be used to calibrate the shaft speed.

From these rules the following list is assembled for each bearing type: peak amplitude and area amplitude. The peak amplitude is the accumulated peak level of all the spectral lines which were matched up. The area amplitude is the accumulated area.

5.4.2.4 Resolution of Conflicts

With the necessary window widths required to accommodate the variable shaft speeds, the frequencies of several bearing types could overlap. Therefore, it is possible for a spectral line to be claimed by two or more bearing assemblies. This is acceptable except when one bearing assembly claims the peak as a side band and another bearing assembly claims the peak as a fundamental or harmonic. In this case the rule applied is that the bearing assembly cannot claim the peak as a harmonic.

5.5 DECISION ANALYSIS

This section presents the processing required to determine if a fault exists in a bearing assembly. The inputs to the module are:

(1) Average and peak signal in 15-35 kHz band
(2) Average and peak signal above 5 kHz
(3) Results from time domain analysis
(4) Results from frequency domain analysis

Figure 98 shows the processing done to decide whether or not a bearing is faulty.

As an added defense against false alarms when a fault is detected, the data is checked against a data base of exception classes. The exception classes are instances where a faulty diagnosis was reached because of an abnormal condition. Rather than try to include the exception handling in the main processing chain, it is more efficient to incorporate it as a separate module. This data base is empty at present due to the lack of field use of the system.

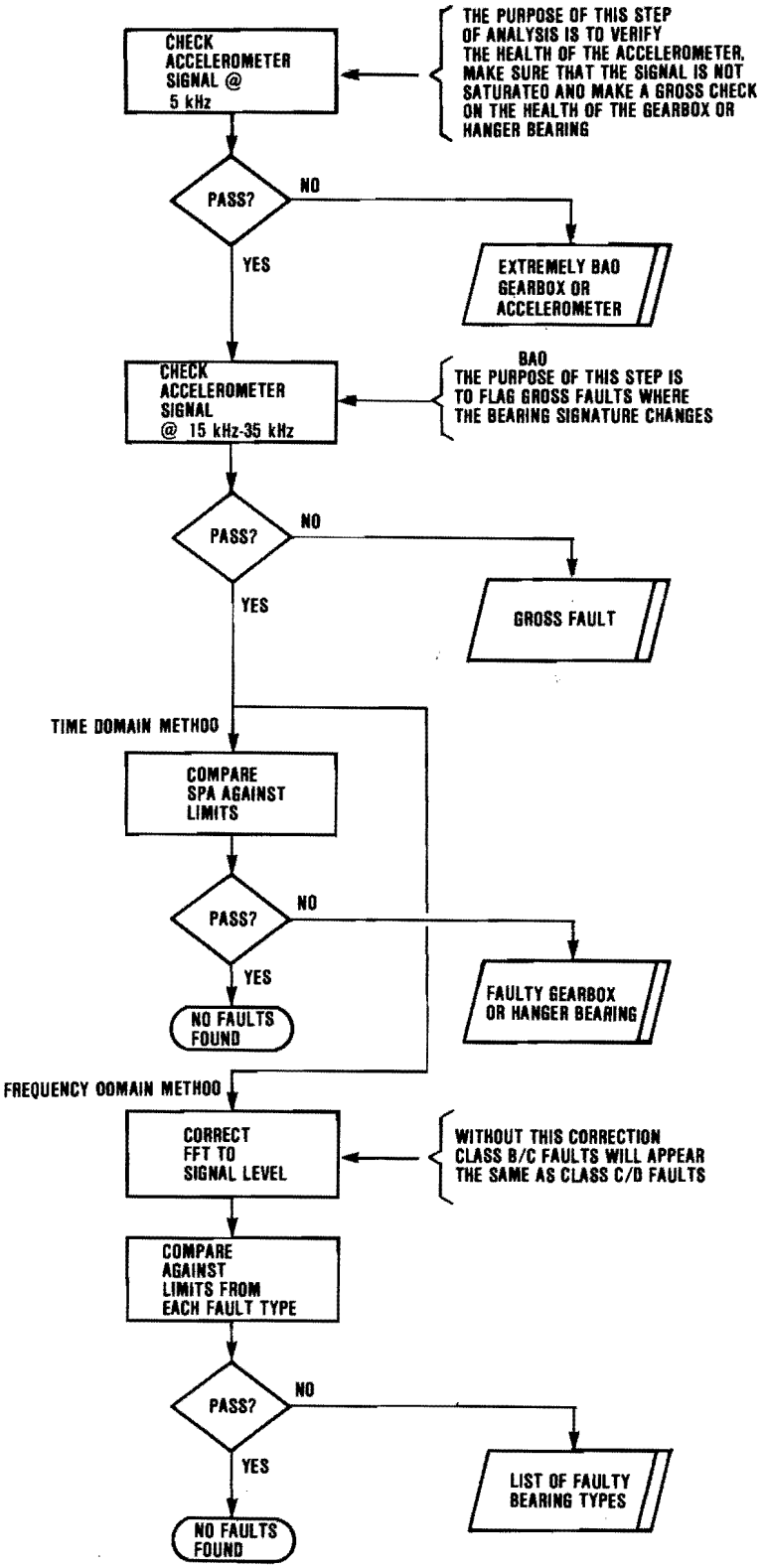

Figure 98. Processing Required to Determine Bearing Assembly Faults

SECTION 6
SPADE ARCHITECTURE

The signal processing requirements and an analysis of the implementation have been separately described for each system element. This section reviews the overall SPADE architecture and describes the entire processing sequence on a signal flow basis. A duplex ball bearing inner race fault signal (Cobra 90-degree gearbox) will be traced through the processing. The SPADE system architecture is comprised of the following functional elements:

(1) Accelerometer
(2) Electrical Front End
(3) Demodulation
(4) Pulse Processing
(5) Frequency Analysis
(6) Variance Reduction (Spectral Lines)
(7) Identification and Classification (Spectral Lines)
(8) Sorting by Fault Categories (Spectral Lines)
(9) Computation of Normalized Energy Content
(10) Computation of Coherent Energy

The discussions which follow will be from a summary point of view. For additional details on any area, the interested reader is referred to the appropriate section in Chapter 5.

6.1 ACCELEROMETER

The accelerometer is designed for a wide bandwidth and a flat spectral response in the frequency range of 15 to 35 kHz.

The design incorporates a 5 kHz high-pass filter to attenuate low frequency machinery noise which might saturate the accelerometer. The accelerometer output is at the DC power supply voltage, with the signal riding on the DC voltage. The accelerometer output waveform (with the DC supply voltage removed) is shown in Figure 99 and the resulting power spectrum in Figure 100.

6.2 ELECTRICAL FRONT END

The accelerometer signal is routed to the SPADE analyzer electrical front end via the signal and fan-out cables. The first function of the electrical front end, shown in Figure 101, is to multiplex the twenty possible accelerometers which can be connected to the SPADE analyzer. The signal then passes through an amplifier to remove possible common mode noise. The DC power supply voltage is removed from the signal at this point.

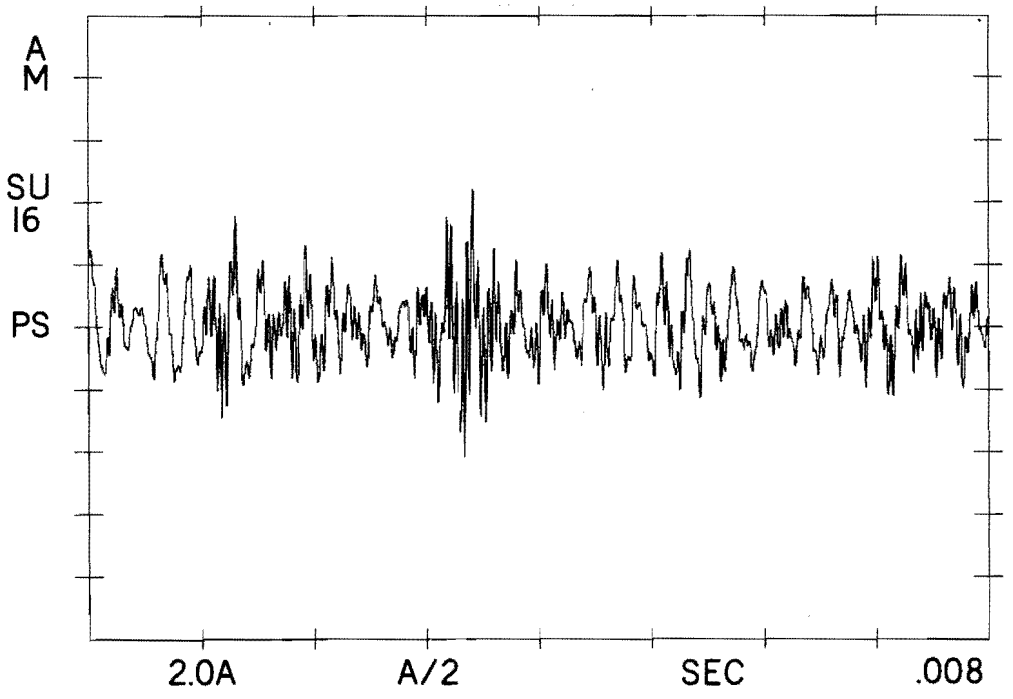

Figure 99. Raw Accelerometer Signal

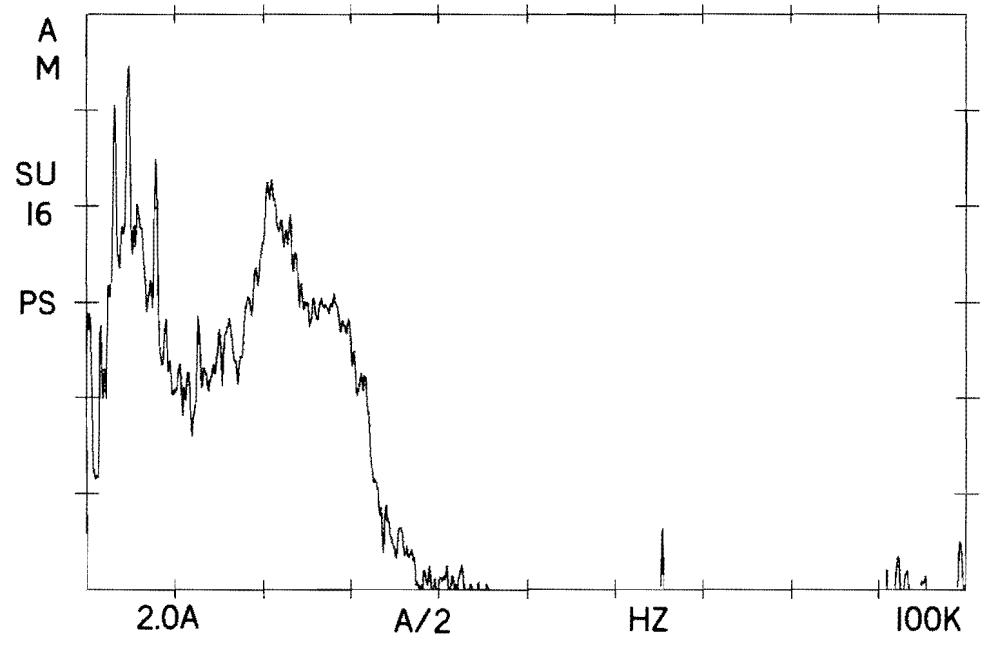

Figure 100. Power Spectrum of Raw Accelerometer Signal

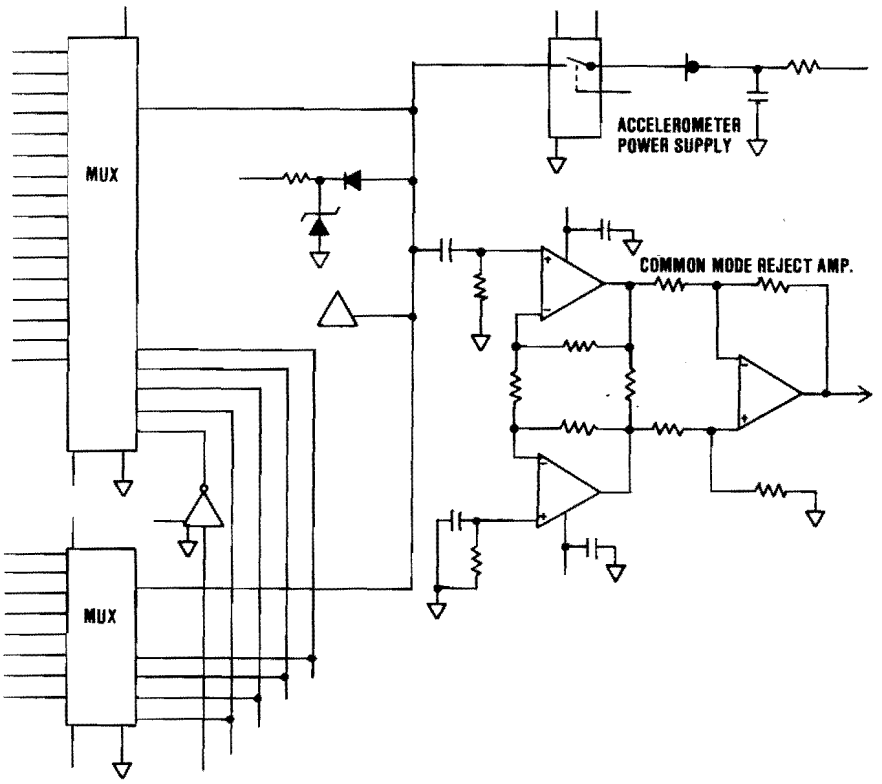

Figure 101. SPADE Analyzer Electrical Front End

Next, the signal is band-pass filtered and amplified. The band-passed signal, shown in Figure 102, reveals the bearing fault signature embedded in the low frequency machinery noise of the raw accelerometer signal (Figure 99). The electrical circuits which accomplish this function are shown in Figures 103 and 104.

The next step is full wave rectification and A/D conversion of the signal. The circuit for this process is shown in Figure 105. The full wave rectification could be done in software. However, the A/D converter has only seven bits of precision and the software rectification would result in a bit reduction in accuracy. The signal, after full wave rectification and at the input to the A/D converter, is shown in Figure 106.

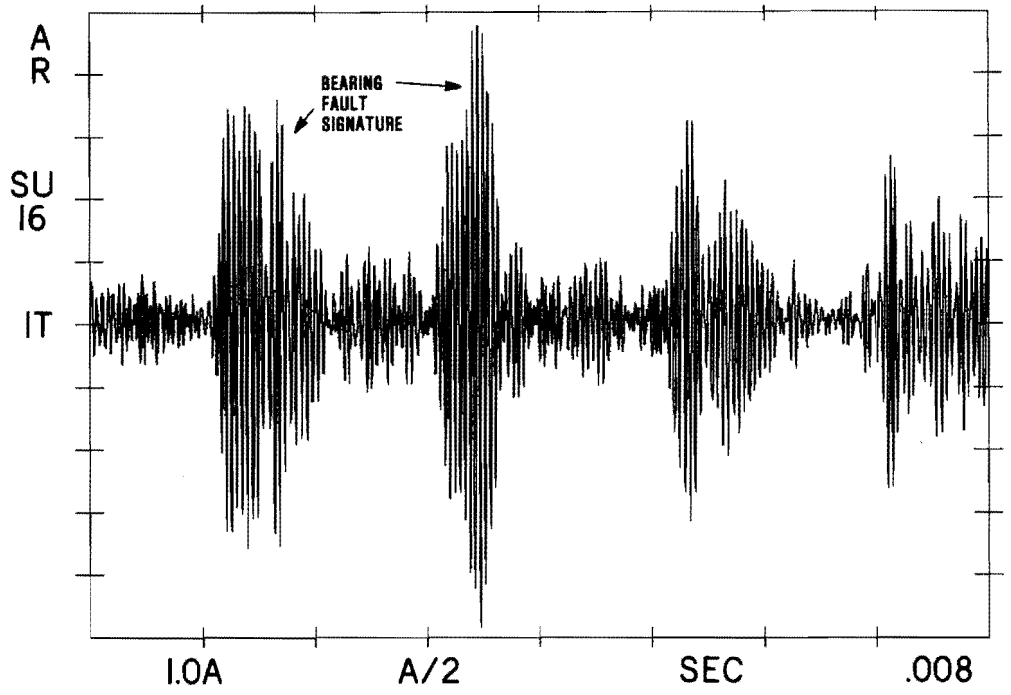

Figure 102. Band-Pass Filtered Signal

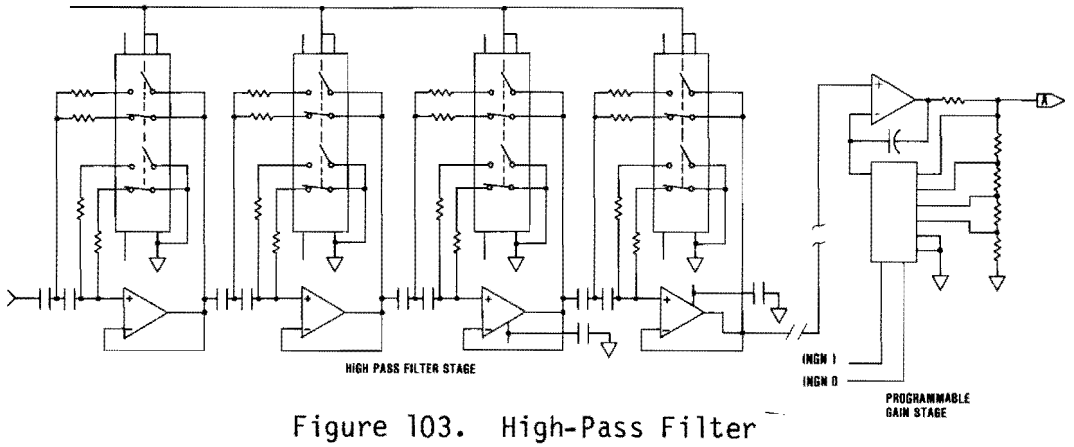

Figure 103. High-Pass Filter

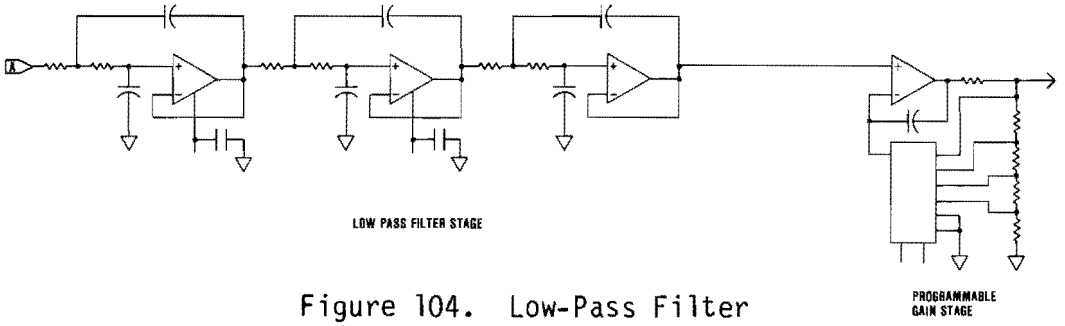

Figure 104. Low-Pass Filter

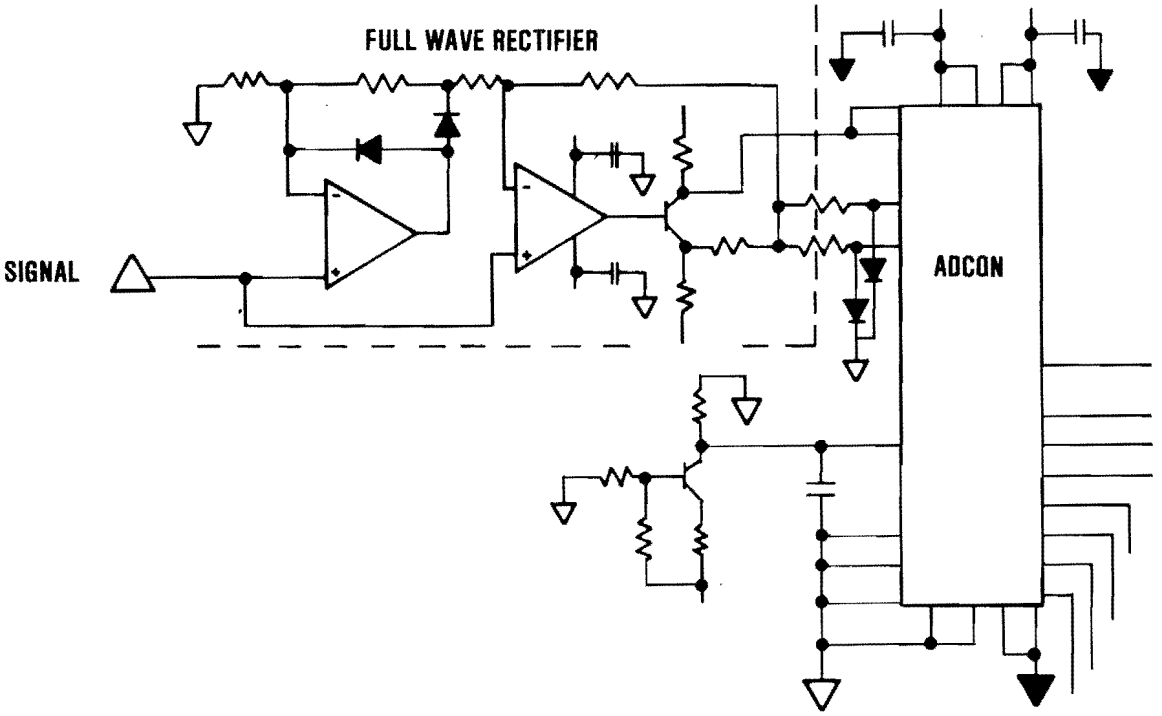

Figure 105. Full Wave Rectifier and A/D Converter

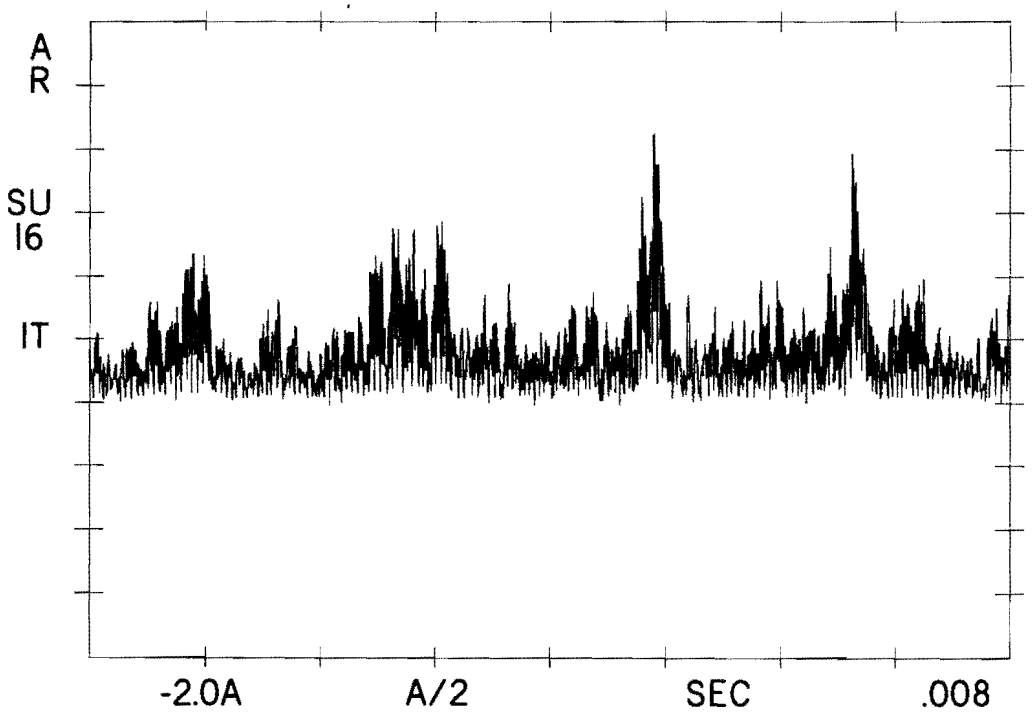

Figure 106. Signal at Input to A/D Converter

6.3 DIGITAL DEMODULATION

The digital demodulation of the signal, performed by a PROM-based TI-TMS 320 signal processor (TMS 320 #1, Figure D-2), consists of three sequential asynchronous stages as shown in the following diagram:

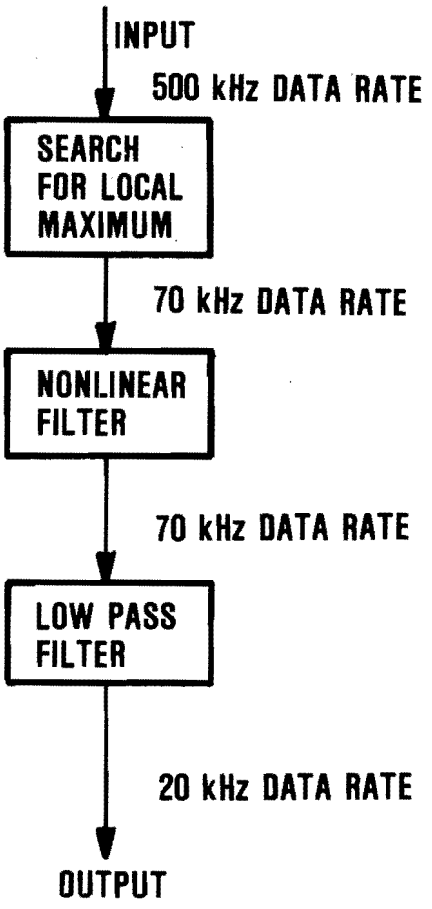

The input signal to the first module is shown in Figure 106. The first module searches for local maximum of the rectified peaks, and its output is shown in Figure 107. As can be seen, the output of the peak detection process is quite grassy. However, this grassy characteristic is effectively removed by the next module, a nonlinear filter, as shown in Figure 108. The signal is then low pass filtered to 20 kHz by the third module and the data is transferred to the pulse processing element. The output of the low pass filter module is shown in Figure 109.

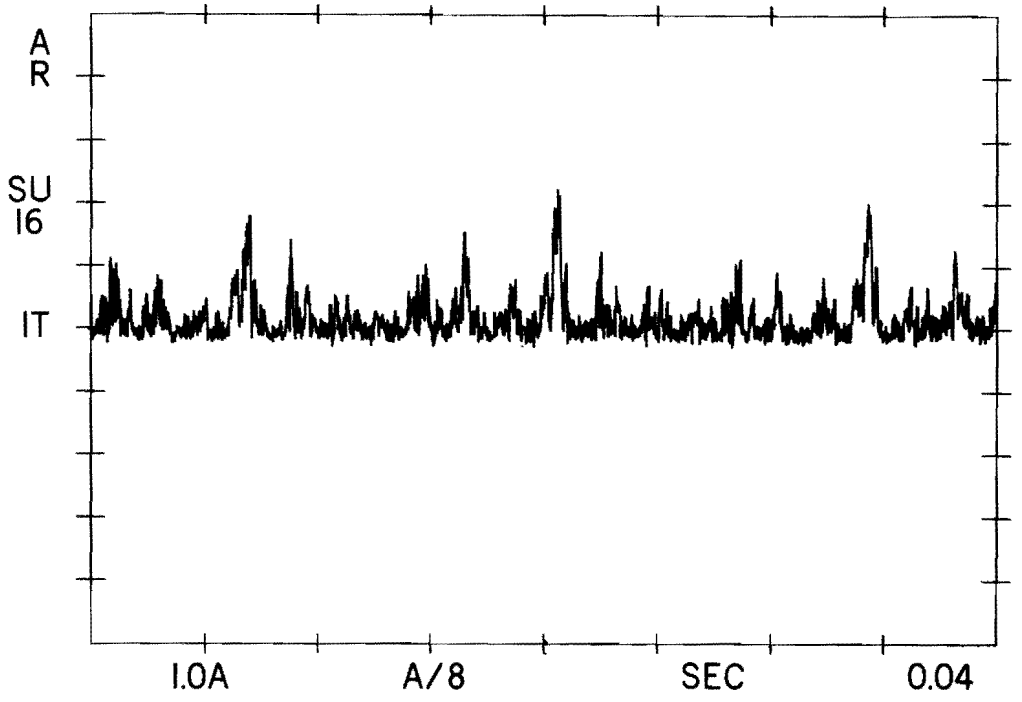

Figure 107. Output of Local Peak Module

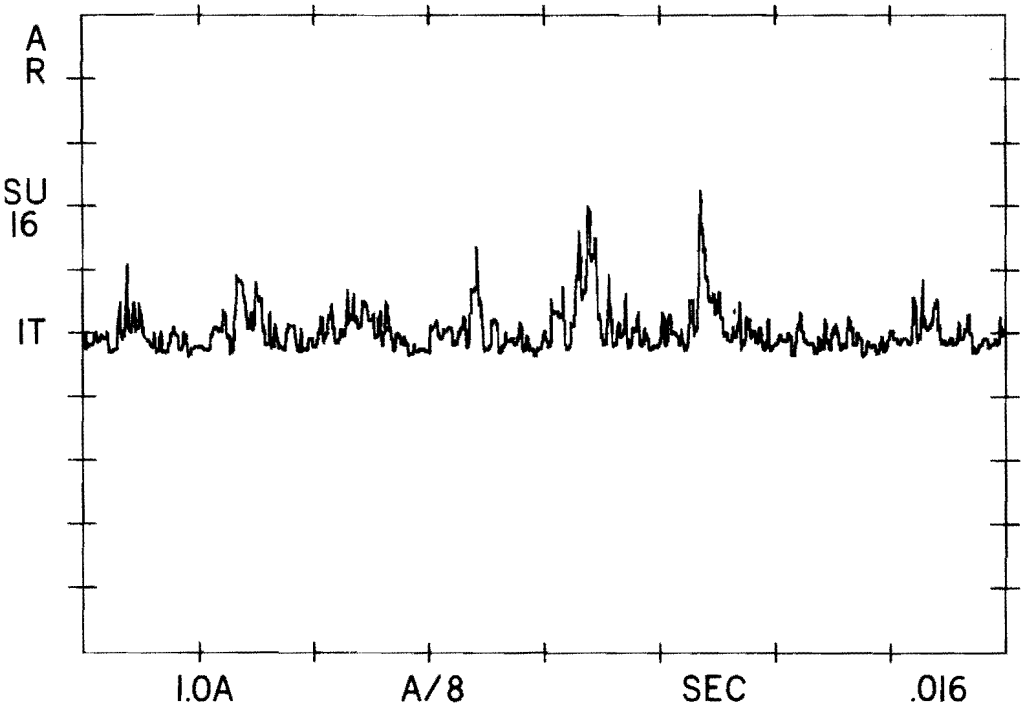

Figure 108. Output of Nonlinear Filter

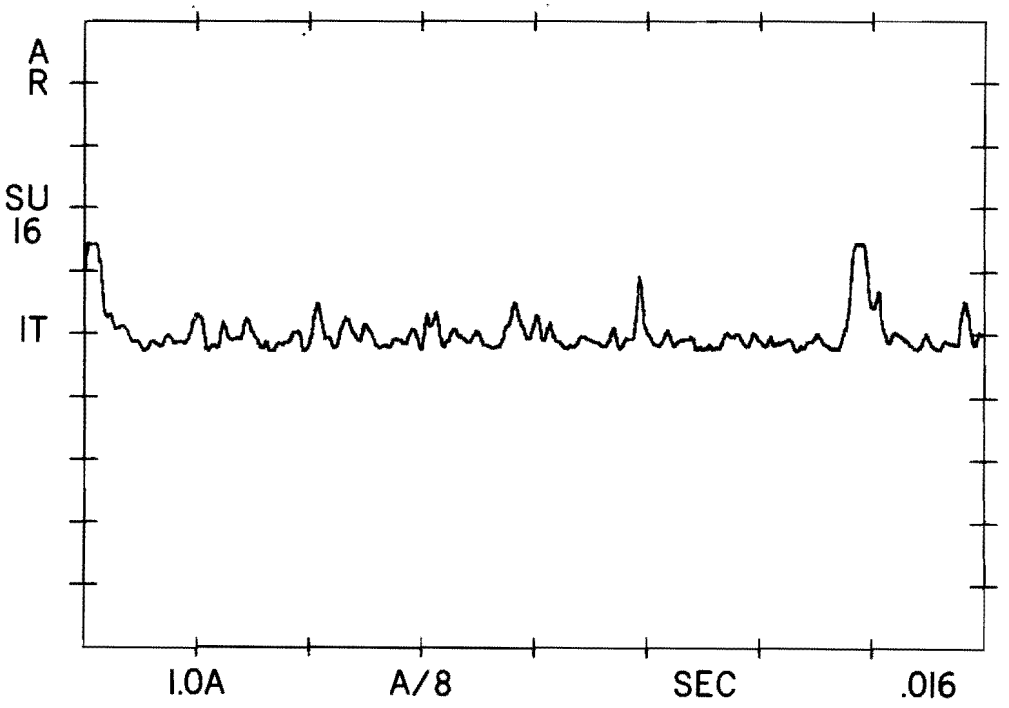

Figure 109. Output of Low-Pass Filter

6.4 PULSE PROCESSING

The purpose of the pulse processing module is to accomplish two tasks:

(1) Reduce the sampling rate from 20 kHz to 2 kHz
(2) Separate bearing fault signatures from other signatures

This module resides in the RAM-based TI-TMS 320 signal processor (TMS #2, Figure D-2) and accepts data from the PROM-based TI-TMS 320 on an interrupt driven basis.

The pulse processing is shown in the following diagram:

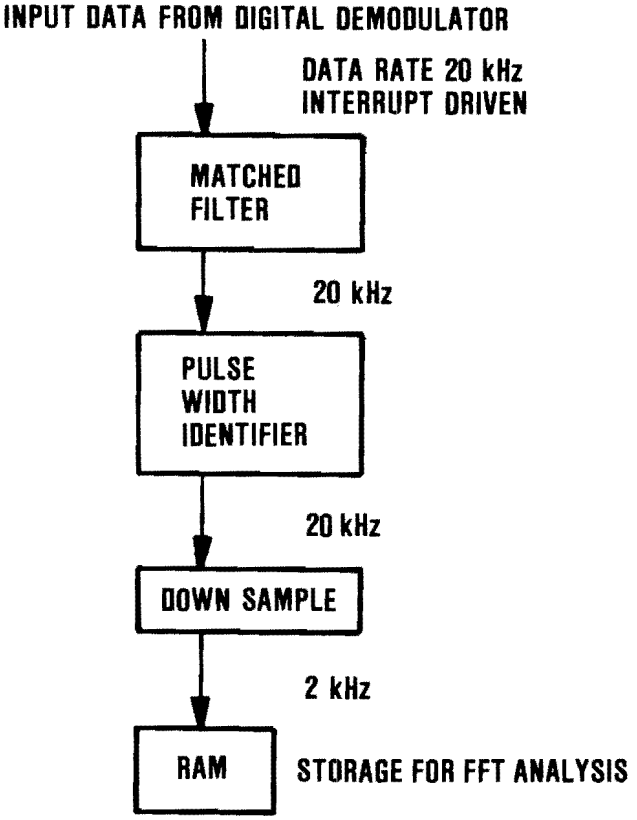

The pulse processing module is interrupt driven and accepts data at a 20 kHz rate from the digital demodulator. The input data stream from the digital demodulator is shown in Figure 110. The data is first passed through a matched filter to extract signals with bearing signature features. The output of the matched filter, shown in Figure 111, demonstrates that the matched filter is quite effective in extracting possible bearing signatures from other signal elements.

The pulse width identifier separates the bearing fault signature from other signals present in the helicopter environment. The frequency content of the input signal to this module (unprocessed spectrum) is shown in Figure 112. As can be seen, there are many large amplitude frequency components in the spectrum which are not related to the bearing fault signature. The module output (processed spectrum) of Figure 113 shows that spectral lines not associated with bearing fault signatures were effectively reduced or completely eliminated.

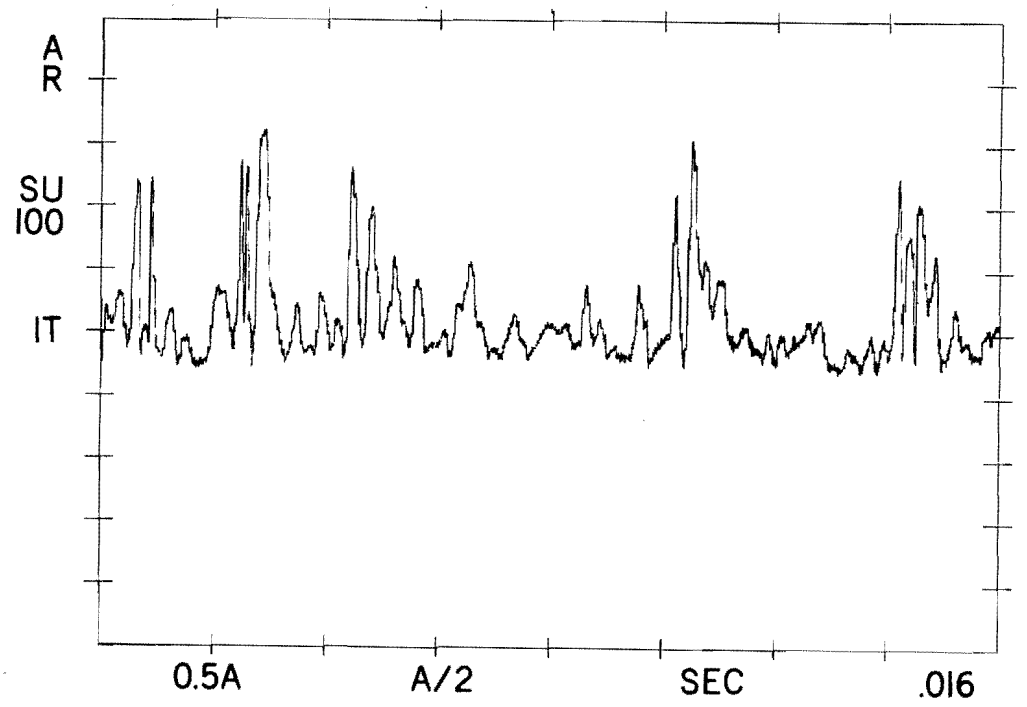

Figure 110. Input Signal to Pulse Processing Module

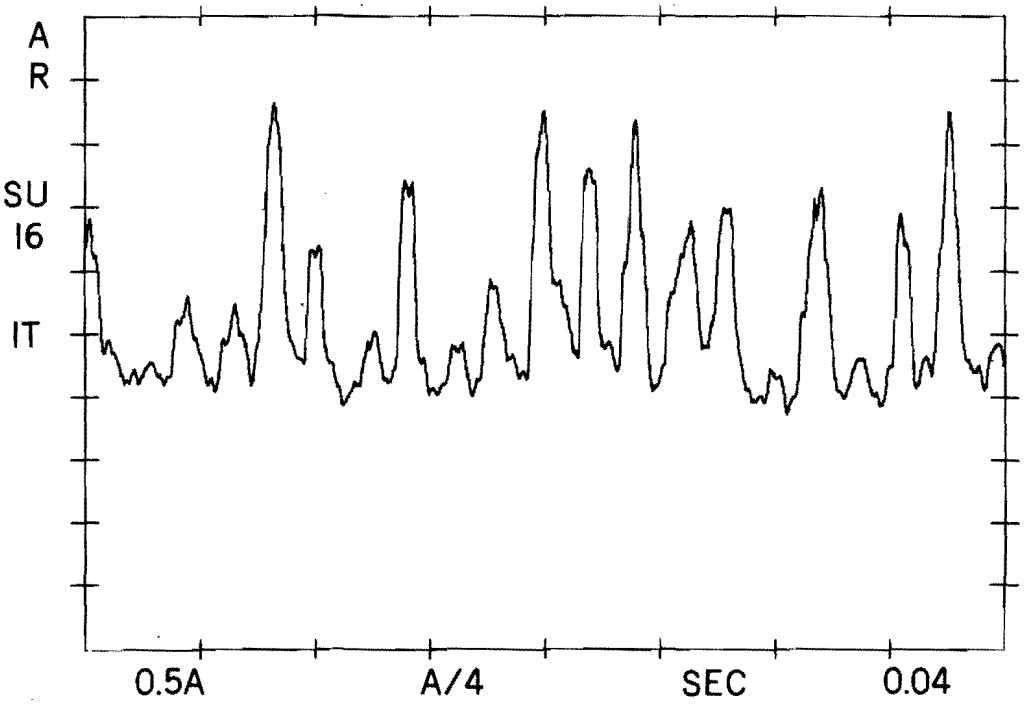

Figure 111. Matched Filter Output Signal

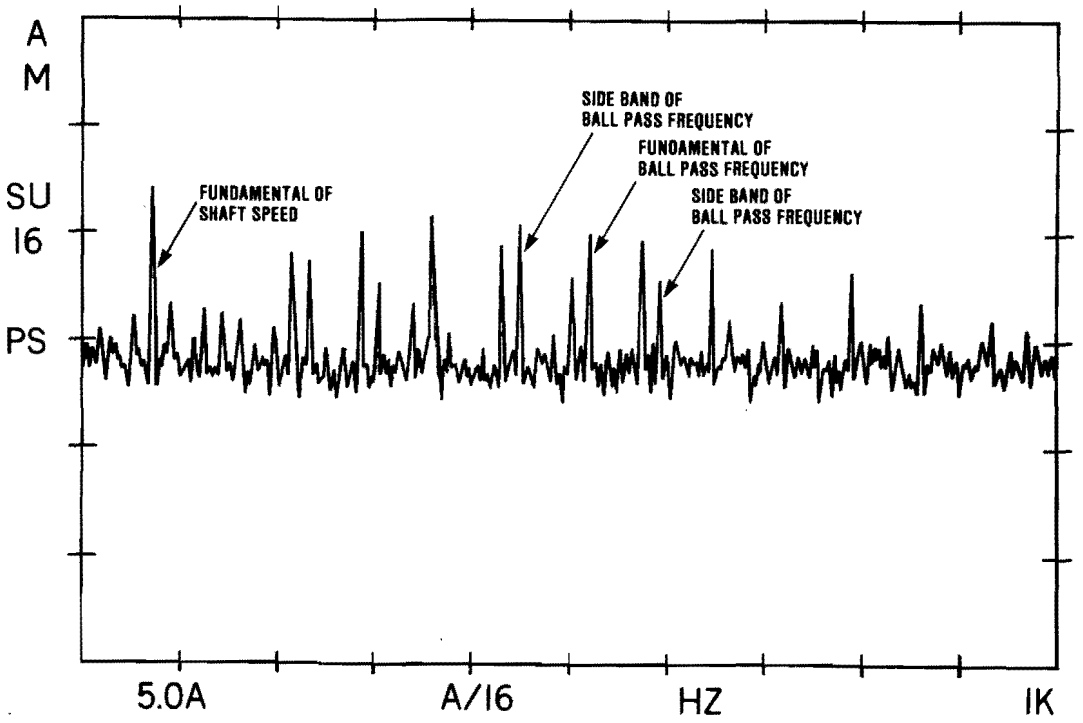

Figure 112. Unprocessed Spectrum

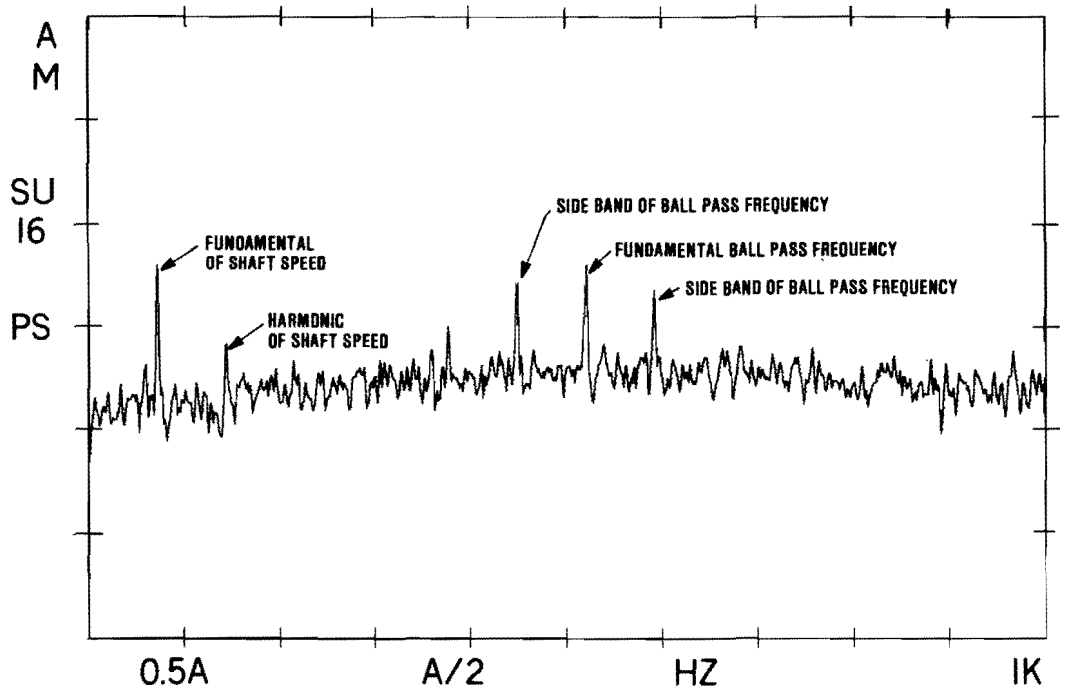

Figure 113. Processed Spectrum

Once a bearing fault signature has been detected and identified, the down sample module integrates the signal level over a 5 millisecond time duration and stores the data in RAM for later frequency domain analysis. Figure 114 shows a comparison between the input signal to the digital signal processing function, and the resulting signal enhancement provided by the digital signal processing.

6.5 FREQUENCY ANALYSIS

The frequency analysis is performed by processing the time domain signal samples (stored in RAM by the pulse processing module) through an FFT algorithm. The result of a single FFT is shown in Figure 115.

6.6 VARIANCE REDUCTION OF SPECTRAL LINES

Considerable enhancement of the bearing fault signal is achieved when the variance in the power spectrum estimate is reduced by a factor of 1/N (where N is the number of averaged FFTs). Figure 116 shows the result of averaging 100 FFTs. The results depicted in this figure show a substantial reduction in variance and enhancement of the fault signal.

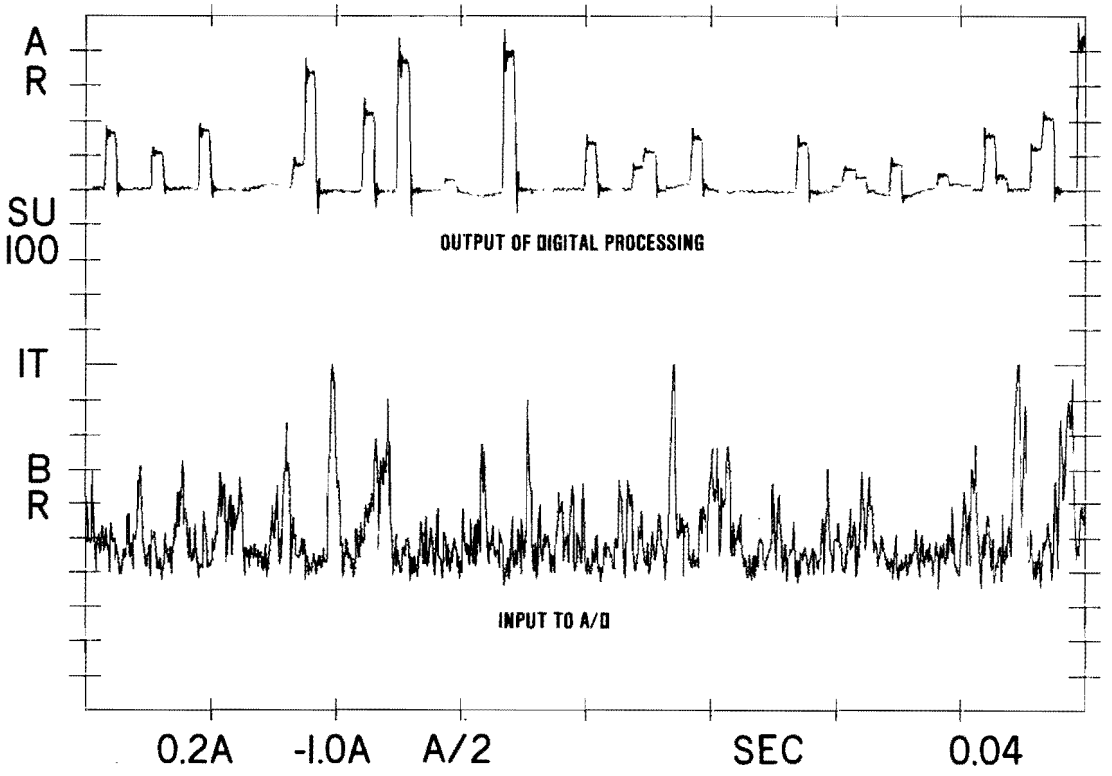

Figure 114. Comparison of Digital Signal Processing Input and Output Signals Demonstrating Signal Enhancement

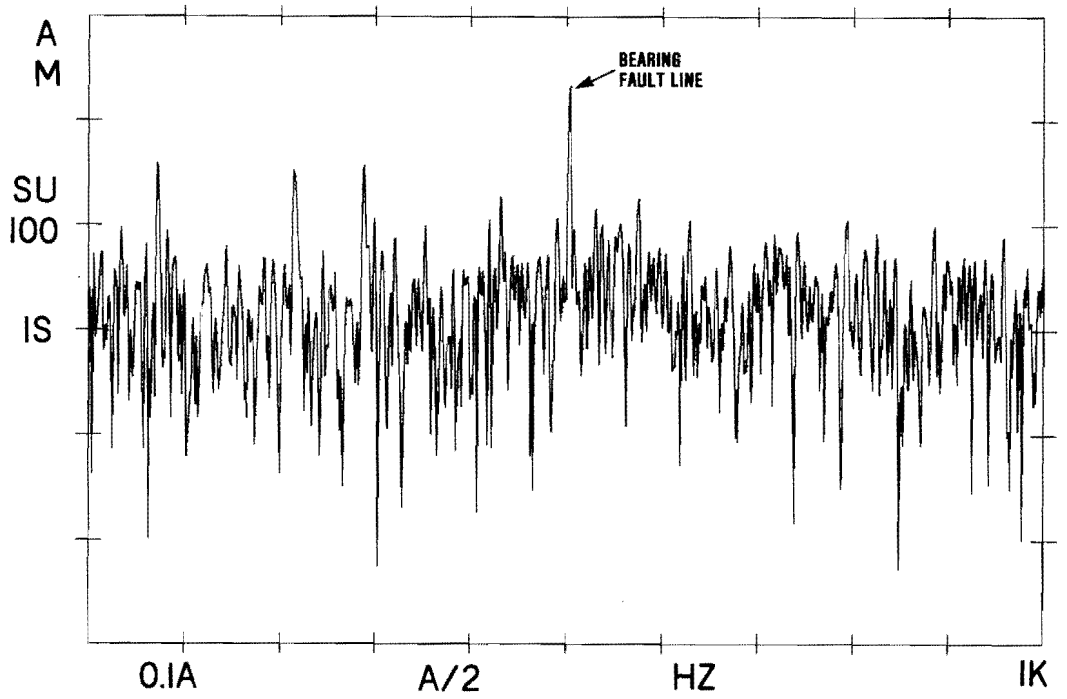

Figure 115. Bearing Fault Signature Resulting From Single FFT

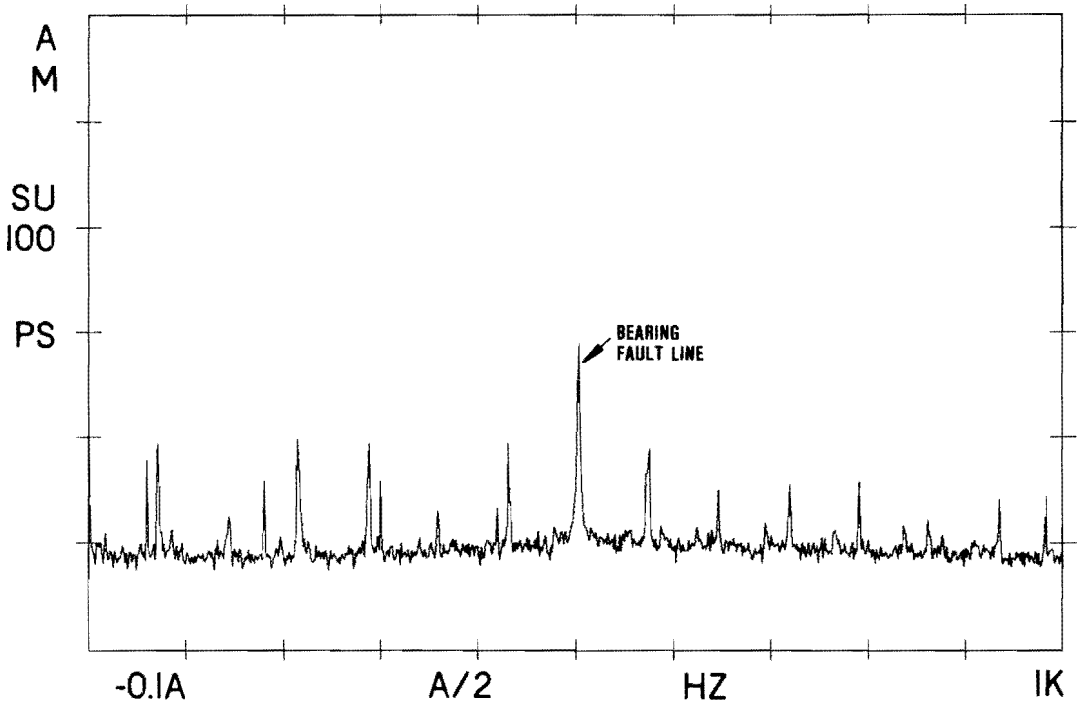

Figure 116. Enhanced Bearing Fault Signal Resulting From Averaging 100 FFTs

6.7 IDENTIFICATION AND CLASSIFICATION OF FEATURES FROM THE SPECTRUM

At this point in the processing, the FFT is represented as a series of numbers which require interpretation for detection of bearing phenomena. Two important quantities must be determined from the FFT line structure: the center frequency of the peak and the magnitude, in dB, that the peak exceeds the background noise (as shown below).

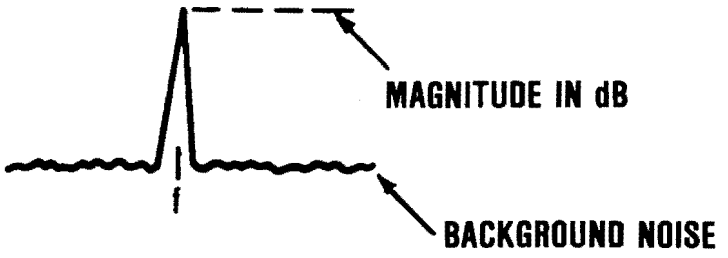

As a fault progresses in severity, the structure of lines in the FFT will change both in width and in amplitude. Figure 117 shows the change in the spectrum from a fault which progressed from the C/D level to the extremely gross category. The identification and classification process is designed to accommodate this possible change in line structure.

6.8 SORTING OF THE SPECTRAL LINES INTO BEARING FAULT CATEGORIES

The next procedure in the processing chain is to find the N largest lines in the spectra. A typical value for N might be 50. For illustration purposes, N = 6 is chosen in the following example. Normally 'largest' refers to peak amplitude; however, factors such as area come into consideration when a peak from a gross fault appears to be indicated. The example presented is for the annotated spectrum shown in Figure 118.

The frequencies and peak values determined from Figure 118 are:

Peak Number	Frequency	Peak Amp (dB)
1	509	19
2	70	11
3	214	11
4	288	10.5
5	455	9.5
6	577	9.5

(Areas under the peak are not calculated for this example.)

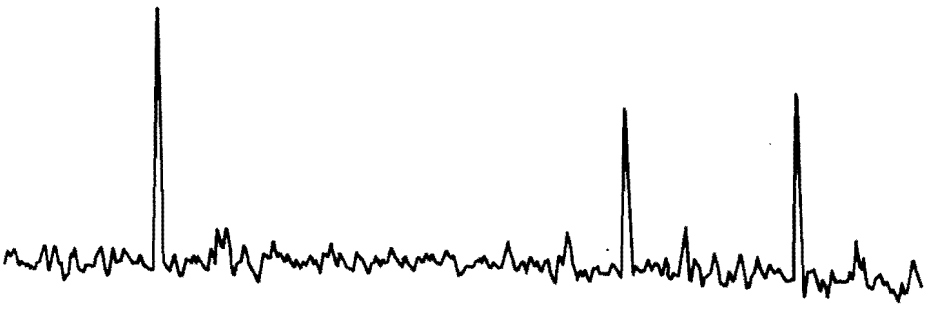

LINE SPECTRUM TYPICAL OF C/D FAULT

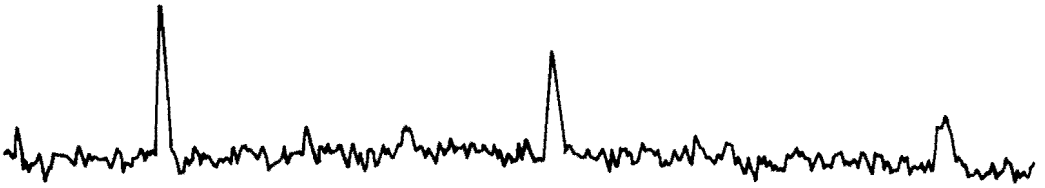

LINE SPECTRUM IN TRANSITION

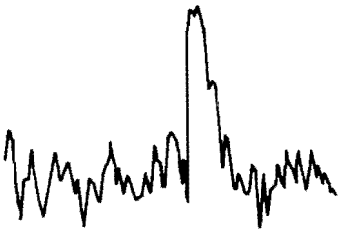

LINE SPECTRUM TYPICAL OF
EXTREMELY GROSS FAULTS

Figure 117. Fault Progression Spectra

The possible bearing fault frequencies which could be present in this spectrum are:

Type	Fundamental	Harmonics
Input Ball OR	351	702 1053
Input Ball IR	509	1018 Outside FFT Range
Input Roller OR	348	696 1044
Input Roller IR	513	1026 Outside FFT Range
Output Ball OR	136	272 408 544 680 816 962
Output Roller OR	134	268 402 540 674 808 942
Output Roller IR	192	384 576 768 960

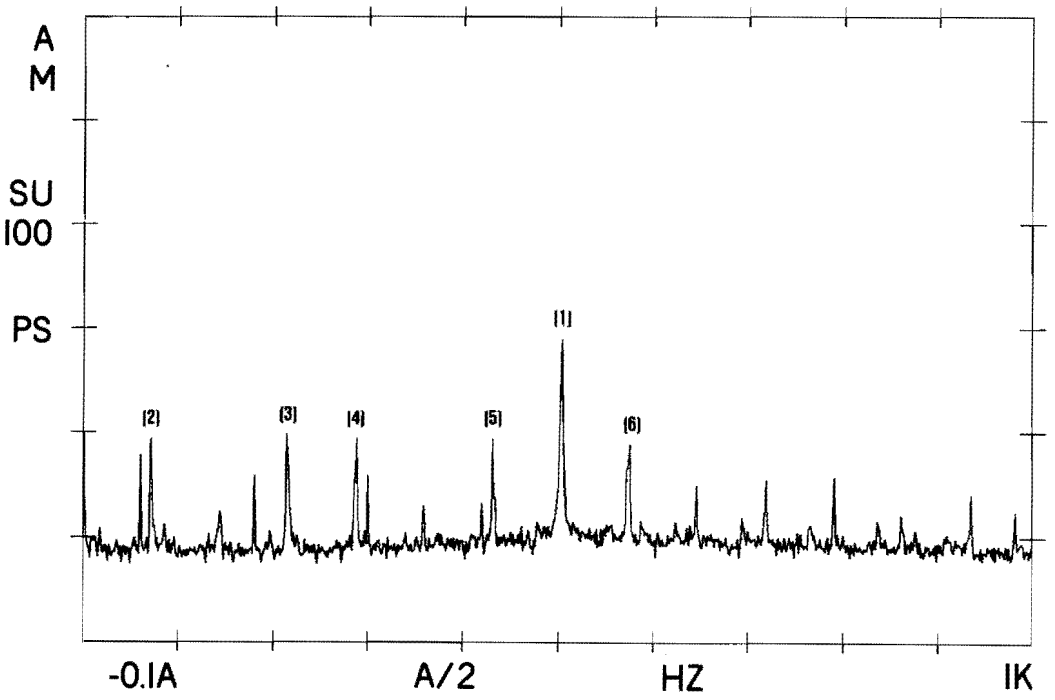

Figure 118. Identification of Six Largest Peaks

The procedure is to search the spectrum lines for frequency matches of the bearing fundamental frequency or second harmonic frequency. The results of the search reveal a single match, peak #1, which corresponds to the input ball IR fault. Next, the first sidebands around the matched frequency are analyzed. The displacement of the sidebands is equal to the shaft frequency, which is around 72 Hz. Again, a match is found for the sidebands which are peaks #5 and #6. The other peaks represent the fundamental and harmonics of the shaft speed. So the results of this search are as follows:

- Input Ball IR Fault Spectral peaks:

  #1 - 509 Hz, 19 dB (fundamental)
  #5 - 455 Hz, 9.5 dB (lower sideband)
  #6 - 577 Hz, 9.5 dB (upper sideband)

6.9 COMPUTATION OF NORMALIZED SIGNAL

The normalized signal is the sum of all identified fault signals. For this example, the normalized signal level is

19 dB + 9.5 dB + 9.5 dB = 23.45 dB (dBs do not directly add)

6.10 COMPUTATION OF COHERENT ENERGY

In order to compute the true signal level, the normalized signal needs to be converted by scaling the signal to the baseline level in the spectrum and to the signal gain contributed by the test set. (Unless this is done, distinguishing between a bearing B-level fault and a C-level fault cannot be done.)

At this point a decision on whether a bearing is good or bad can be made by comparing the energy value to a pre-established limit. Paragraph 7.2 provides the details on setting limit values.

SECTION 7
DATA BASE AND LIMIT DEVELOPMENT

7.1 DATA BASE DEVELOPMENT

A data base of faulted and nonfaulted bearing signals was collected on Government-furnished equipment at RCA, at Fort Rucker, and at Bell Helicopter Textron, Inc. Accelerometer data from faulted and nonfaulted bearings on AH-1S, UH-1H, and OH-58 tail assemblies was direct recorded at 30 in/s on magnetic tape using a Honeywell 5600 recorder. The signal from the accelerometer was processed by adding gain (from 1 to 100) and low pass filtering (two low pass poles at 5 kHz) before recording. Two types of accelerometers were used in collecting data during these tests: a miniature commercial sensor and an RCA specified ruggedized sensor. Both types of accelerometers have a resonant frequency greater than 40 kHz (which is above the region of interest) and a sensitivity of 10 mV/G. Further data on these accelerometers can be found in Section 5.1.3. The commercial accelerometer used RG-58A coax cable to interface to the data recorder, while the ruggedized units used TWIN-X cable. All of the initial data collected at Fort Rucker and at Bell Helicopter Textron, Inc. used the commercial type accelerometer, while subsequent tests on aircraft fault insertion and on the RCA OH-58 test stand used both types of accelerometers.

These accelerometers were placed on gearboxes and hanger bearings by various mounting methods and in a variety of locations to determine optimum mount placement and geometric design. Several permutations of mounts were examined including glued-on mounts, screwed-on mounts, steel mounts, and aluminum mounts. Placement of the accelerometers on the gearbox and hanger bearings, including orientation and location, was examined to provide the optimum position which maximized the signal-to-noise ratio. Two geometric shapes of mounts (L type and cube type) were closely studied to determine which shape has the highest stiffness (therefore the highest resonant frequency) and the flattest response in the region of interest (15-35 kHz). Many mounts have resonances and antiresonances in the region of interest which can be detrimental or advantageous when trying to detect certain faulted bearings. The bearings used for data base development were class C/D faults except for the fault progression data development where faults were incrementally enlarged from class B to gross. These faults were placed on outer races, inner races, and rolling elements. Prior to insertion of the fault, each bearing was disassembled and cleaned. The desired fault was then inserted using a die grinder with diamond-tipped tool. After fault insertion the bearing was cleaned again and reassembled using 0.5 cc of the specified lubricant.

Related experiments to expand the data base were also carried out. These included investigation of gearbox oil temperature effects upon fault sensitivity and the effects of gearbox loading. It appears that oil temperature has little effect upon fault sensitivity although the overall signal level rises as the oil is warmed. Loading effects yield higher

sensitivity at flat pitch as opposed to full pitch, although the optimum sensitivity may be somewhere in between at an intermediate load level. Different lube oil was also examined using arctic lube (MIL-L-7808) as opposed to MIL-L-23699. The major difference in these oils is the viscosity index, which is lower for arctic lube. These tests concluded that there is no appreciable change in sensitivity between the two oil types. A further related test was conducted to determine the effects of tail rotor imbalance on signal sensitivity. These tests showed that the sensitivity is unaffected.

The helicopter tests used components both with known good bearings and implanted faulty bearings. These tests, carried out at Fort Rucker and at Fort Devens on OH-58, UH-1H, and AH-1S helicopters, were used to simulate real test conditions with real background noise and vibration. The data from these tests was recorded either on magnetic tape or as a hard copy of a fast Fourier transform after processing by the developed test set.

7.2 THRESHOLD SETTINGS AND VALIDATION APPROACH

7.2.1 Process of Deriving Threshold Settings from Data

This procedure is designed to obtain 90 percent confidence of 10 percent or less false alarm rate. The quality of the RCA fault detection system is such that 90 percent or greater probability of detection is expected.

7.2.1.1 Procedure Prior to Fielding the Test Set

Owing to the difficulty and expense of collecting data from a large number of aircraft, the system has been designed to detect failures at high signal-to-noise ratios, thereby allowing for the aircraft-to-aircraft variations anticipated during field tests (see Section 2.5). Typically, at the final stage of data processing, the ratio of average signal to RMS noise is 20 dB (10 to 1).

The following steps of data reduction should be followed to establish thresholds prior to field tests. Typically, only three or four independent tests will be required for each bearing for each aircraft:

(1) Measure the signal peak-to-base difference on a decibel scale for as many independent samples as are available. (Include test stand data if statistically similar to aircraft data, as judged by the effectiveness of predetection filters [see Section 5.1.3], and effect of different accelerometer mounts).

(2) Calculate the mean value, M_{s+n}, and standard deviation, S_{s+n}, of the signals. This constitutes the statistics of the signal sample.

(3) Measure the baseline samples, no signal present.

(4) Calculate the mean, M_n, and standard deviation, S_n, of the baseline.

(5) For 90 percent confidence of 10 percent or less false alarm probability, multiply S_n by the number from Table 4 for the sample size (typically three or four). Add this number to the mean level of the baseline. The result is the required threshold setting.

7.2.1.2 Validating and Adjusting Thresholds in the Field

The data processing algorithms incorporated into the SPADE unit have used almost the entire amount of data collected up to the present, to develop a system which yields the highest possible signal-to-noise ratio at the output of the test set. Therefore, independent tests of the system performance can only be made on new data. The procedure for utilizing new data is as follows:

(1) Run the system on live test aircraft (simultaneously recording the filtered accelerometer outputs to preserve data).

(2) For inserted faults, record system response as correct or incorrect to produce the "box score". For natural faults, it is recommended that the bearing assembly be disassembled and inspected for fault conditions or lack thereof.

(3) Repeat the measurements of Section 7.2.1.1, combine the data, and reset the thresholds accordingly. Since the original setting was done for 90 percent confidence on a small sample, it is likely that the new threshold will be smaller than the original, thereby yielding higher probability of detection (see Section 6.2.1.3). Resetting of thresholds should cease at a total number of no more than 10 independent samples and preferably no less than 7.

(4) Once the full set of sample measurements is available, estimate the probability of detection. If greater than 90 percent, it may be desirable to raise the threshold so as to reduce the probability of false alarm below the 10 percent figure.

All threshold changes should be documented with reasons and detailed calculations to support the change and should be approved by engineering management. No other changes should be permitted.

It is recommended that only true independent sample data be used to build the threshold limit data base.

7.2.1.3 Estimation of Performance

Using the procedural steps identified in (2) through (5), performance may be estimated at any stage of data collection as follows:

(1) Subtract the threshold setting from the mean value of the signal plus noise, M_{s+n}, leaving the excess signal available for confidence.

(2) Using the appropriate sample size, multiply all tabular values by the standard deviation of the signal plus noise, S_{s+n}.

(3) Compare the excess signal to these values to determine the confidence level.

SECTION 8
SYSTEM PERFORMANCE EVALUATION

This section defines the method by which performance or effectiveness is evaluated. The approach taken is to adopt the standards defined in Section 7.2. In defining the performance results, the 10-percent false alarm level and the helicopter environment must be determined and the results compared. To offset the limitations of the small sample on-aircraft data base that was available, large fault to baseline signal ratios were required in order to set thresholds and effectively implement the technique. The performance evaluation is presented for the time domain approach (SPA) in Section 8.1 and the frequency domain technique in Section 8.2. The results can be summarized as follows:

- The time domain technique (SPA) performed very poorly, particularly when compared to a 10-percent false alarm rate which is desired in the helicopter environment.

- The frequency domain technique performed very well in fulfilling the goals stated in Section 7.2.

The frequency domain technique had a large ratio between fault level and the 10-percent false alarm level. The effectiveness on all three helicopters was over 90 percent (93 percent, 94 percent, 100 percent) when the 10-percent threshold level was considered.

The third part of this section covers areas where more investigation is suggested to further improve the diagnostic results.

8.1 PERFORMANCE OF TIME DOMAIN APPROACH

The time domain technique or shock pulse technique gave poor performance results. The time domain technique, while not an effective diagnostic technique for C/D level faults, was effective for monitoring the gross power level in the detection of gross bearing faults.

Figures 119 through 121, present the performance of the time domain approach during tests of the 90-degree gearbox for the UH-1 and AH-1 helicopters, the 42-degree gearbox for the same helicopters, and the 90-degree gearbox for the OH-58 helicopter. As can be seen from these figures, one common factor causes the poor performance of the time domain approach on helicopters: the baseline performance in the helicopter environment, and the criterion of a 10-percent false alarm ratio, results in the baseline being above most of the implanted faults. Also, most of the bearing faults which are above the 10-percent false alarm limit are ball bearing faults which are more effectively detected by the frequency domain technique.

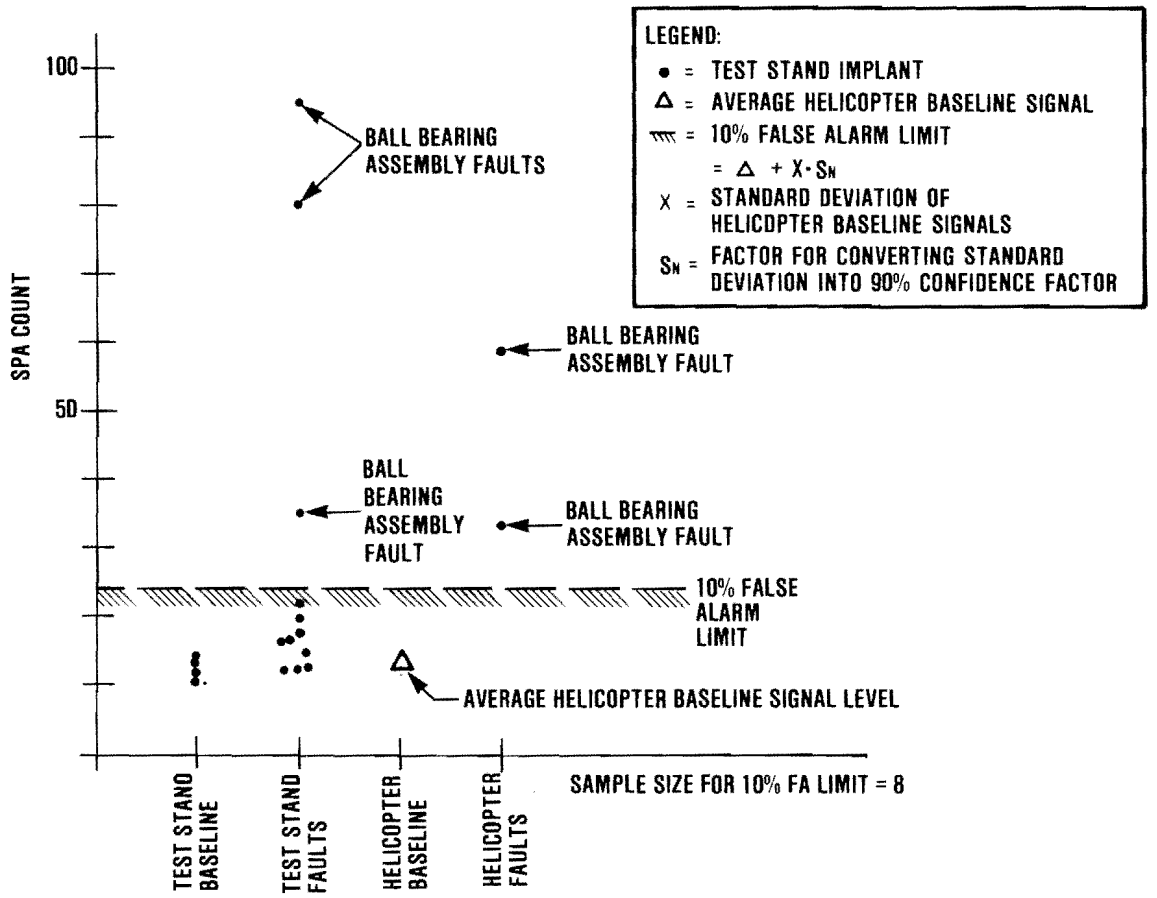

Figure 119. Time Domain Performance, 90-Degree Gearbox Data for UH-1 and AH-1 Aircraft

The time domain method was also unsuccessful in locating bearing rolling element faults because all of the rolling element faults produced signal levels not much above the test stand baseline, which was considerably below the 10-percent false alarm ratio. In an attempt to improve the time domain process performance, an alternative normalized time domain algorithm was tried. However, this algorithm also proved inconsistent in developing a fault trend.

8.2 PERFORMANCE RESULTS FOR FREQUENCY DOMAIN TECHNIQUES

The frequency domain performance data has been divided into the following categories:

(1) Huey/Cobra 42-degree Gearbox
(2) Huey/Cobra 90-degree Gearbox

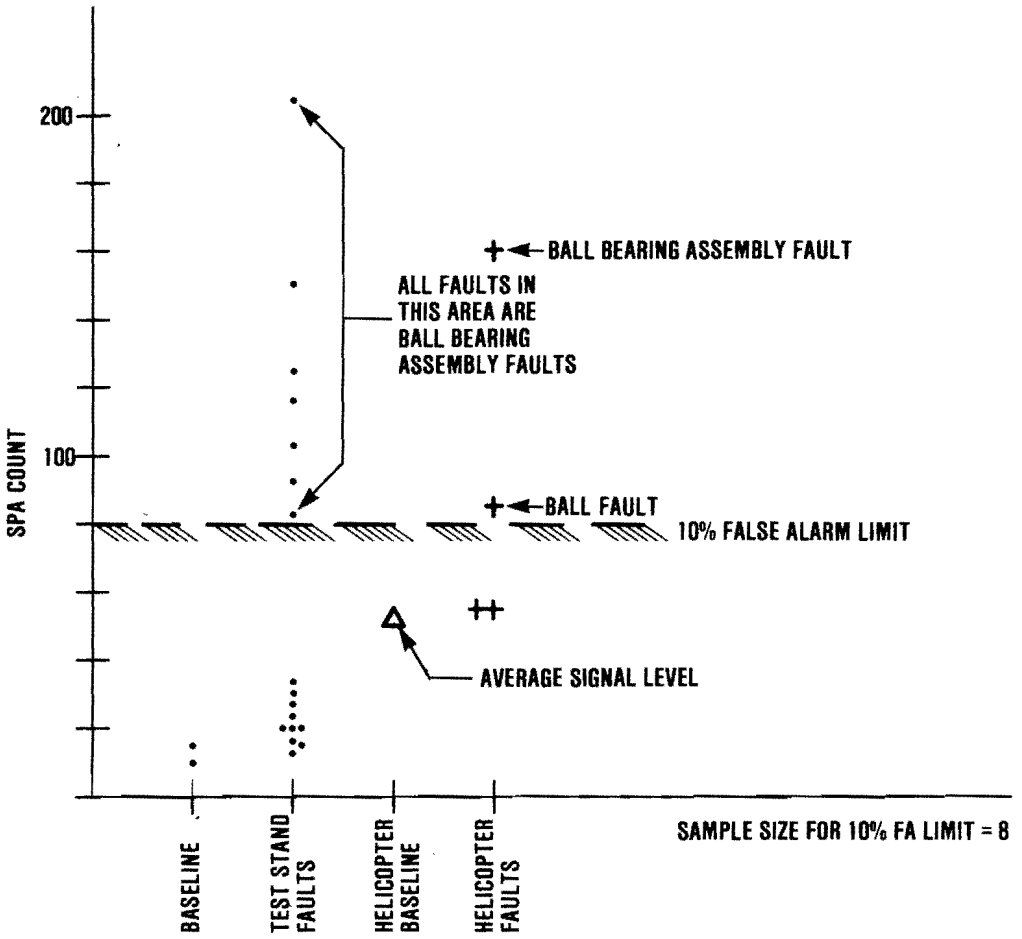

Figure 120. Time Domain Performance, 42-Degree Gearbox Data for UH-1 and AH-1 Aircraft

(3) OH-58 90-degree Gearbox
(4) Hanger bearings (OH-58, Huey and Cobra combined)

The analysis of the background levels, fault levels, and helicopter noise levels indicates that the components in the above categories behave in an equivalent manner. The results for the four categories are shown in Figures 122 through 125 respectively. The results are summarized in Table 7 for each helicopter.

The combined effectiveness is defined as the sum of the product of the number of bearings of a given type times the percent detection for that type divided by the total number of bearings in the helicopter. The only fault not detected was an outer race defect on the 42-degree gearbox of the UH-1 and AH-1. The opinion is held that this fault is detectable, but the fault was incorrectly inserted. This problem will be discussed later in the section on roller element faults.

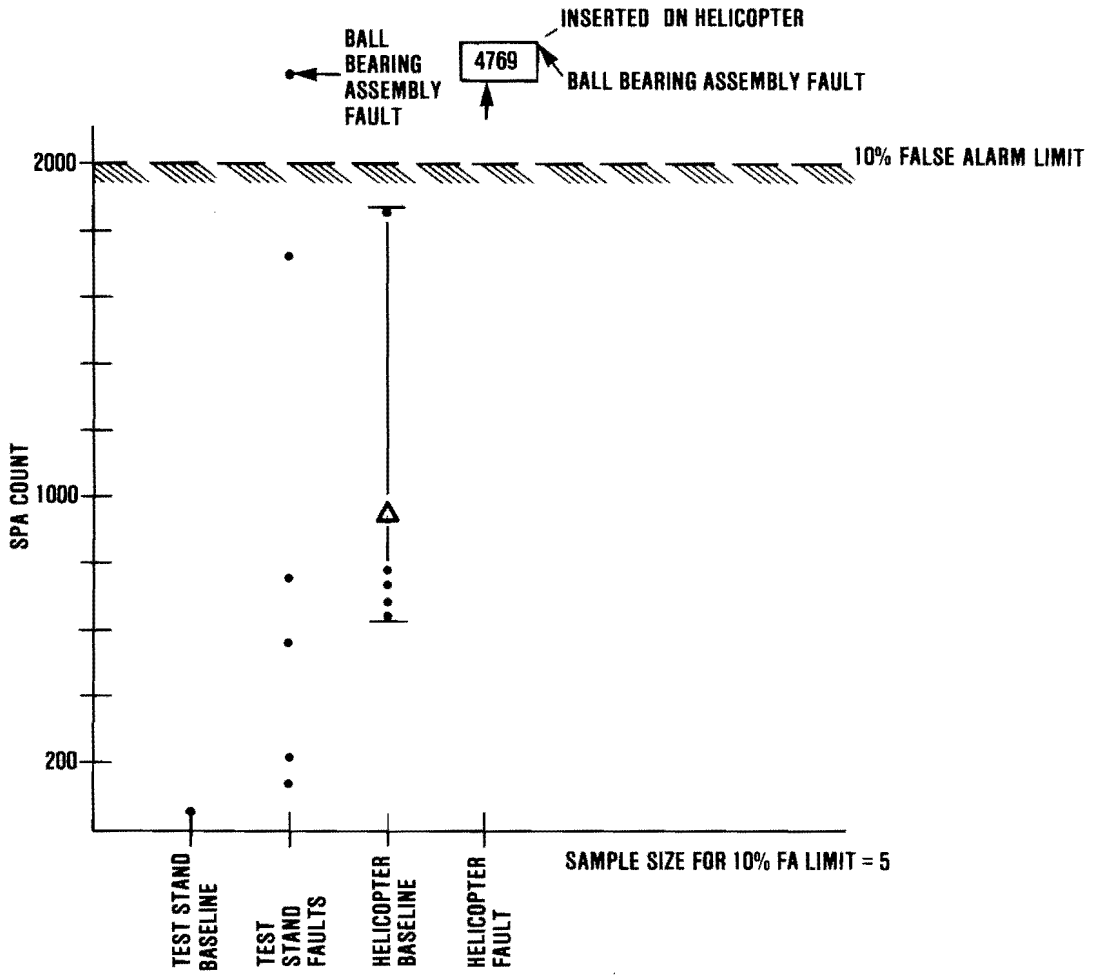

Figure 121. Time Domain Performance, 90-Degree Gearbox Data for OH-58 Aircraft

The number of inserted faults for each bearing type was not sufficient to determine a statistical spread in the fault levels. Therefore, only the range of fault levels were presented in Figures 122 through 125. However, if one compares the 10 percent false alarm level with the spread in the fault levels, one can see the faults are not marginal but are readily detectable. If the 10 percent false alarm ratio was raised by 5 to 10 dB, the level of detection would not change very much.

8.3 AREAS RECOMMENDED FOR FURTHER DEVELOPMENT

This section presents suggested development areas to further improve the bearing fault detection process.

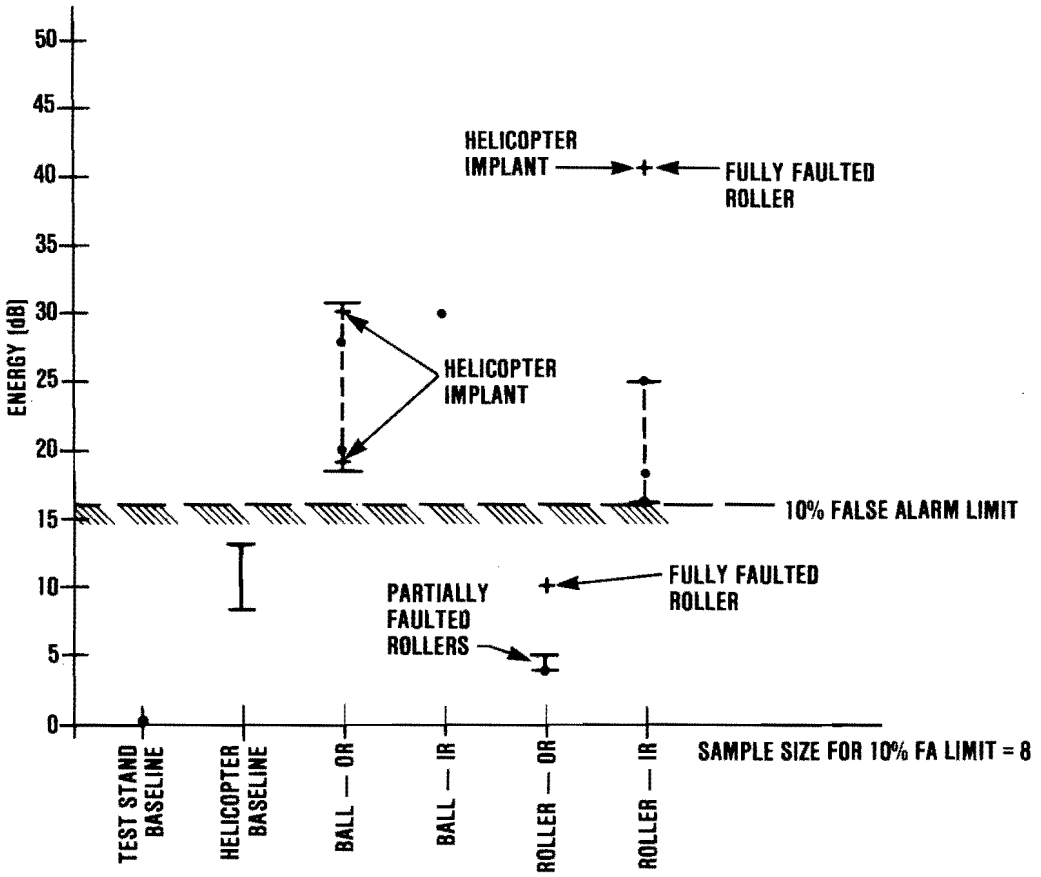

Figure 122. Frequency Domain Performance, 42-Degree Gearbox Data for UH-1 and AH-1 Aircraft

(1) Investigation of the 42-degree gearbox roller bearing outer race fault

The fault data analyzed to date indicates that the implanted outer race fault for the input and output roller bearings of the 42-degree gearbox was not detected. The missed run included two fully faulted rollers which were implanted in the helicopter gearbox. It is believed the reason the fault was not detected was improper insertion; i.e., the faults were not inserted in the load zone of the bearing. Due to the nature of this bearing assembly, most of the load is concentrated on two or three rollers. The load concentration is so great that the unloaded bearing rollers actually skid. If the defect is not in the load zone, the implant process is invalid and no fault signature will be detected. Further effort is suggested to investigate this test result.

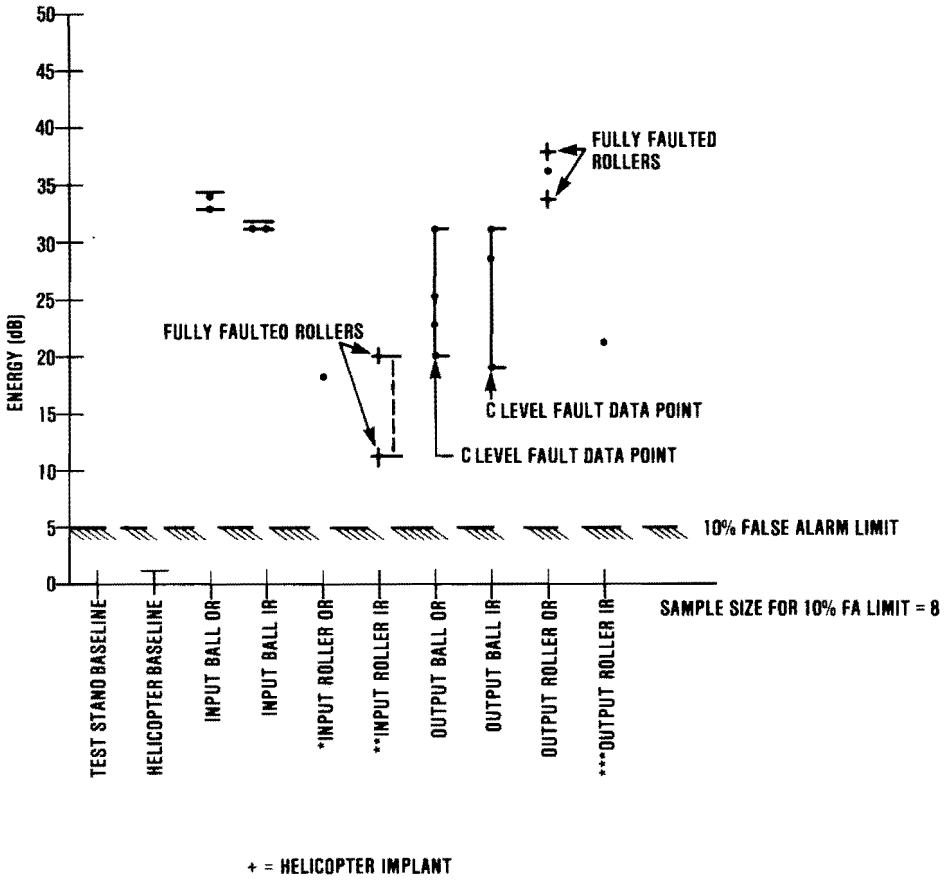

Figure 123. Frequency Domain Performance, 90-Degree Gearbox Data for UH-1 and AH-1 Aircraft

(2) Inconsistency in partially faulted rollers

The roller faults implanted were below the level of the class C/D fault. The class C/D fault is defined as having the fault extend across the length of the ball path. However, on the advice of Bell Helicopter Textron, Inc. personnel, the faults were extended only partially across the roller path. This advice was based upon the observations that early faults do not extend across the roller paths. The results of fault insertion revealed that rollers which were faulted across the length of the path showed excellent fault detection. However, defects that were partially faulted across the roller path showed either very high level signatures or very low level signatures. None of the partial faults showed a mid-range level signature. The cause of the differences in the signals is believed to be alignment mismatches in reassembling the bearing. The rollers are crowned along the surface of the roller on the order of 20 millionths of an inch. Under light loads a very small area of

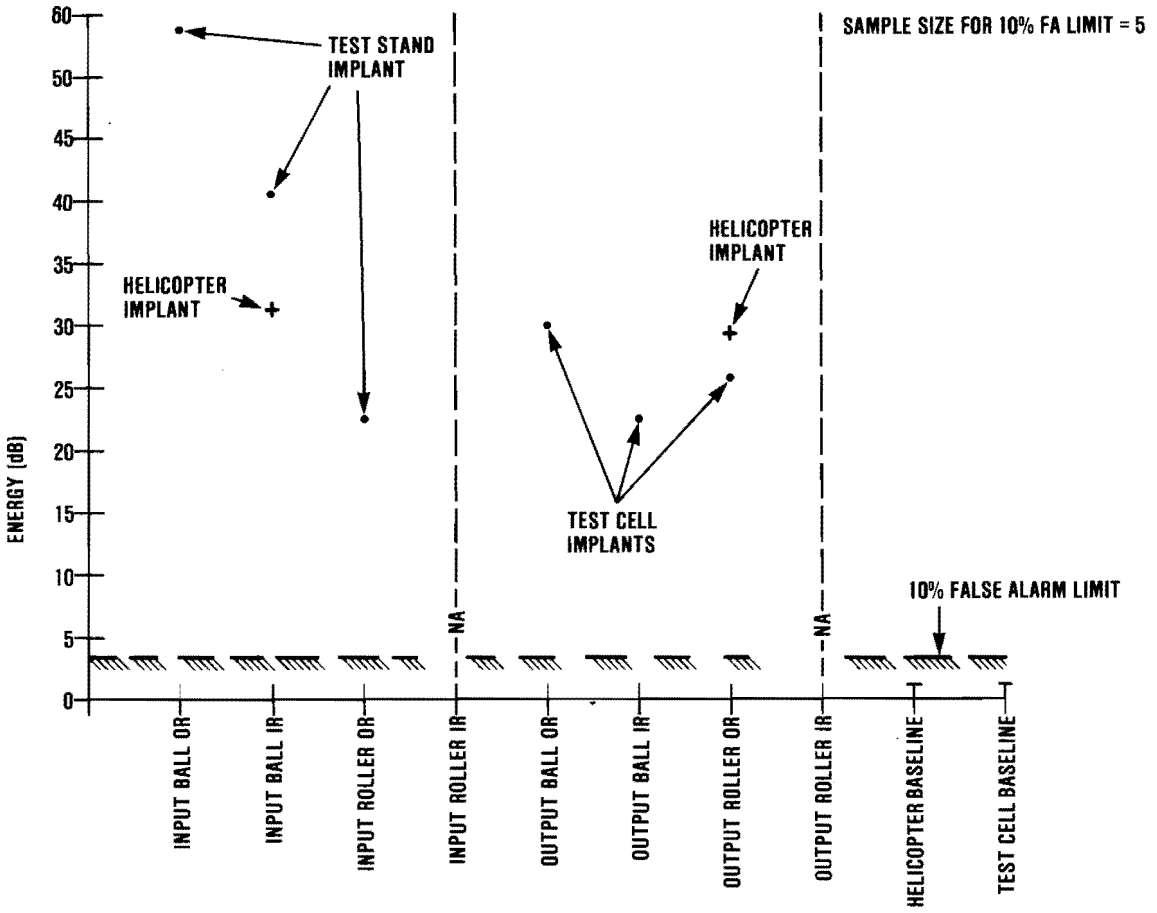

Figure 124. Frequency Domain Performance, 90-Degree Gearbox Data for OH-58 Aircraft

the roller is in contact with the race. As a result, the point of contact of the roller could shift out of the defect zone with a slight misalignment of the two races. This is a plausible explanation, but should be investigated and established conclusively.

(3) Mounts and accelerometers

The performance results presented in this section were taken with the L-shaped mount and the miniature accelerometers. The accelerometer designed for SPADE was not available at the time of the data taking. The thresholds which were computed in this section are valid for the L-shaped mount and the miniature accelerometer and, as of the present time, have not been validated for the SPADE accelerometer. Additional test validation is recommended.

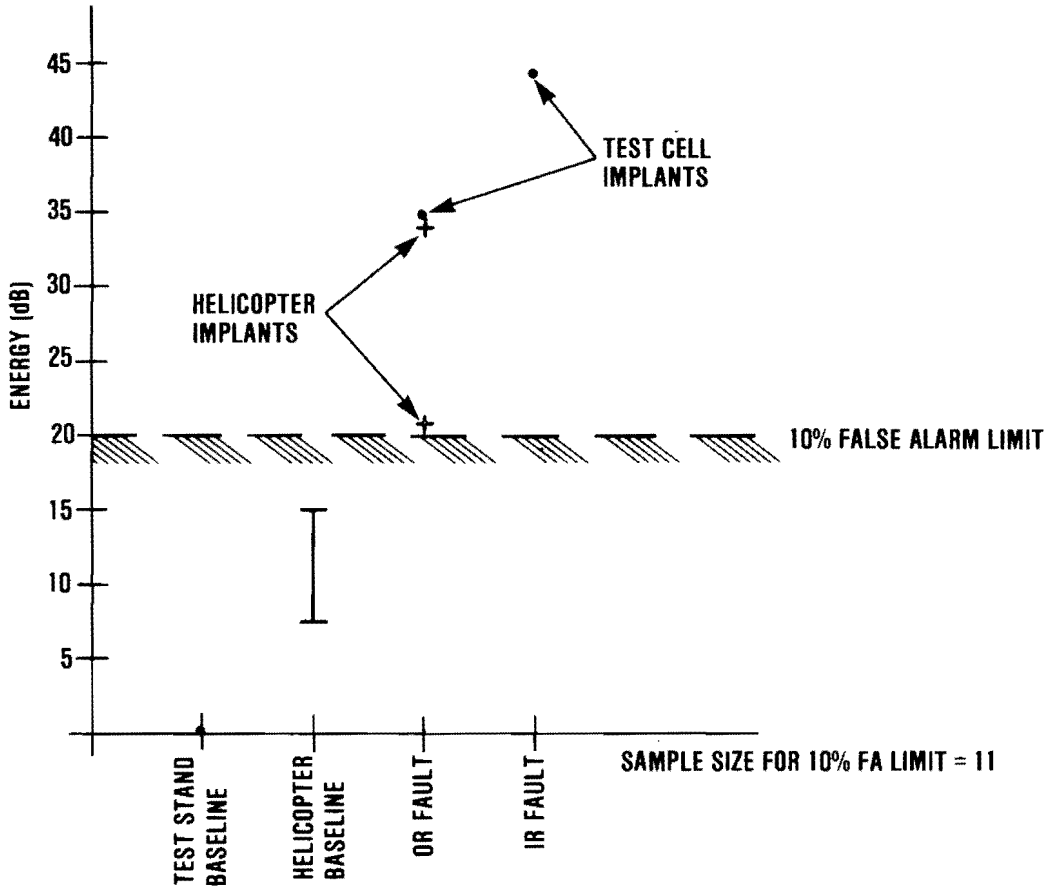

Figure 125. Frequency Domain Performance, Hanger Bearing Data for Bearing Faults

(4) Investigation and possible reduction of the noise floor

The 90-degree gearboxes for the AH-1, UH-1 and OH-58 helicopters had noise levels which were consistent with the noise levels experienced on test stand data. For hanger bearings and 42-degree gearboxes, the on-aircraft noise environment is considerably higher than test stand results. The phenomena behind this rise should be investigated, and it is anticipated that once it is understood, the helicopter noise floor could be reduced.

TABLE 7. SUMMARY OF FREQUENCY DOMAIN PERFORMANCE

Bearing Breakdown		Percent Detection @ 10-Percent False Alarm Rate
AH-1 (Cobra)		
4 hangers		100
90-degree gearbox bearings	4 duplex ball	100
	2 roller	100
42-degree gearbox bearings	4 duplex ball	100
	2 roller	60 percent (Outer race faults were not detected)
Combined effectiveness		94
UH-1 (Huey)		
(The difference between the UH-1 and AH-1 is one less hanger bearing)		
Combined effectiveness		93
OH-58		
8 hangers		100
90-degree gearbox bearings	4 duplex ball	100
	2 roller	100
Combined effectiveness		100

SECTION 9
CONCLUSIONS

The SPADE engineering development achieved a simple, effective means of reliably and accurately detecting class C/D bearing failures. Fault implant tests, in test cells and on aircraft, demonstrated that the method is sensitive only to bearing faults and is immune to extraneous gear and shaft vibrations which characterize the helicopter environment. The technique allows thresholds to be computed from a limited set of data with a 10-percent false alarm rate (which was well below the fault ranges for most bearings). Fault progression test data revealed that the method could detect faults in bearings as low as the B/C fault level.

The bearing fault detection method was based upon the "Shock Model" shown in the illustration below:

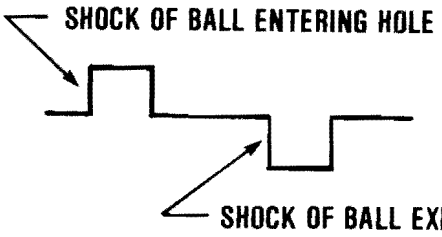

As can be seen, the model deviates from the original model in that two shock pulses, not one, are generated. The first shock pulse originates from the ball entering the fault while the second shock pulse originates from the ball exiting the fault. The detection scheme is based upon an understanding of the physical phenomena of these events, and a signal processing design capable of discriminating the resultant signal characteristics.

The original basis of the SPADE system was the detection of shock pulses by the ringing of a resonant filter. However, it was premised incorrectly on the existence of an impulse-like shock pulse. The elastic compliance of bearing races and even accelerometer mounts is insufficient to allow the impulses as shown in the illustration above to be transferred to the accelerometer. Instead, these elements act as resonant devices, with the bearing fault signature exhibited much like the signal shown in Figure 126. Therefore, the detection scheme which was developed in the original SPADE breadboard was ineffective. The basic mechanism for fault detection remains the same; however, the expected bearing fault waveform is completely different. To complicate matters further, the original SPADE detection scheme overlooked phenomena which interfere with the detection process, such as gear noise and helicopter shaft noise. Based upon acquired knowledge of the fault signature and noise environment, the filtering scheme depicted in Figure 127 was adopted to discriminate bearing fault signatures from signals which are extraneous. Both the current and original system designs employed filtering to remove low frequency machinery noise. In the original SPADE

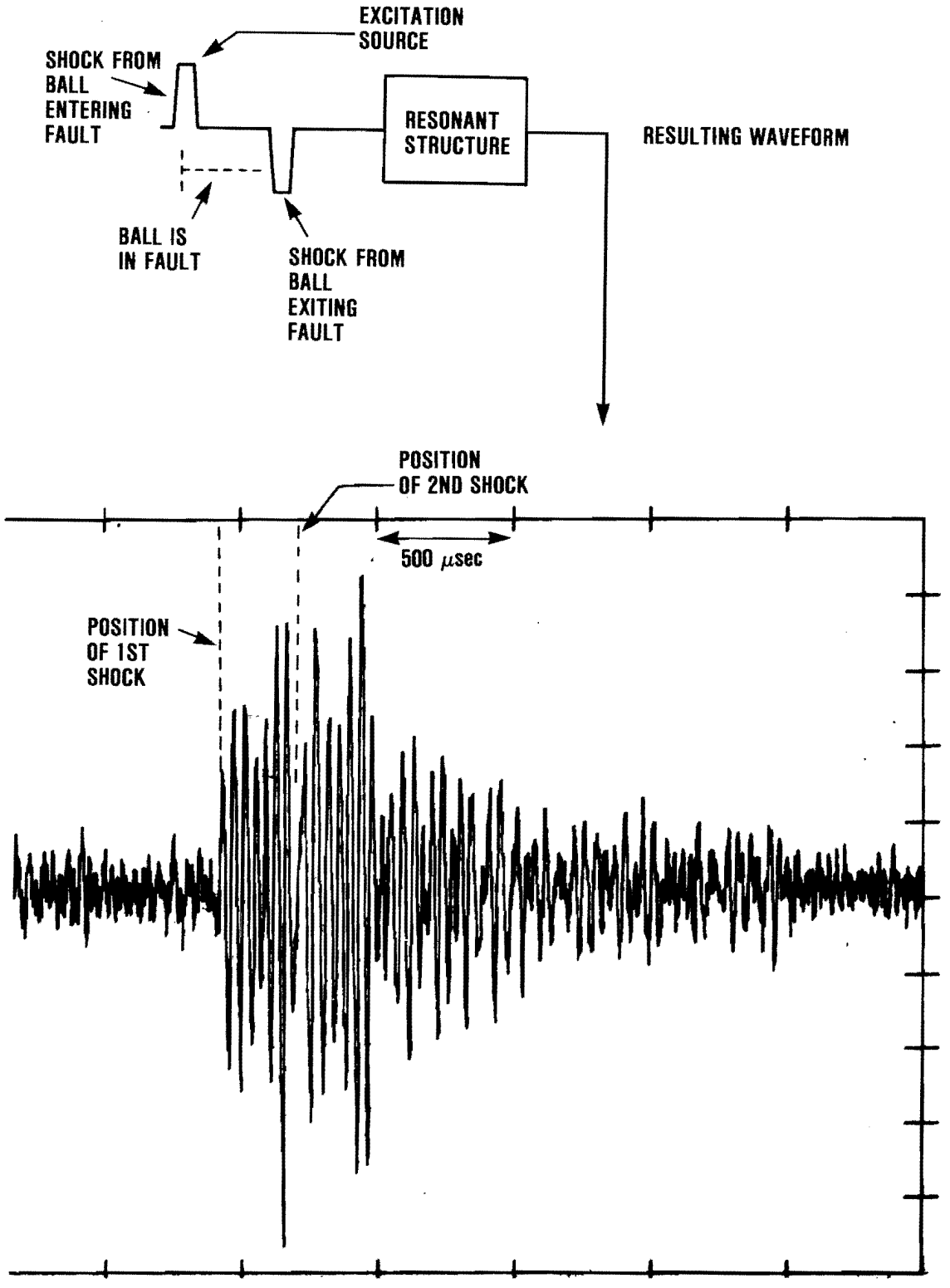

Figure 126. Characteristics of Bearing Fault Signature

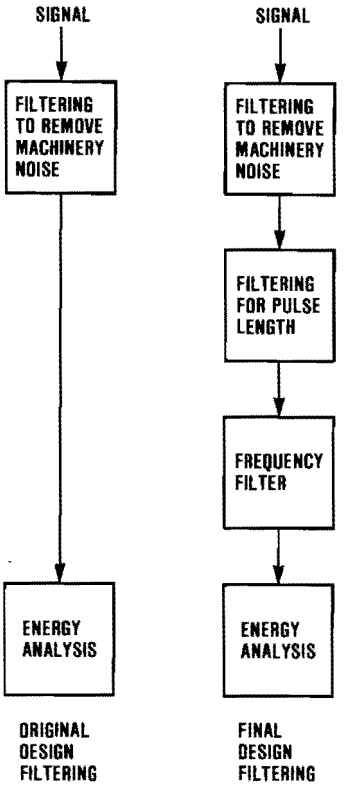

Figure 127. Processing Done by Original SPADE Unit Contrasted to New SPADE Unit

system, a resonant filter was used to remove machinery noise. Since the shock pulse excites a resonant bearing structure, a resonant filter is not needed. The resonant filter was replaced by a very steep band-pass filter which more effectively eliminated machinery noise.

Filtering for pulse length was incorporated in the current design as a discrimination technique to take advantage of the fact that a bearing spall fault produces a constant fault signature as shown in Figure 126. Pulse processing is used to separate fault signatures from gear-mesh noise, which has pulse lengths much smaller than bearing faults, and from shaft imbalance, which has pulse lengths much greater than bearing faults. Due to the periodicity in shaft rotation, the fault signatures can be separated from other sources of noise and each individual bearing fault type can be separated from others by filtering in the frequency domain. An FFT analysis is done solely for the purpose of high resolution filtering. Pattern analysis, or matching, is not employed in the analysis. Rather, each bearing failure mode has a repetition rate which can be easily calculated. Since the signature is not a sine wave, the signature will appear in the frequency domain as a set of frequencies which are computable. For these, a template as shown in Figure 128 can be constructed. By applying this template to the FFT results, the energy which is present for a particular bearing failure can be calculated. A sum of the energy from each of the elements of the template is determined as shown in Figure 129. The result is a single energy value

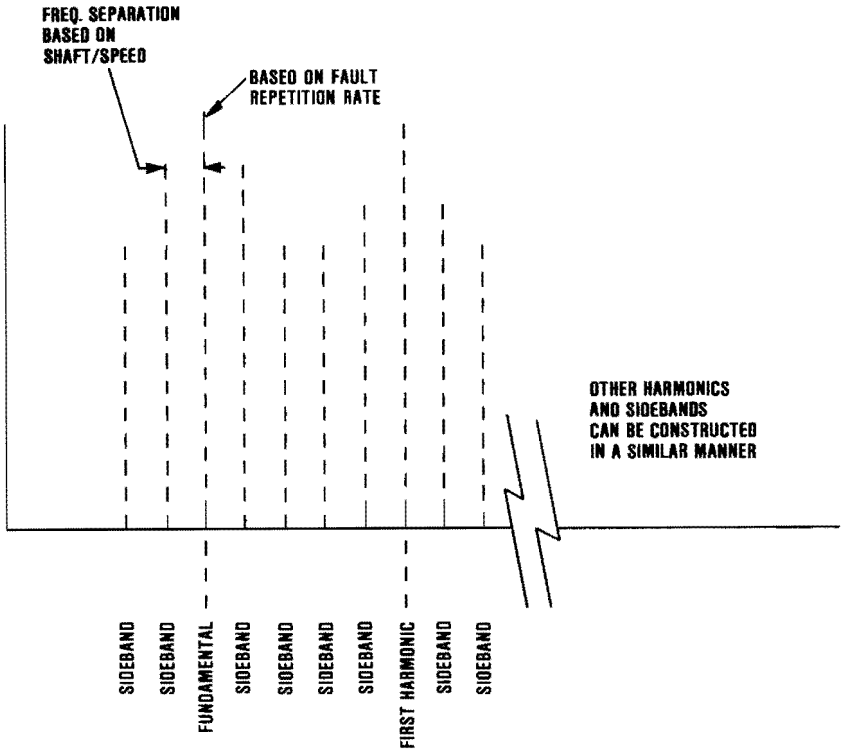

Figure 128. Typical Frequency Template for Bearing Faults

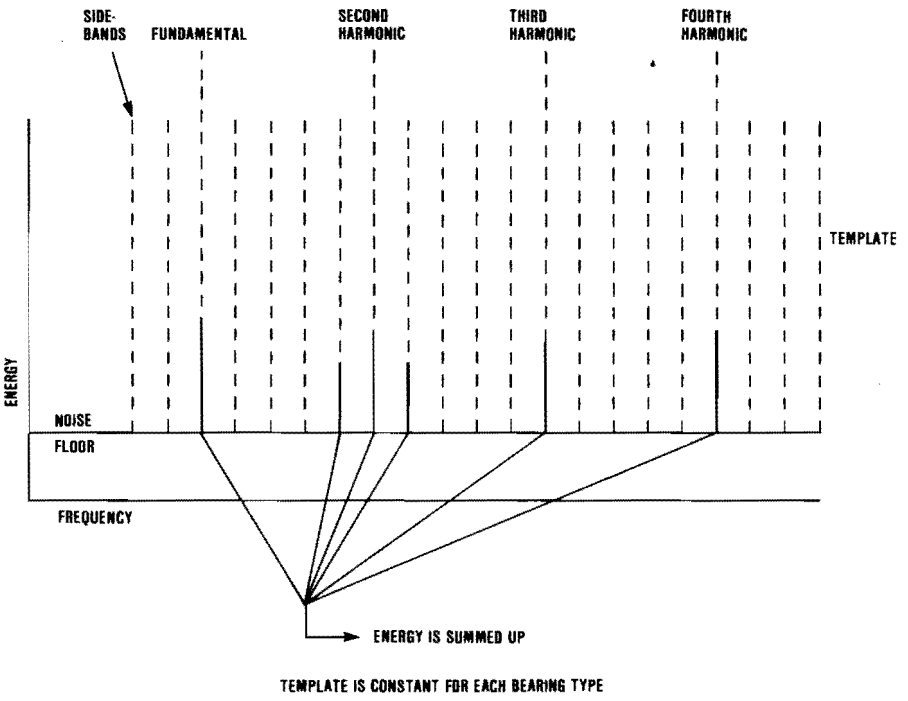

Figure 129. Energy Calculation

for the bearing failure modes which can then be compared to the pre-established threshold limits for the bearing. Figure 130 shows the energy level versus fault severity for a hanger bearing with a progression of inner race fault implants. The energy level is expressed in dB and there is a 25 to 30 dB rise in energy from baseline to a class C/D fault level. From the results shown in Figure 130, as well as the results presented in Chapter 8, the SPADE system was determined to be capable of detecting class C/D faults well within the constraint of a 10 percent false alarm rate.

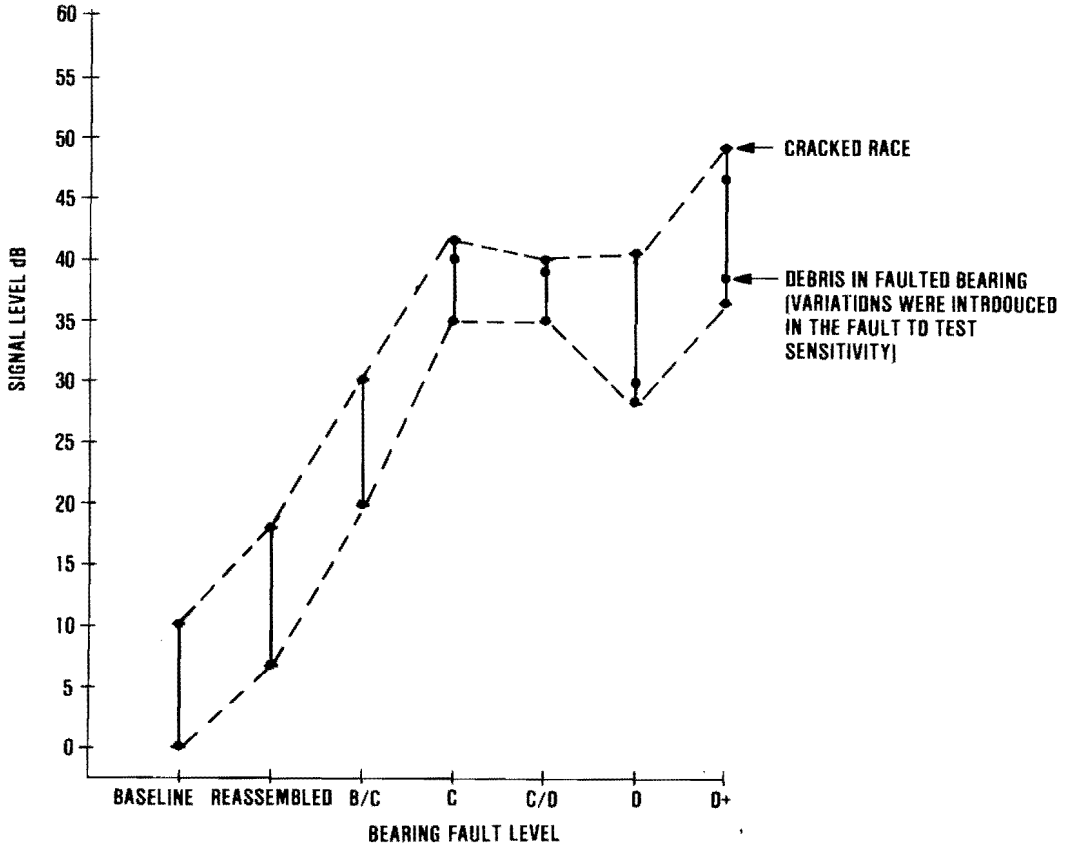

Figure 130. Fault Progression Data

REFERENCES

1. David B. Board, "Small Portable Analyzer Diagnostic Equipment (SPADE), Advance Development Prototype Report," SKF Industries, Incorporated, AVRADCOM TR-80-F-3, September 1979.

2. D. Dyer and R. M. Stewart, "Detection of Rolling Element Bearing Damage by Statistical Vibration Analysis," Journal of Mechanical Doings, April 1978, pp. 229-235.

3. Martin and Thomson, "Robust-Resistant Spectrum Estimation," Proceedings of the IEEE, Vol. 70 No. 9, September 1982, pp. 1097-1115.

4. D. J. Thompson, "Spectrum Estimation Techniques for Characterization and Development of WT4 Waveguide, Part I," Bell Systems Journal, Vol. 56, pp. 1769-1815, 1977.

5. D. J. Thompson, "Spectrum Estimation Techniques for Characterization and Development of WT4 Waveguide, Part II," Bell Systems Journal, Vol. 56, p. 1993, Figure 8, 1977.

6. Martin and Thompson, op. cit., p. 1109, Figures 14-17.

7. Martin and Thompson, op. cit., p. 1111, Figure 27.

8. DiFranco and Rubin, Radar Detection, Prentice Hall, 1968.

APPENDIX A
SPECIFICATION FOR A PIEZOELECTRIC ACCELEROMETER

A-1. SPEC. RCB-002C (EARLY NARROW-BAND VERSION)

Type: Single, axis, external stud-mounted with internal preamp

Operating Temperature Range: -50°F to +250°F

Sensitivity: Specified by an analytic function from 20 kHz to 35 kHz, such function to apply to all deliverable units, to be defined by the vendor, and to be a function of frequency only.

Nominal Sensitivity: 10 mV/g, such value to be achieved at some point within the 20 kHz to 35 kHz range with variation of not more than 30% over that range.

Sensitivity Error: The departure from the sensitivity function, S(F) shall not exceed 10% over the operating temperature range and from unit-to-unit, except that 15% is allowed in the temperature range of 200° to 250°F.

Transverse Sensitivity: 5% maximum

Linear Range: At least 200 g zero-to-peak with operation within the specified sensitivity error.

Low-end Cutoff: At least 5 dB/octave at 5 kHz and lower

Isolation: Case-to-crystal isolation of at least 10 Megohm. The case shall form a full shield for the crystal.

Rated Input Current: 2 $\pm$ 0.2 mA at less than 10 Vdc

Connector: Triax type; directly mounted to case opposite mounting surface; type BJ77 of Trompeter Electronics or equivalent.

Mounting stud: 10 - 32 x 0.20 $\pm$ 0.02 inches

Weight: Not to exceed 20 grams; weight goal is 15 grams

Noise floor: Not to exceed 0.002 g's rms (20 kHz to 35 kHz)

Internal connections: Center conductor to crystal "hi" side; outer shell to base; intermediate conductor to crystal "low".

A-2. SPEC. RCB-003A (FINAL WIDE-BAND VERSION)

Type: Single, axis, external-stud-mounted with internal electronic power amplifier

Operating Temperature Range: -50°F to +250°F

Nominal Sensitivity Envelope: Specified at 70 ±5°F by an analytic function of:

$$K_o \left(\frac{\tau s}{\tau S + 1}\right) mV\text{-}g^{-1} \quad \text{where } \tau \text{ lower} = \frac{1}{2\pi(4000\ Hz)} \text{ sec}$$

$$K_o = 10\ mV - g^{-1} \quad \text{and} \quad \tau \text{ upper} = \frac{1}{2\pi(5000\ Hz)} \text{ sec}$$

Sensitivity Error: Departure from the nominal sensitivity envelope shall not exceed 1 dB from 10 kHz to 20 kHz. From 20 kHz to 25 kHz, departure allowance shall linearly increase from 1 dB to 3 dB. From 25 kHz to 35 kHz, departure shall not exceed 3 dB. All such error limits shall apply across the full operating temperature.

Change in Nominal Sensitivity Envelope with Temperature: The value of the "K_o" parameter (above) in the nominal sensitivity expression is required to vary with temperature as follows:

Temp: °F	Value of K: $mV - g^{-1}$
-50	11.0
70	10.0
150	9.5
200	9.0
250	8.5

This effect is the sole allowance for temperature-induced deviations from 70°F.

Linear Range: At least 200 g zero-to-peak with operation within the specified sensitivity error.

Electrical Isolation: Case-to-crystal isolation of at least 10 Megohm; the case shall form a full shield for the crystal

Rated Input Current: 2 $\pm$ 0.2 mA at less than 10 Vdc

Connector: Triax type; directly mounted to case opposite mounting surface; type BJ77 of Trompeter Electronics or equivalent.

Mounting stud: To be integral with base structure; thread shall be 10 - 32 Class 2B by 0.18 $\pm$ 0.01 inch long

Weight: Not to exceed 22 grams

Noise floor: Not to exceed 0.002 g's rms (10 kHz to 35 kHz)

Internal connections: Center conductor to crystal "hi" side; outer shell to base; intermediate conductor to crystal "low".

APPENDIX B

PRIME ITEM DEVELOPMENT SPECIFICATION
FOR THE
SMALL PORTABLE ANALYZER DIAGNOSTIC EQUIPMENT

1.0 SCOPE

1.1 Scope. This specification establishes the design, construction, performance and test requirements for a one-man portable helicopter bearing analyzer system. This system, identified as the Small Portable Analyzer Diagnostic Equipment (SPADE), shall become a piece of aviation ground support equipment (GSE) to be used alongside operating helicopters during ground runup.

2.0 APPLICABLE DOCUMENTS

2.1 Government

2.1.1 Specifications

MIL-P-11268K	31 Aug 78	Parts, Materials and Processes Used in Electronic Equipment
MIL-F-14072B	19 Apr 76	Finishes for Ground Electronic Equipment
MIL-P-14072B w/Amendment No. 1	2 Aug 76	Parts, Equipment and Tools for Army Material, Packaging of
MIL-P-14232E w/Amendment No. 1	2 Aug 76	Parts, Equipment and Tools for Army Material, Packaging of
MIL-C-83723D w/Supplement No. 1	27 Dec 77	Connectors, Electrical, (Circular, Miniature, Quick Disconnect, Environment Resisting), Receptables and Plugs, General Specification for
MIL-C-22750D	3 Nov 80	Coating, Epoxy-Polyamide
MIL-I-23053/5A w/Amendment No. 1	23 May 77	Insulation Sleeving, Electrical, Heat Shrinkable, Polyolefin, Flexible, Cross-Linked
MIL-C-26482G w/Amendment No. 3	11 Oct 78	Connectors, Electrical, (Circular, Miniature, Quick Disconnect, Environment Resisting), Receptacles and Plugs, General Specification for

MIL-T-28800B w/Amendment No. 1	9 Feb 76	Test Equipment for Use with Electrical and Electronic Equipment
MIL-I-46058C w/Amendment No. 5	3 Apr 79	Insulating Compound, Electrical (for Coating Printed Circuit Assemblies)

2.1.2 Standards

MIL-STD-105D w/Notice No. 2	Apr 63 Nov 63	Coupling Procedures and Tables for Inspection by Attributes
MIL-STD-129	3 Jan 78	Marking for Shipment and Storage
MIL-STD-130E	5 Aug 77	Identification Marking of US Military Property
MIL-STD-454G w/Notice No. 1	29 Aug 80	Standard General Requirements for Electronic Equipment
MIL-STD-461B	1 Apr 80	Electromagnetic Emission and Susceptibility Requirements for the Control of Electromagnetic Interference
MIL-STD-462 w/Notice No. 4	31 Jul 67 4 Apr 80	Electromagnetic Interference Characteristics, Measurement of
MIL-STD-471A w/Notice No. 2	27 Mar 73 8 Dec 78	Maintainability Demonstration
MIL-STD-883	1 May 68	Test Methods and Procedures for Microelectronics
MIL-STD-810C w/Notice No. 1	10 Mar 75	Environmental Test Methods
MIL-STD-648	10 Aug 74	Design Criteria for Specialized Shipping Containers
MIL-STD-1188A	5 Jan 78	Commercial Packaging of Supplies and Equipment
MIL-STD-1472C	2 May 81	Human Engineering Design Criteria for Military Systems, Equipment and Facilities
MIL-STD-1562B	15 Oct 79	List of Standard Microcircuits
MIL-STD-45662	10 Jun 80	Calibration Systems Requirements

2.2 Other Publications

AR 70-38	1 Sep 79	Research, Development, Test and Evaluation of Material for Extreme Climatic Conditions
AR 611-201	1 Feb 82	Enlisted Career Management Fields and Military Occupational Specialities

3.0 REQUIREMENTS

3.1 System Definition. The SPADE system shall meet the physical, reliability, maintainability, environmental conditions, transportability and performance requirements detailed herein. The system shall have the following overall characteristics:

One-man portable
Quick and accurate fault-isolation
Require minimal operator training
Thorough self-test through built-in test (BIT) circuitry
Be easily adaptable to aircraft changes/new applications

3.1.1 General Description. The SPADE system shall be a portable electronic device capable of automatically testing and indicating defective bearings in Army helicopter drive train components, i.e., drive shaft hanger bearings, intermediate and tail rotor gearboxes. The system shall consist of an electronic unit and required application hardware to configure the system to interface and test bearing assemblies for all Army helicopters, specifically Models UH-1H, AH-1S, and OH-58A/C. Hardware and software of the SPADE system shall be expandable to include application to the CH-47C/D, UH-60A, OH-6 and CH-54 aircraft.

3.1.2 SPADE System Description. The SPADE system shall include an analyzer unit which will consist of analyzer electronics, signal conditioning, sensors and displays. The electronic unit shall contain as a minimum: (1) a central processing unit or microprocessor (CPU); (2) nonvolatile memory for software storage; (3) RAM for system execution; and (4) necessary circuitry for self-test functions. The SPADE system shall also include all cabling and sensor mounting hardware, which shall be coded for each aircraft application. The hardware shall be rugged to achieve maximum reliability and shall also have a short setup time while not compromising safety.

3.1.3 Memory Module(s). The SPADE system shall have a removable CPU/memory board configured to facilitate changes in model application and expansion, to include future aircraft types/models. The CPU/memory board shall contain nonvolatile PROM memory devices that shall be removable from the mainframe for reprogramming when required.

3.2 Characteristics

3.2.1 Performance Characteristics

3.2.1.1 The SPADE system shall be designed to have the hardware and software capability required for failure detection of Army helicopter bearings for the following drive train components: tail rotor drive train (hanger bearings), intermediate gearboxes, and tail rotor gearboxes.

3.2.1.2 A minimum of 90 percent of all helicopter component/part removals resulting from the SPADE system indications shall be valid failures or incipient failures.

3.2.1.3 The SPADE system, when used in conjunction with the current maintenance and inspection procedures, shall not fail to detect unsafe-for-flight bearing related component defects more than once every 1,000 flight hours (2,000 desired). The SPADE system shall be used every 25 aircraft flight hours.

3.2.1.4 The SPADE system shall provide a minimum of 20 input channels which shall consist of sensor, cabling, signal conditioning and baseline comparator circuitry.

3.2.1.5 The SPADE system shall be capable of operation in a semiautomatic mode and a manual mode with the following functions:

3.2.1.5.1 Semiautomatic mode will scan through each channel in use, alternately displaying the channel number and a PASS or FAIL message. A failure shall cause the test set to continue monitoring the failed channel until the operator requests continuation to the next channel. If no failures are detected, testing shall loop continuously through the active channels until the operator stops the test.

3.2.1.5.2 Manual mode shall allow the operator to continuously monitor any channel with either a PASS/FAIL display or an interleaving of PASS/FAIL and numerical results. The SPADE system shall allow the operator to rapidly change channels in the manual mode. A special manual mode with open limits will display only numerical results and allow troubleshooting of bearing components which do not have a baseline limit pair stored in memory.

3.2.1.6 The SPADE system shall have the ability to store the last reading from each channel in memory while powered.

3.2.1.7 The SPADE system shall have sufficient memory to store baseline data for at least eight aircraft models.

3.2.1.8 The SPADE system shall have the capability to monitor any single channel continuously.

3.2.1.9 The SPADE system shall be operable with less than the full set of sensors attached.

3.2.2 Physical Characteristics

3.2.2.1 The SPADE analyzer unit, with sensors plus adaptation kit, for any one aircraft type shall weigh no more than 40 pounds.

3.2.2.2 Sensor and cable design shall allow rapid replacement of individual sensors/cables by operating personnel. Modifications to the aircraft shall not be required except for installation of sensor mounting hardware.

3.2.2.3 The SPADE system shall be capable of accommodating at least 20 aircraft test points without relocation of the equipment. The design shall provide provisions for storage of up to 20 sensors when not in use.

3.2.2.4 The SPADE system shall allow installation of all required sensors and cabling and place the SPADE system into operation within 30 minutes by one trained operator for utility, attack, and observation helicopters. The design shall allow two trained operators to accomplish this task within 45 minutes for cargo helicopters (CH-47C/D). (Aircraft preparation time is excluded.)

3.2.2.5 The SPADE system shall be capable of a complete ground test of the monitored aircraft (up to 20 test points) within 15 minutes after preparation and setup and after the aircraft reaches stabilized operating conditions at 100 percent N_r (main rotor rpm) while on the ground.

3.2.2.6 The SPADE system shall have interchangeable sensors without readjustment of channel limits.

3.2.2.7 The SPADE analyzer unit and adaptation kit shall be housed in a watertight, lightweight, suitcase-type container with circular latches and carrying handle capable of withstanding an 80-pound pull.

3.2.2.8 The SPADE system sensor mounting hardware types shall be standardized to minimize the number of types required for each aircraft model.

3.2.2.9 The SPADE system shall allow the operator to rapidly change channels.

3.2.2.10 The SPADE system shall permit reprogramming of individual channel limits at AVIM or general support/direct support maintenance units without the requirement for development of special computer equipment.

3.2.2.11 The SPADE system shall meet the requirements of MIL-STD-1472C. The display shall be of sufficient illumination to be read in direct sunlight.

3.2.2.12 The SPADE system shall allow cabling harness identification by the operator when the harness is connected to the analyzer unit to preclude incorrect installation.

3.2.2.13 The SPADE system shall be capable of operating at any input voltage between 9 and 32 volts DC continuously. The system shall not be damaged under fault-free conditions, when subjected to voltage transients up to 40 Vdc continuous or up to 50 Vdc for up to 15 msec.

3.2.2.14 The SPADE system's memory modules shall be nonvolatile to prevent loss when power is off and in stored configuration.

3.2.2.15 The SPADE system shall be protected with chemical agent resistant paints to facilitate chemical agent exterior decontamination.

3.2.3 Reliability. The SPADE system shall have the following mean time between failure (MTBF) requirements:

(NOTE: Failure in this sense means hardware malfunction.)

	Minimum Acceptable Value	Best Operational Capability
Analyzer Unit	400 mission tasks	3,000 mission tasks
Cabling and Connectors	100 mission tasks	250 mission tasks
Sensors	480 mission tasks	720 mission tasks

The definition of a mission task is one aircraft application with all applicable sensors installed.

3.2.4 Maintainability

3.2.4.1 The maximum mean time to repair (MTTR) for the SPADE system, including all corrective maintenance, test and verification, shall be the following:

Aviation Unit Maintenance (AVUM) .5 man-hours
Aviation Intermediate Maintenance (AVIM) 1 man-hour
Depot 3 man-hours

3.2.4.2 Preventive maintenance for the SPADE system shall not be required more than once every 50 SPADE mission tasks. The mean time for preventive maintenance shall not exceed .2 man-hour.

3.2.4.3 The SPADE system shall be capable of repair and replacement at AVUM and AVIM levels with the common tools available in Army inventory.

3.2.4.4 The SPADE system design shall prevent inadvertent installation of wrong cable harness to an aircraft (color or numerical coding, keying, etc.).

3.2.4.5 The SPADE system circuit cards, display and power modules shall be capable of being easily removed and permit rapid fault isolation by existing Army TMDE and BITE.

3.2.4.6 The SPADE system circuit card designs shall prevent installation in a wrong position/location.

3.2.4.7 The SPADE system shall be operable with the cover removed for troubleshooting purposes. Adequate internal guarding shall be provided for exposed high voltage points in accordance with MIL-STD-1472C and MIL-STD-454G.

3.2.4.8 The SPADE system's display lights, fuses, knobs and switch shall be easily replaceable at the AVUM level.

3.2.4.9 The SPADE system shall require no calibration at AVUM and AVIM levels. Verification of compliance with performance specifications shall be accomplished with self-test and BITE.

3.2.4.10 The SPADE system shall permit operation and maintenance by personnel clothed in appropriate NBC or cold weather clothing.

3.2.4.11 The SPADE system shall have self-test capability to determine the condition of the analyzer unit prior to aircraft setup. The self-test shall indicate if the unit is defective and where the fault is located, i.e., circuit cards, power modules, display electronics, etc.

3.2.4.12 The SPADE system shall be capable of testing and fault isolating sensors and cabling (continuity and faulty pins) at AVUM level. Detected malfunctions shall be indicated by display to identify the failed component.

3.2.4.13 The SPADE system shall be designed to meet the following testability requirements:

AVUM (BITE) 95% failure detection; 98% accuracy
AVIM (BITE) 98% failure detection; 98% accuracy

3.2.4.14 The SPADE system shall be maintained by AVUM and AVIM personnel with skill level descriptions as defined in AR 611-201 for military occupational speciality (MOS) 68F and 35H respectively.

3.2.4.15 The SPADE system shall be maintained by the following baseline maintenance concept:

(1) AVUM level. Personnel at this level will be operators and perform required AVUM functions (MOS 68F). Using the self-test capability, the operator will perform the preoperation tests and corrective maintenance. The SPADE system self-test shall consist of:

(a) Checkout of the primary electronic unit prior to installation on test aircraft.

(b) Checkout of the cabling harnesses and sensors. If defective, provisions shall be provided for individual sensor test and for cable harness fault isolation. Detected malfunctions shall be indicated by display to identify the failed component. Repairs will be accomplished by sensor/electronic unit replacement and/or cabling harness replacement. Other repairs will include replacement of easy-to-remove parts such as knobs, fuses, and lamps. SPADE system preventive maintenance, normal servicing and cleaning shall also be accomplished at AVUM.

(2) AVIM level. Personnel at this level will troubleshoot the SPADE system using BITE, standard tools, multipurpose test, measurement and diagnostic equipment (TMDE), and module substitution (MOS 35H).

(3) Depot level. Depot level maintenance will include repair of modules and PCBs not repaired at lower maintenance levels, and system overhaul, refurbishment and rebuild.

3.2.5 Environmental Requirements

3.2.5.1 The SPADE system shall be capable of operation without damage or malfunction when subjected to the high and low temperature tests specified by Methods 501 and 502, Procedure I of MIL-STD-810. The operating limits shall be as follows:

High Temperature: +120°F
Low Temperature: - 25°F

3.2.5.2 The SPADE system shall be capable of operation without damage or malfunction in atmospheric pressure of 26.0 to 31.0 in. Hg when tested as specified by Method 500.1, Procedure I of MIL-STD-810.

3.2.5.3 The SPADE system shall be capable of operation without damage or malfunction while under exposure to relative humidity when tested as specified by Method 507.1, Procedure II of MIL-STD-810.

3.2.5.4 The SPADE system shall be capable of operation without damage or malfunction while under exposure to solar radiation from 0 to 360 BTU/hr-ft^2 at a maximum of 90°F + 5°F when tested as specified by Method 505.1, Procedure I of MIL-STD-810.

3.2.5.5 The SPADE system shall be capable of operation without damage or malfunction in wind conditions ranging from 0 to 30 knots.

3.2.5.6 When tested as specified in Method 508.1, Procedure I of MIL-STD-810, all nonmetallic materials not inherently fungistatic shall evidence no fungus growth which will affect the operation of the SPADE system.

3.2.5.7 When tested as specified in Method 510.1, Procedure I of MIL-STD-810, the SPADE system shall show no evidence of malfunction due to sand and dust.

3.2.5.8 When tested as specified in Method 516.2, Procedures I and IV MIL-STD-810, the SPADE system shall show no evidence of malfunction due to shock.

3.2.5.9 When tested as specified in Method 514.2, Procedures X, Curve AX of MIL-STD-810, the SPADE analyzer system and a typical vibration transducer shall show no evidence of malfunction due to vibration. An operational performance test shall be performed after each sinusoidal cycling portion of the vibration test. The units shall be nonoperating during cycling runs.

3.2.5.10 The SPADE system shall not be degraded as a result of transport in its case in ambient temperatures of -60°F to +160°F, atmospheric pressure of 3.9 to 31.0 in. Hg and in rain from 0 to 4 in./hr.

3.2.5.11 The SPADE system shall be capable of being transported by all types of military ground, sea, air and rail vehicles.

3.2.5.12 The SPADE system shall be packaged for transport in accordance with Paragraph 4.4 of MIL-STD-648.

3.2.5.13 The SPADE system shall meet performance requirements and shall suffer no detrimental effects after exposure to rain conditions as specified in Method 506.1, Procedure II, of MIL-STD-810. Operational performance tests shall be conducted before and after the tests. The orientation of the test item shall be changed every twenty minutes so that each side will be equally exposed to the rain.

3.3 Design and Construction. Unless otherwise specified herein, the SPADE system design and construction shall be in accordance with the requirements of MIL-STD-454G.

3.3.1 Parts, Materials, and Processes. The selection of parts, materials and processes shall be in accordance with MIL-P-11268K. Maximum design freedom shall be allowed in the selection of parts of commercial origin or in the design of new parts when such parts offer marked improvement in design, performance reliability, or reduction in cost, size or weight. Components already in the Army supply system, which may not be formally designated as standard, shall be used in preference to the creation of a new part.

3.3.2 Microcircuits. Microcircuits shall be selected in accordance with MIL-STD-1562B, with Notice 2, with the following types of 100 percent screening tests in accordance with MIL-STD-883, the minimum extent of which will be specified on the detailed part drawings:

Stabilization bake
Temperature cycle

Burn-in
Final electrical test after burn-in

3.3.3 Cabling. All cabling shall be shielded and shall have the shield terminated in an approved military connector having a conductive finish and be provided with an EMI backshell for peripheral bonding of the shield. Cabling shall be properly supported and secured to prevent undue stress on the connectors and terminals. Cabling and insulated wiring shall be placed and protected to avoid contact with sharp edges. All wires shall allow sufficient slack for servicing and part replacement. Soldered wire terminations shall be mechanically secured so that the connections are not dependent for strength on solder alone. Connectors shall be in accordance with MIL-C-83723D or MIL-C-26482G.

3.3.4 Printed Wiring Assemblies. The printed assemblies shall be in accordance with MIL-STD-454G, Requirement 17. Assemblies not containing cap layers shall be conformally coated in accordance with MIL-I-46058. The board assemblies shall be cleaned of flux and other contaminants before coating. Electrical and mechanical mating surfaces shall not be coated.

3.3.5 Interchangeability. SPADE system interchangeability shall be in accordance with MIL-STD-454G, Requirement 7, and as detailed in MIL-T-28800B.

3.3.6 Workmanship. Workmanship shall be in accordance with MIL-STD-454G, Requirement 9.

3.3.7 Finishes. The external surface of the SPADE analyzer unit shall be finished in accordance with Type I, MIL-F-14072B, and painted a semigloss enamel in accordance with MIL-C-22750D.

3.3.8 Identification and Markings. Identification and marking shall be in accordance with MIL-STD-130E.

3.3.9 Soldering. Soldering shall be in accordance with MIL-STD-454G, Requirement 5.

3.3.10 EMI/EMC. The SPADE system shall meet the EMI requirements of MIL-STD-461B, Notice 4, requirements. The SPADE system, when interfaced to the system under test and operating as intended, shall not cause undesirable response or performance degradation of the system under test and shall not itself exhibit undesirable response or performance degradation.

3.3.11 Safety Engineering. The SPADE system design criteria shall be in accordance with Paragraph 3.2.1 through 3.2.1.1.4 of MIL-T-28800B and paragraph entitled "Labeling" and "Hazards and Safety" of MIL-STD-1472C.

3.3.11.1 Equipment Safety.

(1) The SPADE system shall minimize equipment damage, degradation of efficiency, or mission failure due to the following conditions:

(a) Operator-induced errors

(b) Improper cabling

(c) Power failure or electrical overstress on components

(d) Secondary failures

(e) Installation, storage, operation, handling, maintenance, and transportation

(2) Specific design techniques for equipment protection shall include the following:

(a) Electrical overload protection shall be in accordance with MIL-STD-454G, Requirement 8.

(b) Contacts used on chassis, panels, or cable entrance connectors shall be recessed to prevent breakage or damage.

(c) Positive means shall be provided to prevent the inadvertent reversing or mismating of fittings and electrical connections.

3.3.11.2 Mechanical Safety. The SPADE system design shall include the safety provisions called for in paragraph "Mechanical" of Requirement 1, MIL-STD-454G, and the following:

(1) Exposed edges shall be rounded to a minimum radius of 0.04 inch (1 mm), and exposed corners to a minimum of 0.5 inch (12.7 mm).

(2) Adequate provisions for lifting and handling shall be provided in accordance with paragraph "Unit Design for Efficient Handling" of MIL-STD-1472C.

(3) Color coding of indicator lights shall be in accordance with Table II, MIL-STD-1472C.

3.3.11.3 Electrical Safety. The SPADE system design shall include the safety provisions called for in paragraph entitled "Electrical" of Requirement 1, MIL-STD-454G, and the following:

(1) Accidental contact with current-carrying metal components, terminals, and like devices (greater than 70 volts) shall be controlled by the following:

(a) Wire connections (bare terminals) shall be protected with insulated sleeving in accordance with MIL-I-23053/5A.

(b) All contacts, terminals, and like devices other than wire connections shall be provided with barriers or guards to prevent operating and maintenance personnel from accidental contact.

(c) Small openings shall be provided, where needed, in guards or barriers for maintenance testing without the removal of the guards.

(2) The SPADE system design shall include the grounding provisions in accordance with Requirement 1 of MIL-STD-454G, paragraph entitled: "Ground Potential", "Grounding", "Grounding to Chassis", "Shielding" and "Shorting Rods".

4.0 QUALITY ASSURANCE PROVISIONS

4.1 Responsibility. Unless otherwise specified in the contract, the contractor is responsible for the performance of all quality assurance provisions specified herein. Except as otherwise specified in the contract, the contractor may use his own or any other facility suitable for the performance of the inspection requirements specified herein, unless disapproved by the contracting officer. The contracting officer reserves the right to perform or witness any of the inspections set forth in this specification where such inspections are deemed necessary to assure supplies and services conform to the prescribed requirements.

4.2 Test Equipment and Inspection Facilities. The contractor shall establish or maintain test and measuring equipment and inspection facilities of sufficient accuracy, quality and quantity to permit performance of the required inspection. Calibration of inspection and test equipment shall be in accordance with MIL-STD-45662.

4.3 Inspection Records. The contractor shall maintain detailed inspection records of all inspections and tests performed in accordance with the requirements of 4.4.

4.4 Quality Conformance Inspection. The contractor shall perform a quality conformance inspection in accordance with this paragraph. Unless otherwise specified, testing of the SPADE system shall be conducted at 75 + 5°F ambient air temperature and less than 60 percent relative humidity. An external regulated power source of 28 $\pm$ 4 Vdc shall be used in all tests requiring operation of the SPADE system. During such tests, the test set shall be connected to the external power source with cables supplied as part of the test set. In addition, connections to any other test fixtures or equipment shall be made with the test set cables as required by the applicable test procedure. Unless otherwise specified, nonoperating environmental tests shall be performed on the analyzer unit and cable storage case with case covers installed and latched.

4.4.1 Hardware. The SPADE system hardware shall be tested to determine conformance to the following requirements:

Test	Requirement Paragraph(s)
Aircraft interface	3.1.1 and 3.2.2.13
Nonvolatile memory	3.1.4
Modes of operation	3.2.1.5
Open channel	3.2.1.5
Channel storage	3.2.1.6
Baseline storage	3.2.1.7
Channel monitoring	3.2.1.8
Weight	3.2.2.1
Sensor/cable replacement	3.2.2.2
Aircraft mounting	3.2.2.2
Test point	3.2.2.3
Sensor storage	3.2.2.3
System installation time	3.2.2.4
System operation time	3.2.2.5
Sensor interchangeability	3.2.2.6
Channel advance	3.2.2.9
Reprogramming	3.2.2.10
Illumination requirements	3.2.2.11
Chemical protection	3.2.2.15

4.4.2 Reliability. The reliability requirements specified in Paragraph 3.2.3 shall be verified by analysis of test and failure data including consideration of functional and environmental stress levels which affect the failure rate. Use of test and failure data on similar components is permitted, providing allowances are made for differences in design, usage, and environments. In the event that test history is not sufficient to provide satisfactory evidence of the SPADE system's compliance with reliability requirements, compliance may be determined on the basis of formal reliability predictions employing recognized and approved failure rate data sources and prediction procedures.

4.4.3 Maintainability. The unit and intermediate maintenance requirements shall be demonstrated by a maintenance procedure, maintenance task selection, and maintenance task performance. This demonstration shall determine conformance to the following maintainability requirements:

Test	Requirement Paragraph(s)
Mean time to repair	3.2.4.1
Preventive maintenance	3.2.4.2
Circuit card installation	3.2.4.5 and 3.2.4.6
Circuit card troubleshooting	3.2.4.5 and 3.2.4.5
AVUM replaceables	3.2.4.8 and 3.2.4.5
Self-test	3.2.4.11, 3.2.4.12, 3.2.4.5

4.4.4 Environmental. The SPADE system shall be operated by the contractor during environmental tests in accordance with the contractor prepared, Government approved test plan to determine compliance with the following requirements:

Test	Requirement Paragraph(s)
Temperature	3.2.5.1
Pressure	3.2.5.2
Humidity	3.2.5.3
Solar radiation	3.2.5.4
Wind	3.2.5.5
Fungus	3.2.5.6
Sand and dust	3.2.5.7
Shock	3.2.5.8
Vibration	3.2.5.9
Transport	3.2.5.10, 3.2.5.11, and 3.2.5.12
Rain	3.2.5.13

4.4.5 Design and Construction. Parts and components shall be inspected for workmanship, mechanical fit, loose nuts and screws, and miscellaneous defects in accordance with MIL-P-11268K. Controls and fastening devices shall be inspected for mechanical operation. Wiring, soldered connection, ground connection, weld, finishes, etc., shall be inspected for workmanship. Clearance, dimensions, and mechanical adjustments shall be measured. The visual and mechanical inspection shall include, but not be limited to, the following:

Inspection	Requirement Paragraph(s)
Mainframe	3.1.2
Adaptation kits	3.1.3
Microcircuits	3.3.2
Cabling	3.3.3
Printed wiring assemblies	3.3.4
Interchangeability	3.3.5
Workmanship	3.3.6
Finishes	3.3.7
Identification and markings	3.3.8
Soldering	3.3.9

4.4.6 Electromagnetic Magnetic Interference/Compatibility (EMI/EMC). The SPADE system shall be tested to determine compliance with the requirements of Paragraph 3.3.10. Test methods and procedures shall be in accordance with MIL-STD-462, Notice 3, as implemented by a contractor prepared, Government approved test plan.

4.4.7 Human Engineering Demonstration. The contractor shall perform an actual demonstration to verify final compliance with the human engineering requirements of Section 3 of this specification.

4.4.8 Safety Engineering. A safety evaluation shall be conducted by the contractor to determine that all personnel, equipment, and environment hazards have been identified and eliminated in compliance with Paragraph 3.3.11 of this specification. During acceptance inspection, a visual inspection shall be performed to determine that all requirements, as a result of the safety evaluation, have been incorporated into the SPADE system. Inability to meet the requirements of Paragraph 3.3.11 shall constitute a failure of the test.

4.4.9 Failures. During any testing phase, when a failure is noted, testing shall not proceed until the system has been corrected and the test has passed, unless agreement is reached with the government test director to continue testing. The SPADE system shall be considered to have failed if any of the following occurs.

4.4.9.1 Any malfunction which causes or may cause performance degradation of the test item or system inability to commence or cease operation, serious damage to the test item by continued operation, or personnel safety hazard.

4.4.9.2 Any omission or error in test configuration, test process, or test record such that they prevent demonstration of full conformance with the requirements specified in this specification.

4.4.9.3 Degradation in performance due to deterioration such as permanent warping, deformation or delamination of the equipment. In those cases where compliance with the requirements of this specification cannot be verified by electrical and mechanical measurements, other means of verification shall be employed, such as visual inspection, demonstration, analysis, etc. The test and evaluation plans shall flag tests of the above nature.

5.0 PREPARATION FOR DELIVERY

5.1 Packaging Requirements. Packaging shall be in accordance with MIL-STD-1188A.

5.2 Preservation. Unless otherwise specified, the method and materials used in preservation shall be as specified in MIL-P-14232E.

5.3 Markings. Unless otherwise specified, interior packages and exterior shipping containers shall be marked in accordance with MIL-STD-129.

APPENDIX C
TEST DATA

This appendix describes the testing accomplished by RCA during this contract and lists the data which is available from these tests. No effort has been made to include the actual vibration spectral data in this report due to its voluminous nature. The data collected can be categorized in many ways. Here it is divided into test cell data and on-helicopter data. Helicopter data is subdivided by aircraft types.

C-1. TEST CELL DATA

Throughout this program, test cell data has been collected to support the development of diagnostic and prognostic techniques. Bell Helicopter Textron, Inc., was subcontracted to do testing on the Huey and Cobra tail rotor drive components in their test cell facility. RCA developed a test capability for the Kiowa tail rotor drive in its vehicle test facility.

C-1.1. Bell Helicopter Test Cell Data on the Huey and Cobra

The Bell Helicopter test cell equipment used was comprised of a modified Cobra slave main transmission and a test main transmission; these were externally geared together through a regenerative loop which interconnected the two transmission masts. Power was supplied by a 500 horsepower electric motor connected to a speed increasing gearbox through an electromagnetic coupling. Power to the tail rotor drive train was taken from the tail rotor quill of the test transmission. It was transmitted through a hanger bearing supported driveshaft to the 42-and 90-degree gearboxes, and absorbed by a water brake dynamometer connected to the output of the 90-degree gearbox. Figures C-1 through C-5 illustrate the test setup at Bell Helicopter.

The gearboxes were instrumented with numerous accelerometers, as was the hanger bearing housing. The outputs of these transducers were recorded on magnetic tape for every stabilized diagnostic run. In addition, the gearbox temperatures, shaft speeds, and other test conditions were also recorded, as were certain calibration signals.

Discrete fault implanted bearings were installed on the gearboxes and run as presented in Figures C-6 through C-9 and Tables C-1 and C-2 . Outer race faults were angularly oriented in the direction of the maximum reactive radial loads. The installed orientation of the inner race and rolling element implants is immaterial because these are all rotating members. For the duplex pair ball bearings in these gearboxes, the available data indicated that the member of the bearing set carrying the axial loading is most likely to fail. The duplex ball bearing implants were therefore installed in the axially loaded bearing half. In all cases the fault implants were artificially generated spall-like damage, sized to conform to the boundary between category C and category D defects as outlined in Table C-3.

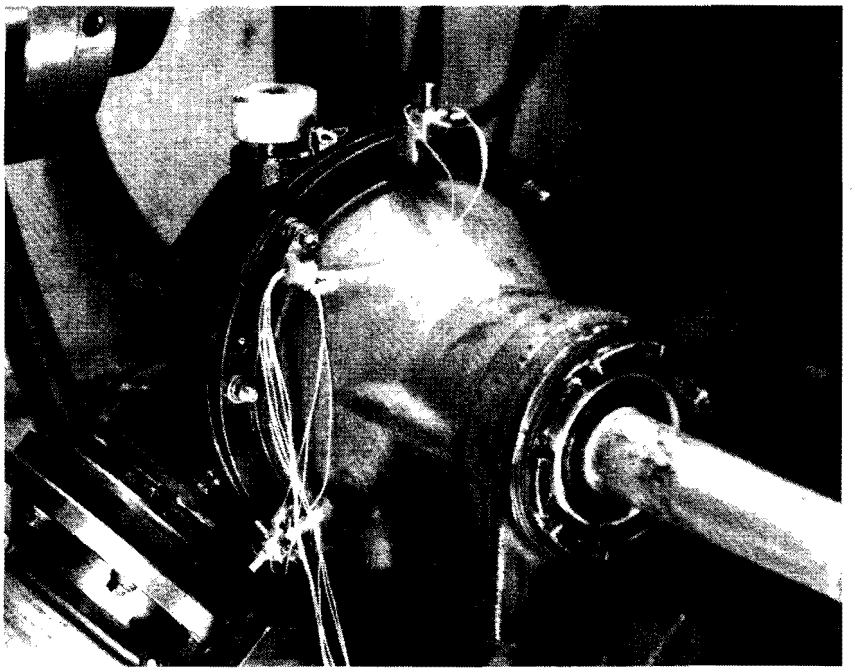

Figure C-1. 90-Degree Gearbox Left Side View

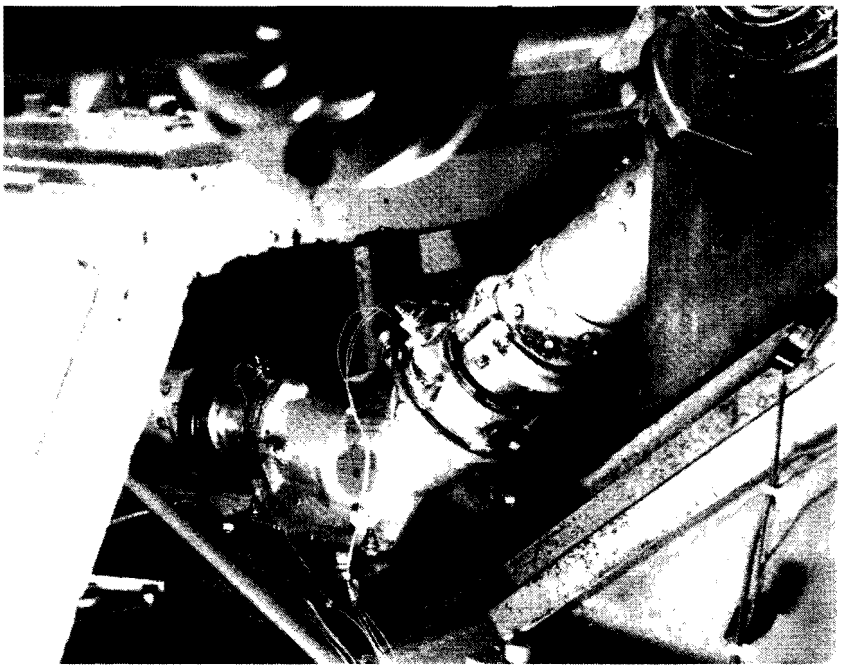

Figure C-2. 42-Degree Gearbox Left Side View

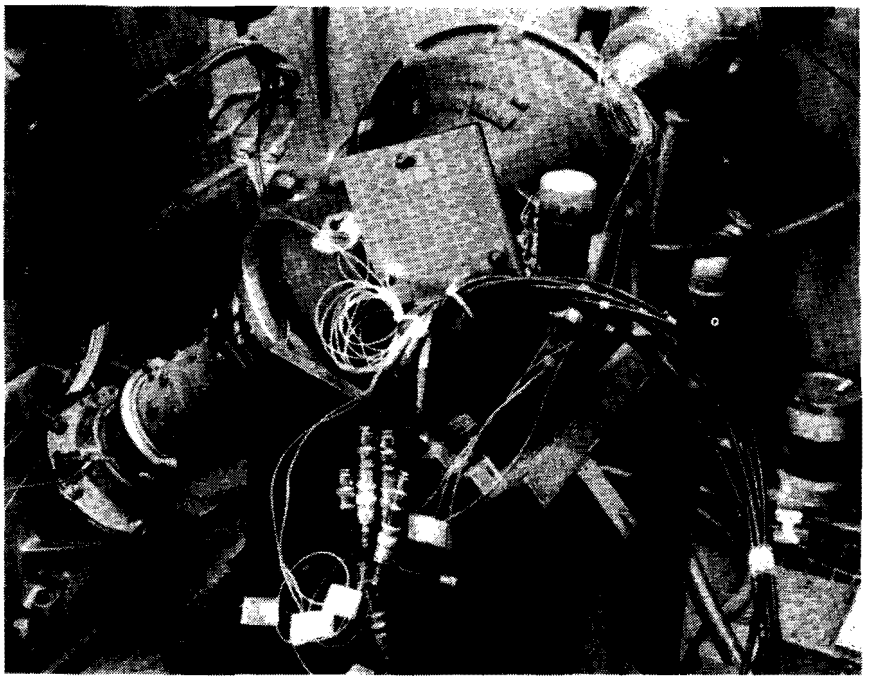

Figure C-3a. Left Side View

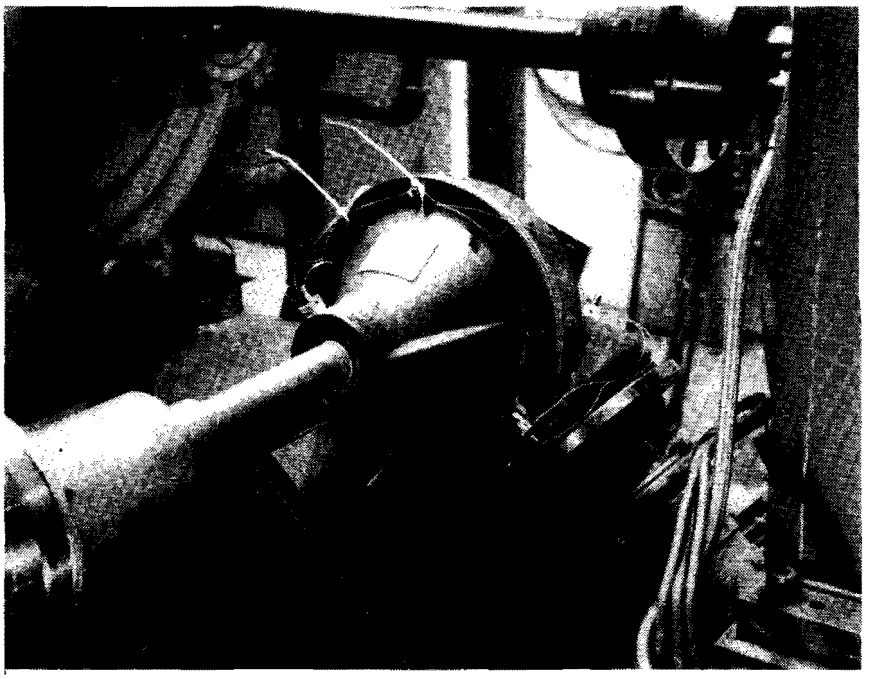

Figure C-3b. Right Side View

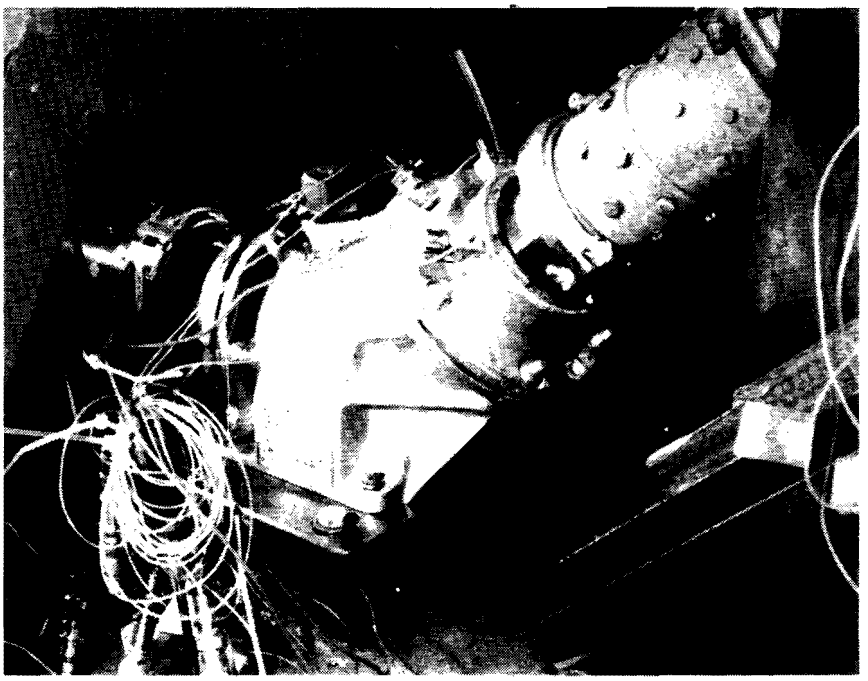

Figure C-4a. View Looking Forward

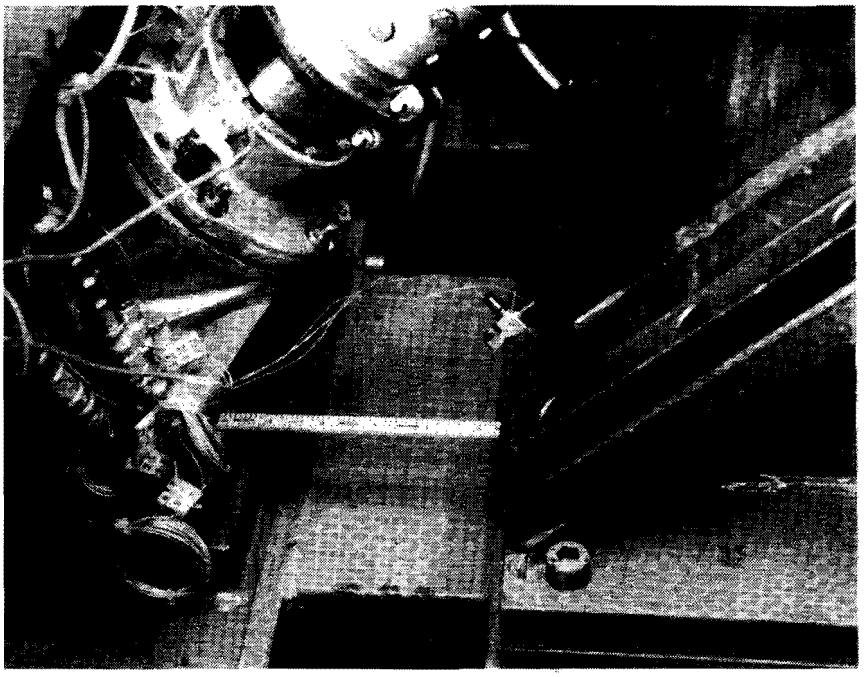

Figure C-4b. Side View at Output

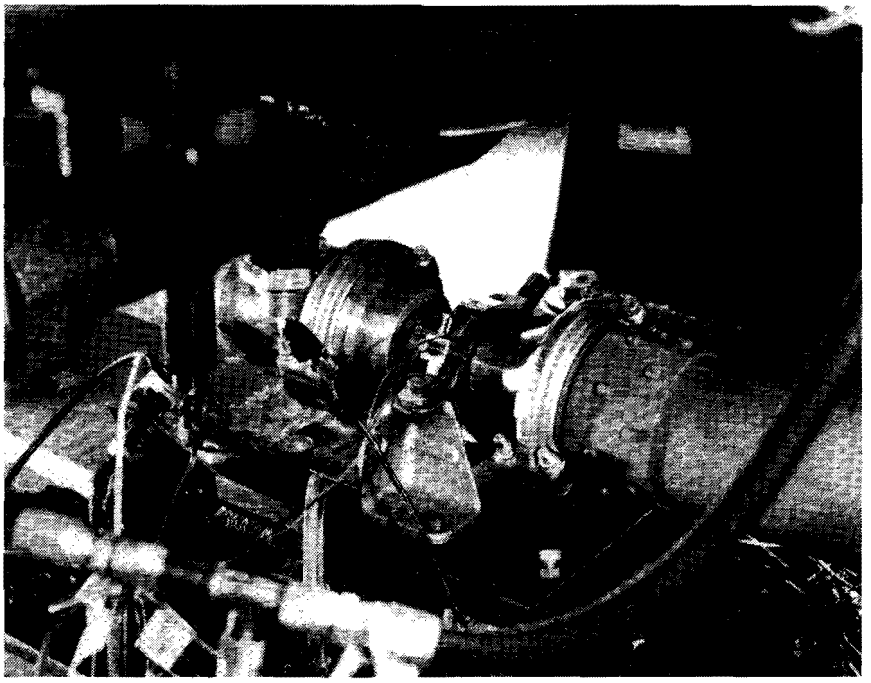

Figure C-5a. View Looking Forward

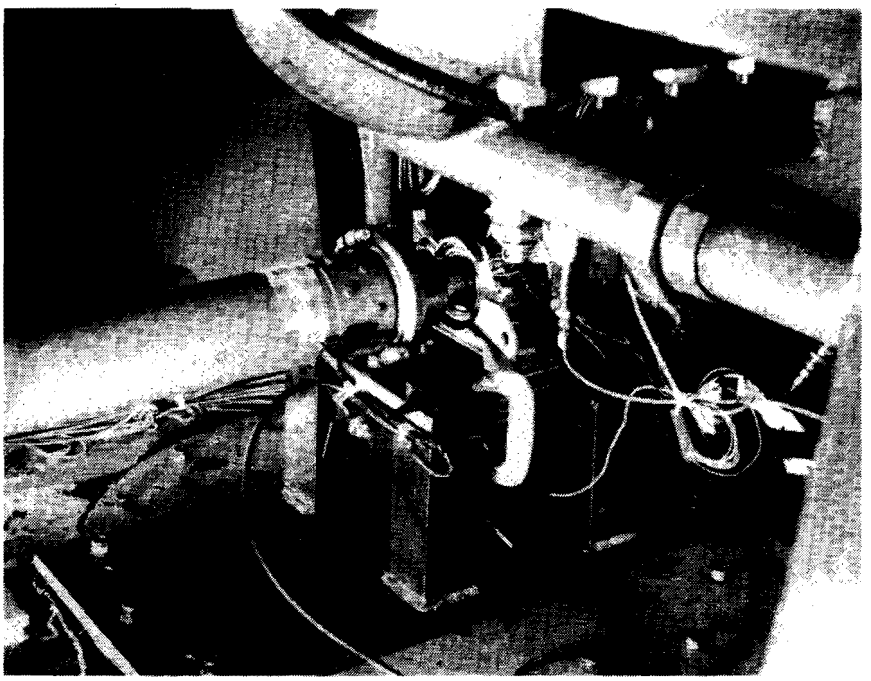

Figure C-5b. View Looking Aft

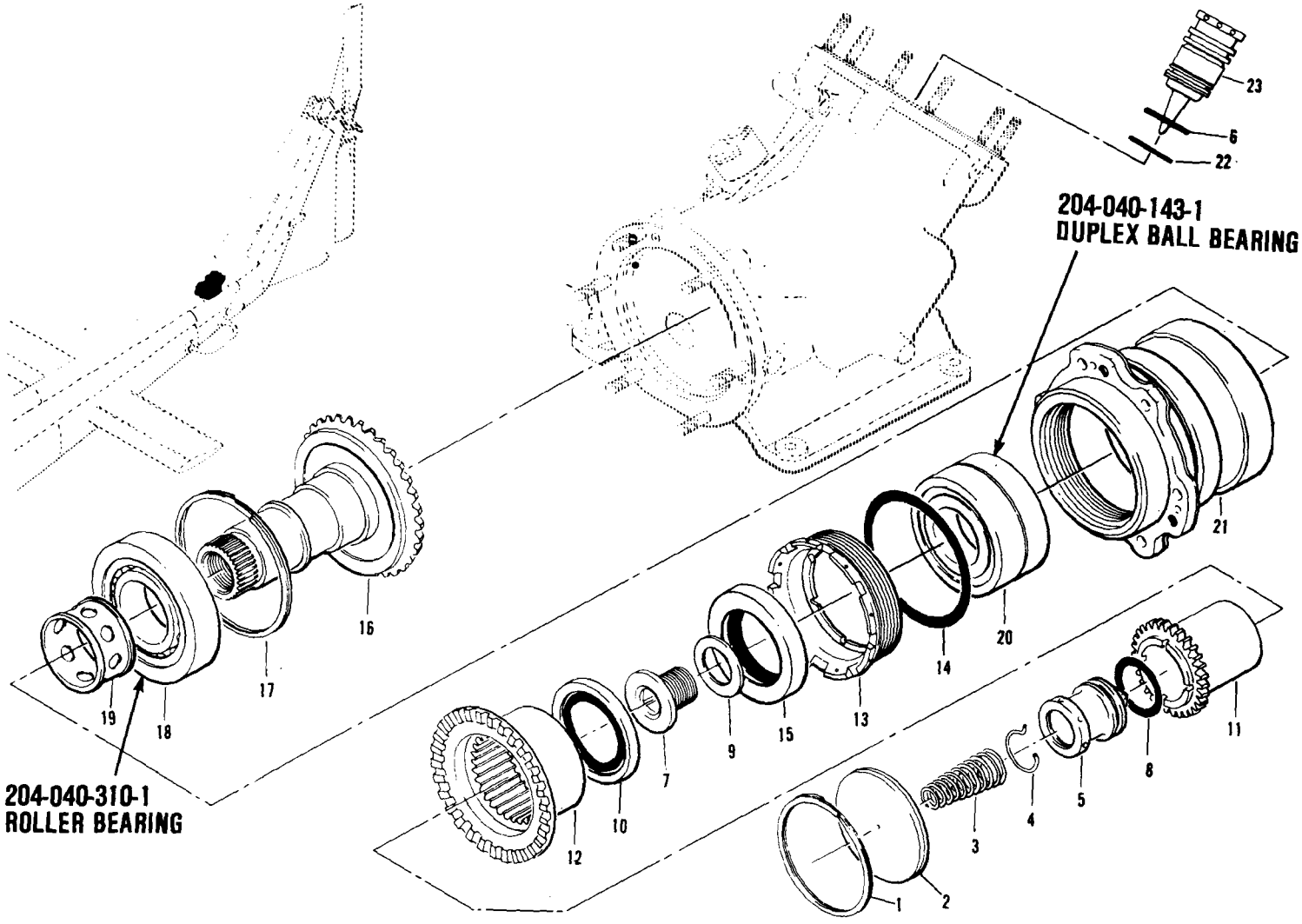

Figure C-6. Quill Assembly, 42-Degree Gearbox, UH-1H

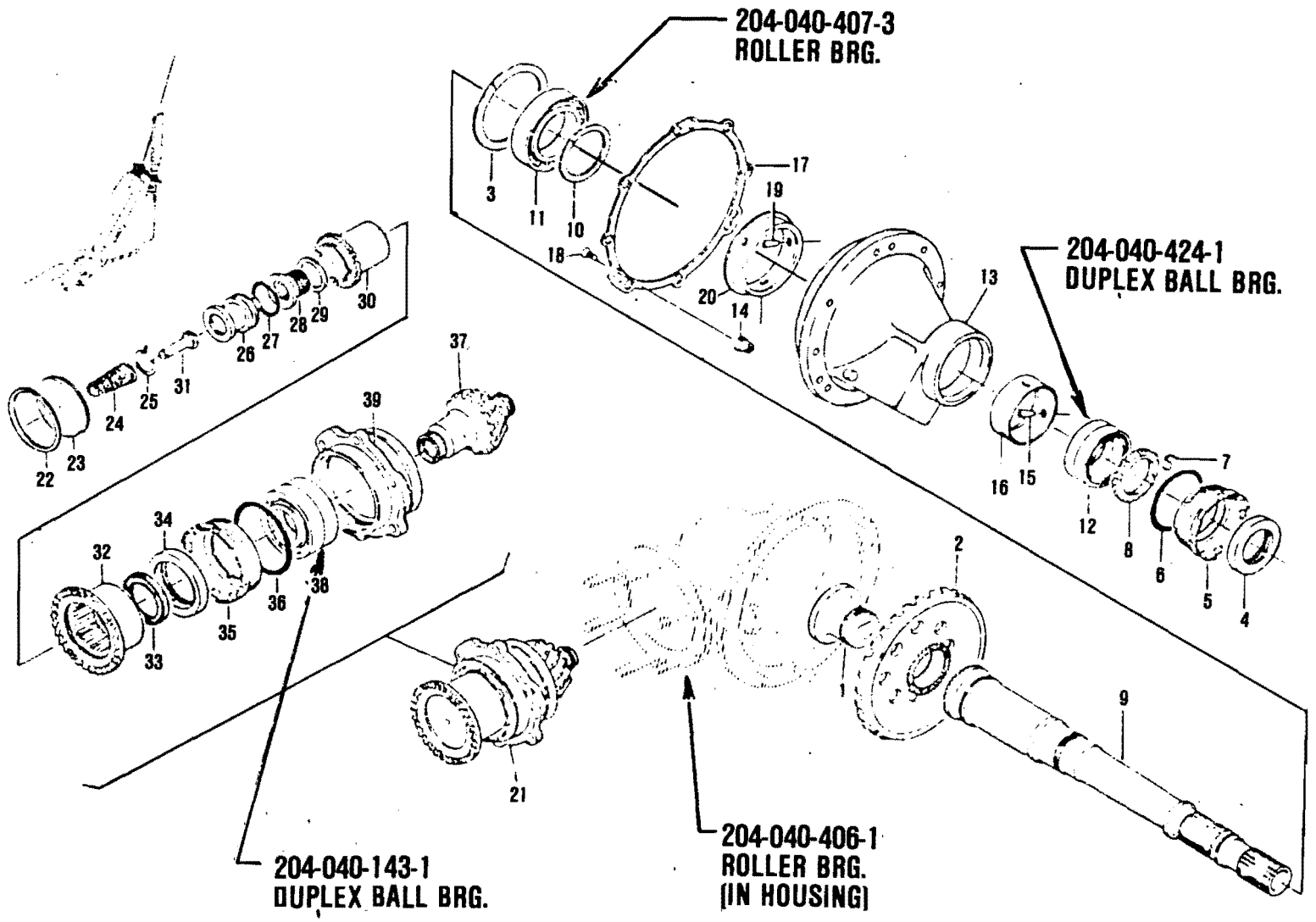

Figure C-7. Quill Assembly, 90-Degree Gearbox, UH-1H

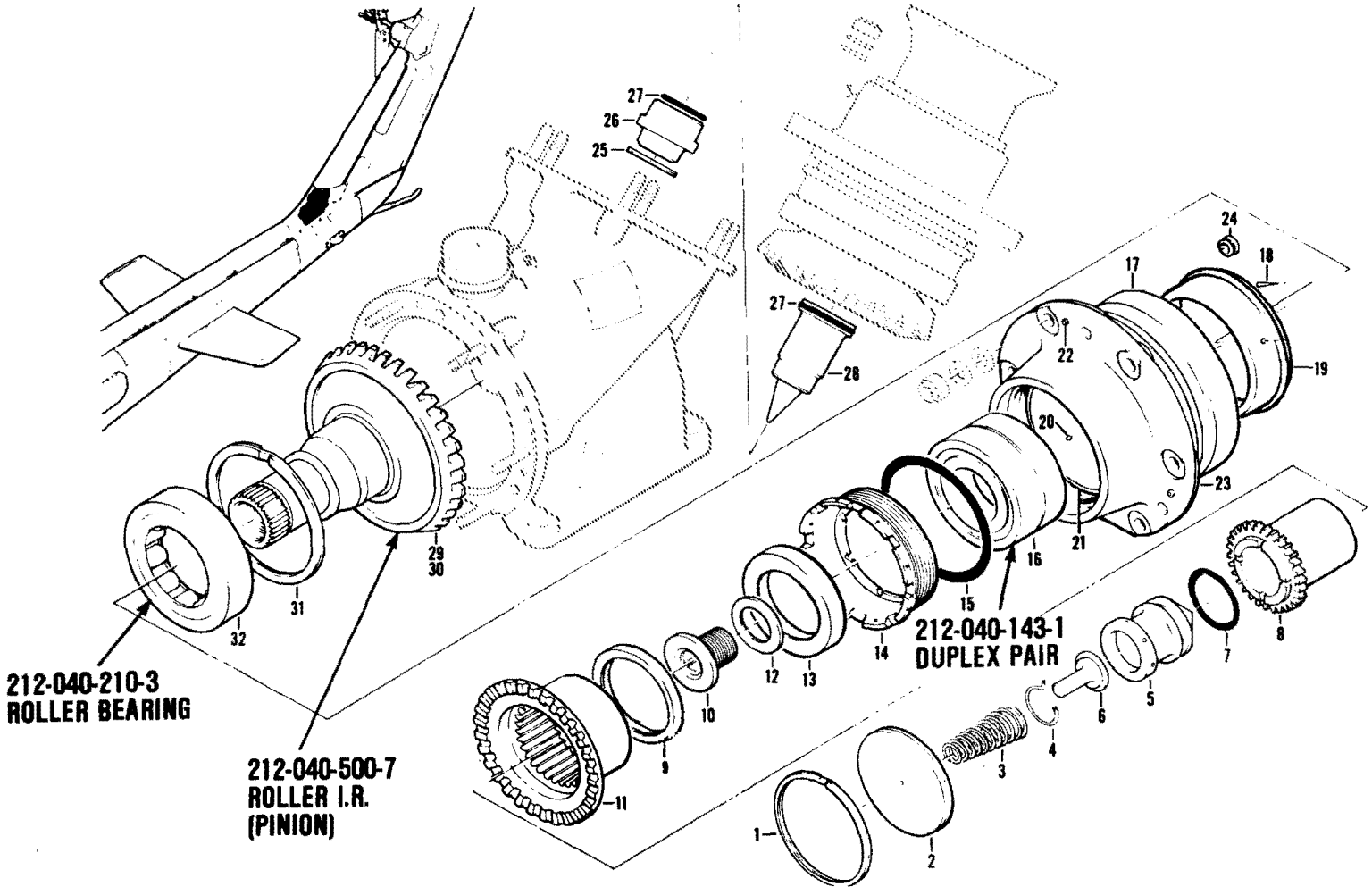

Figure C-8. Quill Assembly, 42-Degree Gearbox, AH-1S

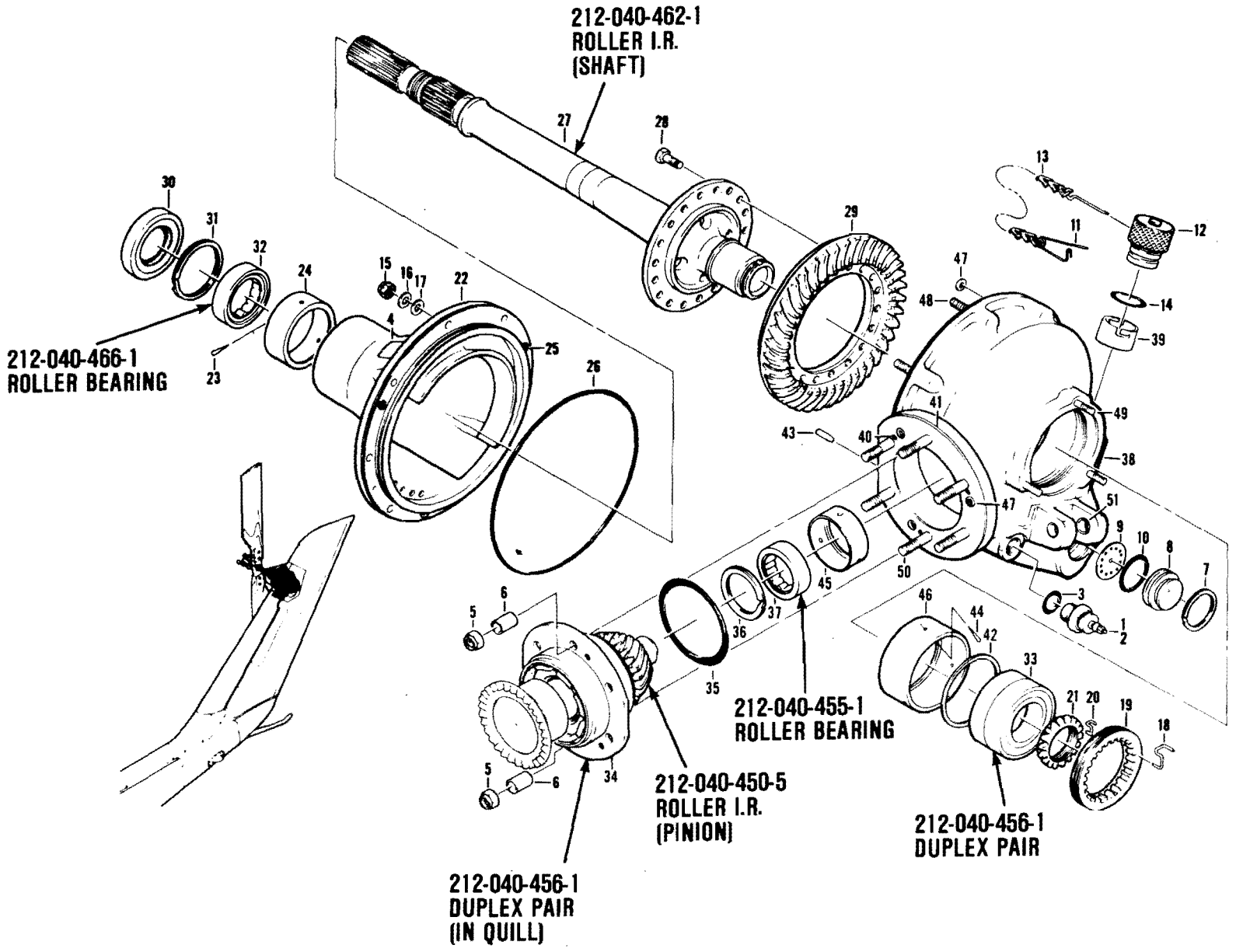

Figure C-9. Gearbox Assembly, 90-Degree Tail Rotor Drive, AH-1S

TABLE C-1. UH-1H RUN SEQUENCE AND BEARING CONFIGURATION

RUN NO	T/R RPM	DYNO HP	42° G/R IMPLANT P/N	SAMPL NO	QUILL (INPT/ OUTPT)	BRG LOC (INPT/ OUTR) (NOTE1)	BRG ELEM (OR,IR, RE)	DEFCT CAT (B,C,D)	ORIENT ±5° DEG (NOTE 2)	DEFCT FREQ HZ	90° G/R IMPLANT P/N	SAMPL NO.	QUILL	BRG LOC	BRG ELEM	DEFCT CAT	ORIENT ±5°	DEFCT FREQ
1A	1654	1R	BASELINE								BASELINE							
1R	1654	100	BASELINE								BASELINE							
2A	1654	1R	143	1	INPT	OUTR	OR	C/D	54	357	143	2	INPT	OUTR	IR	C/D	N/A	503
2R	1654	100	143	1	INPT	OUTR	OR	C/D	54	357	143	2	INPT	OUTR	IR	C/D	N/A	503
3R	1654	100	310	1	INPT	N/A	OR	C/D	139	410	143	1	INPT	OUTR	OR	C/D	139	357
3R	1654	100	310	1	INPT	N/A	OR	C/D	139	594	143	1	INPT	OUTR	IR	C/D	N/A	357
4A	1654	1R	310	2	INPT	N/A	IR	C/D	N/A	594	143	3	INPT	OUTR	RE	C/D	N/A	313
4R	1654	100	310	2	INPT	N/A	IR	C/D	N/A	594	143	3	INPT	OUTR	RE	C/D	N/A	313
5A	1654	1R	310	3	INPT	N/A	RE	C/D	N/A	378	406	1	INPT	N/A	OR	C/D	58	410
5R	1654	100	310	3	INPT	N/A	RE	C/D	N/A	378	406	1	INPT	N/A	OR	C/D	58	410
6A	1654	1R	BASELINE								406	2	INPT	N/A	IR	C/D	N/A	593
6R	1654	100	BASELINE								406	2	INPT	N/A	IR	C/D	N/A	593
7A	1654	1R	BASELINE								406	3	INPT	N/A	RE	C/D	N/A	381
7A	1654	100	BASELINE								406	3	INPT	N/A	RE	C/D	N/A	381
8A	1654	1R	BASELINE								424	1	OUTPT	OUTR	OR	C/D	160	204
8R	1654	100	BASELINE								424	1	OUTPT	OUTR	OR	C/D	160	204
9A	1654	1R	BASELINE								424	2	OUTPT	OUTR	IR	C/D	N/A	264
9R	1654	100	BASELINE								424	2	OUTPT	OUTR	IR	C/D	N/A	264
10A	1654	1R	BASELINE								424	3	OUTPT	OUTR	RE	C/D	N/A	185
10R	1654	100	BASELINE								424	3	OUTPT	OUTR	RE	C/D	N/A	185
11A	1654	1R	BASELINE								407	1	OUTPT	N/A	RE	C/D	315	242
11R	1654	100	BASELINE								407	1	OUTPT	N/A	RE	C/D	315	242
12A	1654	1R	BASELINE								407	2	OUTPT	N/A	IR	C/D	N/A	310
12R	1654	100	BASELINE								407	2	OUTPT	N/A	IR	C/D	N/A	310
13A	1654	1R	BASELINE								407	3	OUTPT	N/A	RE	C/D	N/A	221
13R	1654	100	BASELINE								407	3	OUTPT	N/A	RE	C/D	N/A	221
14A	1654	1R	BASELINE								BASELINE							
14R	1654	100	BASELINE								BASELINE							

NOTE 1: APPLICABLE TO DUPLEX BALL BRGS ONLY (143, 424)

NOTE 2: APPLICABLE TO OR DEFECTS ONLY. ORIENTATION OF DEFECT LOOKING INTO QUILL:

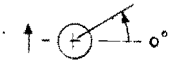

Significant efforts were expended to simulate spalling failures associated with naturally degrading bearings with the exception of generating subsurface fatigue cracks. It is believed that the artificially degraded bearings used were satisfactory for signature analysis. The original test plan included a greater sample of naturally failed bearings that were unavailable during the test period. Figures C-10 through C-43 are photographs and descriptions of the implants tested.

TABLE C-2. AH-1S RUN SEQUENCE AND BEARING CONFIGURATION

RUN #	OTPT HP	HANGER BEARING IMPLANT P/N	#	BRG ELEM (OR,IR RE)	ORNT ±5°	FREQ HZ	42° GEARBOX IMPLANT P/N	#	QUILL (INPT/ OTPT)	BRG LOC (INPT/ OTPT)	BRG ELEM (OR,IR RE))	ORNT ±5°	FREQ HZ	90° GEARBOX IMPLANT P/N	#	QUILL (INPT OTPT)	BRG LOC (INPT OTPT)	BRG ELEM (OR,IR RE)	ORNT ±5°	FREQ HZ
	(1)			(2,3)	(3,4)	(4)				(5)	(2,3)	(3,4)	(4)				(5)	(2,3)	(3,4)	(4)
1A	30	BASELINE					BASELINE							BASELINE						
1B	180	BASELINE					BASELINE							BASELINE						
2A	30	623	1	OR	270°	330	143	1	INPUT	OUTER	OR	302°	307	456	1	INPUT	OUTER	OR	228°	351
2B	180																			
3A	30	623	1	OR	270°	330	143	2	INPUT	OUTER	IR	N/A	504	456	2	INPUT	OUTER	IR	N/A	509
3B	180																			
4A	30	623	1	OR	270°	330	143	3	INPUT	OUTER	RE	N/A	313	456	3	INPUT	OUTER	RE	N/A	327
4B	180																			
5A	30	623	1	OR	270°	330	210	1	INPUT	N/A	OR	138°	344	455	1	INPUT	N/A	OR	160°	348
5B	180																			
6A	30	623	2	IR	N/A	459	500	1	INPUT	N/A	IR	N/A	517	450	1	INPUT	N/A	IR	N/A	513
6B	180																			
7A	30	623	2	IR	N/A	459	210	2	INPUT	N/A	RE	N/A	341	455	2	INPUT	N/A	RE	N/A	359
7B	180																			
8A	30	623	2	IR	N/A	459	143	1	OUTPUT	OUTER	OR	28°	357	456	1	OUTER	INNER	OR	111°	136
8B	180																			
9A	30	623	2	IR	N/A	459	143	2	OUTPUT	OUTER	IR	N/A	504	456	2	OUTPUT	INNER	IR	N/A	197
9B	180																			
10A	30	623	3	RE	N/A	426	143	3	OUTPUT	OUTER	RE	N/A	313	456	3	OUTPUT	INNER	RE	N/A	126
10B	180																			
11A	30	623	3	RE	N/A	426	210	1	OUTPUT	N/A	OR	215o	344	466	1	OUTPUT	N/A	OR	140o	134
11B	180																			
12A	30	623	3	RE	N/A	426	500	2	OUTPUT	N/A	IR	N/A	517	462	1	OUTPUT	N/A	IR	N/A	198
12B	180																			
13A	30	623	3	RE	N/A	426	210	2	OUTPUT	N/A	RE	N/A	341	466	2	OUTPUT	N/A	RE	N/A	138
13B	180																			
14A	30	BASELINE					BASELINE							BASELINE						
14B	180	BASELINE					BASELINE							BASELINE						

NOTES: (1) ALL TESTS RUN WITH T/L OUTPUT AT 1660 RPM
(2) ALL IMPLANTS WITH DEFECT CATEGORY AT C/D LEVEL PER GIUDELINES USED IN AIDAPTS
(3) BEARING ELEMENT: OR - OUTER RACE, IR - INNER RACE, RE - ROLLING ELEMENT
(4) DEFECT ORIENTATION: APPLICABLE TO OR DEFECTS ONLY; ORIENTATION OF DEFECT LOOKING INTO QUILL OR GEARBOX

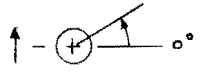

(5) BEARING LOCATION APPLICABLE TO DUPLEX BEARINGS ONLY

TABLE C-3. DEGRADED PART CLASSIFICATION

BALL BEARING DEFECT CATEGORY	
CATEGORY A	NO DEFECT
CATEGORY B	INITIAL SPALLING: ONE ORE MORE VOIDS OR IRREGULARITIES IN THE BALL PATH OR UN THE BALL ITSELF NOT EXCEEDING AN AREA DESCRIBED BY 0.05 X BALL DIAMETER WIDE OR 0.20 X BALL DIAMETER LONG
CATEGORY C	MODERATE SPALLING: UNE OR MORE VOIDS OR IRREGULARITIES IN THE BALL PATH OR ON THE BALL ITSELF BETWEEN THE UPPER LIMIT OF CATEGORY B AND NOT EXCEEDING AN AREA DESCRIBED BY 0.30 X BALL DIAMETER WIDE BY 0.40 X BALL DIAMETER LONG
CATEGORY D	ADVANCED SPALLING. BEARING STILL OPERATIONAL, BUT WITH ONE OR MORE VOIDS OR IRREGULARITIES IN THE BALL BATH OR ON THE BALL ITSELF GREATER THAN THE UPPER LIMIT OF CATEGORY C.
CATEGORY E	FUNCTIONAL FAILURE: BEARING JAMMED OR CONTAINS A BROKEN COMPONENT.
ROLLER BEARING DEFECT CATEGORY	
CATEGORY A	NO DEFECT
CATEGORY B	INITIAL SPALLING ONE OR MORE VOIDS OR IRREGULARITIES IN THE ROLLER PATH OR ON THE ROLLER ITSELF NOT EXCEEDING AN AREA DESCRIBED BY 0.15 ROLLER DIAMETER CIRCUMFERENTIALLY OR 0.30 X ROLLER LENGTH AXIALLY.
CATEGORY C	MODERATE SPALLING: ONE OR MORE VOIDS OR IRREGULARITIES IN THE ROLLER PATH OR ON THE ROLLER ITSELF BETWEEN THE UPPER LIMIT OF CATEGORY B AND NOT EXCEEDING AN AREA DESCRIBED BY 0.30 X ROLLER DIAMETER CIRCUMFERENTIALLY ACROSS THE TOTAL WIDTH OF THE ROLLER OR ROLLER PATH.
CATEGORY D	ADVANCED SPALLING: ONE OR MORE VOIDS OR IRREGULARITIES IN THE ROLLER PATH OR UN THE ROLLER ITSELF GREATER THAN THE UPPER LIMIT OF CATEGORY E.
CATEGORY E	FUNCTIONAL FAILURE BEARING JAMMED OR CONTAINS A BROKEN COMPONENT.

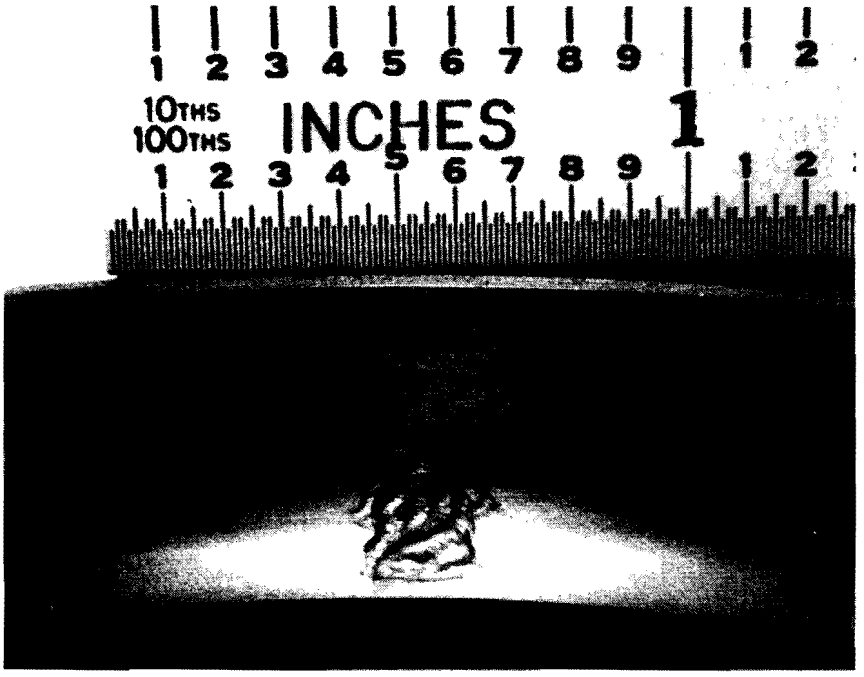

Figure C-10. 42-Degree Gearbox -143 Bearing Outer Race C/D, S/N 33096, Runs 2A + 2B and 3A + 3B

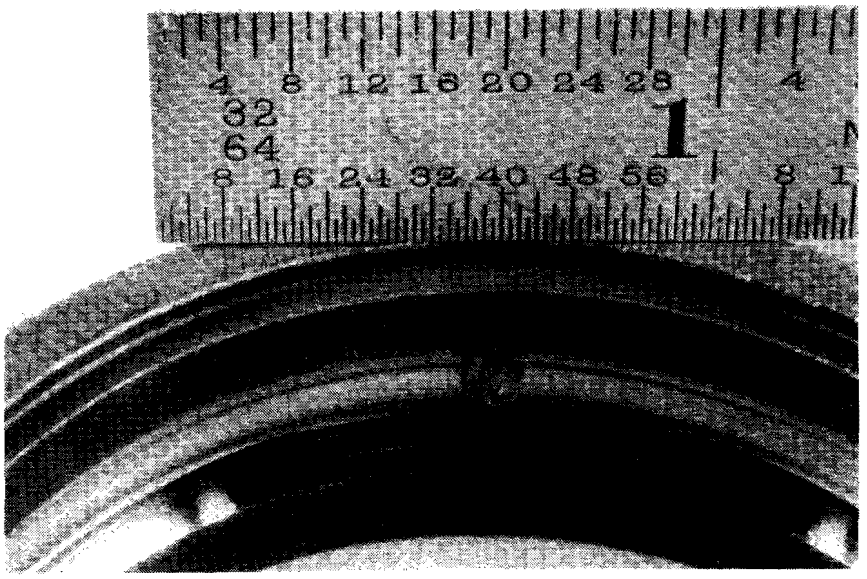

Figure C-11. 90-Degree Gearbox -143 Bearing Inner Race C/D, S/N 3979A, Runs 2A + 2B

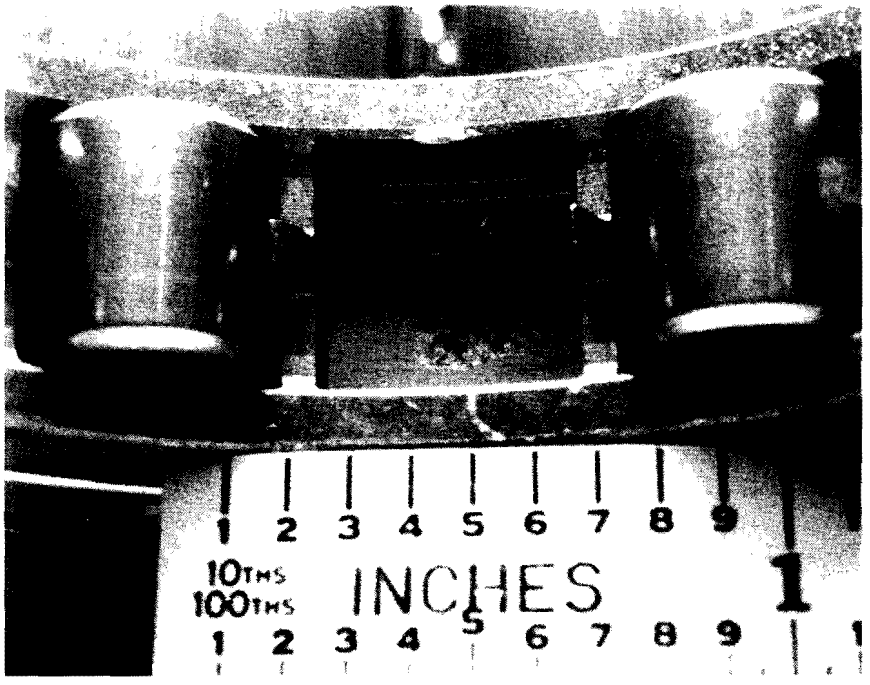

Figure C-12. 42-Degree Gearbox -310 Bearing Outer Race C/D, S/N 167852, Runs 3A + 3B

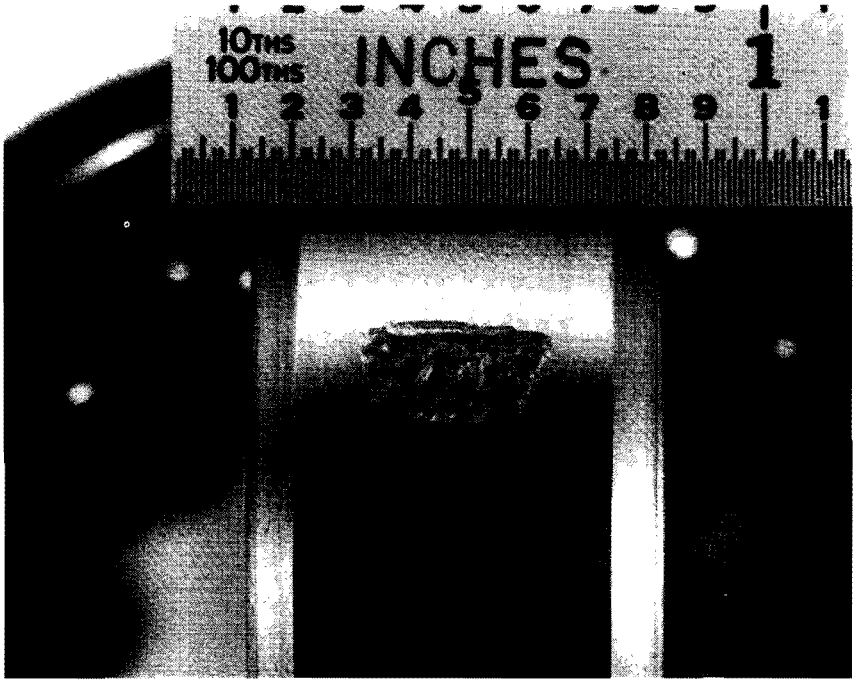

Figure C-13. 42-Degree Gearbox -310 Bearing Inner Race C/D, S/N 145284, Runs 4A + 4B

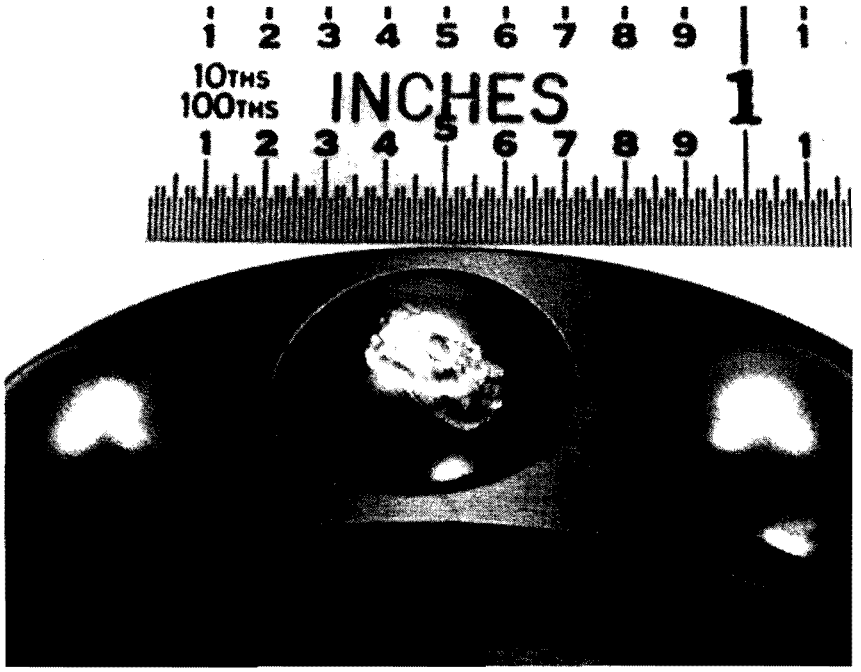

Figure C-14. 90-Degree Gearbox -143 Bearing Ball Fault C/D, S/N 751302, Runs 4A + 4B

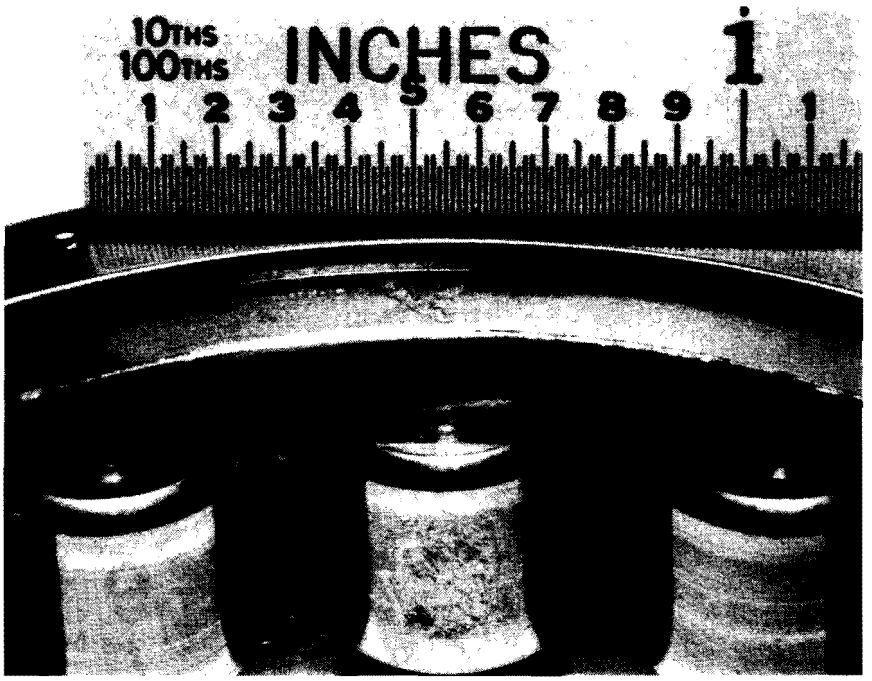

Figure C-15. 42-Degree Gearbox -310 Bearing Roller Fault C/D, S/N 211667, Runs 5A + 5B

Figure C-16. 90-Degree Gearbox -406 Bearing Outer Race C/D, S/N 22902, Runs 5A + 5B

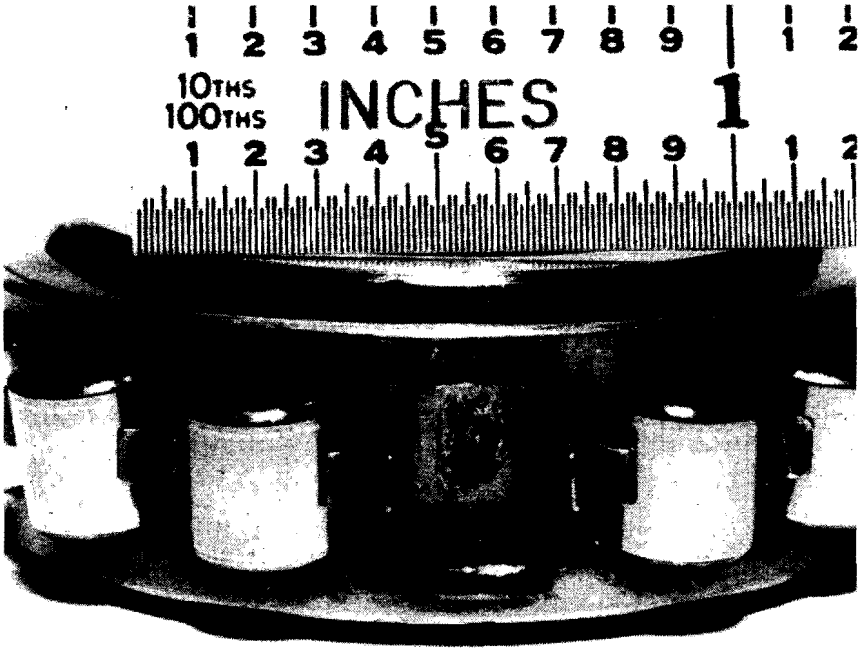

Figure C-17. 90-Degree Gearbox -406 Bearing Inner Race C/D, S/N 2555, Runs 6A + 6B

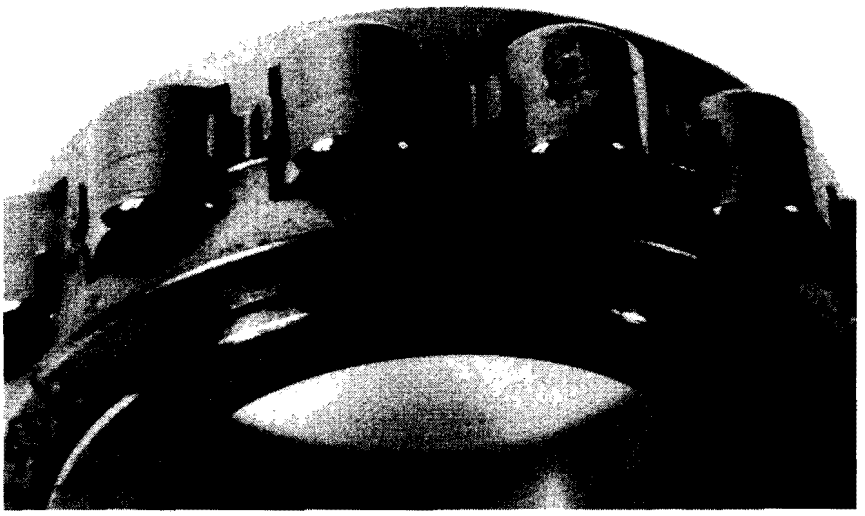

Figure C-18. 90-Degree Gearbox -406 Bearing Roller Fault C/D, S/N 8070, Runs 7A + 7B

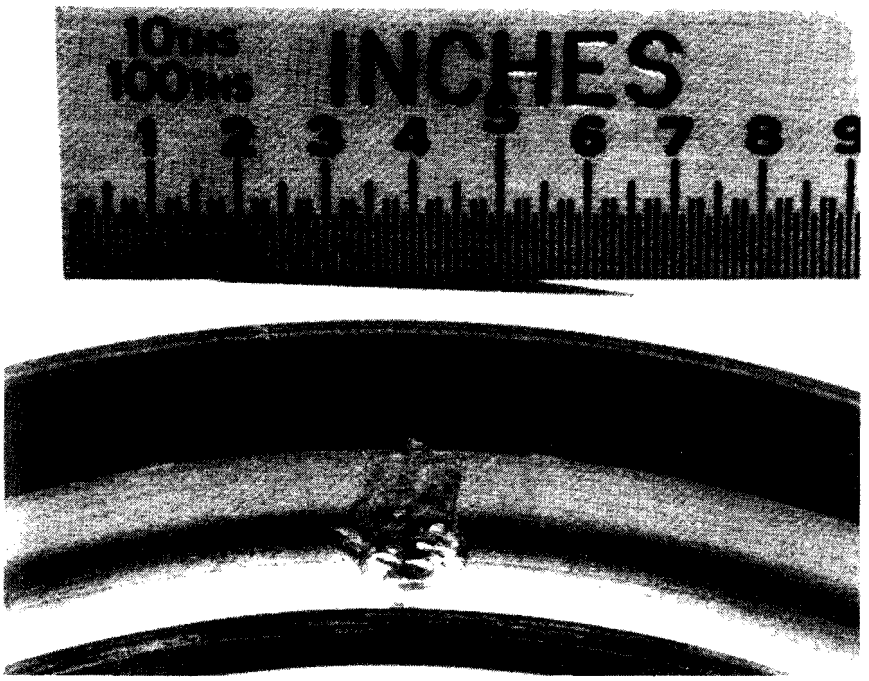

Figure C-19. 90-Degree Gearbox -424 Bearing Outer Race C/D, S/N 32203, Runs 8A + 8B

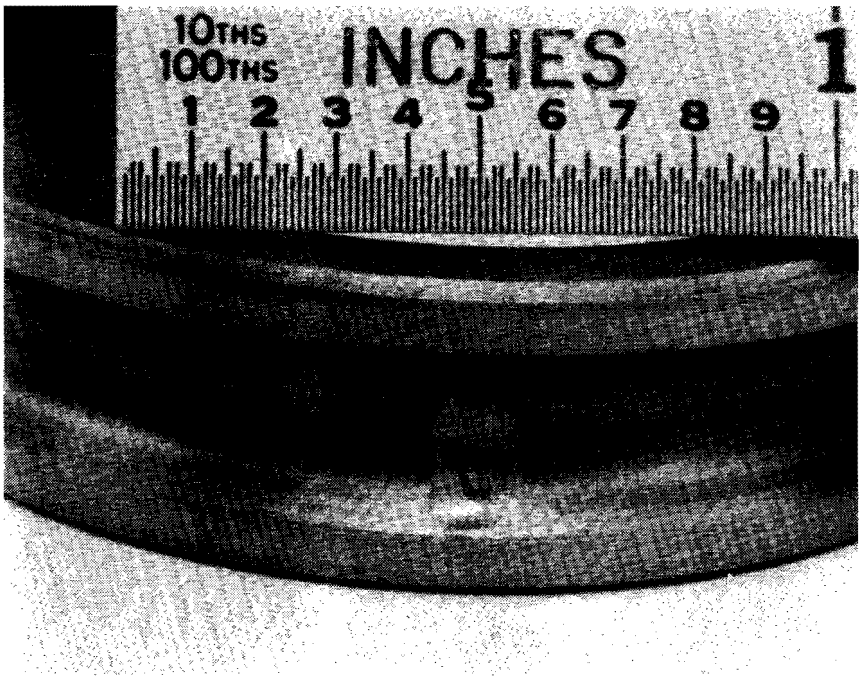

Figure C-20. 90-Degree Gearbox -424 Bearing Inner Race C/D, S/N 38142, Runs 9A + 9B

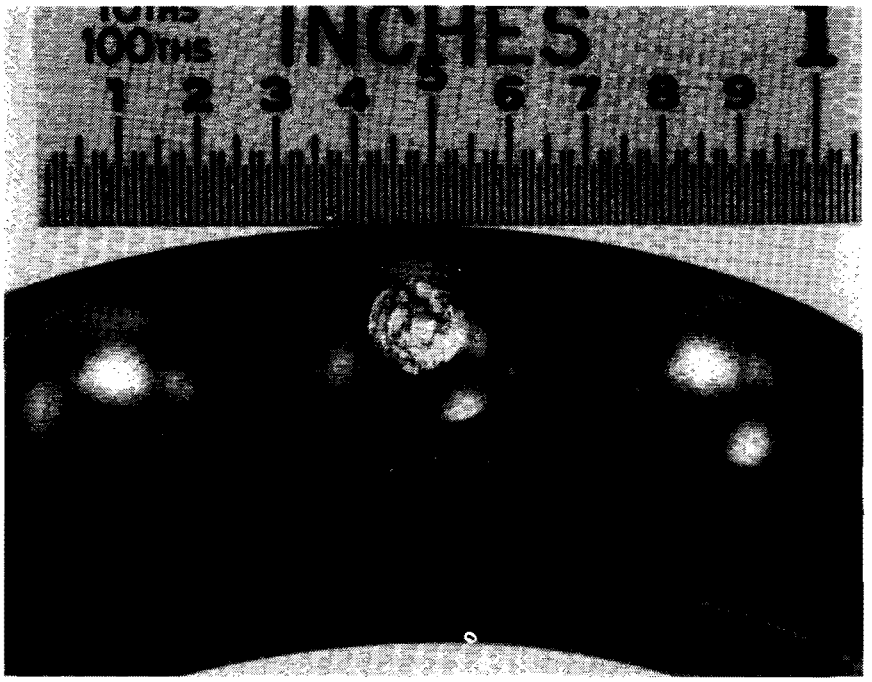

Figure C-21. 90-Degree Gearbox -424 Bearing Ball Fault C/D, S/N 4105, Runs 11A + 11B

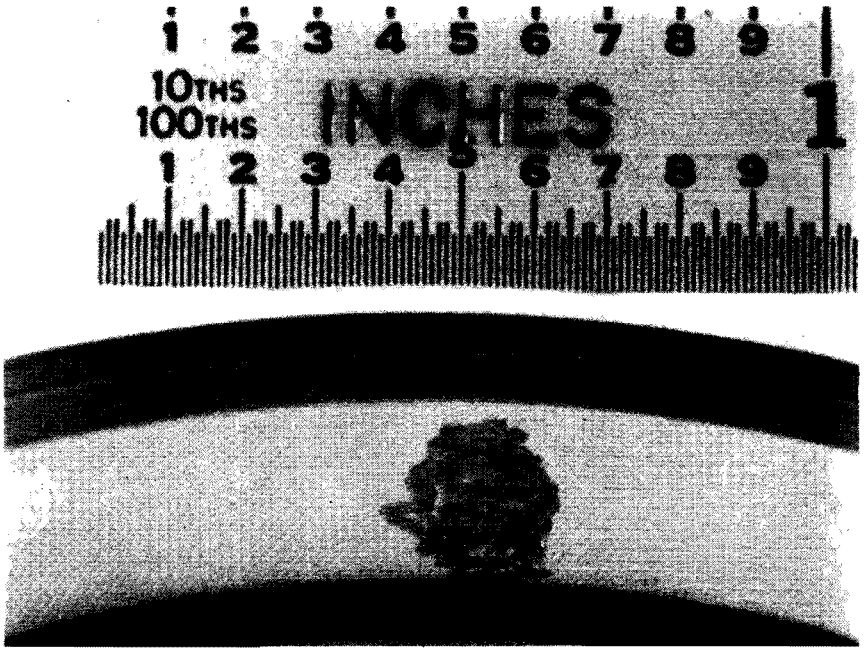

Figure C-22. 90-Degree Gearbox -407 Bearing Outer Race C/D, S/N 4446A, Runs 11A + 11B

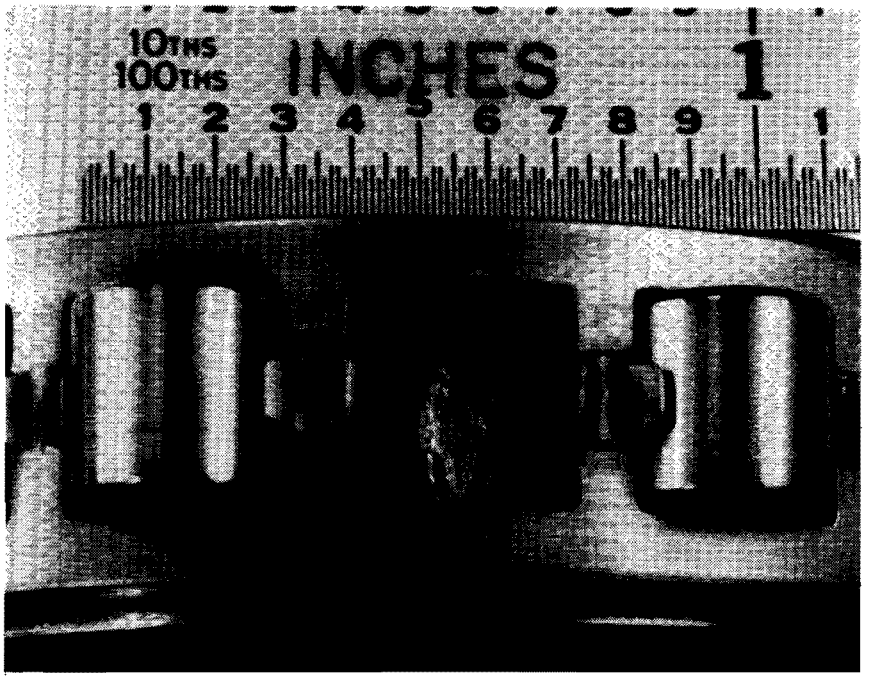

Figure C-23. 90-Degree Gearbox -407 Bearing Inner Race C/D, S/N 1536B, Runs 12A + 12B

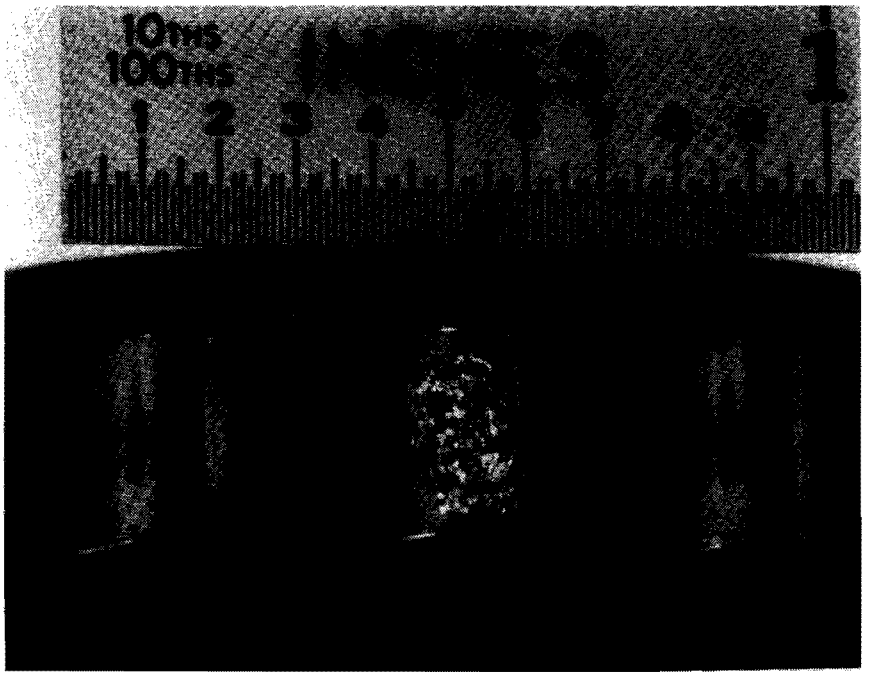

Figure C-24. 90-Degree Gearbox -407 Bearing Roller Fault C/D, S/N 22922, Runs 13A + 13B

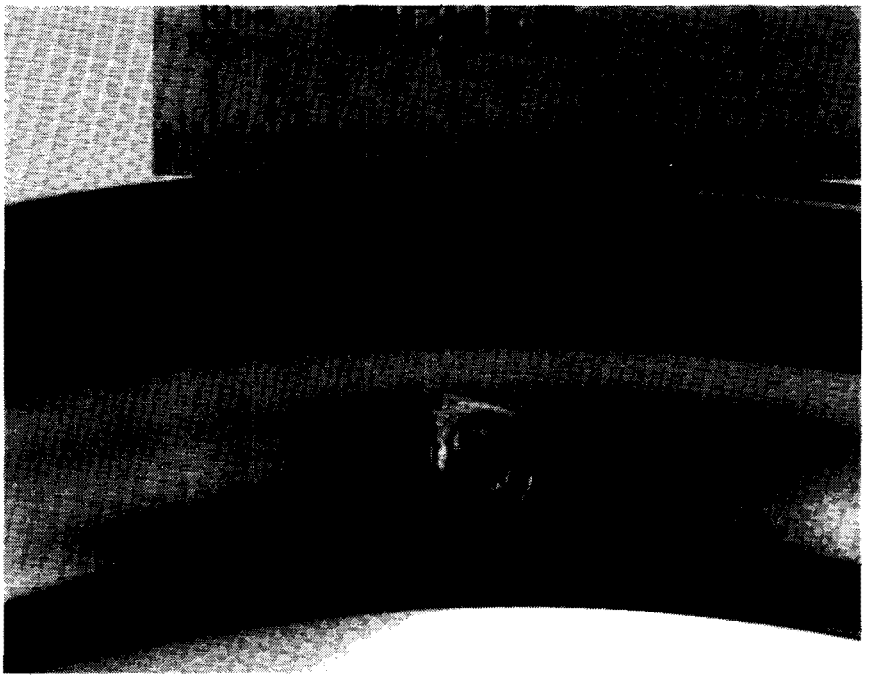

Figure C-25. 90-Degree Gearbox -456 Bearing Outer Race C/D, S/N J0432, Runs 2A + 2B and 8A + 8B

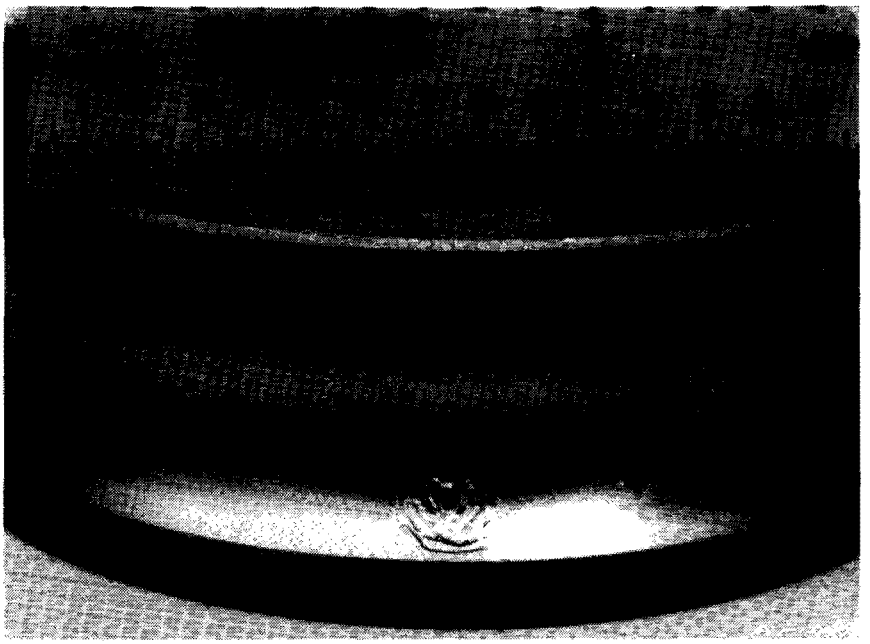

Figure C-26. 90-Degree Gearbox -456 Bearing Inner Race C/D, S/N J0440, Runs 3A + 3B and 9A + 9B

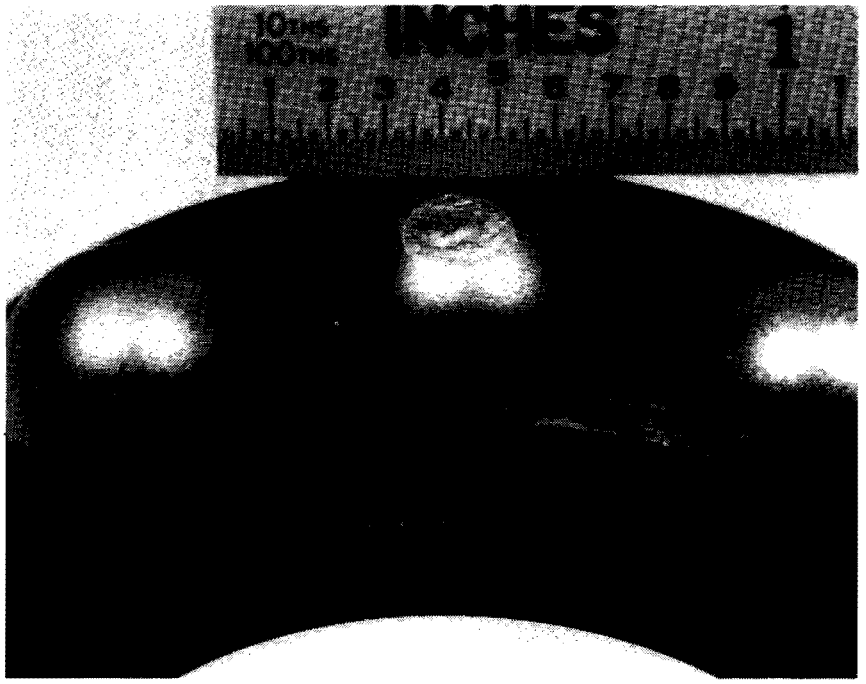

Figure C-27. 90-Degree Gearbox -456 Bearing Ball Fault C/D, S/N J0444, Runs 4A + 4B and 10A + 10B

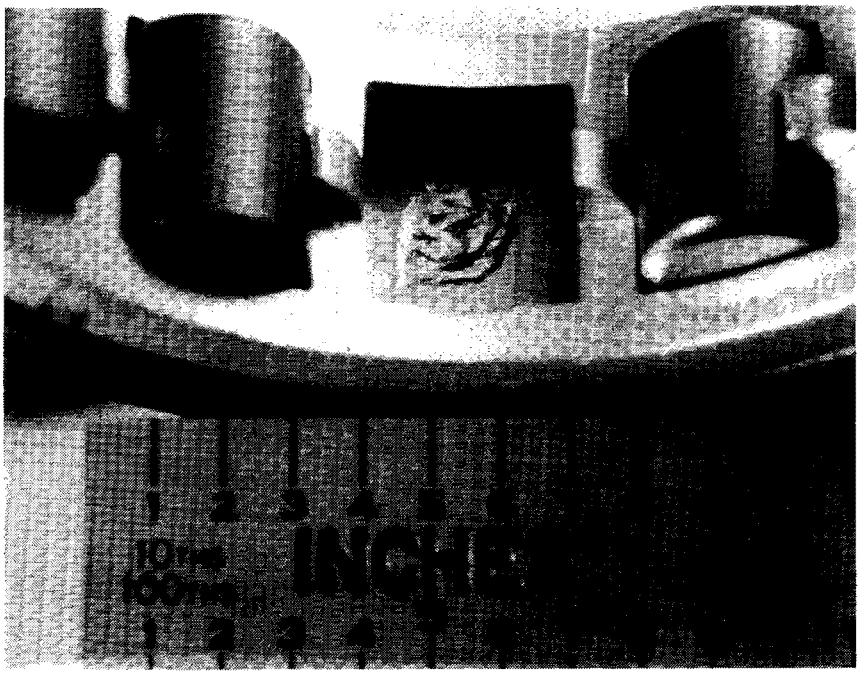

Figure C-28. 90-Degree Gearbox -455 Bearing Outer Race C/D, S/N 6262, Runs 5A + 5B

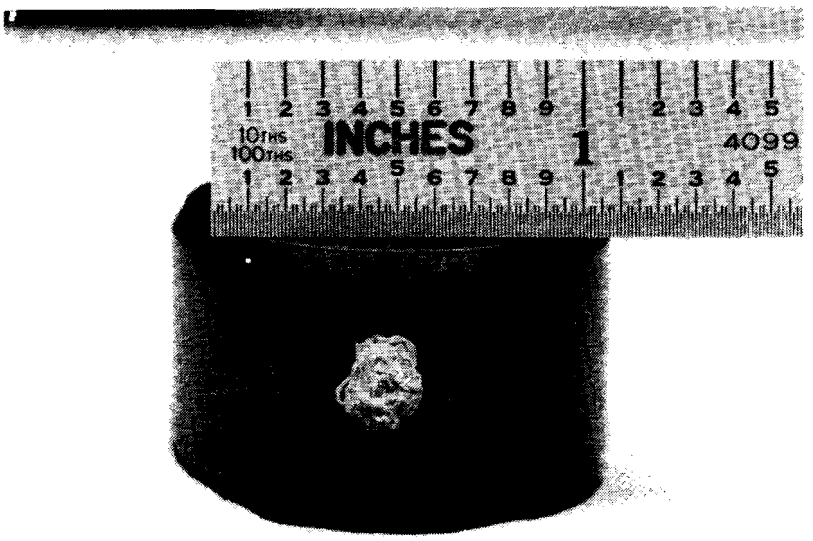

Figure C-29. 90-Degree Gearbox -450 Pinion (Inner Roller Race) C/D Fault, S/N A13-03401, Runs 6A + 6B

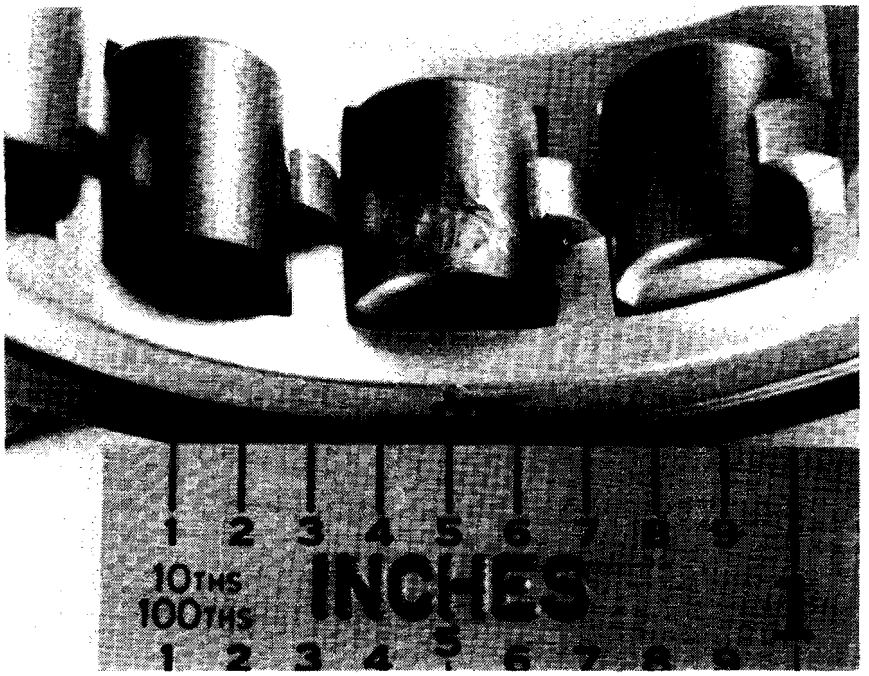

Figure C-30. 90-Degree Gearbox -455 Bearing Roller Defect C/D, S/N 6273, Runs 7A + 7B

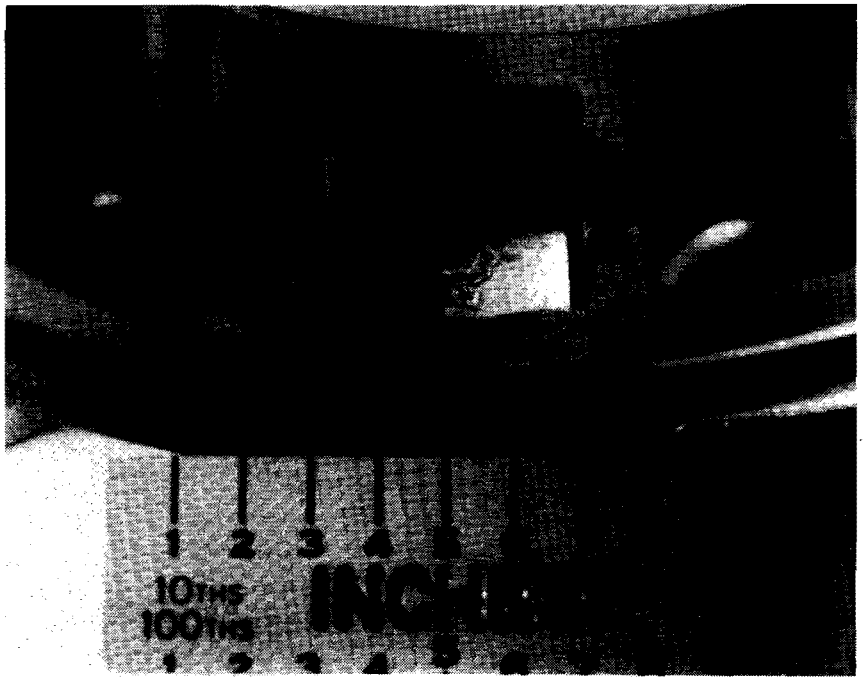

Figure C-31. 90-Degree Gearbox -466 Bearing Outer Race C/D, S/N 6567, Runs 6A + 6B

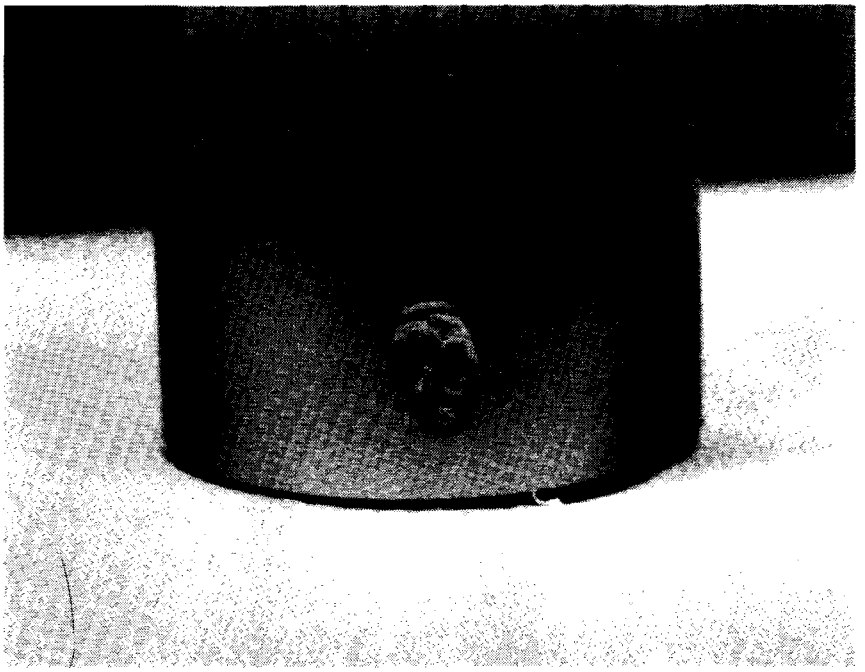

Figure C-32. 90-Degree Gearbox -462 Shaft (Inner Roller BRG Race C/D Fault), S/N A13-05316, Runs 12A + 12B

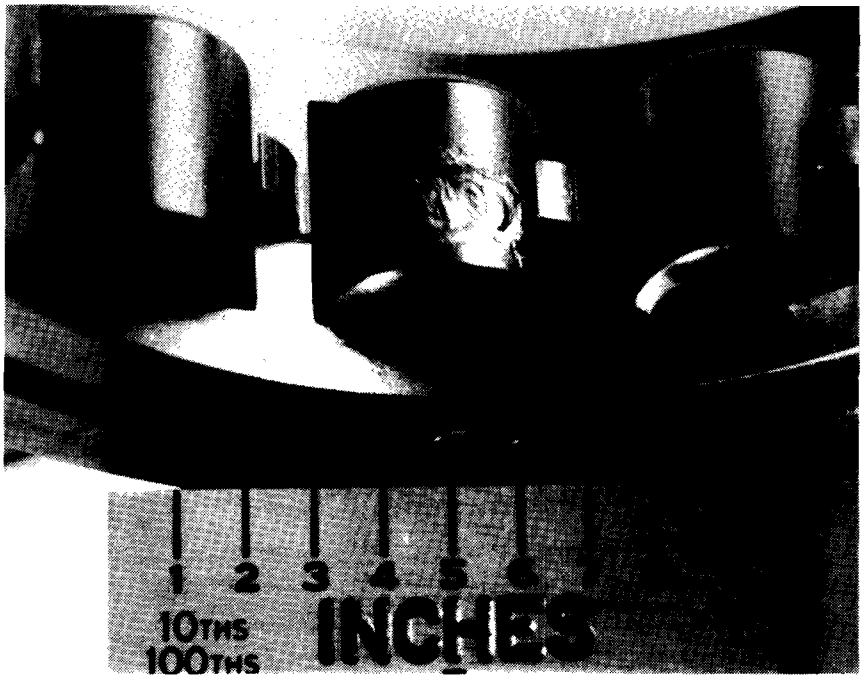

Figure C-33. 90-Degree Gearbox -466 Bearing Roller Defect C/D, S/N 6582, Runs 13A + 13B

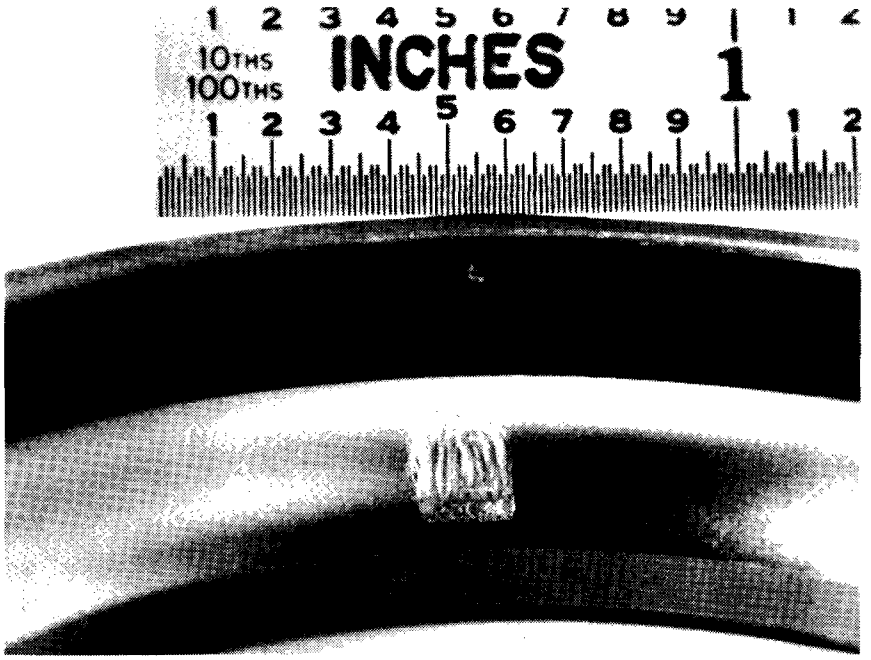

Figure C-34. 42-Degree Gearbox -143 Bearing Outer Race C/D, S/N J0629, Runs 2A + 2B and 8A + 8B

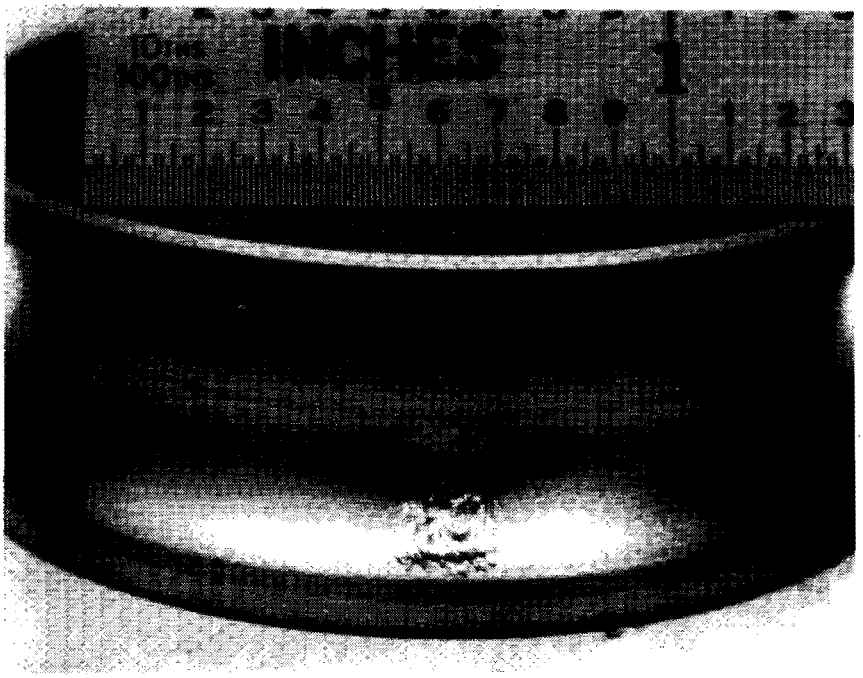

Figure C-35. 42-Degree Gearbox -143 Bearing Inner Race C/D, S/N J0635, Runs 3A + 3B and 9A + 9B

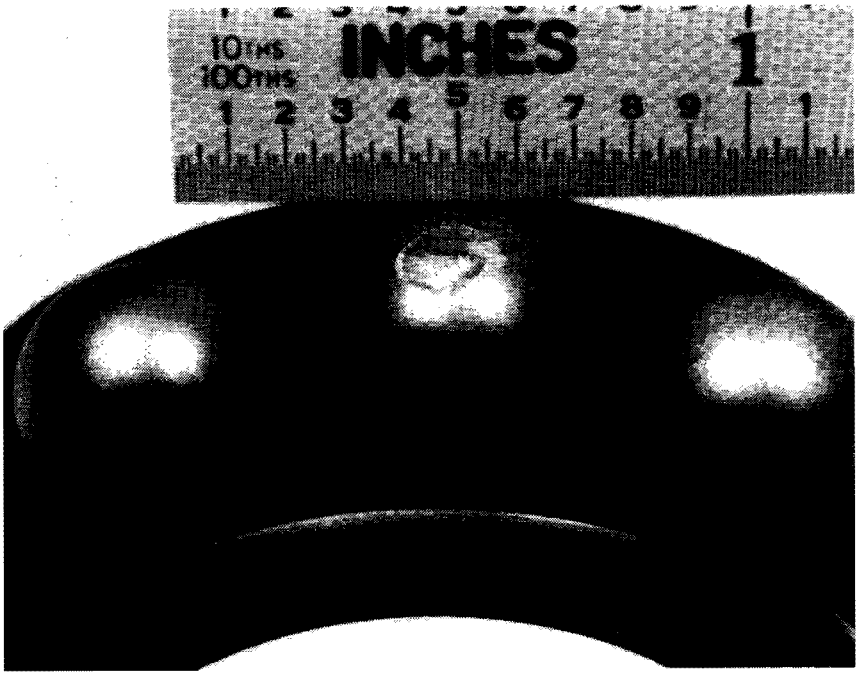

Figure C-36. 42-Degree Gearbox -143 Bearing Ball Defect C/D, S/N J0679, Runs 4A + 4B and 10A + 10B

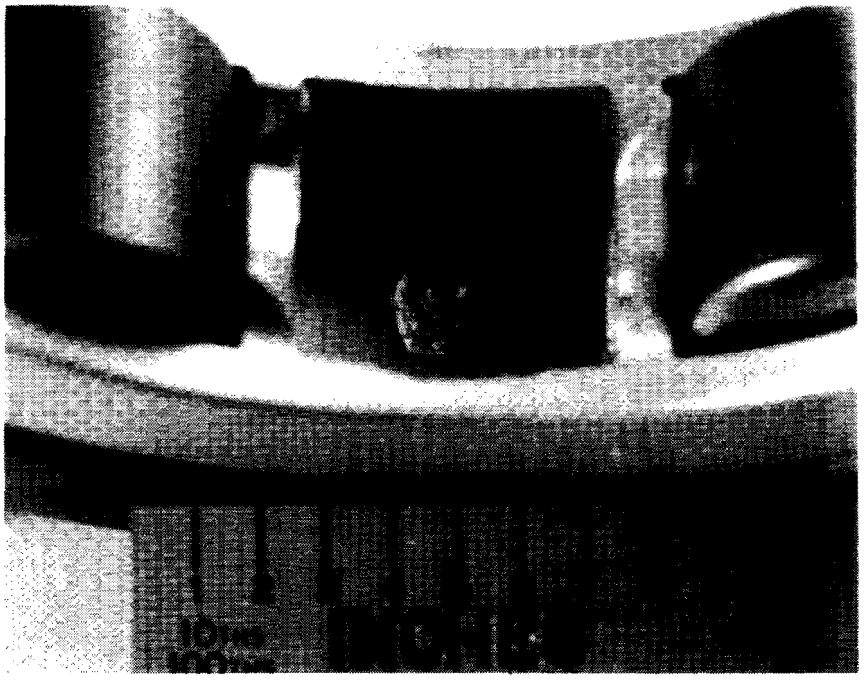

Figure C-37. 42-Degree Gearbox -210 Bearing Outer Race C/D, S/N Z255, Runs 5A + 5B and 11A + 11B

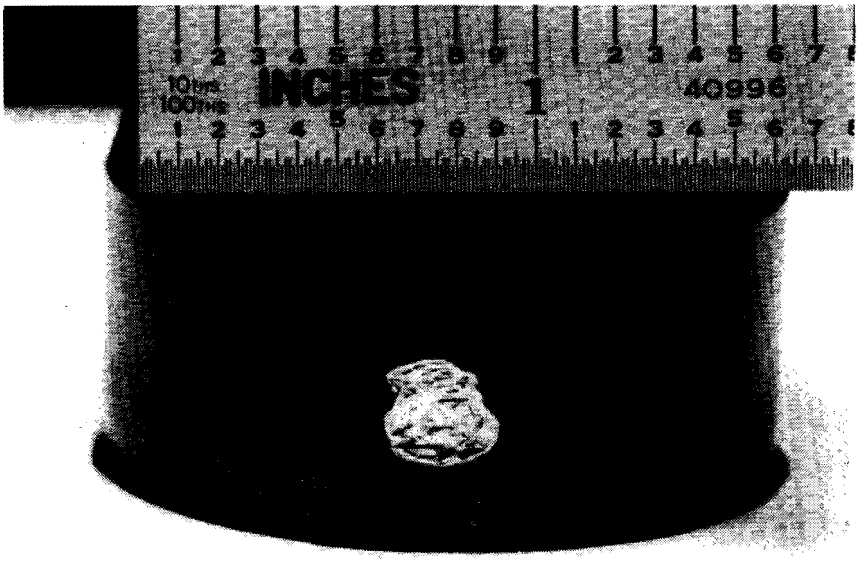

Figure C-38. 42-Degree Gearbox -500-7 Pinion Input Pinion Roller Bearing I.R. Defect, S/N A13-14241, Runs 6A + 6B

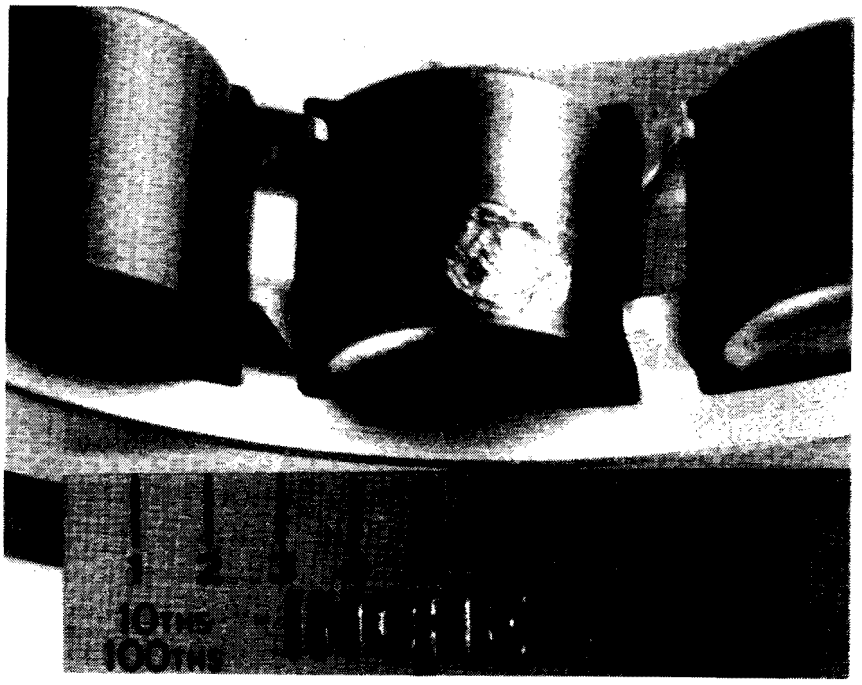

Figure C-39. 42-Degree Gearbox -210 Bearing Roller Fault C/D, S/N Z374, Runs 7A + 7B and 13A + 13B

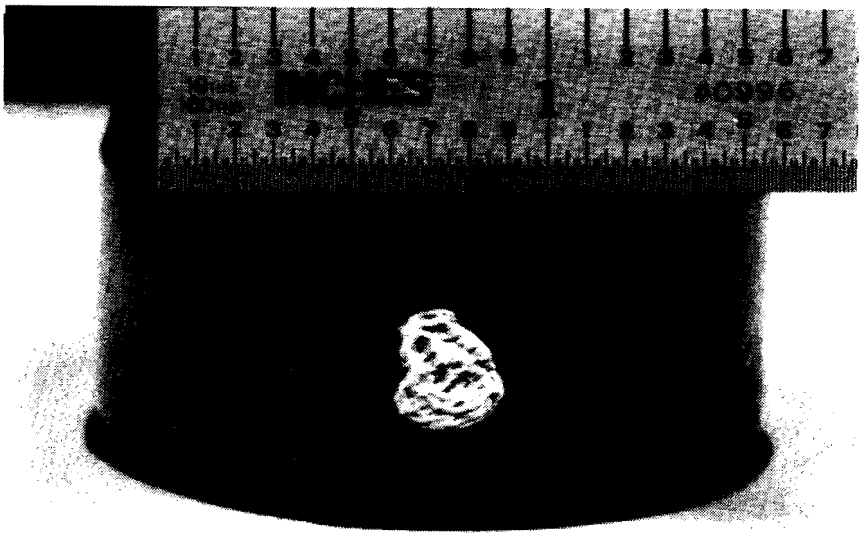

Figure C-40. 42-Degree Gearbox -500-6 Gear Output Gear Roller Bearing I.R. Defect C/D, S/N A13-13064, Runs 12A + 12B

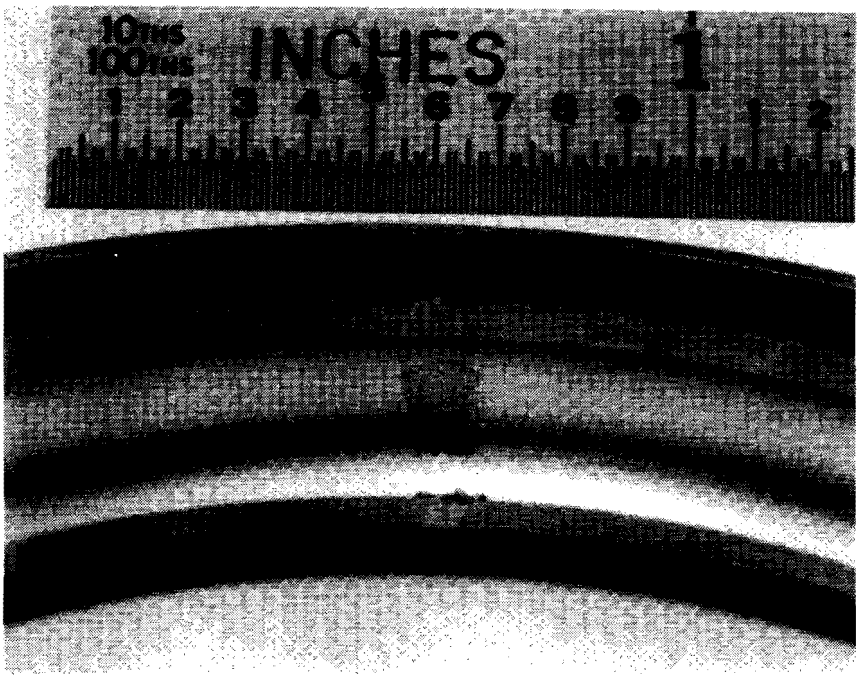

Figure C-41. -623-5 Hanger BRG Outer Race C/D, Runs 2A + 2B and 4A + 4B

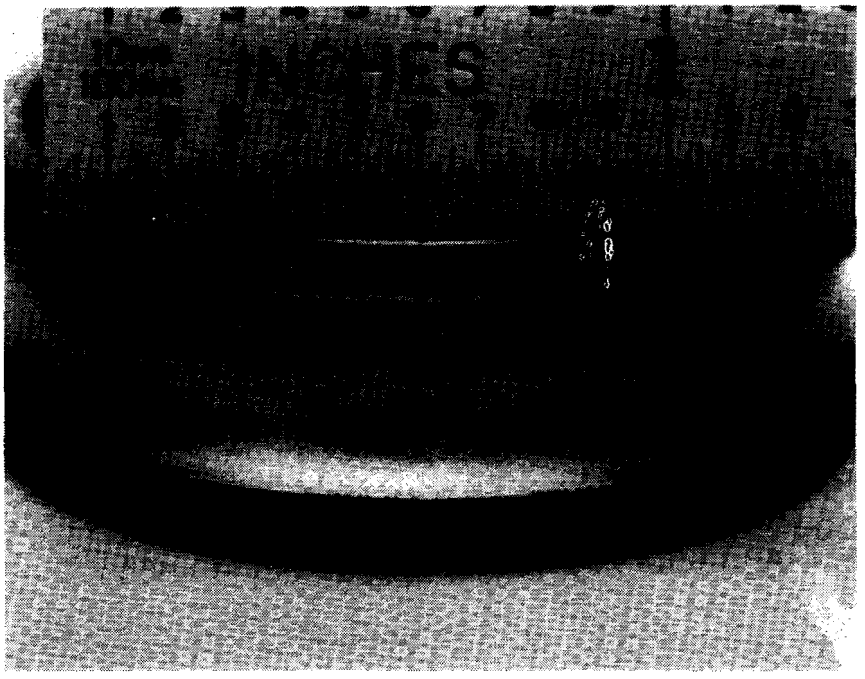

Figure C-42. -623-5 Hanger BRG Inner Race C/D, Runs 6A + 6B and 7A + 7B

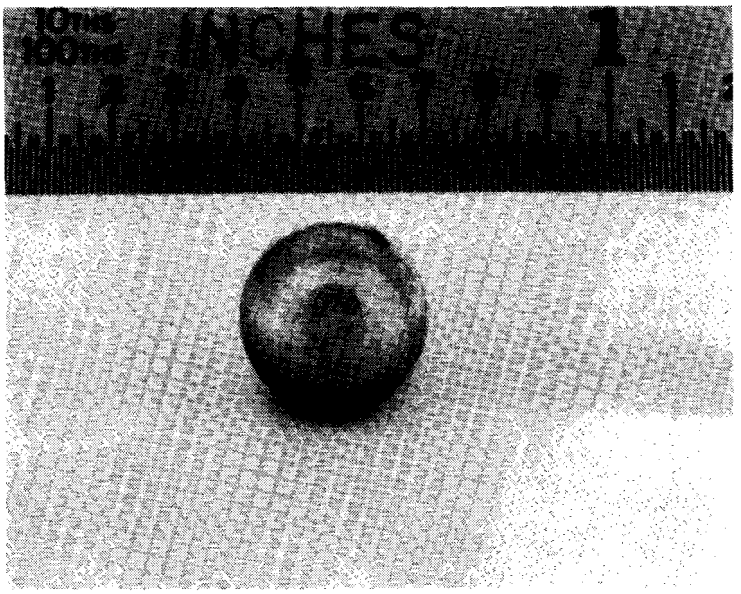

Figure C-43. -623-5 Hanger BRG Ball Fault C/D, Runs 10A +10B and 11A + 11B

C-1.2. RCA Test Cell Data on the Kiowa

RCA constructed a test stand for the evaluation of diagnostic techniques on the OH-58 (Kiowa) tail rotor drive. The apparatus consisted of a helicopter tail boom assembly which was bolted to a rigid steel stand at the main bulkhead. The tail rotor drive assembly was complete beyond the main bulkhead and included the tail rotor blades as a load. Power was supplied by a 25 horsepower electric motor which was belted up to the correct speed. The hanger bearings in positions 1 and 2, normally within the engine dog house, were not used; instead, pillow blocks and a steel driveshaft were used to resist the radial loads of the belt drive. A section of helicopter intermediate driveshaft with its flexible coupling was used to connect the drive to the tail boom assembly. The standard tail rotor driveshaft with its hanger bearings and mounting hardware was mounted on the tail boom as specified in the OH-58 A/C maintenance manual, as was the 90-degree gearbox. A special tail rotor blade pitch control linkage was also installed. The test stand was secured with lag bolts to a concrete pad which allowed operation at up to full tail rotor pitch. Figure C-44 illustrates the test setup.

The hanger bearing housings, numbers 3 through 8, were all instrumented with accelerometers, as was the 90-degree gearbox assembly. The signals from these transducers, along with other data signals, were recorded on magnetic tape in a fashion similar to that which had been done at BHT. Discrete fault

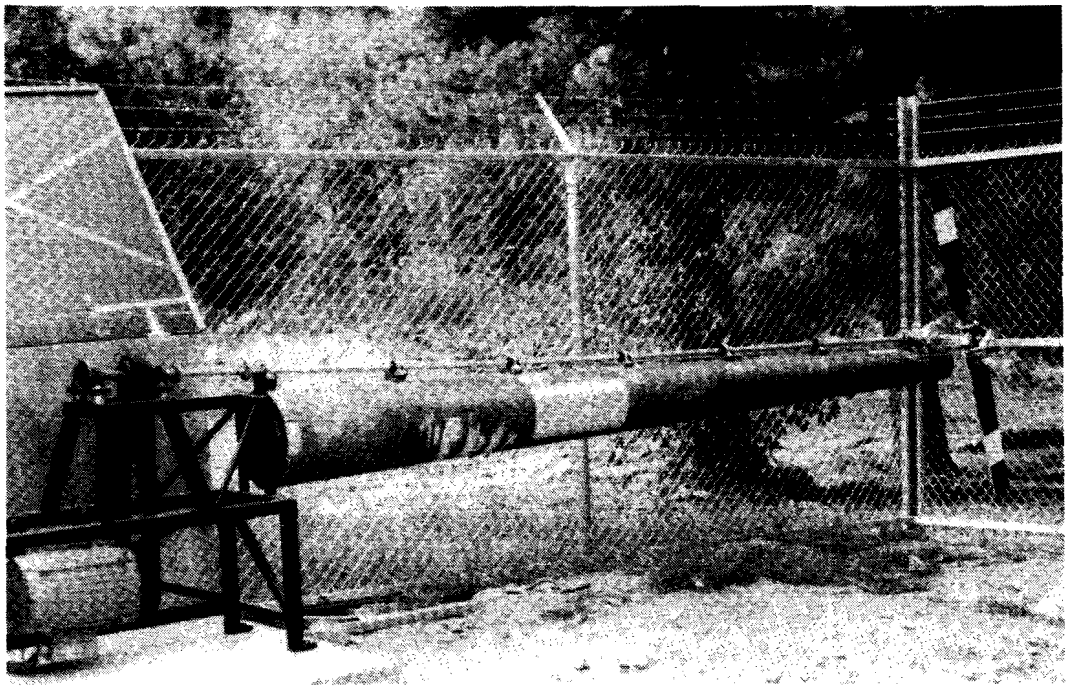

Figure C-44. OH-58 Tail Rotor Test Stand

implanted bearings were run in the gearbox and hanger bearing locations, as outlined in Table C-4 and Figure C-45. The defects were generated and oriented by the same methods that were used for the Huey and Cobra testing at Bell Helicopter. Figures C-46 through C-58 are photographs and descriptions of the implants tested.

The test stand was also used as a signal source for evaluating the performance of the breadboard analyzer. The actual SPADE hardware was connected to the mounted accelerometers through the appropriate cabling at several stages of its development. This test stand has been found to be a very realistic simulation of an actual aircraft and as such it has been important in assessing the performance of the breadboard during its development.

In addition to the fault implantation program outlined in Table C-4, various other tests were conducted on the OH-58 test stand. A sample of four new hanger bearings were installed on the tail boom in positions 3 through 6 which then had their vibration spectra recorded and analyzed. This sample of bearings was then disassembled, faulted, reassembled and rerun on the test stand. Initially, only very small category B faults were inserted in the bearings; they were then disassembled again and the fault size increased to a borderline C/D category.

Table C-4. OH-58 A/C RUN SCHEDULE

Run No.	Hanger Brg. No.	Defect	Defect Frequency	90° G/B Brg. No.	Location	Defect	Defect Frequency
		Baseline					
1				408/1	Inpt	OR-C/D	459
2	1	OR-C/D	471	408/2	Inpt	IR-C/D	647
3				408/3	Inpt	RE-C/D	442
4	2	OR-C/D	471	409/1	Inpt	OR-C/D	288
5				405/1	Inpt	IR-C/D	537
6	3	IR-C/D	662	409/1	Inpt	RE-C/D	312
7				410/1	Outpt	OR-C/D	261
8	4	IR-C/D	662	410/2	Outpt	IR-C/D	352
9				410/3	Outpt	RE-C/D	243
10	5	RE-C/D	595	411/1	Outpt	OR-C/D	257
11				407/1	Outpt	IR-C/D	355
12	6	RE-C/D	595	411/2	Outpt	RE-C/D	267
13							
14		Baseline					

Legend:

OR - Outer race
IR - Inner race
RE - Rolling element
C/D - Borderline Category C to D fault
Inpt - Input Quill
Outpt - Output quill

Bearing Number designation (example)
408/1 206-040-408-1 bearing sample number 1

This precedure was repeated through seven cycles, with data being recorded on the test stand for each new level of fault until the bearings were degraded beyond a category D level. The intent of this experiment was to evaluate the changes in a bearing signature over the time span from initial failure until the failure was severe. The data taken in this experiment is critical in understanding the correlation between the signals emanating from a bearing which is naturally failing in a progressive fashion and the amount of bearing damage.

C-2. ON-AIRCRAFT TEST DATA

In order to confirm the validity of the test cell data, additional data was collected on actual aircraft at Fort Rucker, Alabama. These tests were intended to confirm that there was no degradation in the fault sensitivity on a running aircraft as well as to confirm that the test set would function satisfactorily in the aircraft environment. Two trips to Fort Rucker were made.

During the first trip data was collected on a sample of three ships each of the aircraft of interest. All aircraft were in service and data was acquired in an "as-found" condition. While all aircraft were believed to be fault free, questions about the actual condition arose in several instances. These nine aircraft were instrumented with miniature accelerometers on their tail rotor drive gearboxes and on selected hanger bearings. Vibration signatures were recorded on magnetic tape with the rotor system running at flight idle speed and flat pitch. Table C-5 lists the aircraft tested and the vibration signatures recorded. Figures C-59 through C-62 are photographs of typical accelerometer installations on the aircraft.

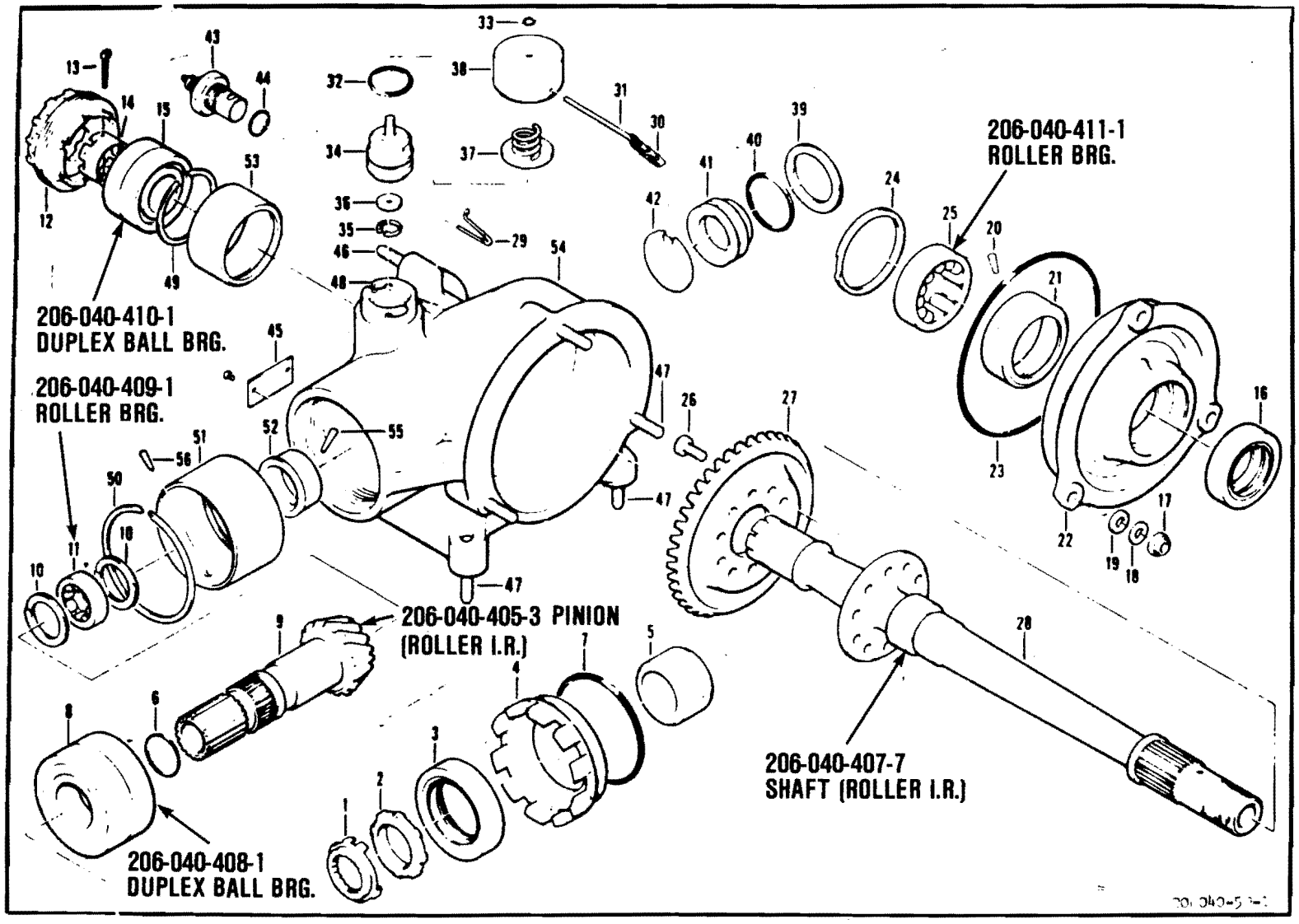

Figure C-45. Tail Rotor Gearbox, OH-58 A/C

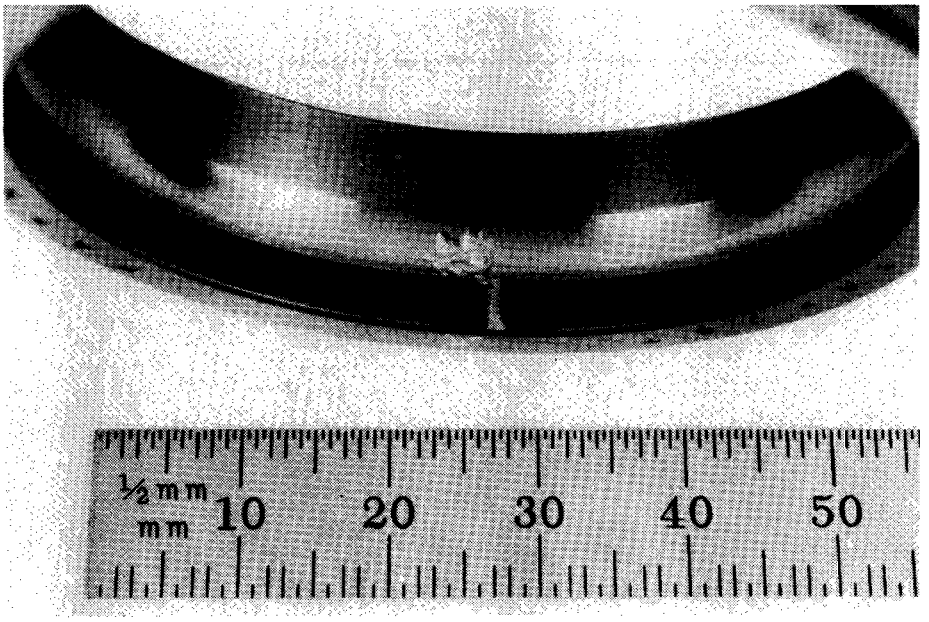

Figure C-46. 90-Degree Gearbox -408 Bearing Outer Race C/D Fault, Runs 2A + 2B

Figure C-47. 90-Degree Gearbox -408 Bearing Inner Race C/D Fault, Runs 3A + 3B

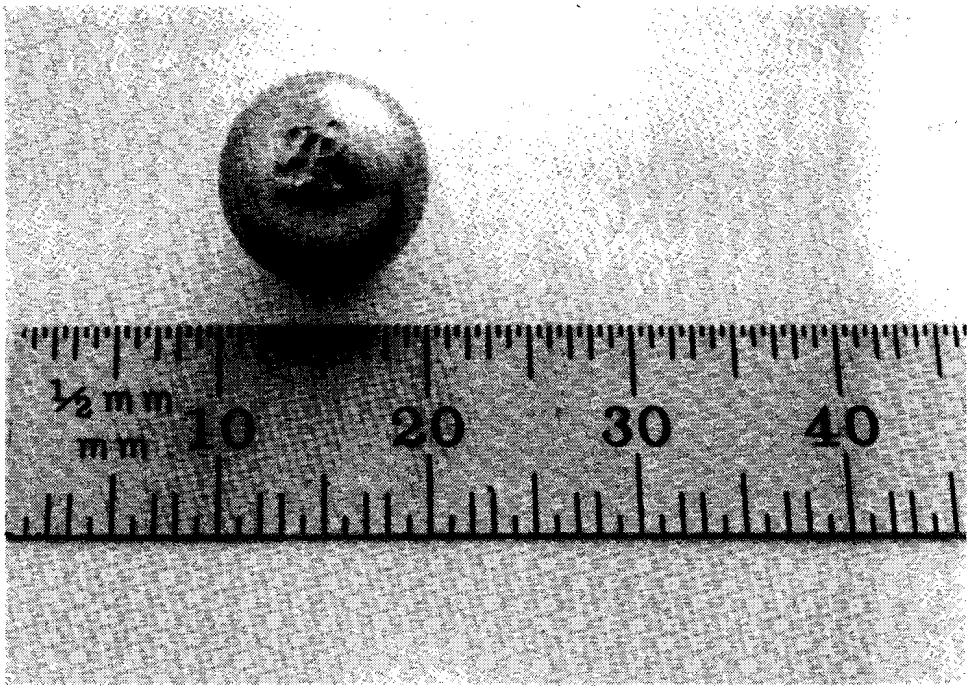

Figure C-48. 90-Degree Gearbox -408 Bearing Ball C/D Fault, Runs 4A + 4B

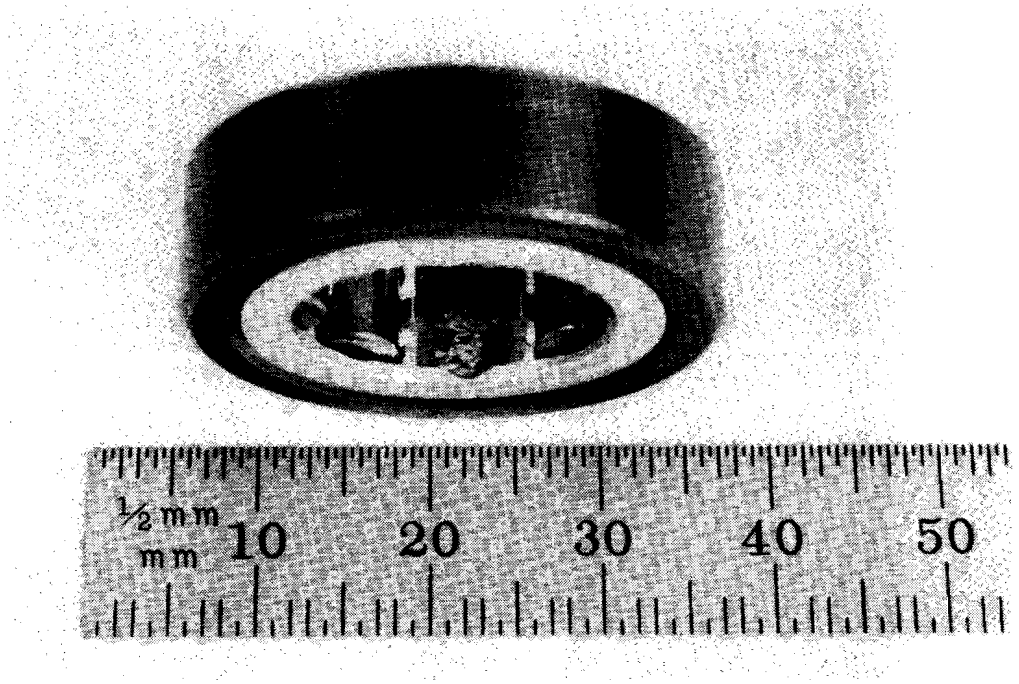

Figure C-49. 90-Degree Gearbox -409 Bearing Outer Race C/D Fault, Runs 5A + 5B

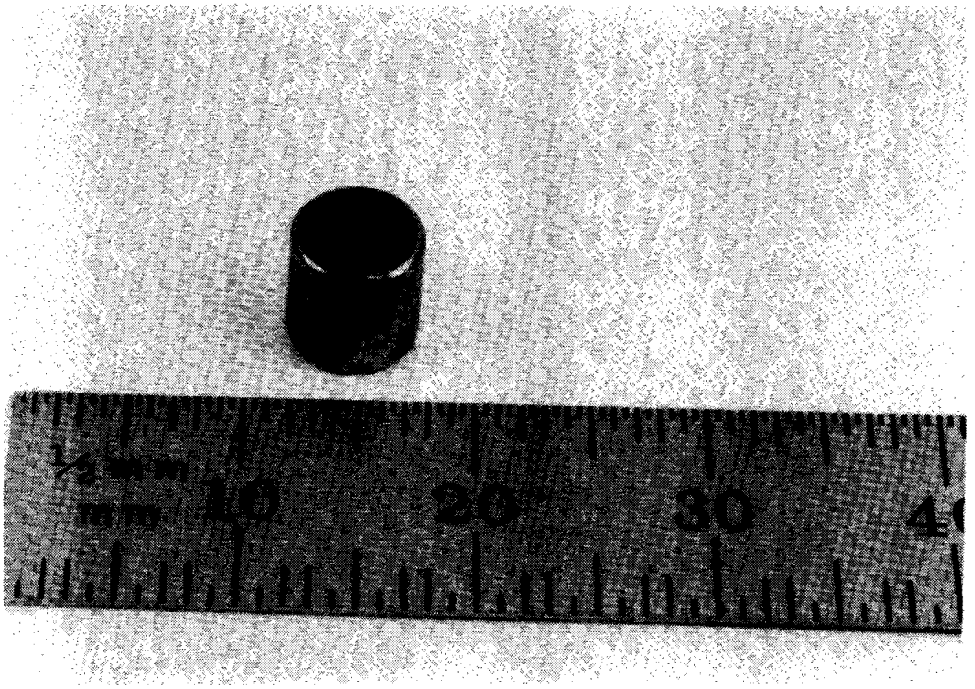

Figure C-50. 90-Degree Gearbox -409 Bearing Roller C/D Fault, Runs 7A + 7B

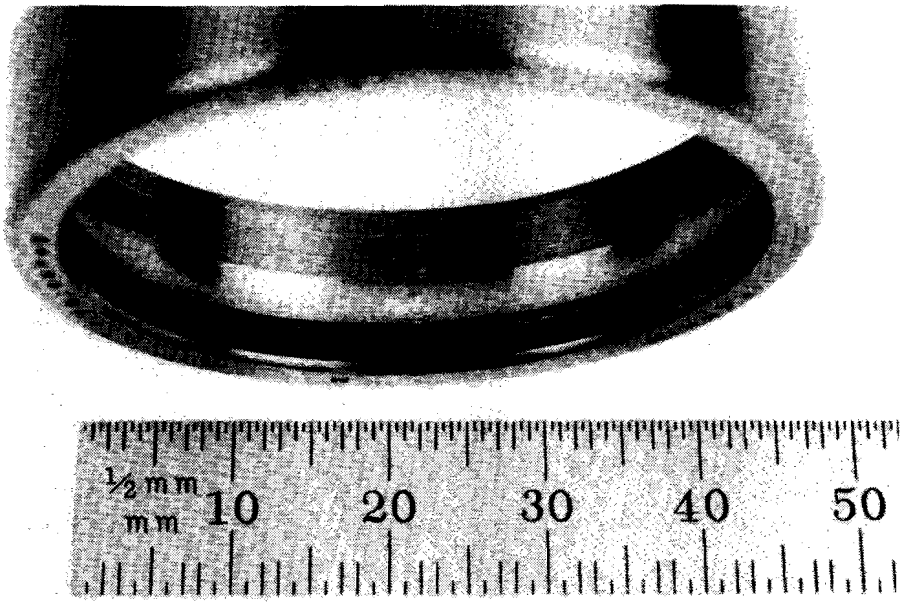

Figure C-51. 90-Degree Gearbox -410 Bearing Outer Race C/D Fault, Runs 8A + 8B

Figure C-52. 90-Degree Gearbox -410 Bearing Inner Race C/D Fault, Runs 9A + 9B

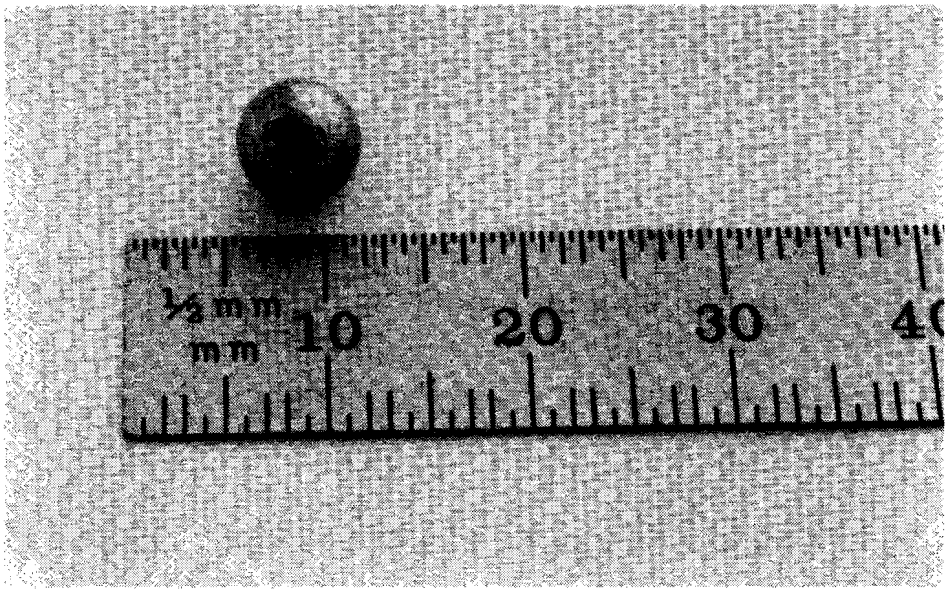

Figure C-53. 90-Degree Gearbox -410 Bearing Ball C/D Fault, Runs 10A + 10B

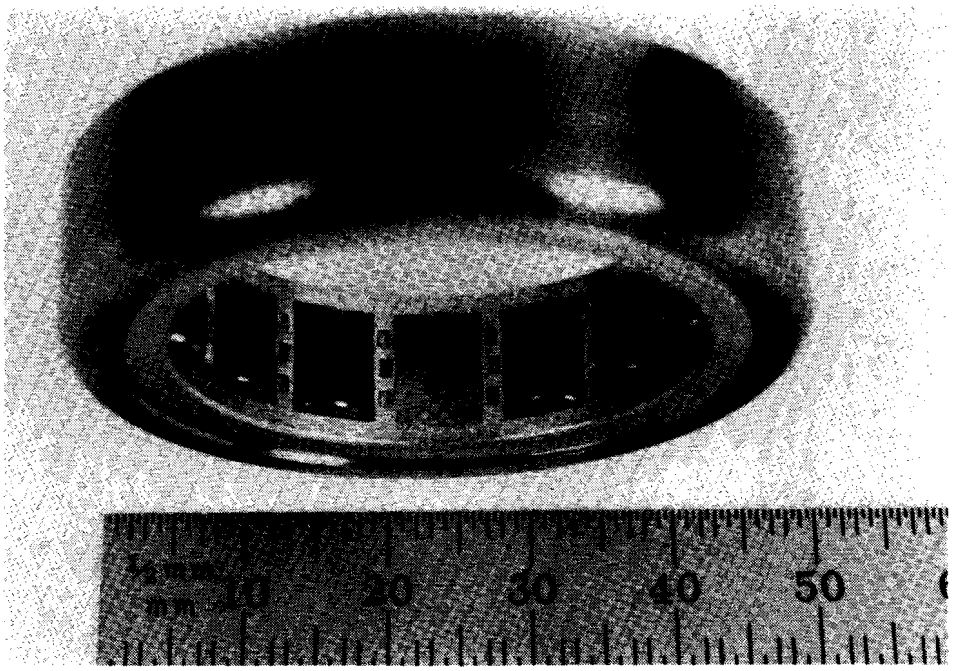

Figure C-54. 90-Degree Gearbox -411 Bearing Outer Race C/D Fault, Runs 11A + 11B

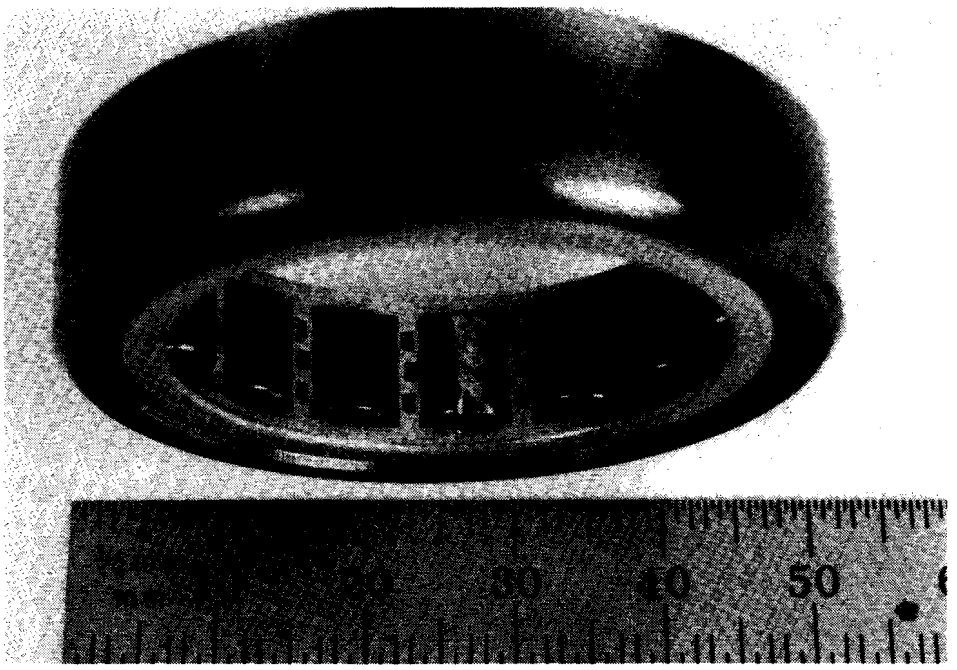

Figure C-55. 90-Degree Gearbox -411 Bearing Roller C/D Fault, Runs 13A + 13B

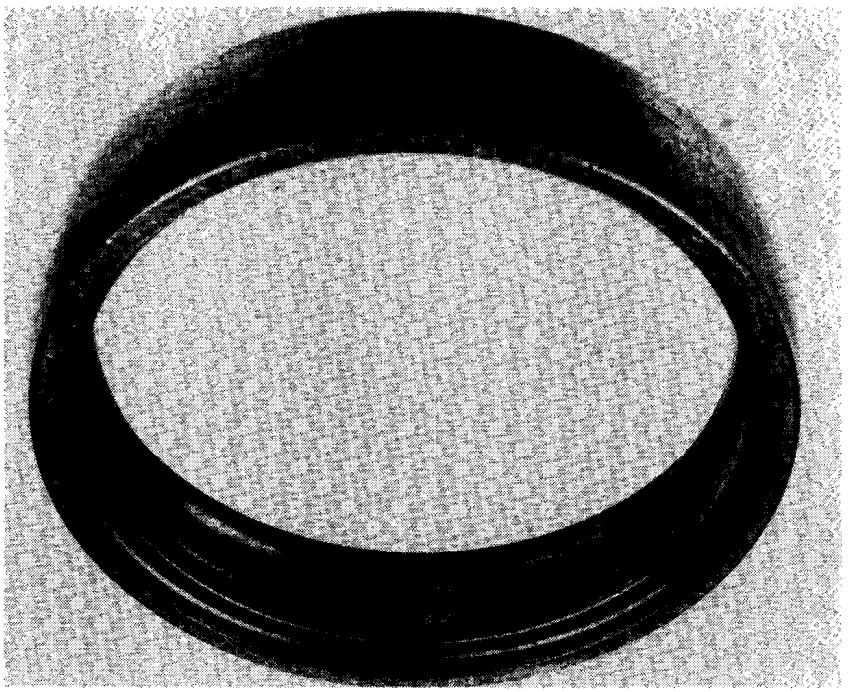

Figure C-56. Typical -339-9 Hanger BRG Outer Race C/D Fault

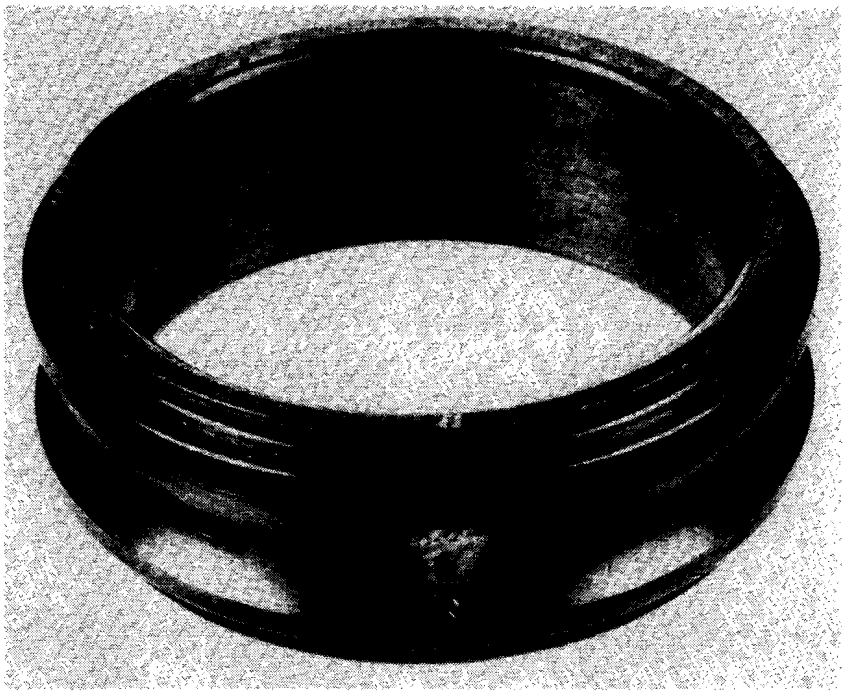

Figure C-57. Typical -339-9 Hanger BRG Inner Race C/D Fault

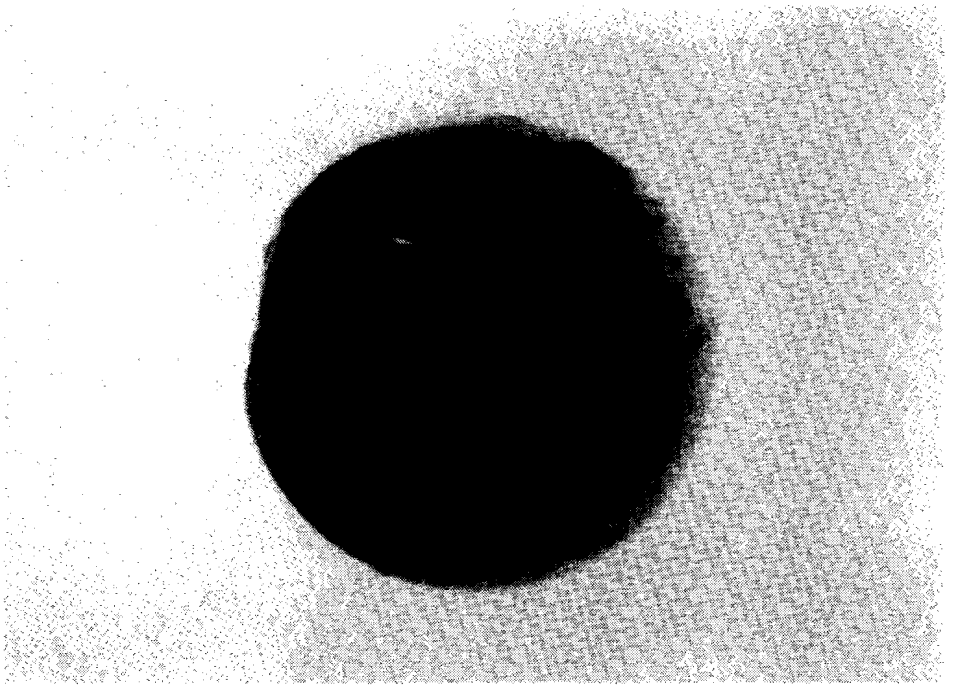

Figure C-58. Typical -399-9 Hanger BRG Ball C/D Fault

TABLE C-5. NOMINAL AIRCRAFT SIGNATURES RECORDED, FT. RUCKER, NOVEMBER 1982

Aircraft Type	Tail Number	90° Gearbox						42° Gearbox						Hanger Bearing				
		Input			Output			Input			Output							
		Axial	Radial	Tang	Axial	Radial	Tang	Axial	Radial	Tang	Axial	Radial	Tang	#1	#2	#3	#4	#8
AH-1S	22573	X	X	X	X	X	X	X	X	X	X	X	X	X				
AH-1S	15339	X	X	X	X	X	X	X	X	X	X	X	X		X			
AH-1S mod	22576	X	X		X	X	X	X	X	X	X	X	X			X		
UH-1H	21574	X	X	X	X	X	X	X	X	X	X	X	X		X			
UH-1H	60850	X	X	X	X	X	X	X	X	X	X	X	X			X		
UH-1H	16330		X	X	X	X	X	X	X	X	X	X	X				X	
OH-58A	16173	X	X	X	X	X	X											X
OH-58A	16954	X	X	X	X	X	X											X
OH-58A	16096	X	X	X	X	X	X											X

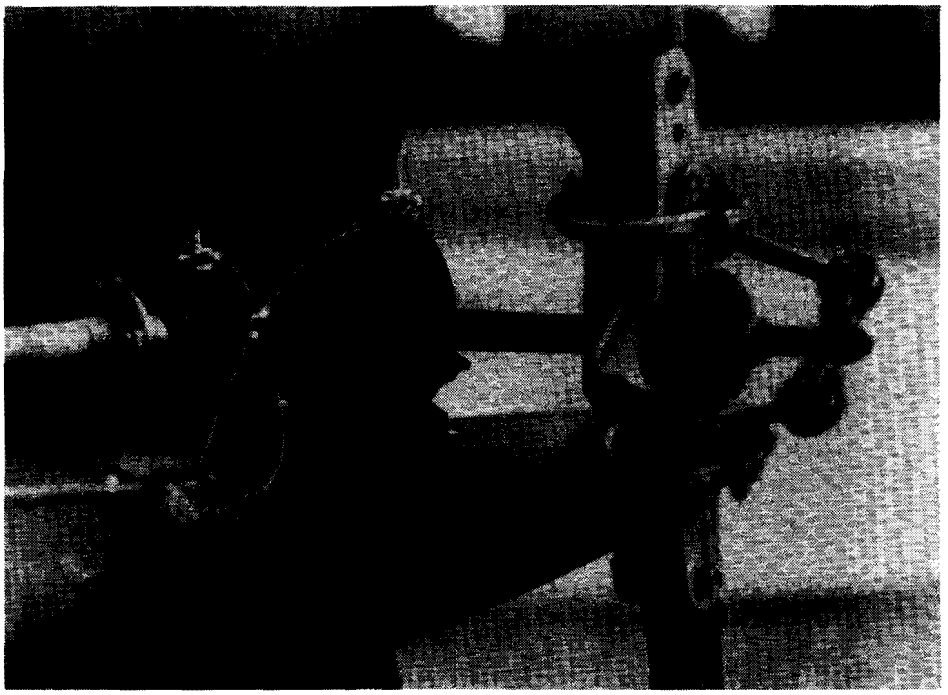

Figure C-59. Typical Accelerometer Mounting on OH-58 90-Degree Gearbox for Nominal Data Recording with Bonded and Bolted Mounts

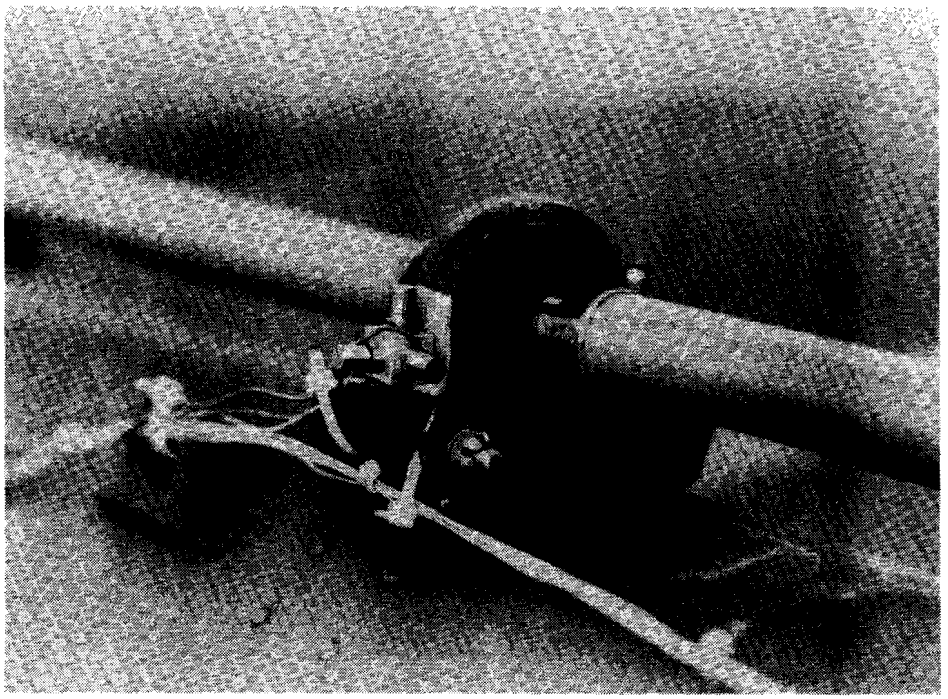

Figure C-60. Typical OH-58 Hanger Bearing Assembly with Bonded Triaxial Accelerometers

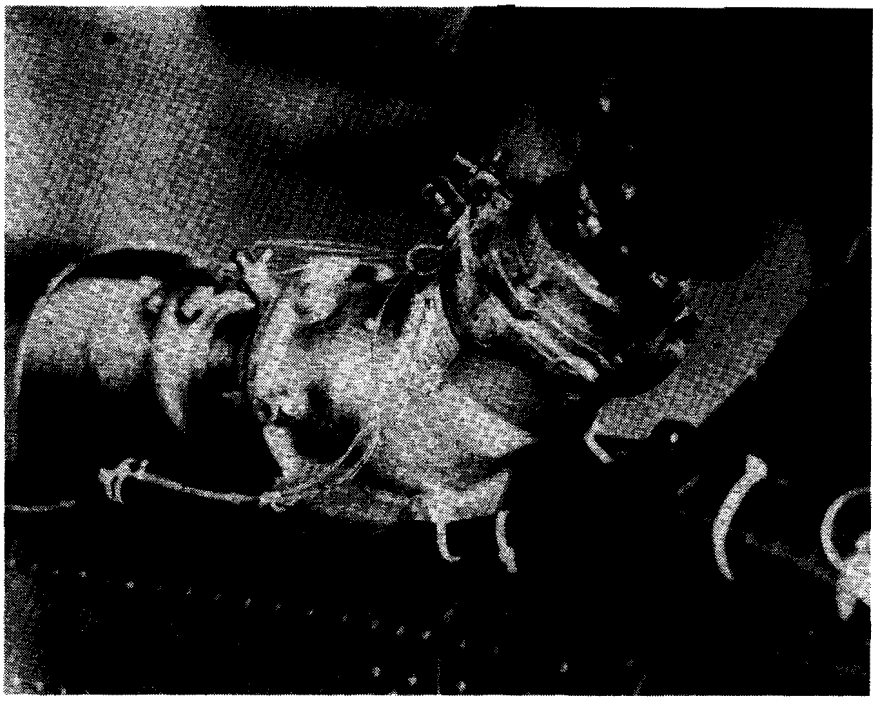

Figure C-61. Typical UH-1H 42-Degree Gearbox with Bolted-on Triaxial Accelerometers for Nominal Data Recording

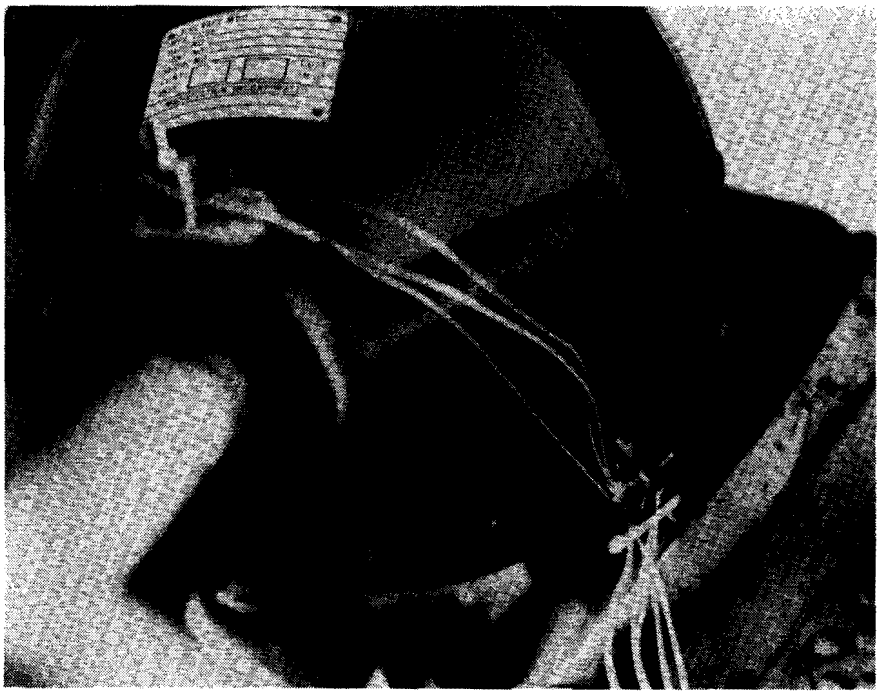

Figure C-62. Typical AH-1S 90-Degree Gearbox with Bolted and Bonded Triaxial Accelerometers for Data Recording

It became apparent during the program, particularly during Diagnostic Software Validation, that fault implant and baseline condition data was required from aircraft tests. A program was structured and a second trip was made to Fort Rucker for additional experimentation. During this trip data was collected on selected bearing implants which were installed on two AH-1S and one OH-58 aircraft. The analysis of the nominal aircraft data previously collected had raised several questions about the condition of the bearings on those aircraft at the time data was collected. It was decided that it was necessary to run gearboxes of known condition on actual aircraft in order to be completely certain of our diagnostic capabilities.

A sample of two Cobra 42-degree gearboxes, two Cobra 90-degree gearboxes, and two Cobra hanger bearing assemblies, all in precisely known condition, as well as the nominal gearboxes in use, were ground run on two Cobra aircraft. Earlier spectral data was available for one of these aircraft. Each of the 42-degree gearboxes contained a single bearing implant which had been evaluated at Bell Helicopter, while one of the Cobra 90-degree gearboxes contained a double fault, each implant of which had been evaluated singly at Bell Helicopter. The second Cobra 90-degree gearbox was fresh from overhaul at Corpus Christi, Texas and was known to be fault free by inspection.

The 90-degree gearbox for the OH-58 was also fresh from overhaul and was ground run on a single ship following data collection on the gearbox originally installed on the ship. That 90-degree gearbox was then faulted with two bearing implants, each of which had been run singly at RCA's test facility. Following data collection on the implanted gearbox, Northrop Worldwide Aircraft Services, Inc. (NWASI) personnel elected to remove for overhaul the original in service 90-degree gearbox due to a high usage time. Vibration data was also collected on the fresh gearbox on the aircraft. Table C-6 details the data recorded and Figures C-63 through C-67 are photographs of typical accelerometer installation on the aircraft.

TABLE C-6. ON-AIRCRAFT IMPLANT TESTING, FT. RUCKER, JULY 1983

Test Specimen	Test Specimen Condition	Aircraft Tested
AH-1S 90° Gearbox	Fresh from overhaul-No Faults	22573 & 23231
AH-1S 90° Gearbox	-450 Input pinion with C/D Spall at roller bearing inner race	22573 & 23231
	-466 Roller bearing on output with outer race C/D spall	
AH-1S 42° Gearbox	-143 Ball bearing on input with outer with outer race C/D spall	22573 & 23231
AH-1S 42° Gearbox	-210 roller bearing on input with with outer race C/D spall	22573 & 23231
AH-1S Hanger Assy.	-623 ball bearing with inner race C/D/ spall	22573 & 23231
OH-58 90° Gearbox	Fresh from overhaul - No Faults	15449
OH-58 90° Gearbox	Fresh from Overhaul - No Faults	15449
OH-58 90° Gearbox	-408 Ball Bearing on Input & with inner race C/D spall	15449
	- 411 Roller bearing on output with outer race C/D spall	

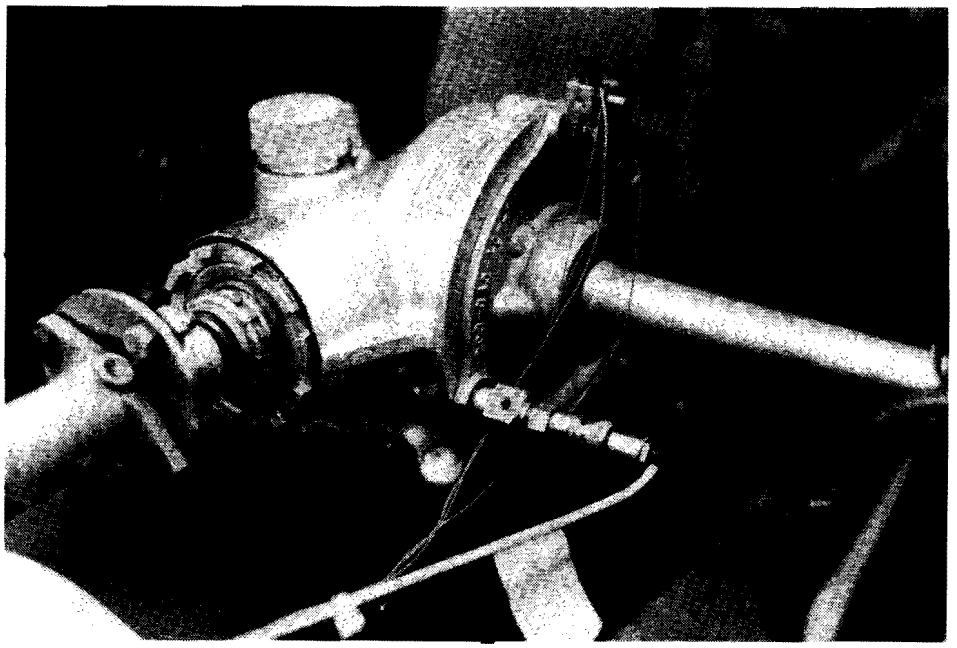

Figure C-63. Typical On-Aircraft Implant Test on OH-58 90-Degree Gearbox with Bolted-on Triaxial and Ruggedized Accelerometers

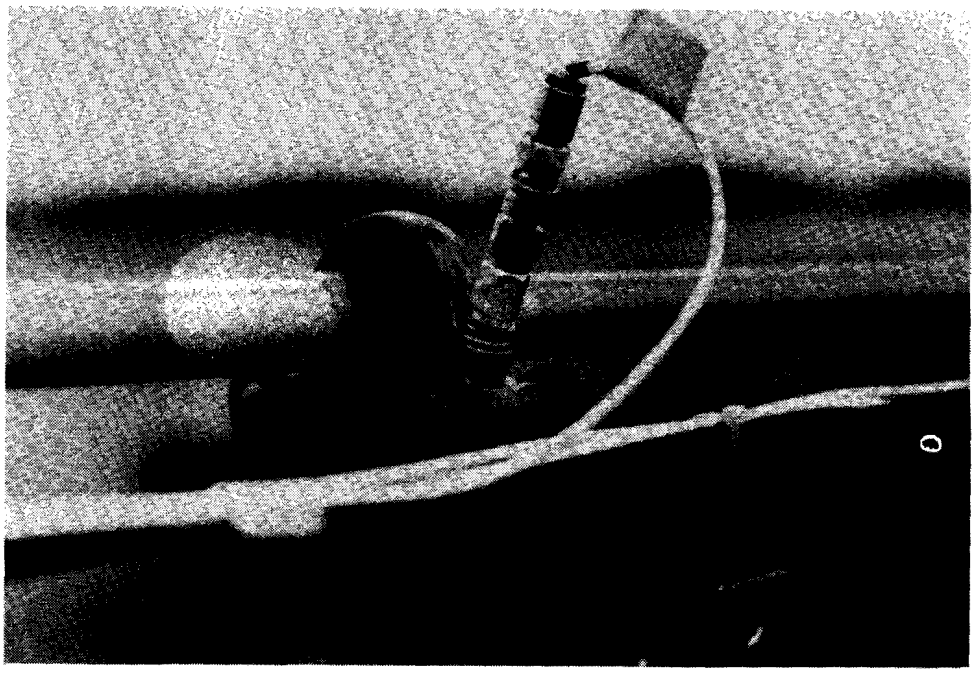

Figure C-64. Typical On-Aircraft Test of OH-58 Hanger Bearing with Bolted-on Ruggedized Accelerometer

Figure C-65. Typical On-Aircraft Implant Test on AH-1S 90-Degree Gearbox with Bolted-on Triaxial and Ruggedized Accelerometers

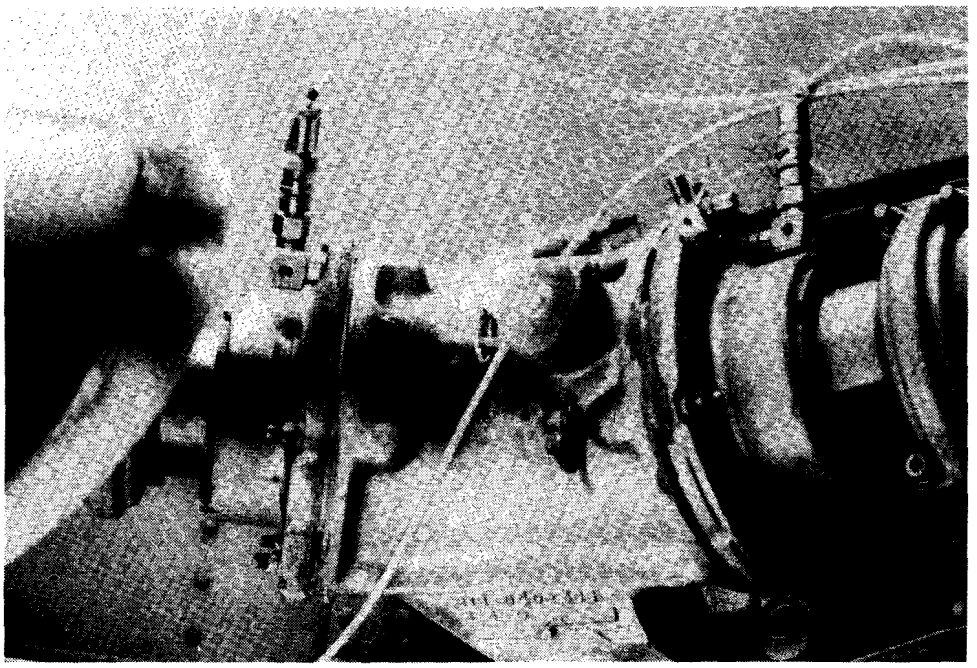

Figure C-66. Typical On-Aircraft Test of AH-1S 42-Degree Gearbox with Bolted-on Triaxial and Ruggedized Accelerometer

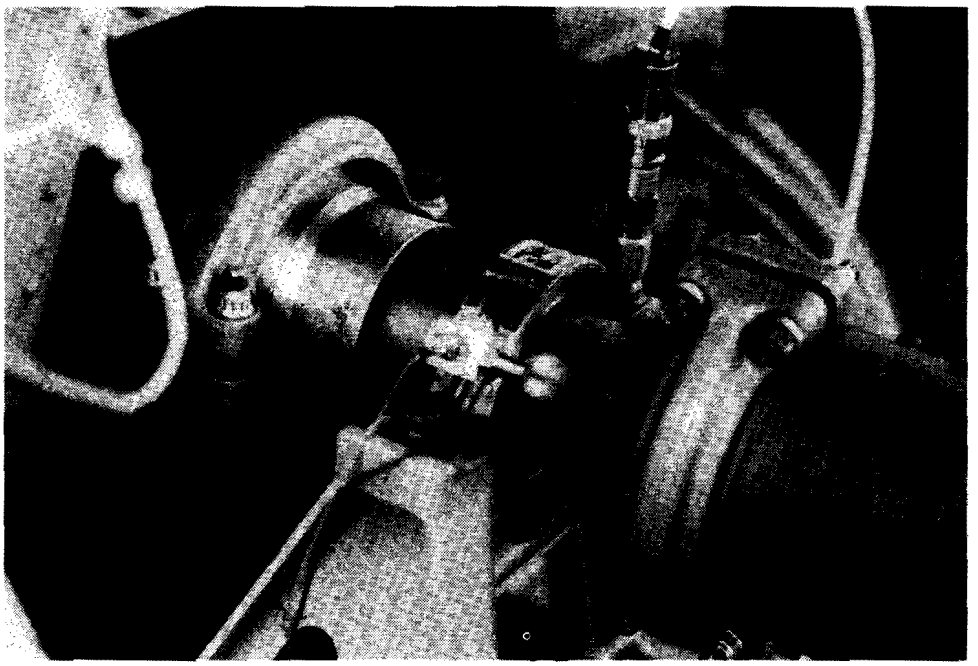

Figure C-67. Typical On-Aircraft Implant Test on AH-1S Hanger Bearing with Bonded Triaxial and Bolted Ruggedized Accelerometers

APPENDIX D
SPADE ELECTRICAL DESIGN

A block diagram of the SPADE analyzer electrical system is shown in Figure D-1. The analyzer-chassis, computer/memory board, display, clock display board and one of the power supplies are designs common with current Army Simplified Test Equipment (STE) production hardware. Exclusive SPADE designs include the Multiplexer/Adcon printed wiring board, the signal processing printed wiring board and the auxiliary power supply.

Figure D-2 shows the detailed block diagrams of the signal processing system. The high speed components such as the A/D converter, D/A converter and the TMS320 signal processors have high power consumption compared to the components of the Army STE production hardware. The auxiliary power supply was added to meet this increased power requirement.

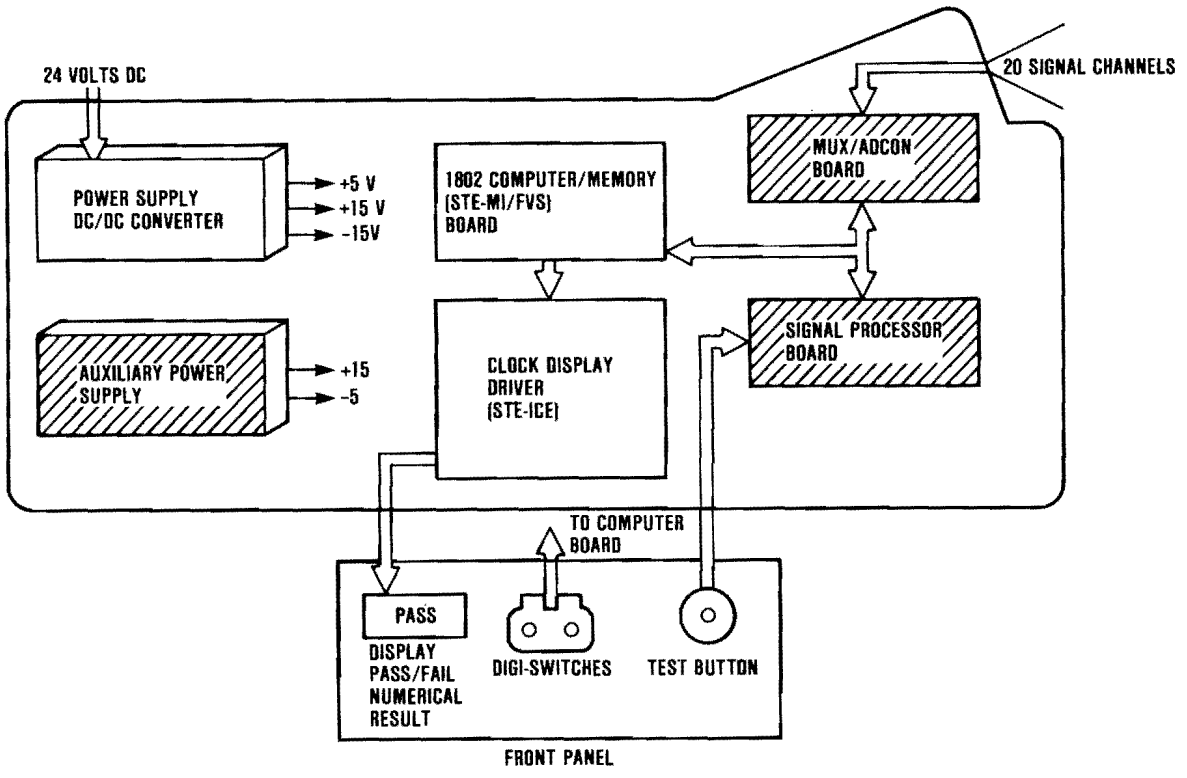

Figure D-1. SPADE Analyzer Electrical Block Diagram

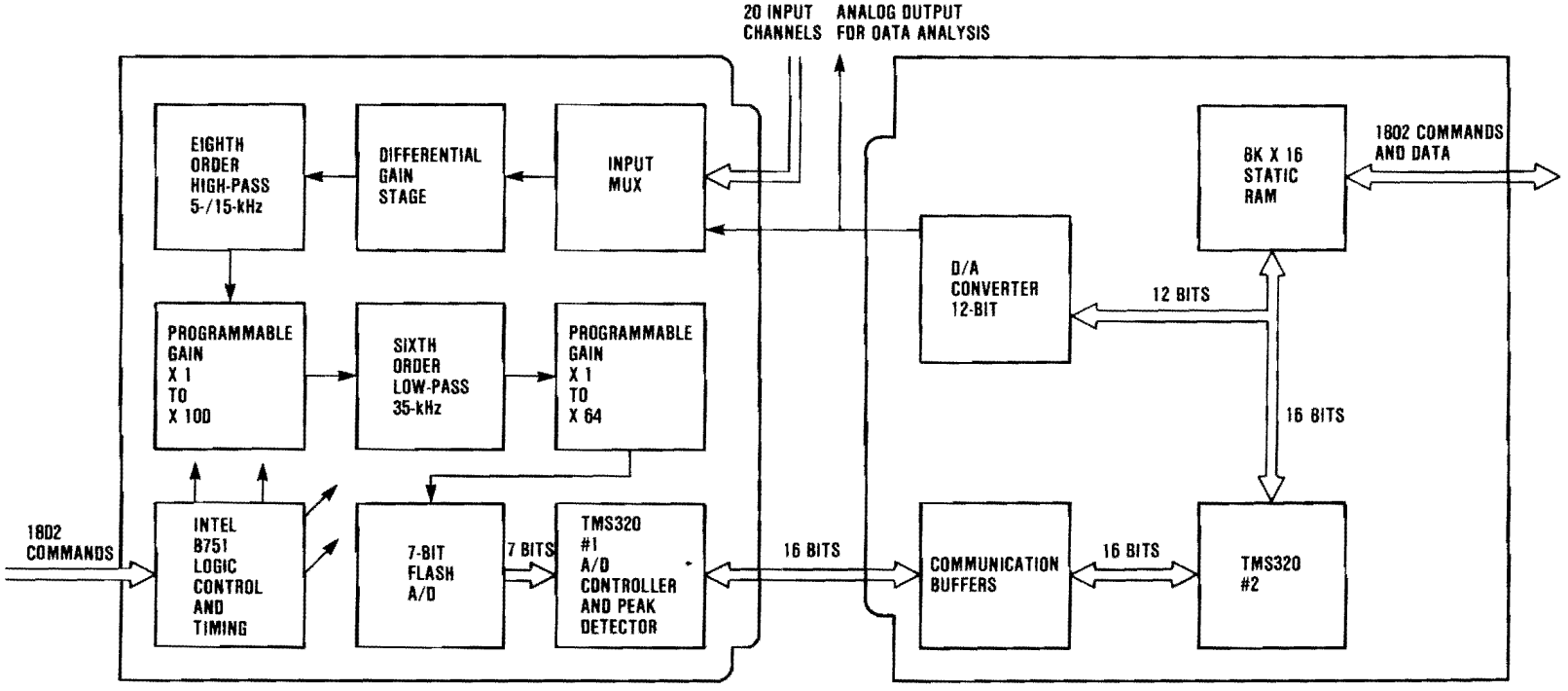

Figure D-2. SPADE Analyzer Signal Processing Block Diagram

Transducer signals are routed through a multiplexer where one signal is selected and routed to a differential amplifier. The amplifier output drives a chain of filters and programmable gain stages, where the signal amplification is automatically adjusted to a proper operating level by a resident computer program. The signals are then sampled by a seven-bit flash A/D converter which is controlled by a TMS320 microprocessor. The TMS320 then performs some signal processing on the data before the data is transferred to the second TMS320 for the execution of the remaining SPADE signal processing algorithms. The results of the signal processing algorithms can then be output through a D/A converter for engineering evaluation, or passed on to the 1802 computer for pass/fail decision making.

APPENDIX E
SELF TEST

E.1 INTRODUCTION

The SPADE system contains four microcomputers interconnected with analog processing as shown in Figure E-1. Data from the accelerometers is multiplexed, filtered, and converted to digital signals prior to processing by the two TMS320 microcomputers. Clocks, control signals and interrupts are generated by the 8751 microcomputer. The 1802 microcomputer serves as master controller. The self-test sequence is shown in Figure E-2. The 1802 first tests its program memory, random access memory, and dual port memory. The 8751 is then instructed to test its clock generators. Next, the two TMS320s are instructed to self test. Finally, a test signal is routed through various multiplexer, filter, and gain paths to test the analog processing and the A/D converter.

E.2 1802 SELF TEST

The 1802 first verifies its program memory (PROM) by computing a checksum and comparing it to the recorded checksum. The checksum is an eight-bit number computed by successively adding the contents of each memory location and truncating the result to eight bits. The 1802 then tests its slow RAM using the byte pattern and address pattern tests shown in Figures E-3a and E-3b. The byte pattern test detects bad memory locations by writing a one to each bit location in turn while zeroing the remaining bits. The address pattern test detects address errors (such as stuck or shorted address lines) that causes data to be written to more than one address at a time. The test writes a unique pattern of bits to each byte in each page of memory. The patterns are then recomputed and compared to those read back from memory. After these memory tests are completed, the 1802 itself can also be assumed functional since the tests exercise most of the 1802's internal registers and data paths.

E.3 8751 SELF TEST

The two major functions of the 8751 are to generate the sample and interrupt clocks and to generate the control signals for the analog multiplexers, gain stages, and filters. The 8751 self test verifies the clock generation function. The control signals will be assumed correct if analog processor self test is passed. The 8751 clock generators are actually self reloading timers. The self test loads each timer in turn with a test value and compares the response time to the 1802's internal clock. This tests the 8751 and 1802 clocks against each other.

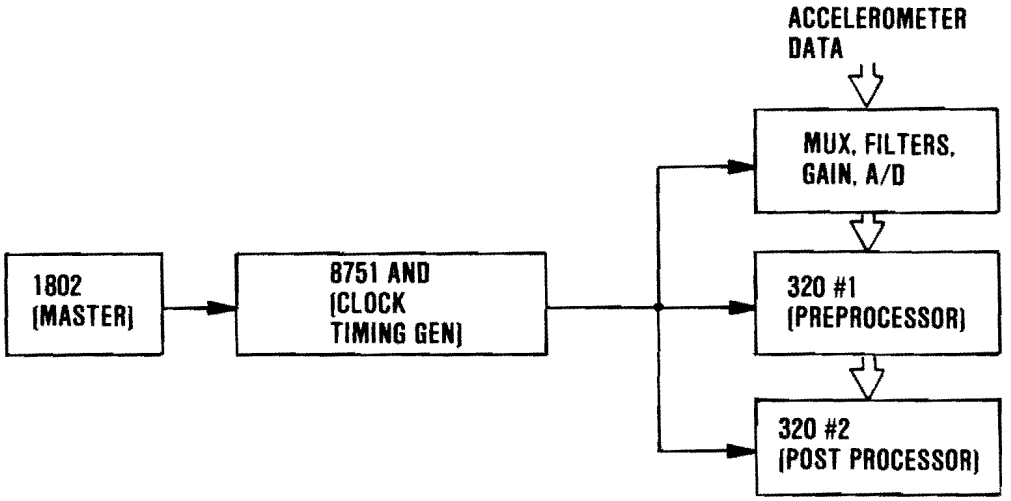

Figure E-1. SPADE System

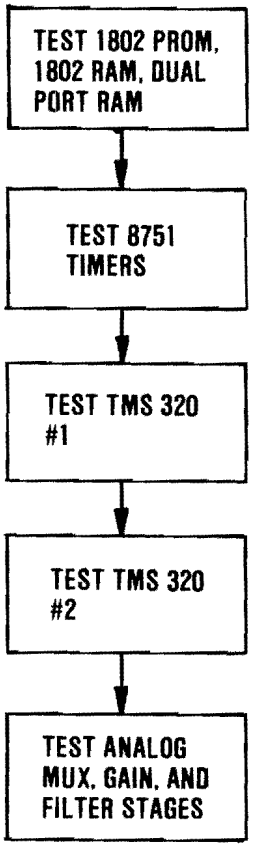

Figure E-2. SPADE Self-Test Top Level

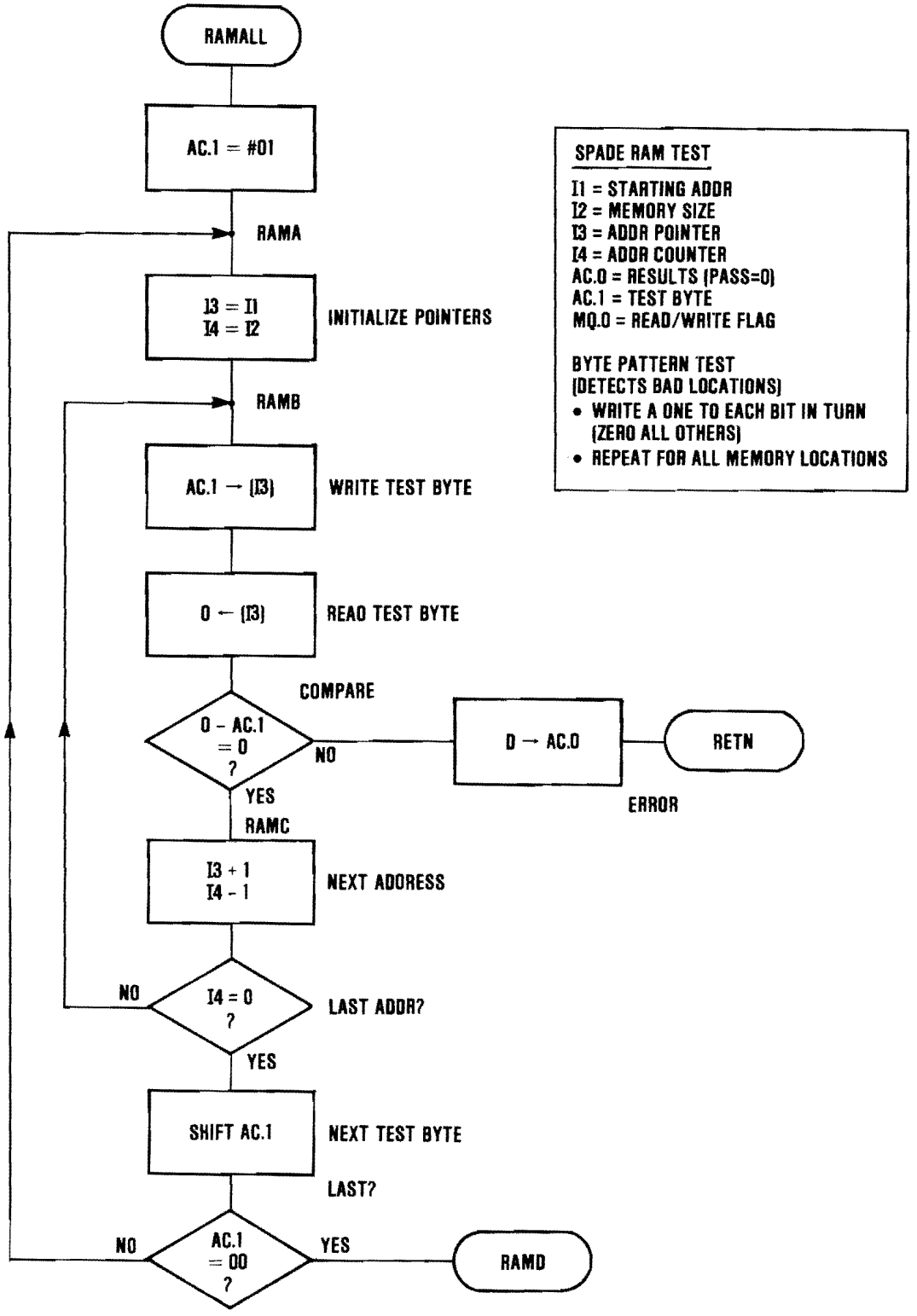

Figure E-3. SPADE RAM Test

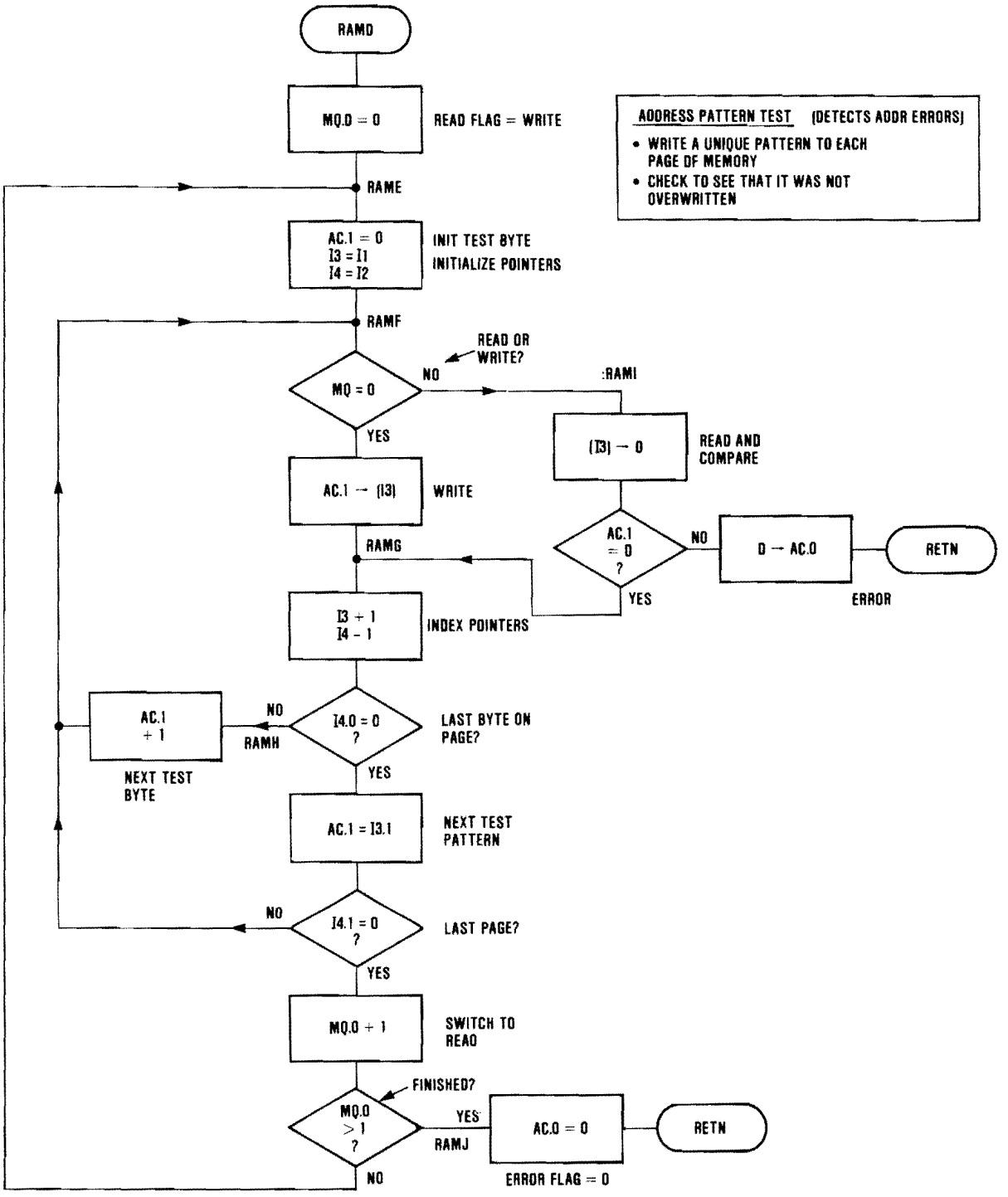

Figure E-3. SPADE RAM Test (Cont.)

E.4 TMS320 SELF TEST

The TMS320 #1 and TMS320 #2 self tests are outlined in Figure E-4. The test for TMS320 #1 begins with a PROM checksum test similar to the 1802 PROM test. The checksum is stored at the top of memory (location OFFF). The TMS320's internal RAM (data memory) is then tested for bit and address errors. These tests are also modeled on the 1802 RAM tests. The arithmetic test uses the shifter and adder as a multiplier and compares the results to the TMS320's on-chip multiplier.

The test for TMS320 #2 is identical to the TMS320 #1 test with two exceptions. The PROM test is replaced by a two-port RAM test and a bit reverse port test is added. The two-port RAM was already tested from the 1802 port. It is now tested for bit and address errors from the TMS320 port. The Bit Reverse port is tested by comparing four patterns to expected responses. Detail flowcharts for the TMS320 self tests are shown in Figures E-5a and E-5b.

E.5 ANALOG PROCESSOR TESTS

The analog multiplexers, gain stages, filters, and A/D converter are tested by applying signals from a D/A converter to predetermined signal paths and comparing the outputs to expected levels. These tests were coded and debugged for the original SPADE hardware but were not modified for the redesigned scientific demonstration hardware due to time limitations.

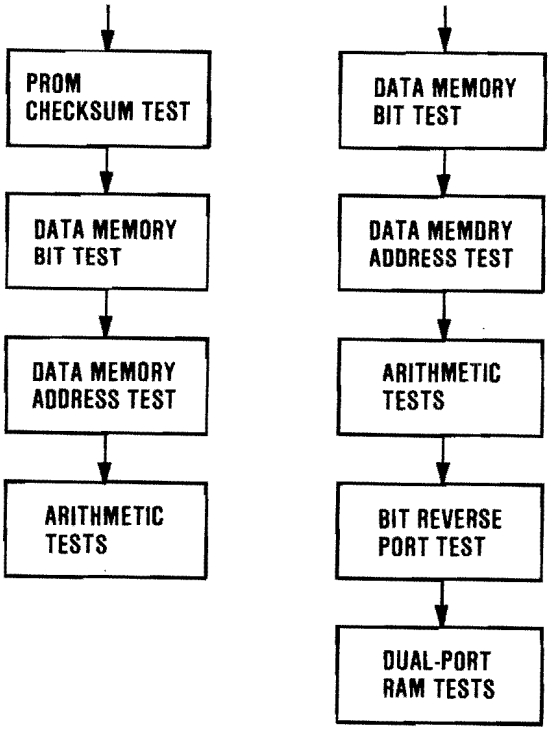

Figure E-4. TMS320 Self Test

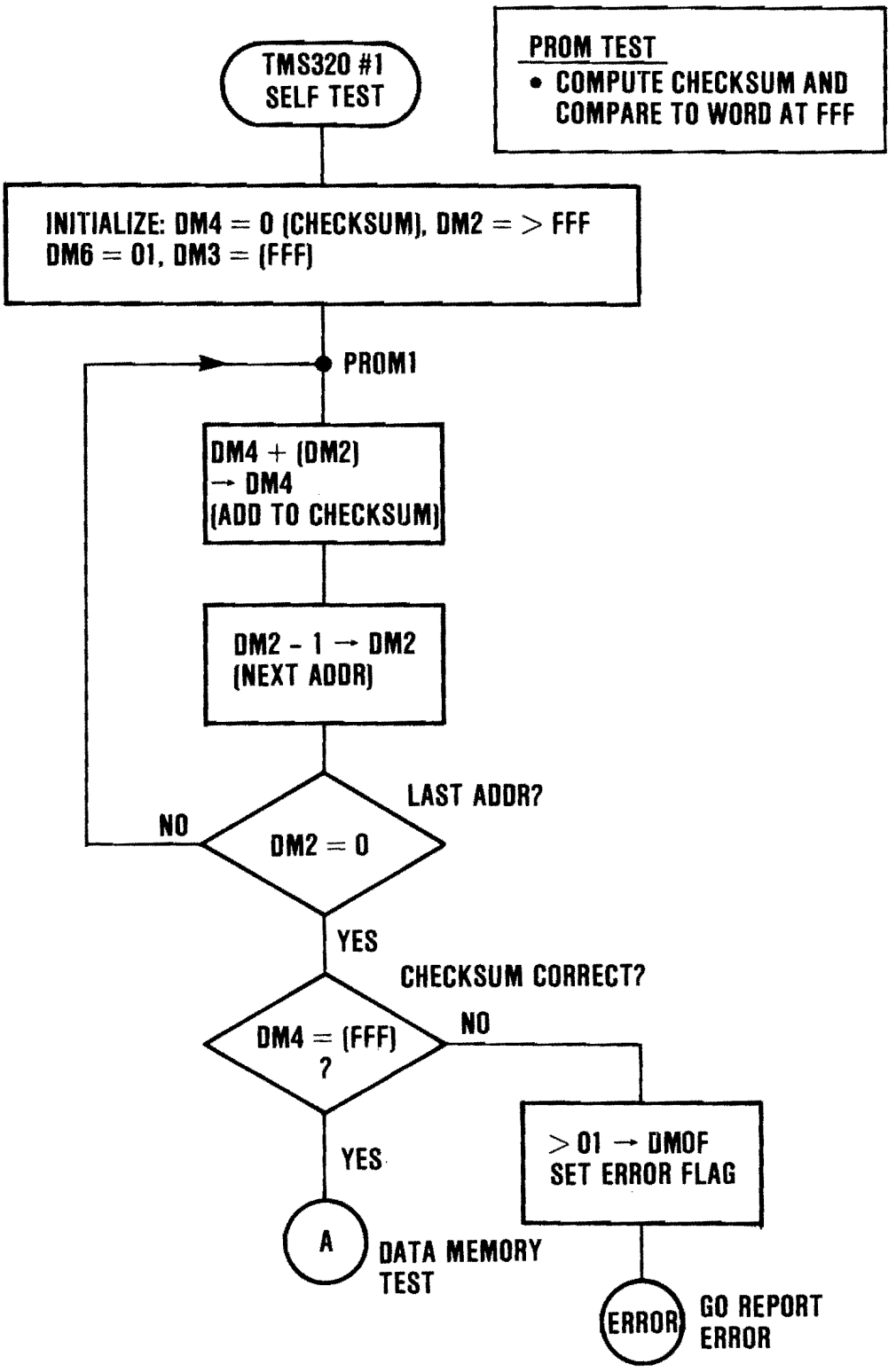

Figure E-5a. TMS320 #1 Self Test

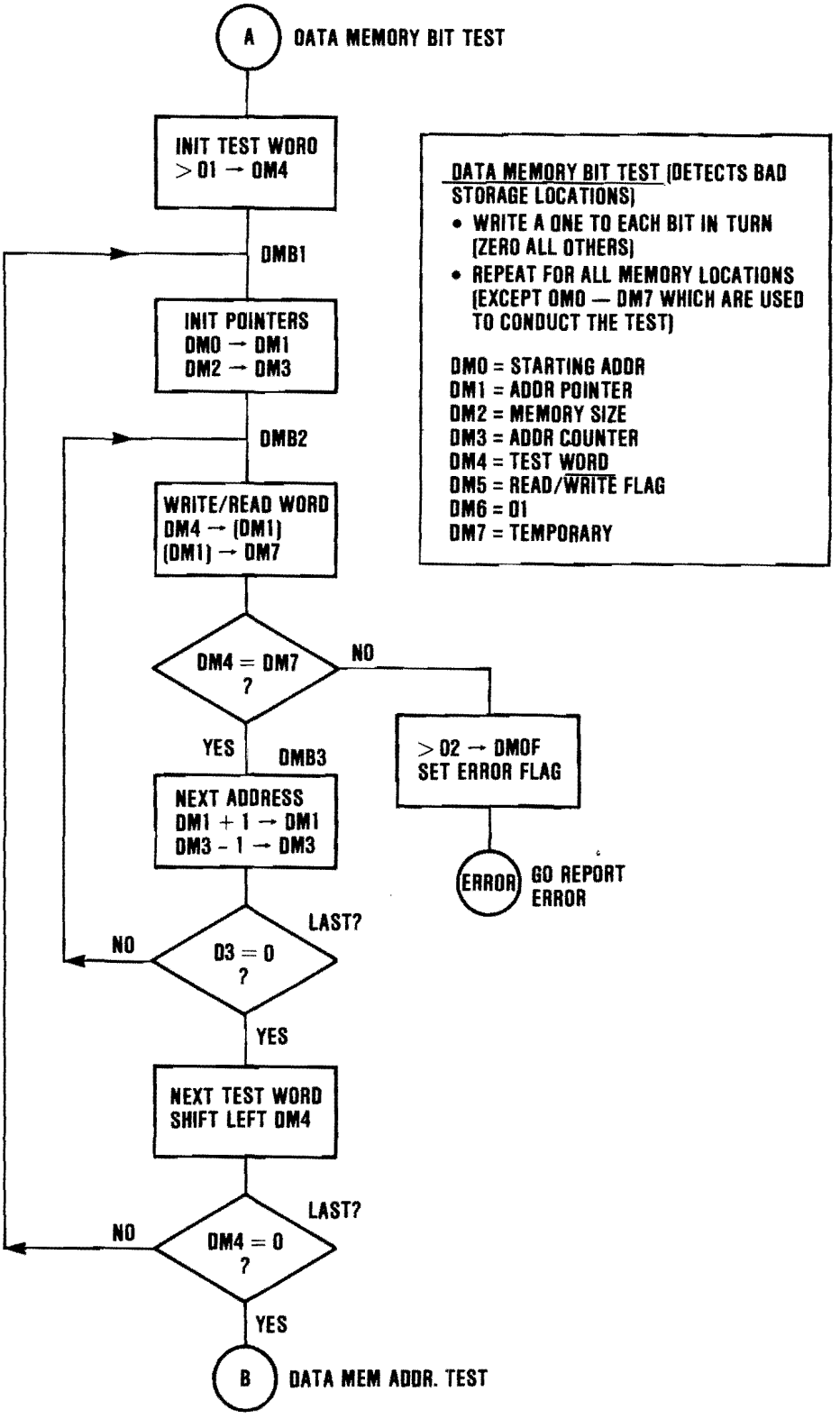

Figure E-5a. TMS320 #1 Self Test (Cont.)

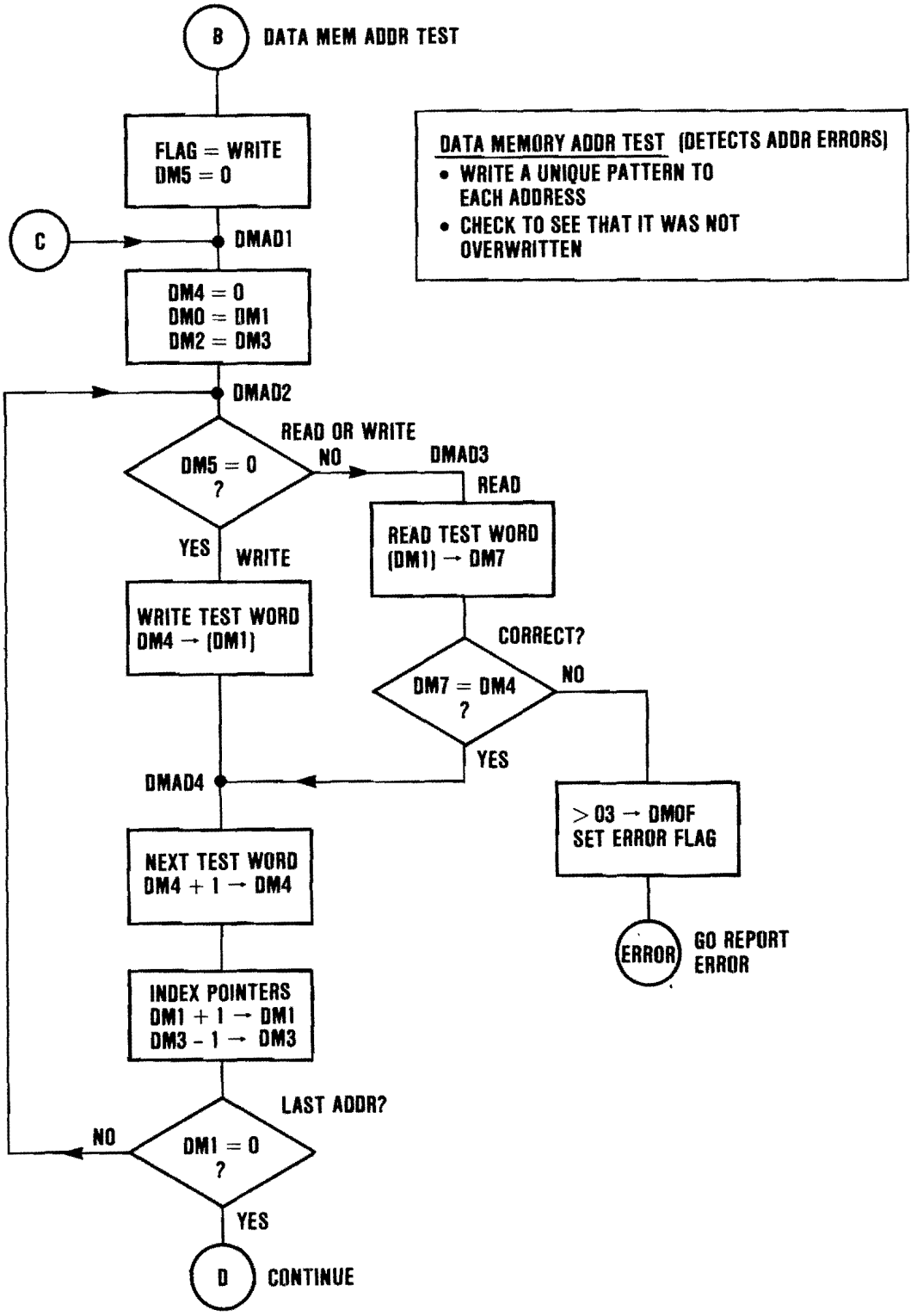

Figure E-5a. TMS320 #1 Self Test (Cont.)

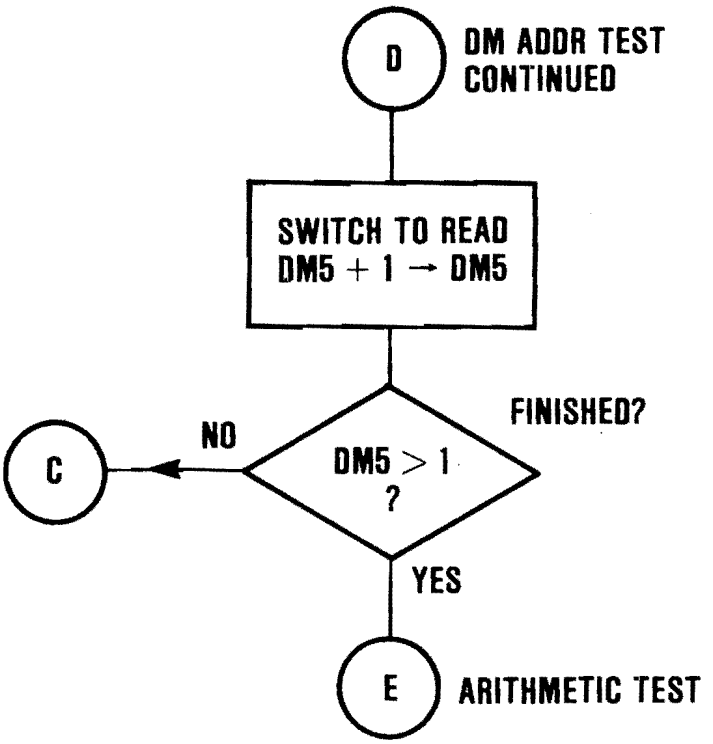

Figure E-5a. TMS320 #1 Self Test (Cont.)

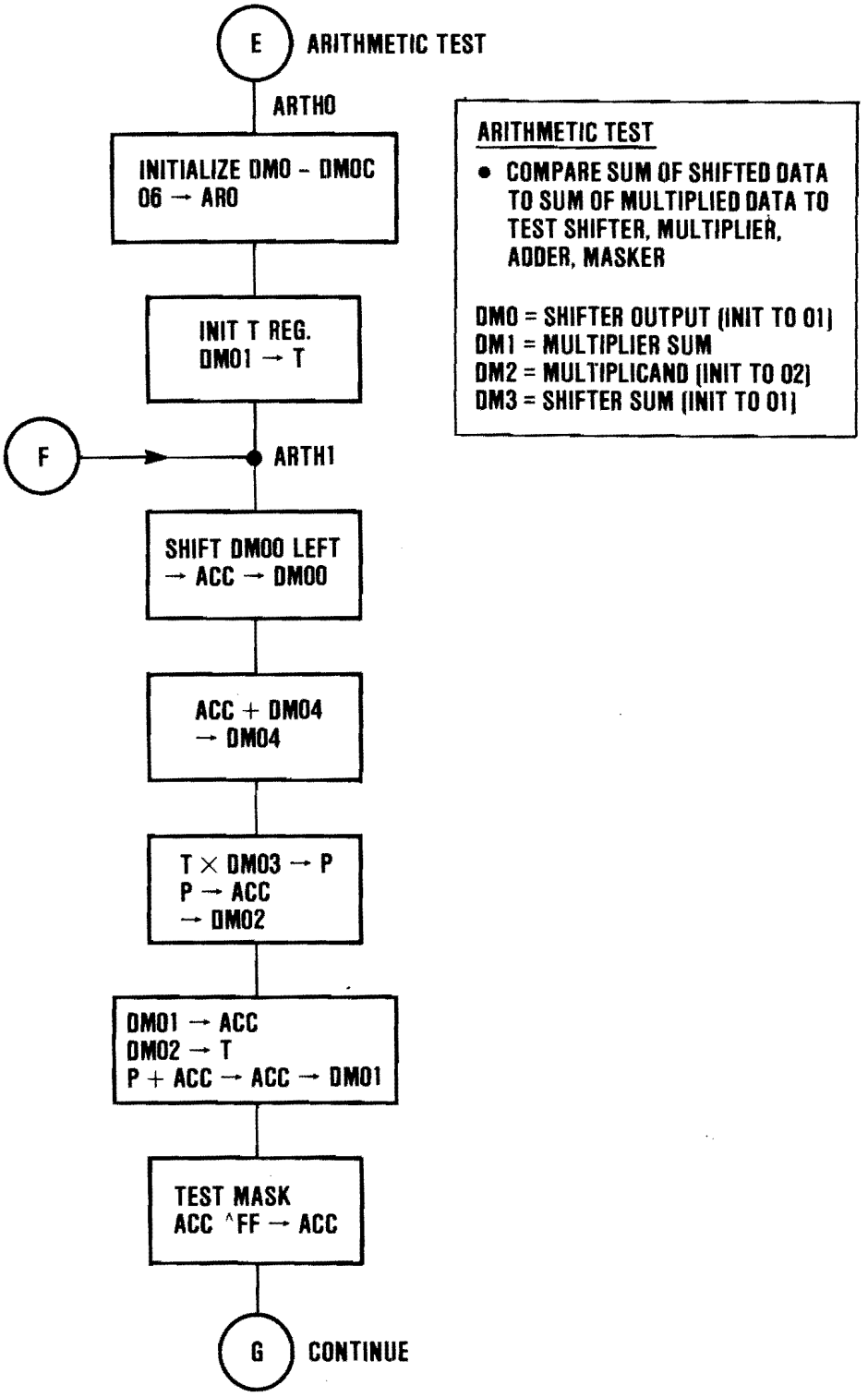

Figure E-5a. TMS320 #1 Self Test (Cont.)

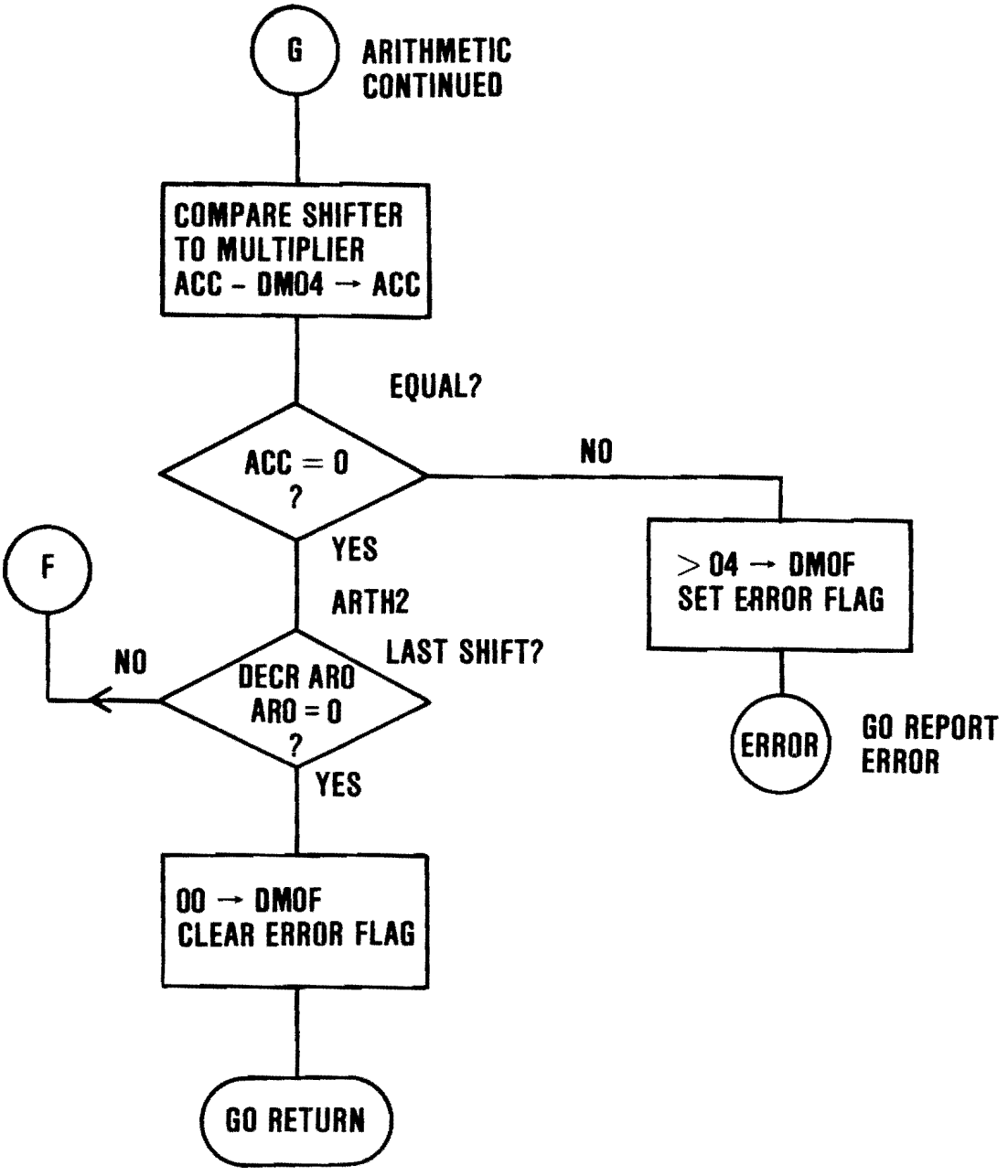

Figure E-5a. TMS320 #1 Self Test (Cont.)

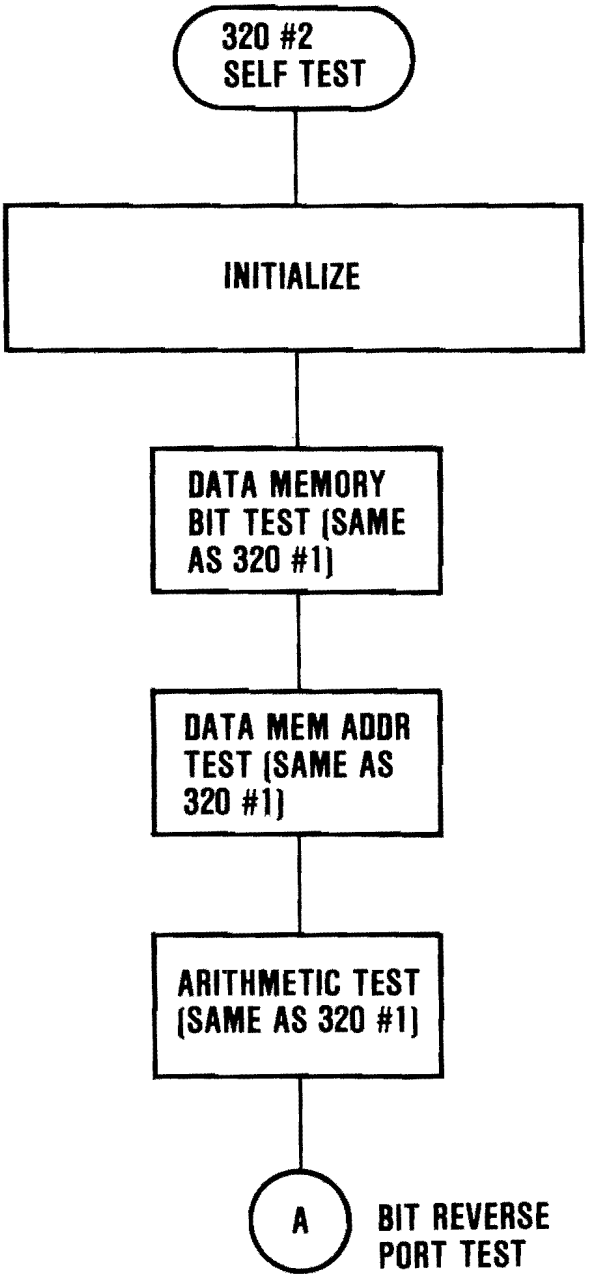

Figure E-5b. TMS320 #2 Self Test

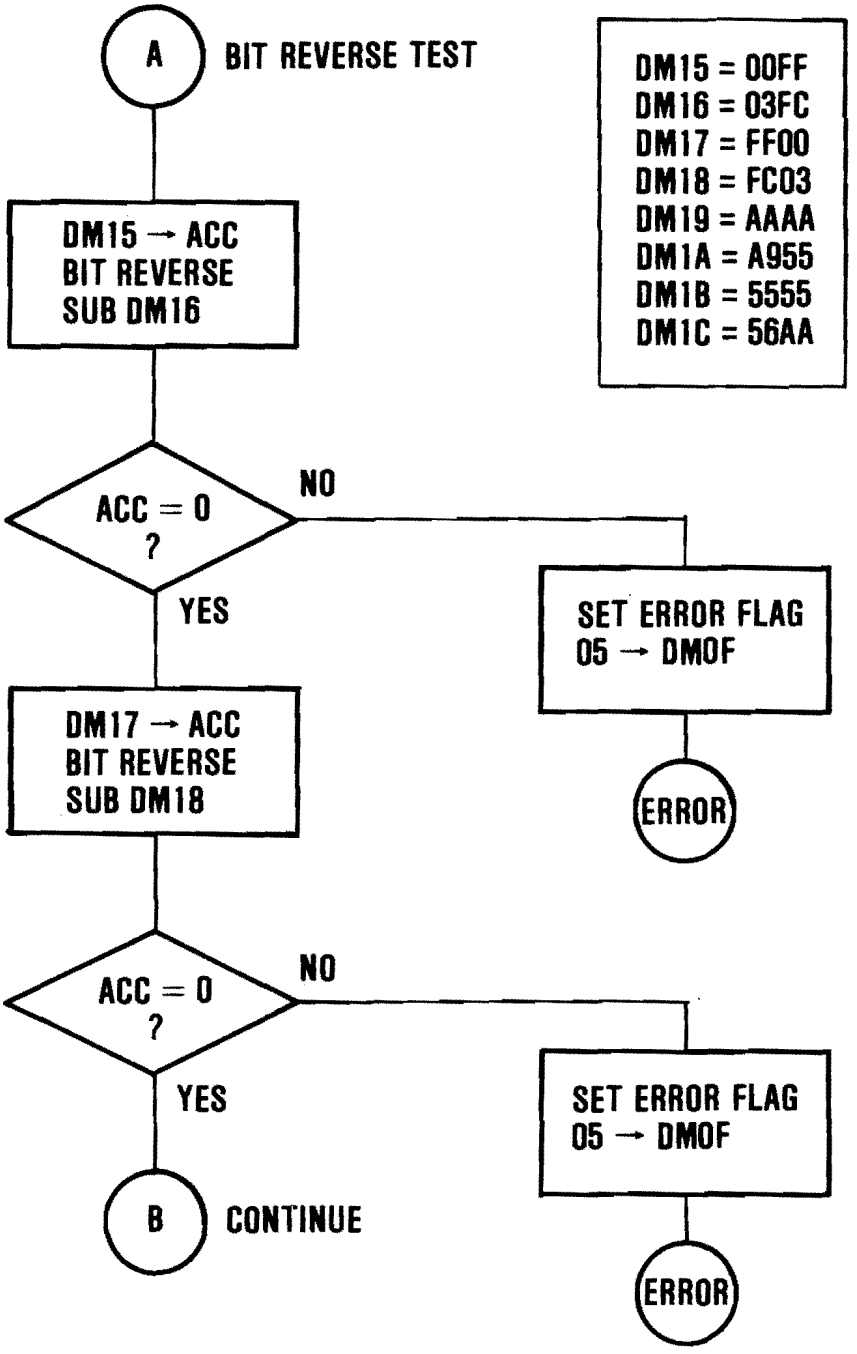

Figure E-5b. TMS320 #2 Self Test (Cont.)

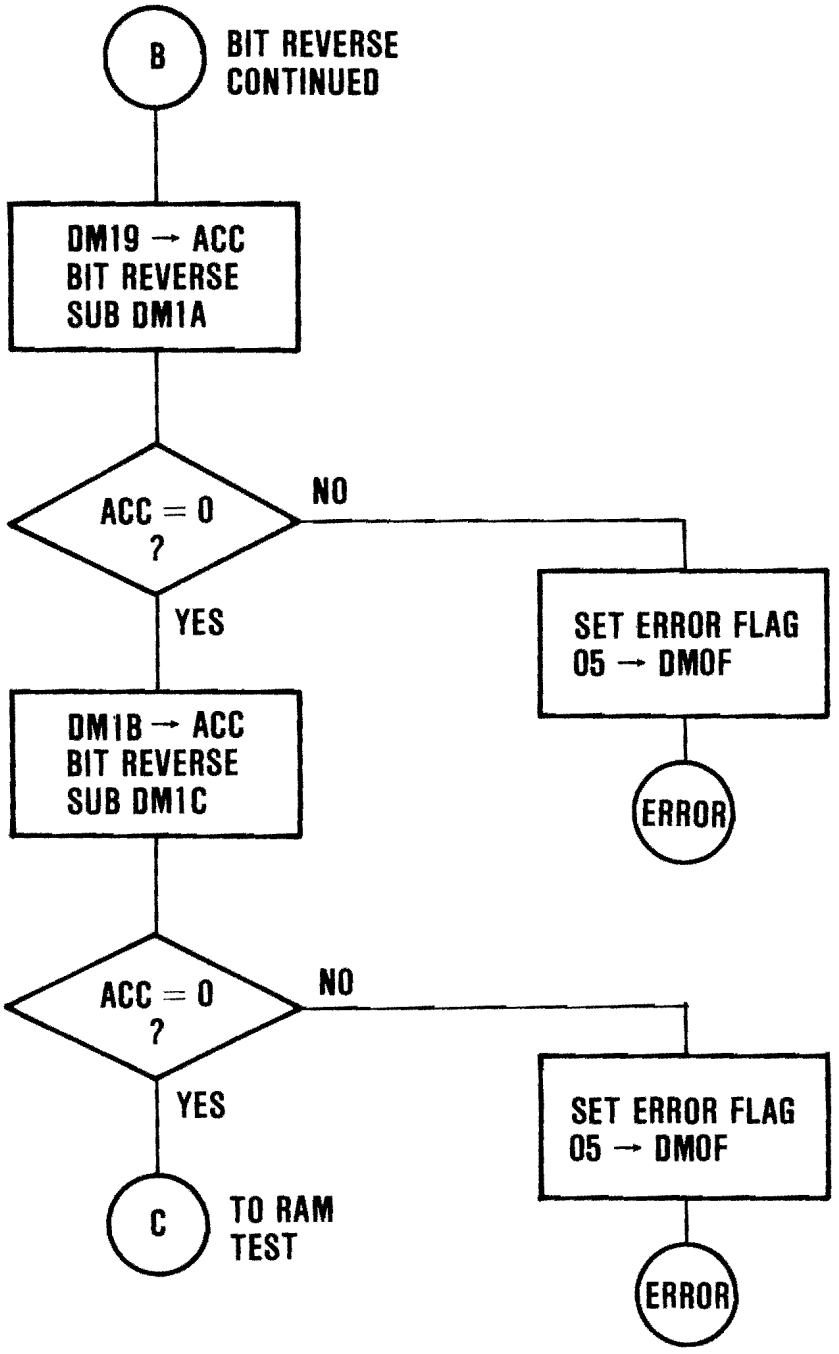

Figure E-5b. TMS320 #2 Self Test (Cont.)

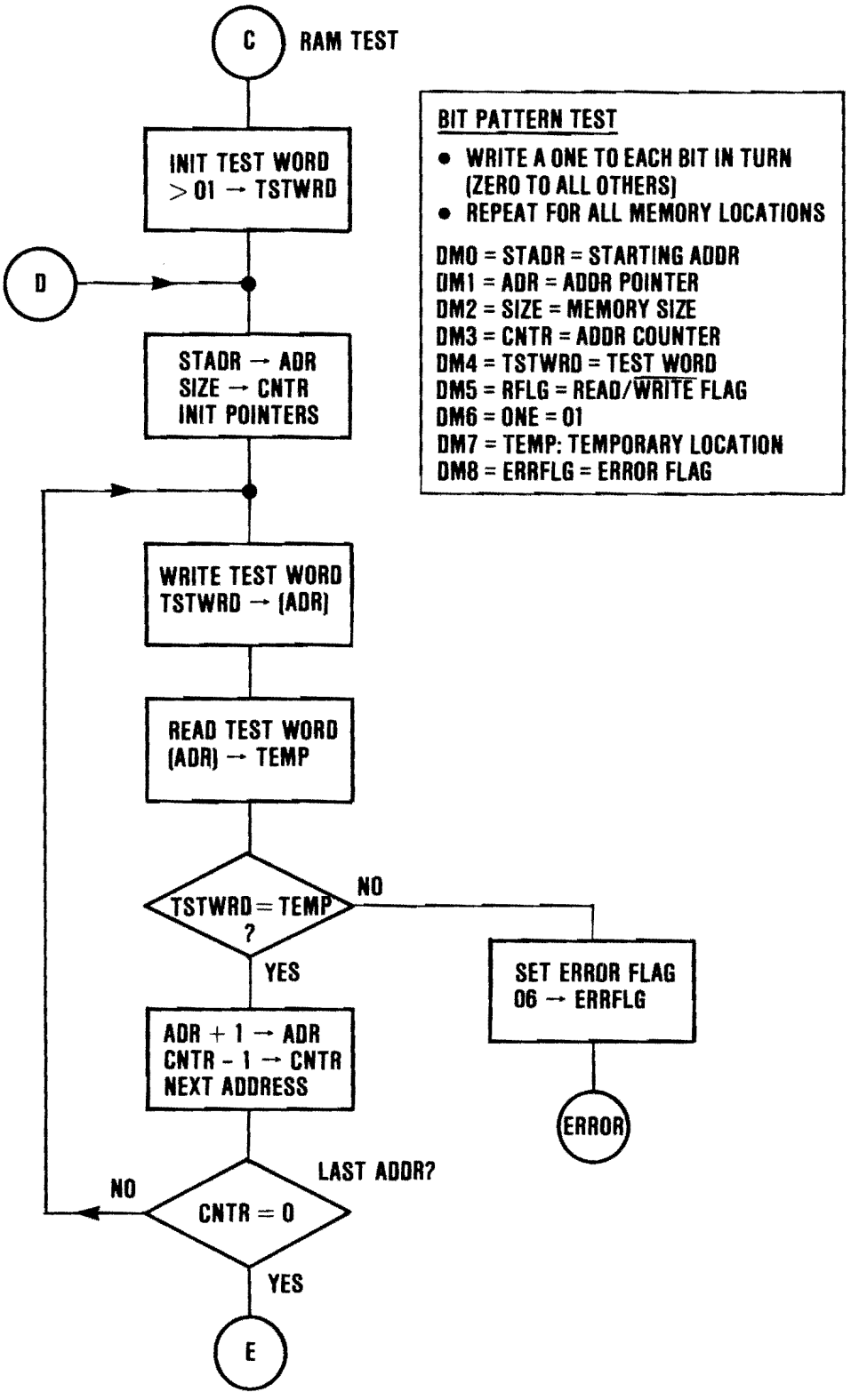

Figure E-5b. TMS320 #2 Self Test (Cont.)

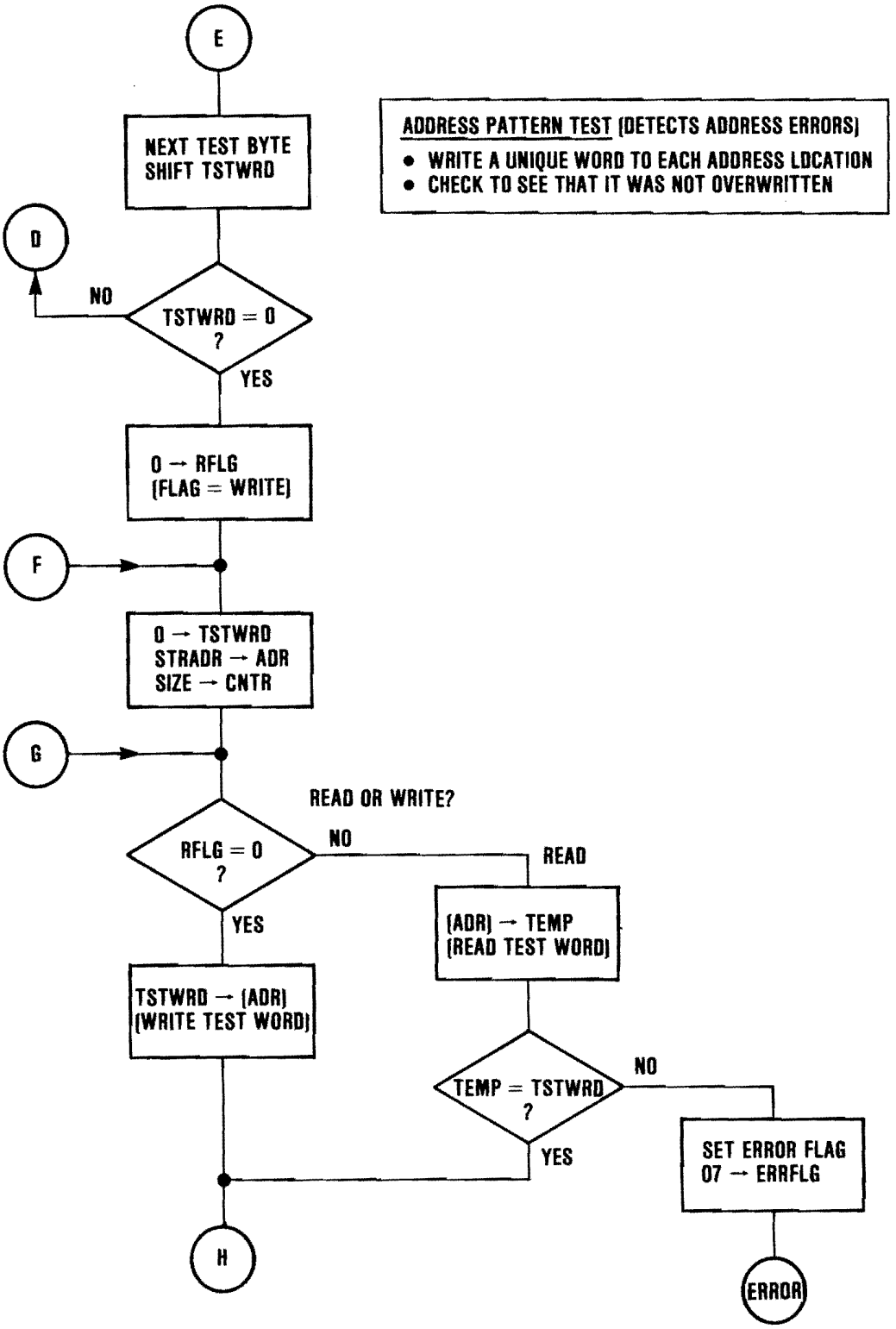

Figure E-5b. TMS320 #2 Self Test (Cont.)

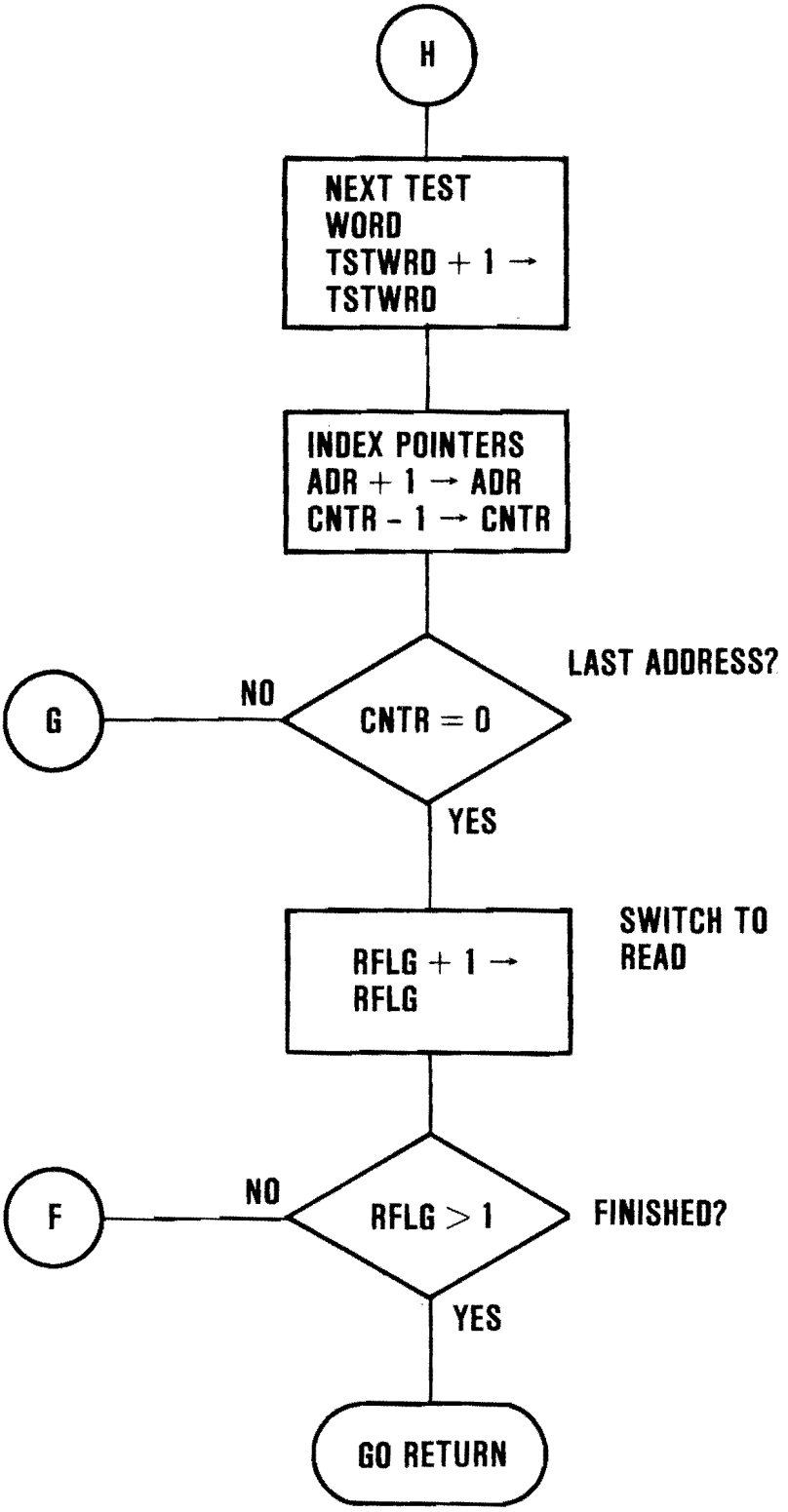

Figure E-5b. TMS320 #2 Self Test (Cont.)

APPENDIX F
NARROW-BAND ELLIPTICAL FILTER

For experimental purposes, a narrow-band sharp-cutoff filter was designed and added to the input of the SPADE processing hardware. Design goals for the filter were as follows:

Center Frequency	=	27 kHz
Lower Stop-band Frequency	=	20 kHz
Lower Pass-band Frequency	=	23 kHz
Upper Stop-band Frequency	=	35 kHz
Upper Pass-band Frequency	=	31.7 kHz
Pass-band Ripple	=	0.1 kHz
Minimum Stop-band Loss	=	60 dB

An elliptical filter of degree twelve was designed and realized to the configuration shown in Figure F-1. An elliptical filter was chosen because of its sharp cutoff properties with small ripple in the pass band (compared to Butterworth, Chebyshev, or inverse Chebyshev).

Figure F-2 shows the frequency response of the filter as computed by a circuit analysis program.

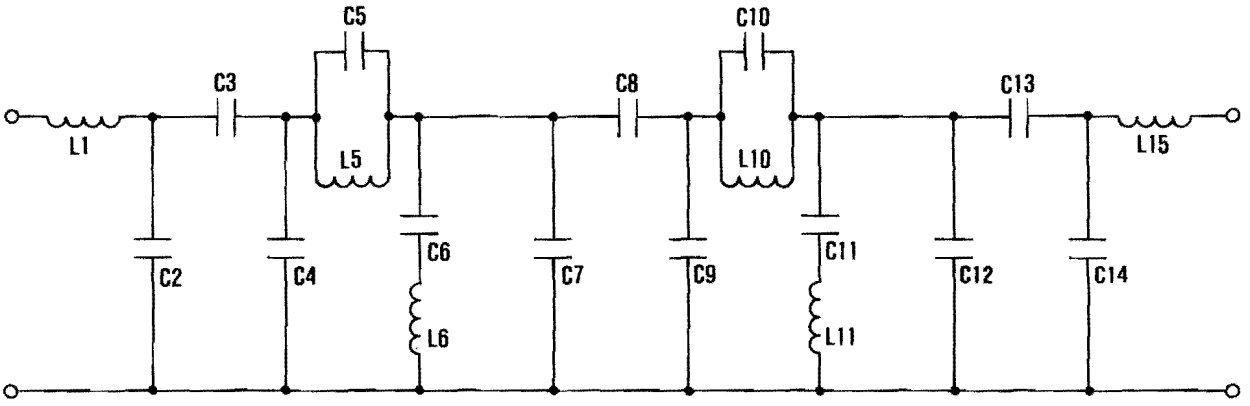

Figure F-1. 27 kHz Elliptical (Cauer) Bandpass Filter

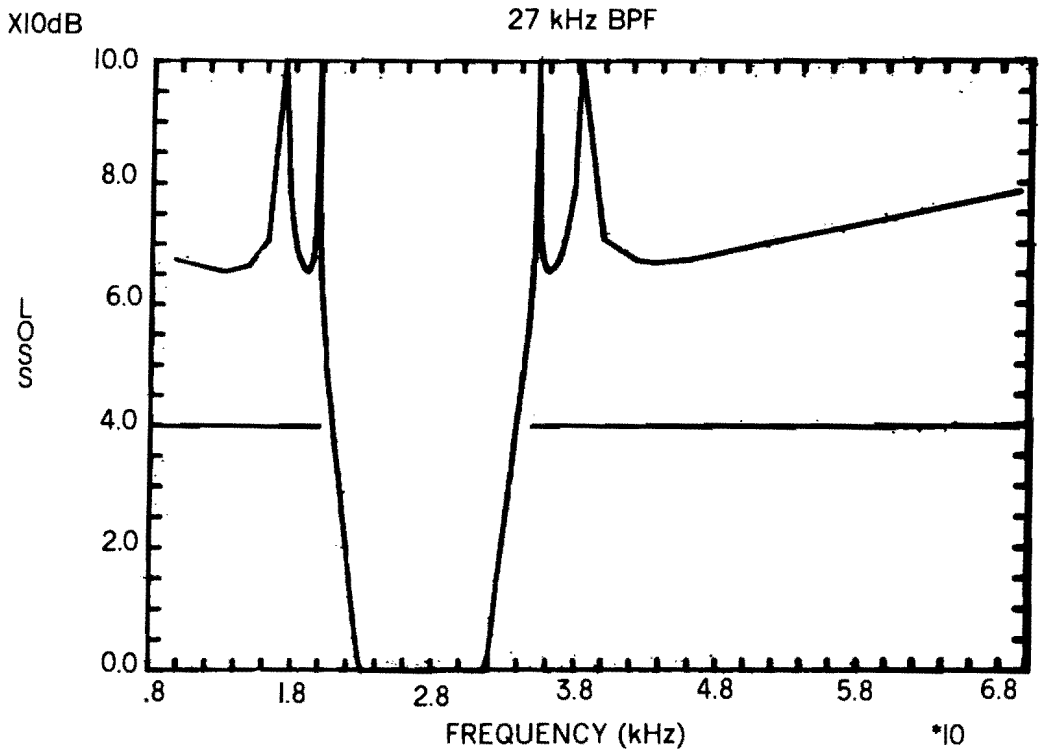

Figure F-2. Narrow-Band Filter Frequency Response

APPENDIX G
ZOOM FFT

The present frequency resolution of the FFT which is employed in the SPADE test set is 2 Hz. The architecture which is employed is not applicable to increasing the size of the FFT; however, there is a procedure which can be used to increase the frequency resolution. It is the zoom FFT. The zoom FFT is based upon the following principle.

A real valued signal

$$F(x) = A \cos(\theta t)$$

can be written as follows:

$$F(x) = A\,(e^{-i\theta e} + e^{i\theta e})$$

When the signal is multiplied by a signal equal to $b\, e^{-i\phi t}$, then

$$F(x) = A\,B(e^{-i(\theta-\phi)t} + e^{-(\theta+\phi)t})$$

The multiplication, which is a heterodyne approach, generates two frequencies. If θ is roughly equal to ϕ, and the appropriate low-pass filtering is done, then the frequency range around θ is translated down to around the zero frequency. This allows an FFT to be employed at a lower sampling frequency and hence greatly increased bandwidth.

The zoom FFT is implemented in the following manner in the SPADE system.

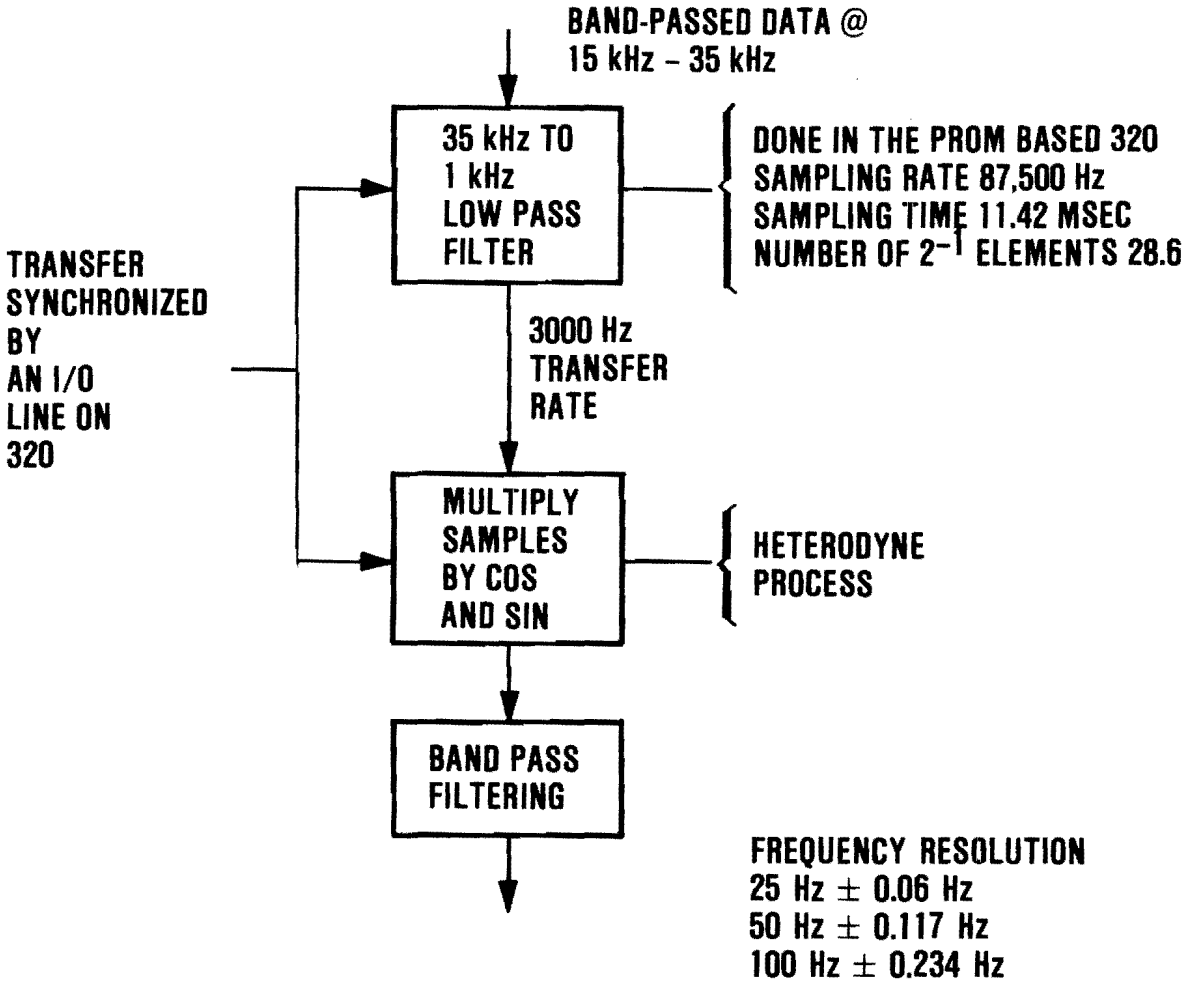

Figure G-1. Zoom FFT Implementation

APPENDIX H
ANALYSIS OF DETECTION AND FALSE ALARM PROBABILITIES

H.1 SIGNAL AND NOISE DISTRIBUTIONS

Figure H-1 shows the distributions of noise or clutter $[f_1(x)]$ and signal plus clutter $[f_2(x)]$. The curves shown are the probability densities of Gaussian or normally distributed random variables. The mean values of the two distributions are m_1 and m_2 respectively, and the variances are $(\sigma_1)^2$ and $(\sigma_2)^2$. The curves apply to any failure indication signal (and associated noise) that is obtained by linear operations on raw accelerometer data. Such operations include frequency filtering, Fourier transforms (especially FFT's), frequency windowing of the Fourier spectrum averaging, and integration.

It is assumed that m_1 is large compared to σ_1, the rms (root mean squared) value of the baseline amplitude variations.

Integrating the probability density curves between specified limits produces the probability that the signal plus clutter, or the clutter alone, lies between the limits. For example, if a threshold is chosen as shown in Figure H-1, the probability that the baseline clutter alone exceeds the threshold is the area under $f_1(x)$ from the threshold to infinity. This is the probability of false alarm, P_{FA}. If $f_2(x)$ is similarly integrated, the result is the probability of detection, P_{DET}. The remaining two areas, to the left of the example threshold, are the probability of calling a good part good and of calling a bad part good respectively.

The design objective parameters, P_{FA} = 10% and P_{DET} = 90%, would be realized by a threshold set at A, the case in which the threshold is set at the crossover of the two curves. This occurs because the selected values of P_{FA} and P_{DET} sum to 100 percent.

It should be noted that many pairs of values such as P_{FA} = 5% with P_{DET} = 90% cannot be realized with the values of $f_1(x)$ and $f_2(x)$ shown. Either a smaller value of σ_1 or σ_2 or larger separation of the means is required.

H.2 SIGNAL-TO-CLUTTER RATIO

The baseline (system output with no failure signal present) is herein referred to as clutter because the baseline is not white noise but contains some components similar to the fault signal. The baseline is mostly made up of machinery noise such as gear mesh and unbalance disturbances, high frequency noise (probably emanating from the engine exhaust and IR

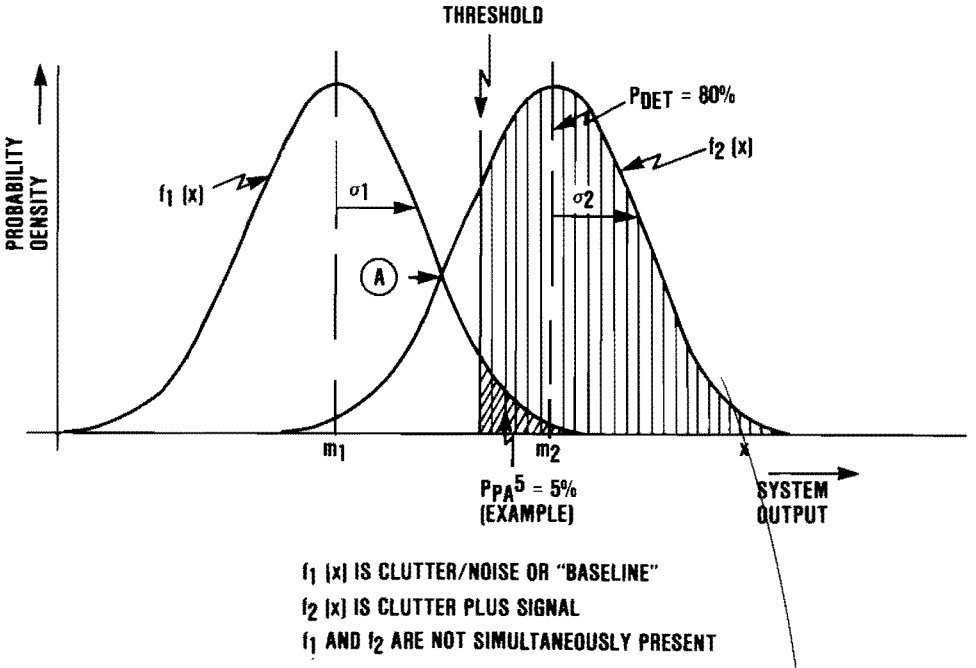

Figure H-1. Relationship of False Alarms and Signal Detection

suppression baffles), and bearing noise caused by microscopic asperities and inaccuracies in race and rolling element dimensions which excite the poorly damped ringing response of the outer race. The latter is also excited by bearing faults, although in a coherent rather than random pattern. Fortunately the machinery noise and the engine noise can be filtered out, leaving a frequency window wide enough to guarantee the presence of at least one bearing ringing mode for every type of bearing to be tested.

H.3 SIGNAL-TO-CLUTTER RATIO FOR SPADE P_{DET} AND P_{FA} REQUIREMENTS

To obtain 10 percent or less probability of false alarm requires a threshold set at the upper 1.25 point on the clutter distribution. To obtain 90 percent probability of detection requires that the lower 1.25 point of the signal plus clutter distribution exceeds the threshold setting. If the sigmas of the two distributions are equal, this amounts to a signal-to-noise ratio of 2.5 to 1.